8-31-2021

Stochastic programming and agent-based simulation approaches for epidemics control and logistics planning

Xuecheng Yin
New Jersey Institute of Technology

Copyright Warning & Restrictions

The copyright law of the United States (Title 17, United States Code) governs the making of photocopies or other reproductions of copyrighted material.

Under certain conditions specified in the law, libraries and archives are authorized to furnish a photocopy or other reproduction. One of these specified conditions is that the photocopy or reproduction is not to be "used for any purpose other than private study, scholarship, or research." If a, user makes a request for, or later uses, a photocopy or reproduction for purposes in excess of "fair use" that user may be liable for copyright infringement,

This institution reserves the right to refuse to accept a copying order if, in its judgment, fulfillment of the order would involve violation of copyright law.

Please Note: The author retains the copyright while the New Jersey Institute of Technology reserves the right to distribute this thesis or dissertation

Printing note: If you do not wish to print this page, then select "Pages from: first page # to: last page #" on the print dialog screen

ABSTRACT

STOCHASTIC PROGRAMMING AND AGENT-BASED SIMULATION APPROACHES FOR EPIDEMICS CONTROL AND LOGISTICS PLANNING

by
Xuecheng Yin

This dissertation addresses the resource allocation challenges of fighting against infectious disease outbreaks. The goal of this dissertation is to formulate multi-stage stochastic programming and agent-based models to address the limitations of former literature in optimizing resource allocation for preventing and controlling epidemics and pandemics. In the first study, a multi-stage stochastic programming compartmental model is presented to integrate the uncertain disease progression and the logistics of resource allocation to control a highly contagious infectious disease. The proposed multi-stage stochastic program, which involves various disease growth scenarios, optimizes the distribution of treatment centers and resources while minimizing the total expected number of new infections and funerals due to an epidemic. Two new equity metrics are defined and formulated, namely infection and capacity equity, to explicitly consider equity for allocating treatment funds and facilities for fair resource allocation in epidemics control. The multi-stage value of the stochastic solution (VSS), demonstrating the superiority of the proposed stochastic programming model over its deterministic counterpart, is studied. The first model is applied to the Ebola Virus Disease (EVD) case in West Africa, including Guinea, Sierra Leone, and Liberia. In the following study, the previous model is extended to a mean-risk multi-stage vaccine allocation model to capture the influence of the outbreak scenarios with low probability but high impact. The Conditional Value at Risk (CVaR) measure used in the model enables a trade-off between the weighted expected loss due to the outbreak and expected risks associated with experiencing disastrous epidemic scenarios. A method is developed to estimate the migration rate

between each infected region when limited migration data is available. The second study is applied to the case of EVD in the Democratic Republic of the Congo.

In the third study, a new risk-averse multi-stage stochastic epidemics-ventilator-logistics compartmental stochastic programming model is developed to address the resource allocation challenges of mitigating COVID-19. This epidemiological logistics model involves the uncertainty of untested asymptomatic infections and incorporates short-term human migration. Disease transmission is also forecasted through deriving a new formulation of transmission rates that evolve over space and time with respect to various non-pharmaceutical interventions, such as wearing masks, social distancing, and lockdown. In the fourth study, a simulation-optimization approach is introduced to address the vaccination facility location and allocation challenges of the COVID-19 vaccines. A detailed agent-based simulation model of the COVID-19 is extended and integrated with a new vaccination center and vaccine-allocation optimization model. The proposed agent-based simulation-optimization framework simulates the disease transmission first and then minimizes the total number of infections over all the considered regions by choosing the optimal vaccine center locations and vaccine allocation to those centers. Specifically, the simulation provides the number of susceptible and infected individuals in each geographical region for the current time period as an input into the optimization model. The optimization model then minimizes the total number of estimated infections and provides the new vaccine center locations and vaccine allocation decisions for the following time period. Decisions are made on where to open vaccination centers and how many people should be vaccinated at each future stage in each region of the considered geographical location. Then these optimal decision values are imported back into the simulation model to simulate the number of susceptible and infected individuals for the subsequent periods. The agent-based simulation-optimization framework is applied to controlling COVID-19 in the states of New Jersey. The results provide

insights into the optimal vaccine center location and vaccine allocation problem under varying budgets and vaccine types while foreseeing potential epidemic growth scenarios over time and spatial locations.

STOCHASTIC PROGRAMMING AND AGENT-BASED SIMULATION APPROACHES FOR EPIDEMICS CONTROL AND LOGISTICS PLANNING

by
Xuecheng Yin

A Dissertation
Submitted to the Faculty of
New Jersey Institute of Technology
in Partial Fulfillment of the Requirements for the Degree of
Doctor of Philosophy in Industrial Engineering

Department of Mechanical and Industrial Engineering

August 2021

APPROVAL PAGE

STOCHASTIC PROGRAMMING AND AGENT-BASED SIMULATION APPROACHES FOR EPIDEMICS CONTROL AND LOGISTICS PLANNING

Xuecheng Yin

Dr. İ. Esra Büyüktahtakın Toy, Dissertation Advisor — Date
Associate Professor of Mechanical and Industrial Engineering, NJIT

Dr. Sanchoy Das, Committee Member — Date
Professor of Mechanical and Industrial Engineering, NJIT

Dr. Athanassios Bladikas, Committee Member — Date
Associate Professor of Mechanical and Industrial Engineering, NJIT

Dr. Wenbo Cai, Committee Member — Date
Associate Professor of Mechanical and Industrial Engineering, NJIT

Dr. Kathleen McEnnis, Committee Member — Date
Assistant Professor of Chemical and Materials Engineering, NJIT

BIOGRAPHICAL SKETCH

Author: Xuecheng Yin

Degree: Doctor of Philosophy

Date: August 2021

Undergraduate and Graduate Education:

- Doctor of Philosophy in Industrial Engineering,
  New Jersey Institute of Technology, Newark, NJ, 2021
- Master of Science in Industrial and Systems Engineering,
  Lehigh University, Bethlehem, PA, 2018
- Bachelor of Science in Mechanical Engineering,
  Huaiin Institute of Technology, Huaian, China, 2015

Major: Industrial Engineering

Presentations and Publications:

Xuecheng Yin, İ. Esra Büyüktahtakın, Sabah Bushaj, and Yue Yuan, "An Integrated Simulation-Optimization Algorithmic Framework to Vaccine Distribution for Controlling the COVID-19," Under preparation, 2021

Xuecheng Yin, İ. Esra Büyüktahtakın, and Bhumi Patel "COVID-19: Optimal Allocation of Ventilators under Uncertainty and Risk," Under review for *European Journal of Operational Research*, 2021

Xuecheng Yin and İ. Esra Büyüktahtakın, "Risk-Averse Multi-stage Stochastic Programming to Optimizing Vaccine Allocation and Logistics in Epidemics Control," Accepted for publication in *IISE Transactions on Healthcare Systems Engineering*, 2021

Xuecheng Yin and İ. Esra Büyüktahtakın, "A Multi-Stage Stochastic Programming Approach to Epidemic Resource Allocation with Equity Considerations," *Health Care Management Science*, Published online ahead of print May 10, 2021. https://doi.org/10.1007/s10729-021-09559-z

Xuecheng Yin, İ. Esra Büyüktahtakın, Sabah Bushaj, and Yue Yuan, "An Integrated Simulation-Optimization Algorithmic Framework to Vaccine Distribution for Controlling the COVID-19," *Institute of Operations Research and Management Sciences (INFORMS) Healthcare Conference*, Virtual, July 2021.

Sabah Bhshaj, İ. Esra Büyüktahtakın, and Xuecheng Yin, "A Simulation-Deep Reinforcement Learning (SiRL) Approach for COVID-19 Epidemic Optimization and Control," *INFORMS Healthcare Conference*, Virtual, July 2021.

Xuecheng Yin, İ. Esra Büyüktahtakın, and Bhumi Patel, "A Data-Driven Stochastic Programming Epidemic Modeling Framework to Controlling the COVID-19," *INFORMS Healthcare Conference*, Virtual, July 2021.

Xuecheng Yin, İ. Esra Büyüktahtakın, and Bhumi Patel, "A Data-Driven Stochastic Programming Epidemic Modeling Framework to Controlling the COVID-19," *Presentation at Yale University*, Virtual, April 2021.

Xuecheng Yin, İ. Esra Büyüktahtakın, and Bhumi Patel, "A Data-Driven Stochastic Programming Epidemic Modeling Framework to Controlling the COVID-19," *Dana Knox Research Showcase* (received the first place in best graduate-student paper presentation), Virtual, April 2021.

Xuecheng Yin, İ. Esra Büyüktahtakın, and Bhumi Patel, "A Data-Driven Stochastic Programming Epidemic Modeling Framework to Controlling the COVID-19," *NSF Student Conference on COVID-19 Modeling*, Virtual, Jan 2021.

Xuecheng Yin and İ. Esra Büyüktahtakın, "Risk-Averse Multi-stage Stochastic Programming to Optimizing Vaccine Allocation and Logistics in Epidemics Control," *INFORMS Conference*, Virtual, Nov 2020.

Xuecheng Yin and İ. Esra Büyüktahtakın, "Multi-stage Stochastic Resource Allocation for the Optimal Control of Epidemic Diseases," *INFORMS Conference*, Seattle, Oct 2019.

Xuecheng Yin and İ. Esra Büyüktahtakın, "Multi-stage Stochastic Resource Allocation for the Optimal Control of Epidemic Diseases," *Modeling and Optimization: Theory and Applications (MOPTA) Conference*, Bethlehem, Aug 2019.

NOT THE NEXT, THE FIRST.

My Future Kid

ACKNOWLEDGMENT

My doctoral study experience at the New Jersey Institute of Technology is a remarkable and unforgettable experience in my life that I cherish a lot.

I would like to especially thank my advisor, Dr. Esra Büyüktahtakın Toy. She is very patient to give me suggestions on my research. She always tries her best to bring me advice and encouragement to conquer the challenges in my research endeavors and my life. I feel very lucky to have such a great advisor. I sincerely thank all my committee members, Dr. Sanchoy Das, Dr. Wenbo Cai, Dr. Athanassios Bladikas, and Dr. Kathleen McEnnis. I would also sincerely thank Dr. Sanchoy Das, who brings me many supports and teach me how to live and how to confront challenges. I truly appreciate all contributions from my committee members.

I gratefully acknowledge the partial support of the National Science Foundation CAREER Award co-funded by the CBET/ENG Environmental Sustainability program and the Division of Mathematical Sciences in MPS/NSF under Grant No. CBET-1554018.

I want to thank all professors who taught me courses at Lehigh University, New Jersey Institute of Technology, and Rutgers University for teaching me the knowledge. I also want to thank all my friends for encouraging me when I feel sad and lonely. I would also like to express sincere thanks to Dr. Sabah Bushaj and Dogacan Yilmaz for their insightful criticism and suggestion on my research. I am also very thankful to my parents, my friends, and many other important people. I am thankful to my parents, my mother Jing Xue and father Zhanghao Yin, for the love, encouragement and unconditional support. Their love gives me the brave to face all difficulties. Without their support, I would not have the opportunity to chase my dream. Last but not least, I would like to especially thank my wife, Dr. Yue Yuan, who gave me a lot of support not only in my life but also in my study and research.

TABLE OF CONTENTS

Chapter **Page**

1 INTRODUCTION 1

1.1 Background 1

1.2 Literature Review 3

1.2.1 Simulation, Compartmental, and Network Models 4

1.2.2 OR Models in Epidemic Resource Allocation 8

1.2.3 Vaccination Models 11

1.2.4 OR Models for Fair Resource Allocation 14

1.2.5 Agent-Based Models 15

1.2.6 Simulation-Optimization Models 18

1.2.7 Literature Focusing on COVID-19 Resource Allocation 19

1.2.8 Mean-Risk Stochastic Programming 22

1.3 Motivation 25

1.4 Summary of Research Objectives and Accomplishments 26

1.4.1 A Multi-Stage Stochastic Programming Approach to Epidemic Control with Equity Considerations 27

1.4.2 Risk-Averse Multi-Stage Stochastic Programming for Vaccine Allocation and Treatment Logistics for Epidemic Response . 28

1.4.3 COVID-19: Optimal Allocation of Ventilator Supply under Uncertainty and Risk 29

1.4.4 An Agent-Based Simulation-Optimization Vaccine Center Location Vaccine Allocation Approach to Controlling COVID-19 . . . 30

1.4.5 Organization of the Dissertation 31

2 A MULTI-STAGE STOCHASTIC PROGRAMMING APPROACH TO EPIDEMIC CONTROL WITH EQUITY CONSIDERATIONS 32

2.1 Introduction 32

2.1.1 Key Contributions and Insights 35

2.2 Problem Formulation 38

TABLE OF CONTENTS
(Continued)

Chapter **Page**

2.2.1 Notation 38

2.2.2 Compartmental Disease Model Description 42

2.2.3 Uncertainty Representation and Scenario Tree Generation Scheme 44

2.2.4 Model Features and Assumptions 47

2.2.5 Model Formulation 48

2.2.6 Equity of ETC and Treatment Resources Distribution 51

2.2.7 Mixed-Integer Linear Program (MIP) Model 56

2.3 Results 57

2.3.1 Model Validation 57

2.3.2 The Value of Stochastic Solution (VSS) 59

2.3.3 Analysis of Budget Allocation 61

2.3.4 Analysis of Different Scenarios 65

2.3.5 Impacts of Equity Considerations 69

2.4 Discussion and Future Research Directions 72

3 RISK-AVERSE MULTI-STAGE STOCHASTIC PROGRAMMING FOR VACCINE ALLOCATION AND TREATMENT LOGISTICS FOR EPIDEMIC RESPONSE 77

3.1 Introduction 77

3.1.1 Key Contributions and Insights 80

3.2 Multi-Stage Risk and Time Consistency 84

3.3 Problem Formulation 85

3.3.1 Notation 86

3.3.2 Compartmental Disease Model Description 90

3.3.3 Uncertainty and Model Assumptions 92

3.3.4 Model Formulation 95

3.4 Case Study and Results 100

3.4.1 Implementation Details 100

TABLE OF CONTENTS
(Continued)

Chapter **Page**

3.4.2 Resource Allocation under Different Budget Levels 102

3.4.3 Analysis of the Risk Trade-off 104

3.4.4 Analyzing the Impact of Delay in Vaccination 110

3.5 Analyzing Vaccine Effectiveness and Acceptance Rates 111

3.6 Discussion and Conclusions 115

4 COVID-19: OPTIMAL ALLOCATION OF VENTILATOR SUPPLY UNDER UNCERTAINTY AND RISK 122

4.1 Introduction 122

4.1.1 Key Contributions and Insights 125

4.2 Problem Formulation 127

4.2.1 Model Notation and Formulation 127

4.2.2 Compartmental Disease Model Description 130

4.2.3 Time- and Space-Varying Transmission Rate 131

4.2.4 Uncertainty and Multi-period Scenario Tree 133

4.2.5 Model Features and Assumptions 134

4.2.6 Multi-Stage Risk and Time Consistency 137

4.2.7 Mathematical Model Formulation and Description 138

4.2.8 Scenario Sub-Problem and Bounds 143

4.3 Case Study Data 143

4.3.1 Population and Migration Data 144

4.3.2 Epidemiological Data 145

4.3.3 Initial Infection, Capacity and Cost Data 147

4.4 Results 148

4.4.1 Model Validation 148

4.4.2 Case Study Implementation Details 150

4.4.3 Transmission Forecast under Different Intervention Strategies . 151

TABLE OF CONTENTS
(Continued)

Chapter **Page**

4.4.4 Optimal Ventilator Allocation 154

4.4.5 Risk Analysis 156

4.5 Discussion and Future Directions 158

5 AN AGENT-BASED SIMULATION-OPTIMIZATION VACCINE CENTER LOCATION VACCINE ALLOCATION APPROACH TO CONTROLLING COVID-19 163

5.1 Introduction 163

5.2 Key Contributions and Insights 165

5.3 Model Description 166

5.3.1 Agent-based Simulation Model 166

5.4 Optimization Model Formulation 169

5.4.1 Important Features and Model Assumptions 169

5.4.2 Notation 171

5.4.3 Optimization Model Formulation 174

5.4.4 Linearization 179

5.4.5 Simulation-Optimization Model 179

5.5 Case Study Data 182

5.5.1 Population and Infection Data 183

5.5.2 Logistics and Operations Cost Data 184

5.6 Model Validation 186

5.7 Case Study Results 189

5.7.1 The Number of Cumulative Infections under Different Budget Levels 189

5.7.2 The Number of Vaccines Allocated to Each County under Different Budget Levels 191

5.7.3 Vaccination Center Location Decision under Medium Budget Levels and Number Restrictions 198

TABLE OF CONTENTS
(Continued)

Chapter **Page**

5.7.4 Vaccine Allocation between Vaccination Centers and Local Pharmacies (and Small Vaccination Sites) 200

5.8 Discussion and Future Direction 202

6 SUMMARY AND FUTURE DIRECTIONS 206

APPENDIX A A MULTI-STAGE STOCHASTIC PROGRAMMING APPROACH TO EPIDEMIC CONTROL WITH EQUITY CONSIDERATIONS . . . 208

A.1 Non-Anticipativity 208

A.2 Linearization 208

A.3 Ebola Case Study Data 210

A.3.1 Population and Migration Data 210

A.3.2 Resource Allocation Cost Data 211

A.3.3 Epidemiological Data 212

A.4 Analysis of Infection and Prevalence Equity Constraints 212

APPENDIX B RISK-AVERSE MULTI-STAGE STOCHASTIC PROGRAMMING FOR VACCINE ALLOCATION AND TREATMENT LOGISTICS FOR EPIDEMIC RESPONSE 216

B.1 Ebola Case Study Data 216

B.1.1 Regional and Population Data 216

B.1.2 Migration Estimation Model and Data for Migration Rates . . 217

B.1.3 Resource Allocation Cost Data 220

B.1.4 Epidemiological Data 221

APPENDIX C AN AGENT-BASED VACCINE ALLOCATION MODEL FOR CONTROLLING COVID-19 222

LIST OF TABLES

Table		Page
2.1	Sets and Indices	38
2.2	Transition Parameters Describing the Rate of Movement between Disease Compartments	39
2.3	Other Parameters	40
2.4	State Variables	41
2.5	Decision Variables	42
2.6	The Range (Lower and Upper Bounds), Mean, and Standard Deviation of Community Transmission Rate in Each Country	45
2.7	The 0.15-, 0.50-, 0.85-Quantiles of the Normal Distribution of the Random Variable ξ_r^n at Nodes 0 and 1 of the Scenario Tree in Figure 2.2	47
2.8	Statistical Analysis to Compare Bi-weekly Predicted Cases and Real Outbreak Data	58
2.9	VSS_t Values up to Four Stages for the 8-Stage Problem with EEV_t Values	60
2.10	Budget and Bed Allocated under Different Budget Levels	63
2.11	Budget and Bed Allocated under Different Scenarios	67
2.12	Model Run Specifics with the Capacity Equity Constraint (2.3)	71
3.1	Comparison of Objective Value, Expected Impact, Expected Risk, and Expected Cost under Various Risk-Averseness Levels	105
3.2	Expected Impact and Expected Risk for Different Risk-averseness Levels	106
3.3	The Budget ($\$M$) Allocation at Each Stage over Four Different Risk-Averseness Levels	107
4.1	The 0.15-, 0.50-, 0.85-Quantiles of the Normal Distribution at Nodes 0, 1, and 3 of the Scenario Tree in Figure 4.2 and the Associated Node of the Uncertain Parameter Realization.	134
4.2	Counties and Population Sizes in New York and New Jersey	145
4.3	Migration Rate Among Counties in New York and New Jersey	145
4.4	Transmission Parameters and Bi-weekly Rates for the COVID-19	146

LIST OF TABLES
(Continued)

Table **Page**

4.5 Transmission Rate ($\sigma_{1,r}$) in New York and New Jersey and Impact of Interventions 147

4.6 Initial Number of Infections, Hospital Capacity, and ICU Capacity for Each County 148

4.7 Statistical Analysis to Compare the Bi-Weekly Predicted New Cases and Real Outbreak Data 150

4.9 Comparison of Objective Value, Expected Impact, and Expected Risk under Various Risk-Averseness Levels 157

4.10 Expected Impact and Risk for Different Risk-Averseness Levels 158

4.8 Optimal Ventilators Allocated under Different Scenarios for Budget Levels 162

5.1 Populations and the Number of Infections (in Thousands) for Each County in New Jersey 184

5.2 COVID-19 Vaccine Cost ($) and Efficiency [Seladi-Schulman, 2021] . . . 185

5.3 Logistics Cost ($) for the COVID-19 Vaccines [WHO, 2021c] 185

5.4 Statistical Analysis to Compare the Weekly Predicted New Cases and Real Outbreak Data 188

5.5 Vaccine Allocation under Limited Budget Level 192

5.6 Vaccine Allocation under Medium Budget Level 194

5.7 Vaccine Allocation under Ample Budget Level 196

5.8 Vaccine Allocation between Vaccination Centers and Local Pharmacies (and small vaccination sites) with Only One Pfizer Center 201

5.9 Vaccine Allocation between Vaccination Centers and Local Pharmacies (and small vaccination sites) with Different Types of Vaccination Centers When Vaccine Center Types and Locations are Fixed a Priori in the Model 202

A.1 Regions, Population Size and Rate in West Africa 211

A.2 The Number of Infected People at the Beginning of the Planning Horizon (August 30, 2014) in West Africa 211

A.3 Bi-weekly Migration Rate between Regions of Guinea and Liberia, Original Data Acquired from the study of Wesolowski et al. [2014] . . 211

A.4 Summary of Ebola Treatment Cost for 50 (100)-bed ETC 212

LIST OF TABLES
(Continued)

Table **Page**

A.5 Transmission Parameters and Bi-weekly Rates for the Ebola Outbreak . 212

A.6 Model Run Specifics with the Infection Equity Constraint (2.2) 213

A.7 Model Run Specifics with the Prevalence Equity Constraint 214

B.1 Regions, Population Size, and Rate in West Africa 217

B.2 The Number of Infected People at the Beginning of the Planning Horizon (June 25, 2019) 217

B.3 Geographical Distance between Regions (KM) 220

B.4 Migration Rate between Regions of North Kivu and Ituri 220

B.5 Summary of Fixed and Variable Treatment Costs in 50 (100)-Bed ETC . 221

B.6 Transmission Parameters and Three-Weekly Rates for the Ebola Outbreak 221

B.7 Three-Weekly Values for Vaccine Supply Upper-Bound (G_j^ω) and the Uncertain Transmission Rate ($\theta_{1,r}^\omega$) for the Ebola Outbreak(High (Low) Realization for G_j^ω Implies Low (High) Realization for $\theta_{1,r}^\omega$) 221

LIST OF FIGURES

Figure		Page
2.1	One-step disease compartmental model.	42
2.2	Scenario tree generation example for Guinea, where each circle, denoted by n, $n := \{0, \ldots, 12\}$, represents a node of the scenario tree.	45
2.3	Comparison of predicted cases with real outbreak data for cumulative infections in Guinea, Liberia, and Sierra Leone.	58
2.4	Total budget allocation under different budget levels.	64
2.5	Total capacity allocation under different budget levels.	64
2.6	Total number of infections and funerals under different budget levels.	65
2.7	Total budget allocation under different scenarios.	68
2.8	Total capacity allocation under different scenarios.	68
2.9	Total number of new infections and funerals under different scenarios.	69
2.10	Optimal budget allocation under different k values for an 8-stage problem with \$24M budget.	71
2.11	Total number of new infections and funerals under different k values for an 8-stage problem with \$24M budget.	72
3.1	One-Step disease compartmental model.	90
3.2	Budget, capacity (bed), and vaccine allocated to each region ($\lambda = 1$ and $\alpha = 0.5$).	103
3.3	Budget allocation over treatment, ETC capacity, and vaccine for four different risk-averseness.	107
3.4	Treatment budget, capacity (bed), and vaccine allocation under different risk-averseness levels.	109
3.5	Cumulative number of infections and funerals for each stage under different types of delay ($\lambda = 10$ and $\alpha = 0.5$).	111
3.6	Non-cumulative number of infections and funerals for each delay option over no delay ($\lambda = 10$ and $\alpha = 0.5$).	111
3.7	Vaccine allocation under different vaccine effectiveness rates ($\lambda = 10$ and $\alpha = 0.95$).	114

LIST OF FIGURES
(Continued)

Figure **Page**

3.8 The first-stage and total vaccine allocation under different vaccine acceptance rates ($\lambda = 10$ and $\alpha = 0.95$). 116

4.1 One-step COVID-19 compartmental model. 130

4.2 Multi-stage scenario tree generation example for the uncertain proportion of untested asymptomatic infections ($\sigma^{\omega}_{2,r}$). 135

4.3 Counties in New York and New Jersey. 144

4.4 Comparison of predicted cases with real outbreak data for new infections in New York and New Jersey. 149

4.5 Number of new infections and deaths under different intervention strategies and actual numbers. 153

4.6 Number of hospitalized individuals and ICU patients under different intervention strategies. 154

5.1 Covasim simulation. 167

5.2 Compartment model of simulation. 168

5.3 Compartment model of optimization. 171

5.4 The loop of simulation-optimization model. 179

5.5 All the counties in New Jersey. 182

5.6 Model validation against real outbreak data in New Jersey. 187

5.7 New Jersey cumulative infections under different budget levels. 191

5.8 Proportion of each type of vaccine under different budget levels. 197

5.9 Vaccination center locations for Pfizer. 198

5.10 Vaccination center locations for all types of vaccines. 199

A.1 Optimal budget allocation under different k values for an 8-stage problem with \$24M budget. 213

A.2 Total number of new infections and funerals under different k values for an 8-stage problem with \$24M budget. 214

A.3 Optimal budget allocation under different k values for an 8-stage problem with \$24M budget. 215

LIST OF FIGURES
(Continued)

Figure **Page**

A.4 Total number of new infections and funerals under different k values for an 8-stage problem with \$24M budget. 215

B.1 Region division in North Kivu and Ituri. The map is constructed using ESRI [2020]. 216

B.2 Steps of calculating the migration rate. 217

C.1 Cumulative infections (thousands) throughout the planning horizon for New Jersey counties - 1. 222

C.2 Cumulative infections (thousands) throughout the planning horizon for New Jersey counties - 2. 223

C.3 Cumulative infections (thousands) throughout the planning horizon for New Jersey counties - 3. 224

C.4 New Jersey cumulative infections under different budget levels - 1. . . . 225

C.5 New Jersey cumulative infections under different budget levels - 2. . . . 226

C.6 New Jersey cumulative infections under different budget levels - 3. . . . 227

CHAPTER 1

INTRODUCTION

1.1 Background

Human beings have suffered from epidemic diseases throughout their history. An epidemic is the rapid spread of an infectious disease that affects a large number of people. Epidemic diseases can disperse widely in a short time, usually two weeks or less, such as influenza, meningitis, and cholera, impacting populations either in a specific area or become a pandemic affecting the lives of millions at a global scale. The outbreaks ruin the economy and weaken the healthcare systems in the region where the epidemic locates. The situation can be even worse in impoverished areas where millions of people do not have an opportunity to receive sufficient treatment. Thus, the number of deaths and infections in poor regions with the epidemic will be much higher than that in other regions. Although some countries may have ample budget to control an outbreak, the shortage of the resource supply during the epidemic still leads to many deaths, degradation in the quality of human life, and economic impediments.

Infectious diseases have changed and continue to change the trajectory of millions of people's lives in both the short-term and long-term. The country, region, and the world have more far-reaching impacts, and some are even irreversible. For example, in 2003, Severe Acute Respiratory Syndrome (SARS) was found to infect humans in South China. A doctor who was infected with the SARS virus in Guangdong Province infected many people when he went to Hong Kong in February 2003. The infected people brought SARS to the rest of the world. The statistics show that the global death toll from SARS is 919, with a fatality rate of nearly 11%. There are 5,327 cases and 349 deaths in Mainland China; 1,755 cases and 300 deaths in

Hong Kong; 665 cases and 180 deaths in Taiwan; 251 cases and 41 deaths in Canada; 238 cases and 33 deaths in Singapore; and 63 cases and 5 deaths in Vietnam [Haccp, 2020].

The H1N1 swine flu broke out in the United States in April 2009, and it was the first outbreak of H1N1 swine flu in a population. The United States is one of the most developed countries, and its response speed is very rapid. The first sample was found on April 15, reported to the International Health Organization (WHO) on April 18, vaccine development began on April 21, and the flue was disclosed to the public on April 23. On April 25, only 10 days after the first sample was found, WHO declared that the H1N1 epidemic had become a public health emergency of international concern. On April 26, 2009, the US government also announced a nationwide public health emergency, and the Centers for Disease Control and Prevention (CDC) began to release the national strategic reserve. WHO and the US government attached great importance to the epidemic. However, the flu epidemic spread rapidly at an unstoppable rate. About one month after the first sample was discovered, the number of infections exceeded 10,000 [Sina, 2021].

At the end of 2019, COVID-19 was detected in China, and suddenly, it spread all over the world. The worldwide spread of COVID-19 caused lots of deaths. Until July 14, 2021, the total number of infections in the world is 188,124,452, and the number of deaths is 4,053,386 [JHU, 2021]. The pandemic has also had adverse economic impacts. Globally, more than one-sixth of young people are unemployed due to the epidemic. Asian Development Bank statistics show that the global economic loss caused by the epidemic is between 5.8 trillion and 8.8 trillion US dollars [News, 2020]. On the other hand, people who are not infected have suffered from losing their relatives, and some lost their income due to the indirect economic influence of the disease.

Consequently, the high impact of epidemics on human life has motivated researchers and practitioners to develop new methodologies to prevent and reduce the effects of infectious diseases. For controlling epidemics, many interventions have been widely used to treat humans and prevent them from getting infected, such as contact tracing, isolation, and vaccination.

With the development of vaccines for different epidemics, people can be immune to the disease, and the health impacts can be significantly reduced. However, for a newly discovered disease, the production quantity of the treatment resource or vaccination may not satisfy the high demand in the early period, and it is also difficult to develop new vaccines. Treatment resources and vaccination supply are almost always limited. In addition, the uncertainty of the epidemic transmission makes the resource allocation decision even harder. The resource allocations decisions should be made ahead of time before knowing the disease's growth trajectory. Once the disease transmission is beyond the estimation, the decisions taken in former time periods can cause a big loss on the number of infections when the resources are limited. Thus, tackling the resource allocation problem under uncertainty is critical for studying logistic issues on epidemic control.

1.2 Literature Review

Operations Research (OR) and mathematical modeling methods have been widely used to determine optimal resource allocation strategies to control an epidemic disease. Those approaches include simulations [Siettos et al., 2015, Ajelli et al., 2016, Kurahashi and Terano, 2015, Wells et al., 2015], differential equations [Craft et al., 2005, Kaplan et al., 2003], network models [Berman and Gavious, 2007, Longini Jr et al., 2007, Porco et al., 2004, Riley and Ferguson, 2006], resource allocation analysis [Zaric et al., 2000, Tebbens and Thompson, 2009, Nguyen et al., 2017, Shaw and Schwartz, 2010], stochastic compartmental models [Lekone and Finkenstädt, 2006,

Tanner et al., 2008, Funk et al., 2017], and mathematical programming [Coşgun and Büyüktahtakın, 2018, Büyüktahtakın et al., 2018a, Ren et al., 2013, Tanner et al., 2008]. The following subsections present a review of the literature in epidemic control and logistics in major categories and present motivations for this dissertation study.

1.2.1 Simulation, Compartmental, and Network Models

The majority of mathematical models in the epidemiological literature use simulation methods to study the logistics of controlling epidemics [Meltzer et al., 2014, Dasaklis et al., 2017, Pandey et al., 2014]. For instance, Rivers et al. [2014] perform simulations of interventions on Ebola to inform public health efforts. They use existing data to parameterize an Ebola Virus Disease (EVD) mathematical model that is used to forecast the progression of the epidemic and the efficacy of several interventions. Their results suggest that contact tracing and infection control, such as decreasing contact rates in hospitals and funerals, have a substantial impact on the number of Ebola cases, but they are not sufficient to halt the spread of the epidemic. On the other hand, they find that the hypothetical pharmaceutical intervention had a smaller effect on the forecast trajectory of the epidemic. Siettos et al. [2015] develop an agent-based simulation model to investigate the dynamics of the Ebola epidemics. The estimated values of key epidemiological variables are found to be very close to the ones reported by the WHO Ebola response team. Jalvingh et al. [1999] modify the InterSpread model for foot-and-mouth (FMD) disease for the case of the classical swine fever (CSF) to evaluate the impact of control measures by changing the assumptions and mechanisms for disease spread from FMD to CSF, and including CSF-specific control measures based on the standard European Union (EU) regulations. They show that InterSpread was a flexible tool that could be adapted to simulate another disease with relative ease.

Several studies have used stochastic compartmental models to analyze different strategies for controlling epidemic diseases, such as vaccination strategies, behavioral changes that impact the interaction between different groups, and regional intervention strategies. Lekone and Finkenstädt [2006] use a stochastic discrete-time approximation to the Susceptible-Exposed-Infectious-Recovered (SEIR) system to model Ebola epidemics and introduced a Markov Chain Monte Carlo (MCMC) simulation algorithm for parameter estimation. They find that intervention measures, such as protective clothing, active surveillance, and community education, have been successful in controlling the disease, and an earlier onset of the control intervention could have saved many more lives. Funk et al. [2017] develop a stochastic compartmental model to analyze the impact of behavior changes on the elimination of Ebola. They report that the expansion of the Ebola Treatment Center (ETC) capacity, occasional interruption of transmission, and improvement in healthcare-seeking behavior contributed to mitigating the epidemic and eventually stop it. Keeling et al. [2001] present an individual farm-based stochastic model of the UK foot-and-mouth epidemic. They show that spatial distribution, size, and species composition of farms influenced the observed pattern and regional variability of the outbreak. Moreover, they assess the history and possible duration of the epidemic, the performance of control strategies, such as movement restrictions, and general implications for disease dynamics in space and time. Onal et al. [2019] present an integrated simulation-optimization framework, which simulates the growth of an agricultural epidemic and uses it as an input into the optimization model. The simulation mimics the growth of an invasive plant over a landscape and multiple years, while a bio-economic optimization model finds an optimal search and treatment path to minimize its economic damage to agricultural production. They find that applying yearly treatment with slow search-and-treatment speed results in the minimum economic damage under most invasion scenarios.

Nguyen et al. [2017] use a multi-scale model to explore Ebola vaccination strategies. They combine a within-host viral dynamics model and a between-host network model of the Ebola virus infection. Their results suggest that an early, age-group specific, and high coverage vaccination program is the most beneficial for controlling the Ebola virus disease. Ball et al. [1997] develop a Susceptible-InfectedRecovered (SIR) model with both local mixing at the household level and global mixing at the community level. Their results show that the allocation of vaccines to those households with the largest number of unvaccinated individuals is the best strategy for controlling an epidemic, given that the efficiency of the vaccine is high. Shaw and Schwartz [2010] study vaccine control of disease spread on a new adaptive network and compare their results with other network models. Their results suggest that vaccine control is much more effective in their adaptive networks than in static networks when the vaccination schedule is Poisson distributed.

Kelly et al. [2019a] employ a non-parametrically estimated Hawkes point process model to generate multiple probabilistic projections of the ongoing 20182019 Ebola Virus Disease (EVD) outbreak size in the Democratic Republic of the Congo (DRC). They compare the forecast results with actual outbreak size under thee-, six-, and nine-week time periods. Their results suggest that the Hawkes point process is an easily-applied statistical model to predict EVD outbreak trajectories to better inform decision-making and resource allocation. Dalziel et al. [2018] perform a retrospective analysis on community deaths during the $2014 - 2016$ Ebola epidemic in Sierra Leone to estimate the number of unreported non-hospitalized cases. Moreover, they quantify how Ebola reporting rates varied across locations and over time and tested if variation in reporting rates affected the estimates of disease transmission rates. They find significant variation in reporting rates among districts and district-specific rates of increases in reporting over time. Thus, correcting for these reporting variations improves the accuracy and precision of estimates of transmission patterns.

Moreover, the literature has often utilized compartmental models with simulations to study the strategies for controlling the Ebola Virus Disease. For example, Jiang et al. [2017] construct a mathematical model to devise the optimal EVD eradication plan. They build a modified epidemic model that takes hospital isolation, Ebola drug, and vaccine into account and later verify the result with a Monte Carlo Algorithm. They investigate the numerical spread of Ebola and eradication pathways, further fit the model against the real total cases data, and calculated infection rate as 1.754. Their results suggest that Ebola eradication requires systematic thinking, effective hospital isolation, and effective EVD drug use and vaccination. Mizumoto et al. [2019] present a quantified effective reproduction number of the ongoing Ebola virus disease epidemic in the Democratic Republic of the Congo. They use the probability mass function and cumulative distribution function of the gamma distribution to calculate the expected number of new incident cases from February 2019 to September 2019. Moreover, they use the next-generation matrix and Monte Carlo Markov Chain to forecast the model parameter from September 2019 to October 2019. They suggest that improving the security situation within the country would reduce the attacks during the vaccination in the affected health zones and thus would have a positive impact on the infection control practices. Rachah [2018] presents a deterministic compartmental model for assessing the impact of isolation to contain the EVD in Sierra Leone. He uses ordinary differential equations with different isolation strategies and studied the numerical simulation in several scenarios. According to his results, the isolation of latent detectable and infectious individuals is the most effective strategy in curtailing the virus. Hart et al. [2019] consider the variation of symptoms between different infection stages in the prediction of Ebola epidemics. They compare the compartmental model that has constant symptoms level to the compartmental model that accounts for various symptoms during infection and apply the models to both EVD cases of the 2019 Democratic Republic of Congo (DRC) and 20142016

Liberia with simulation. According to the results, when the level of surveillance is increased, the various-symptoms model predicts a smaller number of cases than the constant-symptoms model. This means that including different levels of symptoms at different stages of infection in epidemiological models can alter predictions of the effects of intervention strategies compared with assuming a fixed level of symptoms.

1.2.2 OR Models in Epidemic Resource Allocation

Optimal resource allocation is a core problem in many applications ranging from epidemic control [Zaric and Brandeau, 2001, Tanner et al., 2008] to agriculture [Cobuloglu and Büyüktahtakın, 2014, 2015, Kantas et al., 2015], production planning [Hartman et al., 2010, Büyüktahtakın and Liu, 2016, Büyüktahtakın et al., 2018b], and asset replacement [Büyüktahtakın et al., 2014b, Büyüktahtakın and Hartman, 2016, des Bordes and Büyüktahtakın, 2017]. Previous mathematical models that study the epidemic diseases and resource allocation mainly focus on logistics and operation management to control the disease in optimal ways. For example, Zaric and Brandeau [2001] present an approximated operation research model for the allocation of epidemic control resources among a set of interventions. Their results show that approximations yield reasonable estimates of the objective function values when the time horizon is on the order of five years or less. On the other hand, their model can be used as part of effective heuristics for solving large instances of resource allocation. Ekici et al. [2013] develop a disease spread model to estimate the spread pattern of the disease and combined it with a facility location and resource allocation network model for food distribution. They present the estimated number of infections and the number of meals needed in each census tract for a one-year period.

Considering the capacity of hospitals and logistics issues, Büyüktahtakın et al. [2018a] develop a new epidemic-logistics mixed-integer programming model of the epidemic control problem. Their model considers the epidemic spreading over multiple

regions and the logistics simultaneously in a spatio-temporal setting. Different from the classical epidemiological models, the transmission rate between the infected and treated compartment is not constant but instead depended on the treatment capacity and the number of infected people receiving treatment. Also, their model considers the migration between regions to explain how movement patterns contribute to the further spread of an epidemic. The authors further validate the predictions of the model by demonstrating the impact of actual interventions. In the sensitivity analysis of Büyüktahtakın et al. [2018a], the disease transmission rate within the community is found to be the most critical parameter impacting infected and funerals. Later, Liu et al. [2019] adapt the epidemics-logistics model of Büyüktahtakın et al. [2018a] to study the control of the 2009 H1N1 outbreak in China and present similar results for the H1N1 epidemic.

While the disease transmission rates are highly uncertain, relatively fewer studies in the OR community take into account the uncertain parameters for resource allocation in an effort to control the disease. Those OR models that integrate resource allocation with epidemics control use either stochastic dynamic programming (SDP) or two-stage stochastic programming [Coşgun and Büyüktahtakın, 2018, Long et al., 2018, Ren et al., 2013, Yarmand et al., 2014, Tanner et al., 2008]. For example, Coşgun and Büyüktahtakın [2018] propose SDP and approximate dynamic programming (ADP) algorithms to optimally allocate the limited intervention budget for resource allocation to control the human immunodeficiency virus (HIV) disease. They construct the compartmental model as a Markov decision process to capture the progression of the disease among the highest risk group and compare the performance of various ADP algorithms with the SDP. Their results show that the "Dynamic Proportional" strategy that allocates the budget dynamically over a multi-period planning period as the uncertainty in disease transmission is revealed gives the best result among nine different heuristic strategies. Tanner et al. [2008] consider

parameter uncertainty in a two-stage stochastic mixed-integer programming model with chance constraints for finding the optimal vaccination policy that could be applied to a wide class of epidemic models. They consider the seasonal variation of transmission parameters and estimate the parameter distributions for the worst season so that the reliability requirement is guaranteed to be satisfied throughout the entire year.

Long et al. [2018] develop a two-stage model for optimizing the allocation of Ebola treatment units across multiple geographic regions during the outbreak's early phases. They introduce an empirically-estimated coefficient for behavioral adaptation to changing epidemic conditions in the first stage and applied a heuristic, a greedy policy, a myopic linear program, and an approximate dynamic programming algorithm on the second stage. Ren et al. [2013] propose an optimization model to determine efficient distribution strategies of limited resources over multiple locations to address a smallpox outbreak. They introduce approximate representations of disease propagation that are reasonable within parameter ranges and build a large scale multi-city problem. Their results show that for a multi-city outbreak, the proposed assignment of resources saves more lives than allocating medicine proportional to population. Yarmand et al. [2014] develop a simulation model to capture the epidemic dynamics in a region for different vaccination levels and then use the simulation output to formulate a two-stage stochastic linear program for a vaccine allocation problem. Their model solution reduces the number of vaccine doses required to contain the epidemic and allowed for the redistribution of vaccine doses more efficiently.

Operations research models have also been widely used in the context of plant and forestry epidemic diseases, namely invasive species [Büyüktahtakin et al., 2014, Büyüktahtakın et al., 2011, 2014a, 2015, Bushaj et al., 2020b]. For a detailed survey

of such methods, we refer the reader to the systematic review paper of Büyüktahtakın and Haight [2018].

1.2.3 Vaccination Models

Due to the high death rate and difficulties in treating Ebola, vaccination is a widely used strategy that helps control this disease. Thus, many papers have studied various vaccination strategies for Ebola control. The majority of those studies formulate the model based on the uncertainty of the disease transmission or the supply of vaccines. For instance, Kelly et al. [2019b] use a stochastic branching process model to project the size and duration of the $2018-2019$ Ebola outbreak in the Democratic Republic of Congo (DRC) under high (62%), low (44%), and zero (0%) estimates of vaccination coverage. Then they compare the results with the Thiel-Sen regression model. Their results show that the stochastic model with suspected cases and high vaccine coverage predicted total outbreak sizes closest to the true outcome, and a relatively simple mathematical model that is updated in real time may inform outbreak response teams with projections of total outbreak size and duration.

Worden et al. [2019] use a stochastic branching process to project the short-term and long-term course of the 2019 Ebola outbreak in the Democratic Republic of Congo (DRC). They use negative binomial autoregression and Theil-Sen regression to estimate short- and long-term projections. Moreover, they use Gotts rule to estimate a baseline minimum-information projection. The authors conclude that their model generates more accurate short-term forecasts due to the reliable data source that provided weekly case counts and the real-time validation of their models. Also, they estimate that transmission rates were higher than would be expected under target levels of 62% vaccination coverage. Xie [2019] modifies the Susceptible-Exposed-Infective-Hospitalized-Funeral-Removed model of Legrand et al. [2007] to examine disease transmission dynamics after vaccination for the 2014 Ebola

outbreak in Liberia. The author uses a sensitivity analysis of various epidemic scenarios to estimate the basic reproduction number and investigated how vaccination can effectively change the course of the epidemic. He concludes that the ring vaccination strategy would reduce the transmission rate, and the proposed model may be used to better understand the spread of Ebola and develop corresponding strategies.

Brettin et al. [2018] construct a game-theoretic model of the EVD incorporating individual decisions on vaccination to study the effect of a promising Ebola vaccine (rVSV-ZEBOV). They adopt a susceptible-vaccinated-exposed-infected-recovered compartmental model and use differential equations to describe the disease transmission among each compartment. Their results show that Ebola can be eradicated if voluntary vaccination programs are coupled with focused public education efforts. Area et al. [2017] introduce vaccination of the susceptible population into a compartmental model that includes susceptible, infected, exposed, hospitalized, asymptomatic but still infectious, dead but not buried, and buried compartments to control the spread of the disease. They first consider the case where the total number of available vaccines in a fixed period of time is limited and then analyzed the situation where there is a limited supply of vaccines at each instant of time for a fixed interval of time. Finally, they use simulations to compare the models with and without vaccination. They conclude that vaccination of all susceptible individuals at the beginning of the outbreak would give the best result for controlling Ebola, and satisfactory results could be attained if the number of available vaccines meets the needs of the population.

Wells et al. [2019] present a method that can be applied to identify areas at risk during outbreaks of emerging and reemerging diseases. They use a spatial model that incorporates human mobility, poverty, and population density, and assess the effectiveness of the vaccination. As an example, they apply the maximum likelihood

approach to fit the model to the 2019 EVD case in the Democratic Republic of Congo (DRC) from April 5 to May 10. Their results demonstrate that even modest delays in initiating vaccination would have noticeably degraded the impact of the program. Chowell et al. [2019] employ an individual-level stochastic transmission model to evaluate ring and community vaccination strategies for the $2018-2019$ Democratic Republic of Congo (DRC) Ebola transmission. Their simulation model incorporates four different situations, including a proportion of the population that is inaccessible for effective contact tracing and vaccination efforts, two levels of population mixing resembling household and community transmission, two types of vaccine doses with different time periods until immunity, and spatial dependence on transmission rates. Their results indicate that ring vaccination is an effective intervention to contain Ebola epidemics at low levels of household inaccessibility when vaccinating contacts is significantly delayed. Moreover, they find the community vaccination strategies that supplement a ring vaccination strategy could speed up and enhance the probability of epidemic containment.

Liu et al. [2008] study the vaccination effects via two Susceptible-Vaccinated-Infected-Recovered (SVIR) models considering continuous vaccination strategy (CVS) and pulse vaccination strategy (PVS). Their results suggest that vaccination can help disease control by decreasing the basic reproduction number under a necessary level to eliminate the disease successfully. If ignoring the time for the vaccines to obtain immunity, or the possibility for people to be infected before obtaining immunity, the disease can always be eradicated by some suitable vaccination strategies. This may lead to over-evaluating the effect of vaccination. Lee et al. [2010] employ an agent-based computer simulation model to study the vaccine allocation of 2009 H1N1 in the Washington DC region. They compare different vaccination strategies (children first and recommended at-risk individual first). Their results support adherence to the at-risk individual first policy (instead of a children-first policy) for the H1N1

influenza vaccine when the vaccine is in limited supply. Duijzer et al. [2018] study the relationship between the herd effect and the vaccination fraction for the seminal SIR compartmental model and define the dose-optimal vaccine coverage using differential equations. The results indicate the crucial importance of the dose-optimal coverage of the vaccine. Focusing on a limited number of populations can make a significant difference, whereas allocating equally to all populations would be substantially less effective.

Yarmand et al. [2014] present a two-phase stochastic model to study the optimal vaccine allocation. They use a simulation to forecast the epidemic dynamics in each region for different vaccination levels. They also present a Newsvendor model formulation of the problem, which provides a closed-form solution for the optimal allocation and tests an easy-to-implement heuristic for vaccine allocation. The results show that the two-phase vaccination policy potentially results in a lower attack rate of the disease and a considerable saving in vaccine production and administration cost. Preciado et al. [2013] use an arbitrary contact network to distribute vaccination resources throughout the network for epidemic control. They propose a convex framework to find the cost-optimal distribution of vaccination resources when different levels of vaccination are allowed. They present a greedy approach with quality guarantees based on Lagrangian duality and illustrate results using numerical simulations in a real social network.

1.2.4 OR Models for Fair Resource Allocation

Most resource allocation models on epidemic control compute the optimal solution without considering fairness in resource allocation. Fair resource allocation has been studied in the literature, but mainly with different applications. For example, Orgut et al. [2016] consider a food allocation model with equitable and effective distribution of donated food under capacity constraints. Davis et al. [2015] develop a multi-period

linear optimization model for improving geographical equity in kidney allocation while also respecting transplant system constraints and priorities. Their results show that enhancing the practice of sharing kidneys may increase geographic equity in kidney transplantation. Moreover, Lane et al. [2017] give a systematic review of equity in healthcare resource allocation decision-making. Marsh and Schilling [1994] present a literature review of various mathematical methods for equity measures in facility-location decision models. To our knowledge, fairness has not been studied before within the context of resource allocation for epidemic control over large spatial scales.

1.2.5 Agent-Based Models

Many studies on epidemic control use agent-based simulation models to forecast the disease transmission and analyze the interventions such as resource allocation strategies (see, e.g., Müller et al. [2021], Shamil et al. [2021], and Kasaie et al. [2013]). For example, de Mooij et al. [2021] give a data-driven agent-based simulation model to address the challenges of modeling social phenomena in the epidemic. The model incorporates the individual agent's beliefs, objectives, trust in government, and the norms imposed by the government to actual data and is applied in the Virginia state of United States to compare the sensitivity of the COVID-19 outbreak size to the different normative interventions. Müller et al. [2021] present an approach that combines transportation modeling with a mechanistic infection model and a person-centric disease progression model. The model includes various parameters and is validated against the infection dynamics in Berlin (Germany). Their work shows that it is possible to build detailed epidemiological simulations from microscopic mobility models, and the results can be used to inform political decisions. Shamil et al. [2021] define an agent-based model intending to simulate the disease dynamics and transmission of COVID-19 among the inhabitants of a city (Ford County and NYC). They involve the human behavior of different susceptible agents and model how agents

interact with each other. Their results suggest that contact tracing via smartphones, with more than 60% of the population owning a smartphone combined with city-wide lockdown, reduces the effective reproduction number (Rt) below 1 within three weeks of intervention. Furthermore, contact tracing accompanied with early lockdown can suppress the epidemic growth of COVID-19 completely with sufficient smartphone owners. Kasaie et al. [2013] develop an agent-based simulation of a Tuberculosis epidemic in a single population. They use the parameters from the literature and consider a hierarchically structured contact network at different levels. They study the timing of secondary infections from a single source throughout the duration of the disease. They compare the patterns of transmission among different networks and discuss implications. In addition, they do the sensitivity analysis of outputs to illustrate the robustness of the results to variations in the parameter values.

The interventions of disease control have also been incorporated in the agent-based simulations. For instance, Li et al. [2021] present agent-based simulations to study the effectiveness of a nationwide vaccine campaign considering different vaccine efficiencies. The model incorporates the vaccine acceptance rate and different phases of vaccines to characterize the possible outcomes. The study concludes that vaccines alone cannot effectively end the pandemic given the current availability estimates and the adopted vaccination strategy, and thus non-pharmaceutical interventions need to be continued. Jahn et al. [2021] use a dynamic agent-based population model to compare different vaccination strategies for different groups. Outcomes are optimized for an initial number of available vaccines, and optimization is performed deriving a prioritization sequence to maximize the reduction in total hospitalizations and deaths compared to no vaccination. They conclude that elderly and vulnerable persons should be prioritized for vaccination until further vaccines are available. Kerr et al. [2021] present an agent-based simulation model to estimate COVID-19 transmission with interventions applied to control the pandemic. The model involves the human

behaviors and daily activities to simulate the transmission process of the COVID-19 and post different intervention strategies, including testing, treatment, vaccination of COVID-19. The model is able to provide an accurate estimation of the number of infections throughout the planning horizon.

Kasaie et al. [2010] develop an agent-based simulation model of epidemics and study the resource allocation problem by applying response-surface methodology. They compare the solution of the proposed agent-based simulation model and a known mathematical solution in an RA example. In addition, they apply the proposed approach to a more complicated resource allocation problem in which a number of previous restricting assumptions are relaxed. The results show that the model can design detailed individual behaviors and their interactions at the microscopic level, so that the developed models will eventually provide a valid representation of population dynamics and disease prevalence over the course of time. And the flexibility of the model can incorporate new assumptions about populations' characteristics and disease characteristics. Kasaie and Kelton [2013a] provides an extended discussion of their former paper on the calibration, analysis, and optimization of an agent-based simulation model of an epidemic.

The agent-based model is not only used in the epidemic control, but also in other fields. For instance, Mashhadi et al. [2016] develop an agent-based simulation (ABS) framework to model the overall product take-back and recovery system. They consider the Sociodemographic properties of the consumers, attributes of the take-back programs, specific characteristics of the recovery process, and product life cycle information. They use a numerical example of an electronic product take-back system and simulation-based optimization. They notice that the global optima cannot be guaranteed due to the non-linearity of the problem.

1.2.6 Simulation-Optimization Models

In recent years, many studies combine simulation and optimization in their own field. Carson and Maria [1997] review the area of simulation-optimization. They introduce the basic concept of simulation-optimization and review the methods and application in this area. In addition, they discuss the corresponding software tool. April et al. [2003] summarize the most relevant approaches that have been developed for the purpose of optimizing simulated systems. They concentrate on the metaheuristic black-box approach used in commercial software. They present an example of simulation optimization in the context of a simulation model developed to predict performance and measure risk in a real-world project selection problem. Xi et al. [2013] develop a simulation-optimization model that determines where to locate electric vehicle chargers to maximize their use by privately owned electric vehicles. They explore interactions between the optimization criterion used and the budget available. The results show that although the optimal location is sensitive to the specific optimization criterion considered, overall service levels are less sensitive to the optimization strategy. Nsoesie et al. [2013b] present a simulation-optimization approach for forecasting the influenza epidemic curve. The study combines an individual-based model and the Nelder-Mead simplex optimization method. The results suggest that the peak infected and total infected are also accurately forecasted for Montgomery County in Virginia within the forecasting period. Kasaie and Kelton [2013b] propose a simulation-optimization framework to address a general form of the resource allocation problem on epidemic control. They discuss implementation steps with application to the control of the influenza pandemic with several interacting healthcare interventions. Nsoesie et al. [2013a] use a simulation-optimization approach to forecast influenza epidemics. They combine an individual-based model and a simple root-finding optimization method for parameter estimation and forecasting. They use web-based estimates of influenza activity from

Google Flu Trends (GFT) to forecast seasonal influenza epidemics. The results indicate that if the overall trend of the epidemic is accurately captured, GFT could be used for peak forecasts as illustrated, but probably not for forecasting other epidemic measures such as peak height and attack rate. Ghamizi et al. [2020] propose an actual data-driven model to enhance epidemiological predictions, which will learn to fine-tune predictions in different contexts. The model includes deep learning estimation of the epidemiological parameters and a genetic algorithm component searching for optimal trade-offs/policies between constraints and objectives. The results show that the model yields predictions with much lower error rates than pure epidemiological models.

1.2.7 Literature Focusing on COVID-19 Resource Allocation

Many studies focus on the intervention and its impact on controlling the transmission of the COVID-19 [Zhang et al., 2020a, Patel et al., 2020, Saldaña et al., 2020, Ambikapathy and Krishnamurthy, 2020]. Fisman et al. [2020] use a next-generation matrix approach to estimate the conditions under which masks would reduce the reproduction number of COVID-19. Their model takes into account the possibility of assortative mixing, where mask users interact preferentially with other mask users. They observe that the usage of masks could decrease the reproduction number of COVID-19 if widely used, and widespread masking may be sufficient to suppress epidemics when the reproduction number has been brought close to 1 via other measures. Zhang et al. [2020a] extend a previously established agent-based disease transmission model and implement non-medical mask-wearing, shelter-in-place, and case isolation as control measures, and quantify their impact on reducing the attack rate and adverse clinical outcomes. They find that non-medical mask-wearing by 75% of the population reduced infections, hospitalizations, and deaths by 37.7%. In addition, sheltering individuals aged 50 to 64 years of age was the most efficient

strategy. Eikenberry et al. [2020] develop a compartmental model for assessing the community-wide impact of masks used by the general population. They suggest that broad adoption of even relatively ineffective face masks may meaningfully reduce community transmission of COVID-19 and decrease peak hospitalizations and deaths. Masks are found to be useful with respect to both preventing illness in healthy persons and preventing asymptomatic transmission.

Optimization Models. Optimization models have also been widely studied for resource allocation in the fight against COVID-19. Queiroz et al. [2020] provide a systematic review of various supply chain and logistics approaches for optimizing the distribution of critical resources amid the COVID-19. To tackle the shortage of ventilators, Mehrotra et al. [2020] develop a two-stage stochastic programming model, optimizing ventilator allocation during the pandemic under various demand scenarios. The authors find that when 60% of the ventilator inventory is allocated to non-COVID-19 patients, there is no shortfall. In comparison, when 75% of the stock is allocated to the non-COVID-19 patients, a shortfall in the supply of the ventilators to the COVID-19 patients occurs. Also, they find that it is essential to ramp up the production of the ventilators to meet the additional requirements of the ventilators that might come up during the peak times of the pandemic. Lacasa et al. [2020] come up with an algorithm for optimizing the allocation of the ventilators and ICU beds and validate their algorithm during the peak and declining times of the pandemic based on the data from the United Kingdom and Spain cases.

Bertsimas et al. [2020] develop a four-step approach, combining descriptive, predictive, and prescriptive analytics and propose an optimization model for the re-allocation of the ventilators throughout the U.S. during the COVID-19 pandemic. Blanco et al. [2020] present a two-stage stochastic mixed-integer programming model, which minimizes the expected non-covered demand, using robust objective functions of type minmax and maxmin regret. Billingham et al. [2020] present a network

optimization model to tackle the problem of scarce ventilator distribution. Parker et al. [2020] develop mixed-integer programming and robust optimization models to redistribute patients instead of resources, such as ventilators among different hospitals under demand uncertainty. Govindan et al. [2020] develop a practical decision support system hinge on the knowledge of the physicians and the fuzzy interference system (FIS) to help manage the demands of essential hospital services in a healthcare supply chain, to break down the pandemic propagation chain, and reduce the stress among the health care workers.

The literature on the optimal allocation of ventilators is not limited to COVID-19. For example, Zaza et al. [2016] present a conceptual framework that identifies the steps in planning the distribution of stockpiled mechanical ventilators during an emergency. Meltzer et al. [2015] develop a spreadsheet model, which estimates mechanical ventilator demand in the United States during an influenza pandemic. They estimate a need of 35,000-60,500 additional ventilators to avert 178,000-308,000 deaths in a highly severe pandemic scenario. Huang et al. [2017] introduce a two-stage method for optimizing stockpiles of mechanical ventilators, which are critical for treating hospitalized influenza patients in respiratory failure under a pandemic situation. They also incorporate their model into a web-based decision-support tool for pandemic preparedness and response.

Vaccine Models. Many articles focus on the vaccine development and allocation on controlling COVID-19 [Foy et al., 2021, of Sciences Engineering et al., 2020, Ferranna et al., 2021]. The majority of the vaccine models use the simulation method to simulate the vaccination results under different intervention strategies or use the optimization model to generate the optimal vaccine allocation for the simulation. For instance, Shim [2021] uses an age-structured model to understand the epidemiological characteristics of COVID-19. The model determines optimal vaccine allocation for minimizing infections, deaths, and years of life lost while accounting

for population factors, such as country-specific age distribution and contact structure, and various levels of vaccine efficacy. The results suggest that a transmission-blocking vaccine should be prioritized in adults aged between 20 and 49 years old and those older than 50 years to minimize cumulative incidence and mortality. Leithaeuser et al. [2020] use mathematical programming for computing an optimal selection of vaccination sites out of a given set for controlling COVID-19. The model incorporates the assignments of patients and doctors to facilities, the number of vaccines per site, as well as maximum travel time. Their results demonstrate that the number of required physicians can, in most scenarios, be limited to 2,000 in the case of free assignments. However, when travel distances for the patients are to be minimized, an increased number of physicians is unavoidable. Rastegar et al. [2021] present an optimization model for flu vaccine distribution. The model considers the fears of COVID-19 that have intensified the shortage of flu vaccines in developing countries and utilizes an equitable objective function to distribute vaccines to high-risk people. The results demonstrate the applicability of the model proposed in this study for influenza vaccine distribution during the COVID-19 pandemic.

1.2.8 Mean-Risk Stochastic Programming

Stochastic programming has been widely used in many fields, including but not limited to healthcare [Yin and Büyüktahtakın, 2021a], agriculture [Cobuloglu and Büyüktahtakın, 2017], and finance [Birge and Louveaux, 2011]. The expectation is the most widely-used objective criterion in stochastic programming [Ahmed, 2006]. However, it does not capture the variability in the objective function, in particular, the situations with high-impact and low-probability. However, when some extreme cases occur, there could be a big loss when only the expected value over all scenarios is considered. For example, at the beginning of an epidemic outbreak, disease characteristics may not be known, and the disease growth could be highly uncertain,

and thus a large number of infections and losses could happen in shorter time periods than expected. In order to capture the impact of such events, we will consider a risk measure in the objective function in addition to the expectation criterion.

Since conditional value-at-risk (CVaR) is a coherent risk measure that can be used in an optimization model without losing convexity [Rockafellar and Uryasev, 2002], many former studies considered mean-risk models with CVaR in stochastic programming models [Ahmed, 2006, Rockafellar and Uryasev, 2002, Schultz and Tiedemann, 2006, Miller and Ruszczyński, 2011]. CVaR-based mean-risk stochastic programming has been studied in various applications, such as supply chain management [Alem and Morabito, 2013], reverse logistic network design problem [Soleimani and Govindan, 2014], water resources allocation [Zhang et al., 2016], humanitarian relief network [Elçi and Noyan, 2018].

Among the application of mean-CVaR models, Dai et al. [2014] incorporate the CVaR into a two-stage stochastic model to address the problem of long-term planning of municipal solid waste management system in the city of Regina, Canada. While considering the uncertainty of waste-generation rates in the formulation of the model, they consider a decreasing expansion cost along with the time. Their results suggest that the model with the mean-CVaR can better quantify the systems' risk, and it is useful for helping decision maker analyze the trade-offs between cost and risk. Thus, it would help them identify desired waste management strategies under complex uncertainties. Soleimani and Govindan [2014] consider a risk-averse two-stage stochastic programming approach to the design and planning of a reverse supply chain network. They use CVaR as a risk evaluator and consider return amounts and prices of second products as two stochastic parameters. Moreover, they compare the mean-risk model with the risk-neutral model through the mean-risk value of the stochastic solution (VSS). Their results prove that the model behaves more conservatively (lower costs) by increasing the weight of the CVaR (λ) in the objective

function and decreasing the value of α in CVaR. Also, solving the risk-averse model is shown to be efficient in obtaining more reliable solutions.

Furthermore, many papers proposed methodology and decomposition algorithms for mean-CVaR stochastic programming models. For example, Zhang et al. [2016] consider a risk-averse multi-stage stochastic linear programming model with the application to the water allocation problem under uncertainty. They incorporate CVaR into the objective function to control high-risk events, supplementing the mean. To solve the model, they use a nested L-shaped framework to survey different ways of decomposing the resulting problem. Their results indicate that separated the approximations of mean and CVaR related expressions generally work better than combined approximations, and multicut versions work better than single cut versions within the nested L-shaped method for the problem they studied. On the other hand, multicut would lower the optimality gap when a unique VaR representative variable exists. Moreover, both the risk of water shortage and the cost of most expensive scenarios are lower under a higher level of risk aversion because it saves more water and uses less of the water supply source. Elçi and Noyan [2018] develop a two-stage risk-averse model to address the problem of the threat of hurricanes in the Southeastern part of the United States. They enforce a joint probability constraint on the feasibility of the second stage problem, and considered CVaR as the risk measure. In addition, they employ an exact Benders decomposition-based branch-and-cut algorithm for solving the model. Their results show that the algorithm can significantly benefit from parallelization, and it can find better initial first stage decisions. Noyan [2012] specifies the conditional value-at-risk (CVaR) as a risk measure and applied the proposed model to disaster management. The author considers the problem of determining the response facility locations and inventory levels of the relief supplies at each facility in the presence of uncertainty in demand and the damage level of the disaster network. To solve the model, two decomposition

algorithms are constructed based on the generic Benders-decomposition, which are single-cut and multi-cut. Their results suggest that the proposed problem in the paper could be solved for different risk parameters, and this would help the decision makers to evaluate different allocation decisions under uncertainty. Homem-de Mello and Pagnoncelli [2016] discuss the incorporation of risk measures into multi-stage stochastic programs. They introduce the expected conditional risk measures and illustrated the idea of a pension fund problem. Their results show that the expected conditional risk measures (ECMRs) overcome some issues that arise with other alternative risk measures for multi-stage stochastic programs, such as the time consistency.

1.3 Motivation

Former studies above have made outstanding contributions to the epidemic control and logistics planning literature. However, there still exist research gaps in decision-making for resource allocation on epidemic control. To begin with, the majority of the studies use simulations and differential equations to forecast the transmission of the disease, which is hard to incorporate with the optimization model. In addition, researchers study the uncertainty of resource allocation problems using the two-stage models, which are unable to capture the changes in the decision throughout a planning horizon involving multiple time periods. Moreover, none of the literature has considered fair resource allocation when the resource is limited. Last but not least, the current researches on the decisions for epidemic control do not consider the risk of the realization of the extreme scenarios. Once the realization of the transmission is significantly different from the estimated values, there will be a huge loss in the number of infections.

The former epidemic-logistics model presented in Büyüktahtakın et al. [2018a] has incorporated the logistics of treatment into a disease spread model, which foresees

the disease growth over a spatial scale, and allocates limited resources to control the spread of the disease. The mathematical model of Büyüktahtakın et al. [2018a] is deterministic and assumes expected values for disease transmission rates. However, in reality, the disease transmission rate could be quite uncertain, changing over time and space under various scenarios. Thus, a stochastic OR model is necessary to represent the uncertainty in transmission in a more realistic way. In this dissertation, we address these shortcomings and the research gaps in the literature by formulating multi-stage stochastic programming models and simulation-optimization models, which optimizes the resource allocation for the prevention and control of epidemic outbreaks and pandemics, such as the Ebola Virus Disease (EVD) and the Coronavirus Disease 2019 (COVID-19). A summary of the research objectives and accomplishments of this dissertation is discussed in the next section.

1.4 Summary of Research Objectives and Accomplishments

Overall, this dissertation develops multi-stage stochastic models and agent-based models to address the resource allocation issue that lies at the core of epidemic control and logistic planning. The first study presents a multi-stage stochastic model and considers fair resource allocation when the resources are limited, such as in West Africa. The second study extends the model in the first study to a mean-risk multi-stage stochastic model to address the risk-aversive resource allocation problem in the Democratic Republic of the Congo (DRC). The ring vaccination and short-term migration are also considered in this study. The third study involves the uncertainty of the proportion of untested asymptomatic infections in the transmission of COVID-19 and government intervention strategies while providing the optimal ventilator allocation among New York City regions. The fourth study develops a simulation-optimization model to optimize the vaccination center locations and vaccine allocation among the counties in New Jersey. The optimization model imports

the results from the simulation and generates the optimization results that are used to be sent back to the simulation. The results presented in this dissertation also lead to important insights into decision-making and policies in epidemic control.

Each subsection below discusses a summary of research goals and accomplishments under each chapter of this dissertation. The detailed research contributions of this dissertation and related insights into healthcare decision-making are discussed in each chapter, respectively, under a subsection titled "Key Contributions and Insights."

1.4.1 A Multi-Stage Stochastic Programming Approach to Epidemic Control with Equity Considerations

Existing compartmental models in epidemiology are limited in terms of optimizing the resource allocation to control an epidemic outbreak under disease growth uncertainty. In Chapter 2, we address this core limitation by presenting a multi-stage stochastic programming compartmental model, which integrates the uncertain disease progression and resource allocation to control an infectious disease outbreak. The proposed multi-stage stochastic program involves various disease growth scenarios and optimizes the distribution of treatment centers and resources while minimizing the total expected number of new infections and funerals. We define two new equity metrics, namely infection and capacity equity, and explicitly consider equity for allocating treatment funds and facilities over multiple time stages. We also study the multi-stage value of the stochastic solution (VSS), which demonstrates the superiority of the proposed stochastic programming model over its deterministic counterpart. We apply the proposed formulation to control the Ebola Virus Disease (EVD) in Guinea, Sierra Leone, and Liberia of West Africa to determine the optimal and fair resource-allocation strategies. Our model balances the proportion of infections over all regions, even without including the infection equity or prevalence equity

constraints. Model results also show that allocating treatment resources proportional to population is sub-optimal, and enforcing such a resource allocation policy might adversely impact the total number of infections and deaths, and thus resulting in a high cost that we have to pay for the fairness. Our multi-stage stochastic epidemic-logistics model is practical and can be adapted to control other infectious diseases in meta-populations and dynamically evolving situations. The work based on this chapter is published in Yin and Büyüktahtakın [2021a].

1.4.2 Risk-Averse Multi-Stage Stochastic Programming for Vaccine Allocation and Treatment Logistics for Epidemic Response

Existing compartmental-logistics models in epidemics control lack methods in optimizing the allocation of vaccines and treatment resources under a risk-averse objective. In Chapter 3, we present a mean-risk, multi-stage, stochastic epidemics-vaccination-logistics model that evaluates various disease growth scenarios under the Conditional Value-at-Risk (CVaR) risk measure to optimize the distribution of treatment centers, resources, and vaccines, while minimizing the total expected number of infections, deaths, and close contacts of infected people under a limited budget. We integrate a new ring vaccination compartment into a Susceptible-Infected-Treated-Recovered-Funeral-Burial epidemics-logistics model. Our formulation involves uncertainty both in the vaccine supply and the disease transmission rate. Here, we also consider the risk of experiencing scenarios that leads to adverse outcomes in terms of the number of infected and dead people due to the epidemic. Combining the risk-neutral objective with a risk measure allows for a trade-off between the weighted expected impact of the outbreak and the expected risks associated with experiencing extremely disastrous scenarios. We incorporate human mobility into the model and develop a new method to estimate the migration rate between each region when data on migration rates is not available. We apply our multi-stage stochastic mixed-integer programming model to

the case of controlling the 2018-2020 Ebola Virus Disease (EVD) in the Democratic Republic of the Congo (DRC). Our results show that increasing the risk-aversion by emphasizing potentially disastrous outbreak scenarios reduces the expected risk related to adverse scenarios at the price of the increased expected number of infections and deaths over all possible scenarios. We also find that isolating and treating infected individuals are the most efficient ways to slow the transmission of the disease, while vaccination is supplementary to primary interventions on reducing the number of infections. Furthermore, our analysis indicates that vaccine acceptance rates affect the optimal vaccine allocation only at the initial stages of the vaccine rollout under a tight vaccine supply. The work based on this chapter is published in Yin and Büyüktahtakın [2021b].

1.4.3 COVID-19: Optimal Allocation of Ventilator Supply under Uncertainty and Risk

Chapter 4 presents a new risk-averse multi-stage stochastic epidemics-ventilator-logistics compartmental model to address the resource allocation challenges of mitigating COVID-19. This epidemiological logistics model involves the uncertainty of untested asymptomatic infections and incorporates short-term human migration. Disease transmission is also forecast through a new formulation of transmission rates that evolve over space and time with respect to various non-pharmaceutical interventions, such as wearing masks, social distancing, and lockdown. The proposed multi-stage stochastic model overviews different scenarios on the number of asymptomatic individuals while optimizing the distribution of resources, such as ventilators, to minimize the total expected number of newly infected and deceased people. The Conditional Value at Risk (CVaR) is also incorporated into the multi-stage mean-risk model to allow for a trade-off between the weighted expected loss due to the outbreak and the expected risks associated with experiencing disastrous pandemic

scenarios. We apply our multi-stage mean-risk epidemics-ventilator-logistics model to the case of controlling the COVID-19 in highly-impacted counties of New York and New Jersey. We calibrate, validate, and test our model using actual infection, population, and migration data. The results indicate that short-term migration influences the transmission of the disease significantly. The optimal number of ventilators allocated to each region depends on various factors, including the number of initial infections, disease transmission rates, initial ICU capacity, the population of a geographical location, and the availability of ventilator supply. Our data-driven modeling framework can be adapted to study the disease transmission dynamics and logistics of other similar epidemics and pandemics. The work based on this chapter is under review for publication in Yin et al. [2021].

1.4.4 An Agent-Based Simulation-Optimization Vaccine Center Location Vaccine Allocation Approach to Controlling COVID-19

In Chapter 5, we introduce a simulation-optimization approach to address the vaccination facility location and allocation challenges of the COVID-19. We extend an agent-based model of the COVID-19 by adding two new vaccination compartments, "Vaccinated 1" and "Vaccinated 2". The "Vaccinated 1" represents the people who have taken the first shot of the vaccine and the "Vaccinated 2" means the people who have taken the second shot of the vaccine. In addition, we formulate a resource allocation optimization model, which can decide the optimal vaccination center locations for each type of vaccine and generate the optimal vaccine allocation strategies in each region considered. We combine the agent-based simulation model with the vaccination center and vaccine-allocation optimization model into one single simulation-optimization framework. The simulation model forecasts the number of susceptible individuals and infections for the current period, and the results are inputted into the optimization model. The optimization model incorporates the

available budget, the potential vaccination center locations, as well as the available vaccines to generate the vaccination center locations and optimal vaccine allocation decisions for the next period. The generated results will be imported back to the simulation model to estimate the number of infections in the future. We calibrate, validate, and test our model against real outbreak data. The results show that more vaccines with lower costs should be allocated under a limited budget level, and more vaccines with a higher efficiency should be allocated under an ample budget level. In addition, the regions that have a high population or initial infections should receive more vaccines compared with those other with a lower population and initial infections.

1.4.5 Organization of the Dissertation

This Ph.D. dissertation is organized in chapters that correspond to four journal papers. Chapter 2 presents a multi-stage stochastic programming model and considers fair resource allocation for epidemic control when the resources are limited. Chapter 3 extends the model in the first study to a mean-risk multi-stage stochastic programming model to address the risk-aversive resource allocation problem for controlling the Ebola virus disease in the Democratic Republic of the Congo (DRC). Chapter 4 involves the uncertainty of the proportion of untested asymptomatic infections in the transmission of COVID-19 and government intervention strategies while providing the optimal ventilator allocation among New York City regions. Chapter 5 introduces a simulation-optimization approach to addressing the vaccination facility location and allocation challenges of the COVID-19. Finally, in Chapter 6, we summarize our contributions and future research directions inspired by this dissertation.

CHAPTER 2

A MULTI-STAGE STOCHASTIC PROGRAMMING APPROACH TO EPIDEMIC RESOURCE ALLOCATION WITH EQUITY CONSIDERATIONS

2.1 Introduction

An epidemic is the rapid spread of an infectious disease that impacts a large number of people. Epidemic diseases can disperse widely in a short time period, usually, two weeks or less, such as influenza, meningitis, and cholera, impacting populations either in a specific area, or become a pandemic affecting the lives of millions at a global scale, such as the ongoing the coronavirus pandemic. All over the world, outbreaks continue to take lives, ruin the economy, and weaken the health-care system. Unfortunately, the toll is higher in the less-developed countries because millions of people in poor regions of the world do not have the opportunity to receive sufficient treatment in case of an outbreak.

Ebola virus disease (EVD) is a prime example of a devastating epidemic. The EVD, also known as Ebola hemorrhagic fever, is a severe, often fatal illness affecting humans and other primates [WHO, 2019d]. The 2014-2016 outbreak in West Africa was the biggest Ebola outbreak in history, causing more than 28,600 cases and 11,325 deaths by the end of June 2016 [CDC, 2019b]. The virus started in Guinea, and then moved across countries to Sierra Leone and Liberia. The tenth outbreak of the Ebola virus disease has been ongoing in the Democratic Republic of the Congo (DRC) since August 2018. The outbreak has started from the northeast region of the country, centered in the North Kivu and Ituri provinces. More than 3000 cases have been verified by March 2020 [MSF, 2020], and it is the country's largest-ever Ebola outbreak.

There are no specific cure or treatment for Ebola-infected individuals. Multiple investigational Ebola vaccines have been developed and tested in numerous clinical

trials around the world, some of them have been licensed to prevent the Ebola virus disease [NIH, 2019]. Short term intervention strategies, including quarantine, isolation, contact tracing, and safe burial, have been helpful to Ebola control. Moreover, Ebola treatment centers (ETCs), which mainly isolate and treat infected individuals, play a significant role in controlling the Ebola virus disease.

The optimization problem of allocating resources to control an epidemic, such as Ebola, is an immense challenge, especially in the regions where available treatment facilities and funds are scarce. The decision-maker has to make difficult decisions to allocate limited resources to the right locations and in the right amount for slowing down the outbreak and minimize its impacts. Due to the insufficiency of intervention resources, some regions may not receive their fair share of treatment resources, compared to other regions that are also impacted by the disease. Furthermore, the EVD can spread from one individual to another through multiple mechanisms, such as through person-to person-contact or by touching the dead body infected by the EVD. The rates of disease transmission can change under various conditions and thus could be highly unpredictable.

Operations Research (OR) and mathematical modeling methods have been widely used to determine optimal resource allocation strategies to control an epidemic disease. Those approaches include simulations [Siettos et al., 2015, Ajelli et al., 2016, Kurahashi and Terano, 2015, Wells et al., 2015], differential equations [Craft et al., 2005, Kaplan et al., 2003], network models [Berman and Gavious, 2007, Longini Jr et al., 2007, Porco et al., 2004, Riley and Ferguson, 2006], resource allocation analysis [Zaric et al., 2000, Tebbens and Thompson, 2009, Nguyen et al., 2017, Shaw and Schwartz, 2010], and stochastic compartmental models [Lekone and Finkenstädt, 2006, Tanner et al., 2008, Funk et al., 2017, Kibis et al., 2021].

The majority of previous work focuses on analyzing the impact of different intervention strategies on disease transmission. Most of those studies consider disease

growth and resource allocation problems separately in different models or enumerate each resource allocation policy in a simulation model one by one. Moreover, few studies incorporate fairness in resource allocation optimization models. The former epidemic-logistics model presented in Büyüktahtakın et al. [2018a] incorporate the logistics of treatment into a disease spread model, which foresees the disease growth over a spatial scale, and at the same time allocates limited resources to control the spread of the disease. Büyüktahtakın et al. [2018a] consider the varying treatment capacity based on a limited budget. The mathematical model of Büyüktahtakın et al. [2018a] is deterministic and assume expected values for disease transmission rates. However, in reality, the disease transmission rate could be quite uncertain, changing over time and space under various scenarios. Thus, a stochastic OR model is necessary to represent the uncertainty in transmission in a more realistic way. Moreover, the majority of the OR models do not consider equity and fairness in resource allocation, resulting in solutions that may provide few or no resources to some regions impacted by the disease, especially when resources are quite limited.

The objective of this chapter is to develop a multi-stage stochastic programming extension of the deterministic epidemic-logistics model of Büyüktahtakın et al. [2018a] with equity considerations and present realistic insights into controlling the EVD under disease transmission uncertainty. Considering different budget levels and various tightness of the equity constraints, we analyze the optimal resource allocation strategies in a meta-population over three countries in West Africa. In our paper, the stochastic program incorporates various scenarios of disease transmission rates through person-to-person contact, thus capturing the uncertainty and variability in the infection transmission rate better compared to its deterministic counterpart. The objective function of our multi-stage stochastic programming epidemic-logistics model is to minimize the expected number of new infections and deceased individuals overall scenarios, all time periods, and all regions considered. We study the Value of

the Stochastic Solution (VSS), a well-known stochastic programming measure that compares the efficiency of the deterministic and the stochastic models. Furthermore, we introduce two new equity metrics for fair resource allocation in epidemics control and analyze the impact of various budget distribution strategies on the number of infected people and deceased individuals under each of these equity metrics.

2.1.1 Key Contributions and Insights

Former stochastic programming approaches on epidemic control involved a time domain with only two periods. Furthermore, there is a need for analyzing the equity and efficiency tradeoff in a mathematical programming formulation when allotting resources for controlling infectious diseases. Our approach contributes to the epidemiology and OR literature in the following ways.

Modeling Contributions. Firstly, to the best of our knowledge, our study presents the first multi-stage stochastic programming (SP) model for infectious disease control, considering the uncertainty in the disease transmission parameter. Multi-stage SP is superior over two-stage SP models because disease transmission dynamically changes over multiple time stages. Our stochastic programming approach is also preferable to probabilistic sensitivity analysis, which considers a single scenario at a time and also to robust optimization (RO), which could provide highly conservative results by focusing on the worst-set of outcomes in a hostile environment [Defourny et al., 2012]. Due to the temporal and spatial dimensions considered in our resource allocation model, multi-stage SP is also computationally more amenable to dynamic programming, which cannot tackle such a high-dimensional problem.

Second, we present the multi-stage VSS, which shows that the proposed stochastic programming model is superior to its deterministic counterpart.

Third, we introduce and formulate two new equity metrics and incorporate equity measures as a constraint in the mathematical formulation to balance efficiency and equity for fair resource allocation in epidemics control. To our knowledge, this study is the first one that models equity in a multi-stage stochastic programming formulation. Our multi-stage model provides an advantage of adjusting the level of equity over time with respect to evolving disease dynamics, as opposed to using a standard equity measure, which is not updated over time. Furthermore, unlike former work, we address equity in both establishing treatment centers and allocating treatment resources over metapopulations and multiple periods using mathematical optimization.

The infection equity constraint is also easier to implement than using standard equity metrics, such as the absolute difference between regional prevalence (cases per population in a region) and the overall prevalence (cases per population over all regions), because the absolute gap value using the prevalence metric could be tiny and difficult to adjust compared with the absolute gap value defined by the infection equity constraint. Furthermore, computational results imply that our model balances the proportion of infections in each region, even without including the infection equity or prevalence equity constraint.

Fourth, while we tailor our epidemics-logistics stochastic programming modeling framework for the EVD, it can be adapted to study different diseases to determine the optimal and fair resource-allocation strategies among various regions and multiple planning periods to curb the spread of an epidemic.

Applied Contributions and Policy Insights: Our mathematical model could be used as a decision support tool to aid policymakers in understanding disease dynamics and making the most effective decisions to fight epidemics under uncertainty. In particular, our model could be used by the stakeholders in epidemic control (e.g., governments, UN entities, non-profit organizations) to determine the optimal location

and timing of ETCs opened and treatment resources allocated to minimize the total expected infections and deaths over metapopulations in multiple locations and over multiple time periods.

Our model provides significant insights into the control of the Ebola Virus Disease in West Africa that would not be possible with existing models and methods in infectious disease control. Our multi-stage stochastic program foresees various disease growth scenarios to optimize resource allocation, as opposed to solving the problem for an average scenario and myopically for one stage at a time with fixed periodic budgets, which could provide sub-optimal solutions and thus less effective resource allocation. Specifically, our study provides the following several policy insights and recommendations to decision-makers:

(**i**) Our analysis emphasizes that quick response, such as allocating treatment centers and resources in the early stages of the epidemic, is critical for minimizing the total number of infected individuals and deaths related to the disease.

(**ii**) The value of the stochastic solution demonstrates that the optimal timing and location of resource allocation vary with respect to the disease transmission scenario, and thus possible disease growth scenarios should be considered when planning for an epidemic instead of considering a single scenario of the expected value.

(**iii**) Our results show that the infection level ("the number of infected people in a region" / "the total number of infected people" - "population in a region" / "total population") is a key factor for resource allocation.

(**iv**) Our analysis suggests that the region with the highest infection level has the priority to receive the majority of the resources at the beginning of the time horizon to minimize the number of infections and funerals.

(**v**) Model results also show that allocating treatment resources proportional to population is sub-optimal.

(**vi**) While equitable resource allocation is important in decision-making, too much focus on the equity of resource allocation might adversely impact the total number of infections and deaths and thus resulting in a high cost that we have to pay for fairness. Therefore, decision makers are advised to be cautious about enforcing fairness when allocating resources to multiple regions.

2.2 Problem Formulation

This section gives the formulation of a multi-stage stochastic programming model, including the compartmental model, description of the scenario tree, formulation, equity constraints, and their explanation.

2.2.1 Notation

Model notations that are used throughout the rest of Chapter 2 are presented in Tables 2.1–2.5 below.

Table 2.1 Sets and Indices

Notation	Description
J	Set of time periods, $J = \{0, ..., \overline{J}\}$.
A	Set of ETC types, $A = \{1, ..., \overline{A}\}$.
R	Set of regions, $R = \{1, ..., \overline{R}\}$.
M_r	Set of all surrounding regions of region r.
Ω	Set of scenarios, $\Omega = \{1, ..., \overline{\Omega}\}$.
j	Index for time period where $j \in J$.
r	Index for region where $r \in R$.
a	Index defining type of ETC, where $a \in A$.
ω	Index for scenario where $\omega \in \Omega$.

Table 2.2 Transition Parameters Describing the Rate of Movement between Disease Compartments

Notation	Description
$\lambda_{1,r}$	Disease fatality rate without treatment in region r.
$\lambda_{2,r}$	Disease fatality rate while receiving treatment in region r.
$\lambda_{3,r}$	Disease survival rate without treatment in region r.
$\lambda_{4,r}$	Disease survival rate with treatment in region r.
$\lambda_{5,r}$	Safe burial rate of Ebola-related dead bodies in region r.
$\chi_{1,r}^{\omega}$	Transmission rate per person due to community interaction in region r under scenario ω.
$\chi_{2,r}$	Transition rate per person during traditional funeral ceremony in region r.

Table 2.3 Other Parameters

Notation	Description
$b_{1j,r}$	Unit cost of treatment for an infected individual in region r at end of period j.
$b_{2j,r}$	Unit cost of safe burial for a dead body in region r at end of period j.
$g_{aj,r}$	Fixed cost of establishing type a ETC in region r at end of period j.
k_a	Capacity (number of beds) of type a ETC.
u_r	The population in region r.
Δ	Total available budget for treatment.
π_r	Initial number of susceptible individuals in region r.
ϖ_r	Initial number of infected individuals in region r.
θ_r	Initial number of treated individuals in region r.
ϑ_r	Initial number of recovered individuals in region r.
υ_r	Initial number of unburied dead bodies (funerals) in region r.
τ_r	Initial number of buried dead bodies (safe burials) in region r.
ς_r	Initial treatment capacity in terms of number of ETC beds in region r.
$\alpha_{l\to r}$	Migration rate of susceptible individuals from surrounding regions $l \in M_r$ to region r.
$\phi_{l\to r}$	Migration rate of infected individuals from surrounding regions $l \in M_r$ to region r.
$\nu_{r\to l}$	Migration rate of susceptible individuals from region r to surrounding regions $l \in M_r$.
$\rho_{r\to l}$	Migration rate of infected individuals from region r to surrounding regions $l \in M_r$.

Table 2.4 State Variables

Notation	Description
$S^{\omega}_{j,r}$	Number of susceptible individuals in region r at end of period j under scenario ω.
$I^{\omega}_{j,r}$	Number of infected individuals in region r at end of period j under scenario ω.
$T^{\omega}_{j,r}$	Number of individuals receiving treatment in region r at end of period j under scenario ω.
$R^{\omega}_{j,r}$	Number of recovered individuals in region r at end of period j under scenario ω.
$F^{\omega}_{j,r}$	Number of deceased individuals due to the epidemic in region r at end of period j under scenario ω.
$B^{\omega}_{j,r}$	Number of buried individuals in region r at end of period j under scenario ω.
$\hat{S}^{\omega}_{j,r}$	Number of susceptible individuals migrating into region r at end of period j under scenario ω.
$\widetilde{S}^{\omega}_{j,r}$	Number of susceptible individuals emigrating from region r at end of period j under scenario ω.
$\hat{I}^{\omega}_{j,r}$	Number of infected individuals migrating into region r at end of period j under scenario ω.
$\widetilde{I}^{\omega}_{j,r}$	Number of infected individuals emigrating from region r at end of period j under scenario ω.

Table 2.5 Decision Variables

Notation	Description
$C^{\omega}_{j,r}$	Total capacity (number of beds) of established ETCs in region r at end of period j under scenario ω.
$\overline{I}^{\omega}_{j,r}$	Number of infected individuals hospitalized (and quarantined) in region r at end of period j under scenario ω.
$y^{\omega}_{aj,r}$	Number of type a ETCs established in region r at end of period j under scenario ω.

2.2.2 Compartmental Disease Model Description

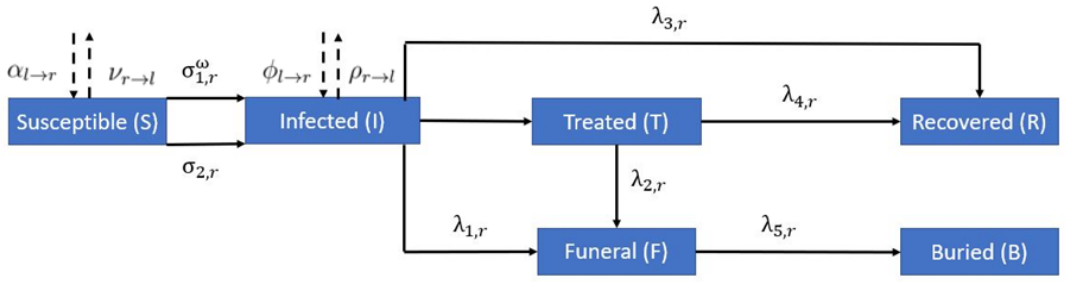

Figure 2.1 One-step disease compartmental model.

Figure 2.1 shows the transmission dynamics of the Ebola Virus Disease (EVD) in a region r of a country located in West Africa. The disease spreads among the susceptible population (S), by either person-to-person contact at a periodic rate of $\chi^{\omega}_{1,r}$ under scenario ω or through touching Ebola-related dead bodies that are not yet buried during traditional funerals at a periodic rate of $\chi_{2,r}$. Thus, susceptible individuals (S) are infected and become infected (I) with a rate of $\chi^{\omega}_{1,r}$ as a function of I and with a rate of $\chi_{2,r}$ as a function of funerals (F), who represent deceased but unburied people. Without treatment, some of the infected individuals in the compartment (I) will die and move to the funeral (F) compartment with the rate of

$\lambda_{1,r}$, while some of the infected individuals will recover with a rate of $\lambda_{3,r}$, moving into the recovered compartment (R). However, the number of individuals that will be hospitalized for treatment (T) is based on the treatment capacity variable $C^{\omega}_{j,r}$, which gives the total available number of beds in the ETCs in region r under scenario ω in period j. Thus, there is no constant transition rate from I to T. Meanwhile, individuals who did not receive treatment will remain in the community and continue to spread the disease. In treated compartment (T), some of the individuals will recover with a periodic rate of $\lambda_{4,r}$, and a fraction of them will die with a periodic rate of $\lambda_{2,r}$. The deceased individuals in the funeral compartment are safely buried at a rate of $\lambda_{5,r}$, moving into the buried compartment (B). Thus, we assume that every death (F) leads to a safe burial (B). In order to describe the migration of susceptible and infected individuals within a given country, we define $(\alpha_{l\to r}, \upsilon_{r\to l})$ as the rates of migration of susceptible individuals into and out of region r, respectively, and $(\psi_{l\to r}, \rho_{r\to l})$ as the rates of migration of infected individuals into and out of region r, respectively. The multi-stage stochastic programming epidemic-logistics model is defined in detail in the next section.

The latent period for the EVD is highly variable, changing from 2 to 21 days [WHO, 2020c]. In our model, we assume that each time stage represents two weeks, in which an infected but asymptomatic individual can become symptomatic and infect others. For this reason, and to avoid computational complexity, we do not include an explicit latent compartment in the model; instead, we fit those individuals within the infected compartment. Similarly, the Ebola modeling literature focusing on logistics usually omit the latent period to avoid further computational complexity (see, e.g., Büyüktahtakın et al. [2018a], Long et al. [2018]).

2.2.3 Uncertainty Representation and Scenario Tree Generation Scheme

It is beyond the scope of this work to introduce a new methodology for multi-period scenario tree generation; we refer the reader to Heitsch and Römisch [2009], Leövey and Römisch [2015], and Pflug and Pichler [2015] for different approaches to generate scenario trees. To generate the scenario tree for our case, we follow a similar approach presented in the study of Alonso-Ayuso et al. [2018]. Here, we focus on the most uncertain parameter: the community transmission rate based on former research stating that transmission rates impact the infections and deaths the most among all different input parameters based on sensitivity analysis [Büyüktahtakın et al., 2018a].

We model the future uncertainties regarding the progression of the disease by a discrete set of scenarios, denoted $\omega \in \Omega$. Each scenario has a probability, p^{ω}, where $\sum_{\omega \in \Omega} p^{\omega} = 1$. We assume that the uncertain community transmission rate follows a normal distribution. The data regarding the distribution of the community transmission rate parameter is not available. Thus, we use the lower and upper bounds on the transmission rate in the community based on the data gathered from literature (Table 2.6) to generate the normal distribution function for the transmission rate parameter at time zero. The upper and lower bounds, thus the distribution functions for the uncertain parameter, are specified for each country and are different at each node of the scenario tree. Accordingly, the mean μ_r^n is defined for each region $r \in R$ and node $n \in N$. The lower bound and upper bound are considered as the value of 0.001- and 0.999-quantiles of the normal distribution, respectively. The standard deviation σ_r is defined according to a normal distribution using the initial lower and upper bounds provided for each region $r \in R$. Also, we use Q_h to represent the value of the h-quantile of the normal distribution.

Table 2.6 The Range (Lower and Upper Bounds), Mean, and Standard Deviation of Community Transmission Rate in Each Country

Region	Rate Range	Mean	Standard Deviation
Guinea	[0.24, 0.84]	0.54	0.10
Sierra Leone	[0.24, 0.88]	0.66	0.07
Liberia	[0.24, 0.64]	0.44	0.07

Source: [Althaus, 2014, Towers et al., 2014]

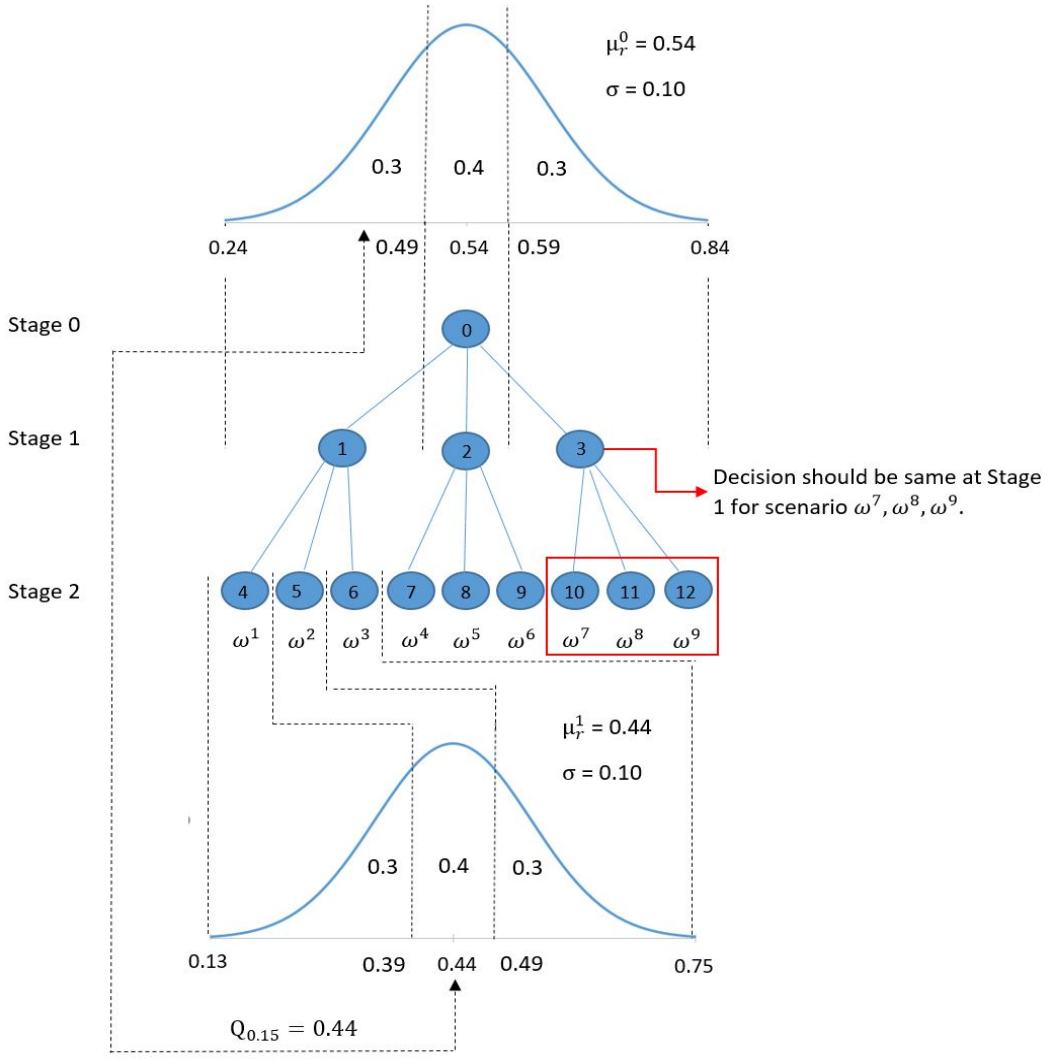

Figure 2.2 Scenario tree generation example for Guinea, where each circle, denoted by n, $n := \{0, \ldots, 12\}$, represents a node of the scenario tree.

As shown in an example scenario tree in Figure 2.2, a particular scenario could give the community transmission rates ($\chi^{\omega}_{1,r}$) into the future for the next two stages in all considered regions. In our model, we consider three realizations for each node of the scenario tree, namely as low, medium, and high. The low and high realizations have a probability of 0.3, and the medium realization has a probability of 0.4. Each path from the root node to the leaf node of the scenario tree represents a scenario ω. In the example shown in Figure 2.2, we have two stages, and thus $3^2 = 9$ scenarios. In addition, two scenarios are inseparable at stage j if they share the same scenario path up to that stage. This implication is modeled using non-anticipativity constraints, as described in Appendix A.1. For example, for scenarios ω^1 to ω^9, the decision at node 0 should be the same as we do not know the values of the uncertain parameters at stage 0. Similarly, for scenarios ω^1 to ω^3, the decision at node 1 should be the same because these scenarios cannot be differentiated at stage 1 due to uncertainty.

The probability of a scenario ω, p^{ω}, is calculated as the multiplication of probabilities on the scenario path. For example, the probability of scenario ω^1, which corresponds to a low realization in the first and second stages, is 0.09, while the probability of scenario ω^9, which corresponds to a medium realization in the first stage and a high realization in the second stage, is 0.12.

For each node $n \in N$ in the scenario tree, the low realization value of the random variable ξ^n_r is given by the value of the 0.15-quantile ($\mu^n_{r,low} = E(\xi^n_r | Q_{0.001} \leq \xi^n_r \leq Q_{0.30}) = Q_{0.15}$), the medium realization is given by the value of the 0.50-quantile ($\mu^n_{r,medium} = E(\xi^n_r | Q_{0.30} \leq \xi^n_r \leq Q_{0.70}) = Q_{0.50}$), and the high realization is equal to the value of the 0.85-quantile of the normal distribution ($\mu^n_{r,high} = E(\xi^n_r | Q_{0.70} \leq \xi^n_r \leq Q_{0.999}) = Q_{0.85}$). In our example, at node 0 the normal distribution of the uncertain community transmission rate parameter in Guinea has $\mu^0_r = 0.54$ and $\sigma^0_r = 0.10$. The low, medium, and high realizations of the uncertain parameter at nodes 0 and 1 are given in Table 2.7 below.

Table 2.7 The 0.15-, 0.50-, 0.85-Quantiles of the Normal Distribution of the Random Variable ξ_r^n at Nodes 0 and 1 of the Scenario Tree in Figure 2.2

	Low	Medium	High
node 0:	$Q_{0.15}$=0.44	$Q_{0.50}$=0.54	$Q_{0.85}$=0.64
node 1:	$Q_{0.15}$=0.26	$Q_{0.50}$=0.44	$Q_{0.85}$=0.62

The normal distribution of community transmission rate associated with nodes 1, 2, and 3 at stage 1 have a mean of $Q_{0.15} = 0.44$, $Q_{0.50} = 0.54$, and $Q_{0.85} = 0.64$, respectively. While scenarios ω^1, ω^2, and ω^3 at stage 1 has a single realization value of 0.54 for the random parameter at node 1, the realizations of scenarios ω^1, ω^2, and ω^3 at stage 2 correspond to nodes 4, 5, and 6, with a mean of $Q_{0.15} = 0.26$, $Q_{0.50} = 0.44$, and $Q_{0.85} = 0.62$, respectively.

2.2.4 Model Features and Assumptions

In this study, we have considered six regions, each consisting of multiple districts, in the three countries most affected by the 2014-16 EVD. West Africa is poor and the budget for the Ebola treatment comes from an international consortium of partners, including governments, international financial Institutions, regional organizations, and private foundations [United Nations, 2020]. Those funding is either directly provided to the affected governments or the United Nations (UN) entities. In this chapter, we took the perspective of the UN entities, such as the World Health Organization (WHO), where the total funding is collected centrally and allocated among those three countries to optimize the use of treatment resources and the donated funding.

The actual capacity of ETCs varies from 20 to 200 operational beds [WHO, 2020d]; however, we used 50 and 100-bed ETCs in our model to reduce the computational complexity. It is essential to differentiate the small and large ETCs

in the model because each ETC type has a different setup cost, which impacts the optimal allocation of resources. We assume that each Ebola patient will receive the same treatment in either a large or small capacity ETC. The treatment capacity parameter is cumulative and only reflects total ETC beds.

Furthermore, the cost of burying dead bodies safely is shown to be minor compared to the ETC and treatment cost [WHO, 2020b, Büyüktahtakın et al., 2018a]. In addition, changing the burial rate into a variable that is optimized in the model would have complicated the model considerably, and so we only focus on adjusting the variable values of treatment resources. Thus, we assume that the burial rate is constant, and burials and treatment are operated separately using different budgets.

2.2.5 Model Formulation

Following the convention of Büyüktahtakın et al. [2018a], the multi-stage stochastic programming epidemic-logistics model (2.1) can be formulated as follows:

$$\min \quad \sum_{j\in J-1}\sum_{r\in R}\sum_{\omega\in\Omega} p^{\omega}((I^{\omega}_{j+1,r}-I^{\omega}_{j,r})+F^{\omega}_{j+1,r}) \tag{2.1a}$$

$$\text{s.t.} \quad S^{\omega}_{0,r}=\pi_r, \quad I^{\omega}_{0,r}=\varpi_r, \quad T^{\omega}_{0,r}=\theta_r, \quad R^{\omega}_{0,r}=\vartheta_r,$$

$$F^{\omega}_{0,r}=\upsilon_r, \quad B^{\omega}_{0,r}=\tau_r, \quad C^{\omega}_{0,r}=\zeta_r, \quad r\in R, \forall\omega\in\Omega \tag{2.1b}$$

$$S^{\omega}_{(j+1),r}=S^{\omega}_{j,r}+\hat{S}^{\omega}_{j,r}-\widetilde{S}^{\omega}_{j,r}-\chi^{\omega}_{1,r}I^{\omega}_{j,r}-\chi_{2,r}F^{\omega}_{j,r},$$

$$j\in J\setminus\{\overline{J}\}, r\in R, \forall\omega\in\Omega, \tag{2.1c}$$

$$I^{\omega}_{(j+1),r}=I^{\omega}_{j,r}+\hat{I}^{\omega}_{j,r}-\widetilde{I}^{\omega}_{j,r}+\chi^{\omega}_{1,r}I^{\omega}_{j,r}+\chi_{2,r}F^{\omega}_{j,r}-(\lambda_{1,r}+\lambda_{3,r})I^{\omega}_{j,r}-\overline{I}^{\omega}_{j,r},$$

$$j\in J\setminus\{\overline{J}\}, r\in R, \forall\omega\in\Omega, \tag{2.1d}$$

$$T^{\omega}_{(j+1),r}=T^{\omega}_{j,r}+\overline{I}^{\omega}_{j,r}-(\lambda_{2,r}+\lambda_{4,r})T^{\omega}_{j,r},$$

$$j\in J\setminus\{\overline{J}\}, r\in R, \forall\omega\in\Omega, \tag{2.1e}$$

$$R^{\omega}_{(j+1),r}=R^{\omega}_{j,r}+\lambda_{4,r}T^{\omega}_{j,r}+\lambda_{3,r}I^{\omega}_{j,r},$$

$$j\in J\setminus\{\overline{J}\}, r\in R, \forall\omega\in\Omega, \tag{2.1f}$$

$$F^{\omega}_{(j+1),r}=F^{\omega}_{j,r}+\lambda_{1,r}I^{\omega}_{j,r}+\lambda_{2,r}T^{\omega}_{j,r}-\lambda_{5,r}F^{\omega}_{j,r},$$

$$j \in J \setminus \{\overline{J}\}, r \in R, \forall \omega \in \Omega, \tag{2.1g}$$

$$B^{\omega}_{(j+1),r} = B^{\omega}_{j,r} + \lambda_{5,r} F^{\omega}_{j,r}, \qquad j \in J \setminus \{\overline{J}\}, r \in R, \forall \omega \in \Omega, \tag{2.1h}$$

$$\hat{S}^{\omega}_{j,r} = \sum_{l \in M_r} \alpha_{l \to r} S^{\omega}_{j,l}, \qquad j \in J, r \in R, \forall \omega \in \Omega, \tag{2.1i}$$

$$\hat{I}^{\omega}_{j,r} = \sum_{l \in M_r} \phi_{l \to r} I^{\omega}_{j,l}, \qquad j \in J, r \in R, \forall \omega \in \Omega, \tag{2.1j}$$

$$\widetilde{S}^{\omega}_{j,r} = \sum_{l \in M_r} \nu_{r \to l} S^{\omega}_{j,r}, \qquad j \in J, r \in R, \forall \omega \in \Omega, \tag{2.1k}$$

$$\widetilde{I}^{\omega}_{j,r} = \sum_{l \in M_r} \rho_{r \to l} I^{\omega}_{j,r}, \qquad j \in J, r \in R, \forall \omega \in \Omega, \tag{2.1l}$$

$$\sum_{r \in R} \Big(\sum_{j \in J \setminus \{0,j\}} \sum_{a \in A} g_{aj,r} y^{\omega}_{aj,r} + \sum_{j \in J} b_{1j,r} T^{\omega}_{j,r} \Big) \leq \Delta \quad \forall \omega \in \Omega, \tag{2.1m}$$

$$C^{\omega}_{j,r} = \sum_{m=1}^{j} \sum_{a \in A} k_a y^{\omega}_{amj,r} + C_{0,r}, \qquad j \in J \setminus \overline{J}, r \in R, \forall \omega \in \Omega, \tag{2.1n}$$

$$\overline{I}^{\omega}_{j,r} = min\{I^{\omega}_{j,r}, C^{\omega}_{j,r} - T^{\omega}_{j,r}\}, \qquad j \in J \setminus \overline{J}, r \in R, \forall \omega \in \Omega, \tag{2.1o}$$

$$S^{\omega}_{j,r} \quad I^{\omega}_{j,r} \quad T^{\omega}_{j,r} \quad R^{\omega}_{j,r} \quad F^{\omega}_{j,r} \quad B^{\omega}_{j,r} \quad \overline{I}^{\omega}_{j,r} \geq 0,$$

$$j \in J, r \in R, \forall \omega \in \Omega, \tag{2.1p}$$

$$y^{\omega}_{aj,r} \in \{0, 1, 2, \ldots\}; \quad y^{\omega}_{aj,r} \leq I^{\omega}_{j,r},$$

$$a \in A, j \in J \setminus \{\overline{J}\}, r \in R, \forall \omega \in \Omega, \tag{2.1q}$$

$$y^{\omega}_{at(n),r} - y_{an,r} = 0, \quad \overline{I}^{\omega}_{t(n),r} - \overline{I}_{n,r} = 0, \quad C^{\omega}_{t(n),r} - C_{n,r} = 0,$$

$$a \in A, \forall \omega \in \beta(n), \forall n \in N, \tag{2.1r}$$

The objective function (2.1a) minimizes the total expected number of newly infected individuals plus funerals over all scenarios, in all regions throughout the planning horizon. Constraints (2.1b) represent the number of individuals in susceptible, infected, treated, recovered, funeral, and buried compartments and the total ETC capacity, respectively, in each region r at the beginning of the planning horizon. Equations (2.1c)–(2.1h) represent the dynamics of the population in each disease compartment, as shown in Figure 2.1. Specifically, constraint (2.1c) implies that the number of susceptible individuals in region r at the end of period $j+1$ under

scenario ω is equal to the number of susceptible individuals from the previous year plus the number of susceptible individuals who immigrate into region r minus the number of susceptible individuals who emigrate from region r and minus the number of newly infected individuals at the end of period j under scenario ω. Constraint (2.1d) gives the number of infected individuals at the end of period $j+1$ in region r under scenario ω, which is equal to the number of infected individuals from the previous year plus immigrated infected individuals minus emigrated infected individuals, plus newly infected individuals and minus individuals who recovered, died, or were accepted for treatment at the end of period j under scenario ω. Constraint (2.1e) describes the total number of treated individuals in region r at the end of time period $j+1$ under scenario ω, which is equal to the number of treated individuals at the end of period j plus infected individuals who accepted treatment based on the availability of beds minus treated individuals who died or recovered. Constraint (2.1f) ensures that the cumulative number of recovered individuals in region r at the end of the period $j+1$ under scenario ω is equal to the number of recovered individuals from the previous year plus newly recovered individuals. Constraint (2.1g) defines the total number of unburied funerals in region r at the end of time period $j+1$ under scenario ω, which is equal to the infected and treated individuals who moved to the funeral compartment minus the buried dead bodies. Constraint (2.1h) gives the cumulative number of buried dead bodies at the end of the period j under scenario ω. Constraints (2.1i)–(2.1l) present the number of immigrated and emigrated individuals in susceptible and infected compartments. Specifically, constraints (2.1i) and (2.1j) give the number of susceptible and infected individuals who immigrated into region r from region $l \in M_r$ under scenario ω. Constraints (2.1k) and (2.1l) represent the number of susceptible and infected individuals, who emigrated from region r into neighboring region $l \in M_r$ under scenario ω. Constraints (2.1m)–(2.1o) represent the restrictions regarding logistics and operation management. Specifically, constraint

(2.1m) denotes the budget limitation on the sum of the fixed costs of opening ETCs and the variable cost of treating infected individuals over all regions r in all periods j under scenario ω. Constraint (2.1n) shows the total capacity in region r at the end of period j under scenario ω. Constraint (2.1o) ensures that the number of hospitalized individuals is limited by the number of available beds in ETCs in region r. In particular, the number of hospitalized individuals ($\overline{I}$) is equal to the minimum of the number of infected individuals and the capacity available at established ETCs after considering currently hospitalized individuals in ETCs. Constraints (2.1p) present non-negativity restrictions on the number of susceptible, infected, treated, funeral, buried, and recovered individuals, respectively, under scenario ω. Constraints (2.1q) denote the integer requirements on the number of type-n ETCs to be opened in region r at the end of period j under scenario ω. In addition, if the number of infected individuals is less than 1 in a region r, the value of the integer variable corresponding to opening an n-bed ETC is forced to be zero, and thus no ETC will be opened in that region. Constraints (2.1r) represent nonanticipativity restrictions, which state that if two scenarios share the same path up to stage j, the corresponding decisions should be the same, as described in Appendix A.1.

2.2.6 Equity of ETC and Treatment Resources Distribution

Equitable resource allocation has long been studied in health-care resource allocation decision-making [Lane et al., 2017]. Some examples include equity in facility location [Marsh and Schilling, 1994, Ares et al., 2016], organ allocation for kidney transplantation [Su and Zenios, 2006, Bertsimas et al., 2013], vaccine coverage [Enayati and Özaltın, 2020], and health-care fleet management [McCoy and Lee, 2014].

In the health-care sector, an equity metric compares two or more populations based on the service or utility the health system provides to the different populations.

The comparison of various populations could be based on the health status, distribution of resources, expenditures, utilization, and access [Goddard and Smith, 2001, Culyer and Wagstaff, 1993].

While it is essential to clearly define equity to be used for fair resource allocation, there is no universal consensus on the definition and measurement of equity in public health decision making [Stone, 2002]. Lane et al. [2017] find a large disparity in the description of equity in health care resource allocation based on their review of the related literature.

Among numerous definitions of equity, Young [1995] defines three equity concepts on resource allocation: parity (claimants should be treated equally), proportionality (goods should be divided in proportion to differences among claimants), and priority (the person with the greatest claim to the good should get it). Savas [1978] describes equity as fairness, impartiality, or equality of service. Culyer [2001] discusses utilitarian principles dictating that resources should be allocated in such a way as to maximize the overall health and wellbeing of a society, and egalitarian principles dictating that all people are equal and that inequalities between groups should be removed. McCoy and Lee [2014] use utilitarian, proportionally fair, and egalitarian principals to incorporate equity into optimal resource allocations.

Marsh and Schilling [1994] present a list of 20 equity measures within the context of facility location. Among the most commonly-used equity measures are the sum of absolute deviations (SAD), the mean absolute deviation (MAD), the minimum effect (ME), and the Gini coefficient (GC). Love-Koh et al. [2020] categorize methods used to define equity measures into five: 1) gap measures, regression-based measures, Lorenz and concentration curves, measures incorporating inequality aversion, and health-related social welfare. The equity measures defined by absolute and relative gaps are commonly used by international agencies, such as the WHO, to distribute

resources, such as vaccines and medical treatment, between population groups in low- and middle-income countries [Casey et al., 2017].

Equitable resource allocation has also been studied considering the tradeoff between the efficiency and equity in resource allocation for infectious diseases, such as HIV and influenza (e.g., Mbah and Gilligan [2011], Zaric and Brandeau [2007], Kaplan and Merson [2002], Enayati and Özaltın [2020]). For example, Earnshaw et al. [2007] develop a linear programming planning tool to help policymakers understand the effectiveness of different allocations of HIV prevention funds under fairness constraints. Enayati and Özaltın [2020] propose an equity constraint in a mathematical program to help public health authorities consider fairness when making vaccine distribution decisions. In a food allocation problem, Orgut et al. [2016] present a deterministic linear programming model to optimize the allocation of donated food, considering objectives of both equity and effectiveness.

Similar to these works, we will follow an approach that would balance the efficiency and equity in epidemics resource allocation. Specifically, we will focus on equity over meta-populations and multiple spatial dimensions. We define our equity measures within the context of proportionality and priority, as described in Young [1995]. Our formulations of equity are gap-based, combining absolute and relative gaps. Our approach is seeking a balance between utilitarian and egalitarian objectives studied in Culyer and Wagstaff [1993] and McCoy and Lee [2014] by determining a resource allocation strategy that will minimize total infections and deaths but at the same time incorporates equality dimensions as a constraint. Unlike former work, we address equity in the resource allocation for both treatment centers and treatment resources using mathematical optimization.

Our definition of equity is similar to the descriptions of Mbah and Gilligan [2011], who defines social equity as the equal opportunity for infected individuals to access treatment, Marsh and Schilling [1994], who define equity within the context of

facility location, and Orgut et al. [2016] who study equity in the fair allocation of food. Specifically, we define equity as the case where each region and country receives its fair share of the ETCs and medical treatment resources during an epidemic outbreak.

The majority of studies on fair resource allocation define the equity as a one-period metric, which does not change over time. In our multi-stage stochastic programming model, the equity standard is adjusted over time with respect to the changing disease dynamics throughout the planning horizon, increasing the efficiency of the resource allocation. To the best of our knowledge, our study is the first to model the fair resource allocation using a multi-stage stochastic programming model.

Infection Equity Constraint In the first formulation, we will address the objective of equity by limiting the absolute deviation between a regions relative number of infections and its relative population with respect to all regions, while effectiveness corresponds to minimizing the expected number of infections and deaths. In this equity measure, namely infection equity constraint, we consider priority concerning the proportions of infections and enforce resource allocation to limit the proportion of infections with respect to the population for each region. The infection equity constraint is given as follows:

$$\left|\frac{\sum_{j\in J}\sum_{\omega\in W} p^{\omega} I^{\omega}_{j,r}}{\sum_{j\in J}\sum_{r\in R}\sum_{\omega\in W} p^{\omega} I^{\omega}_{j,r}} - \frac{u_r}{\sum_{r\in R} u_r}\right| \leq k \tag{2.2}$$

The infection equity constraint (2.2) gives a bound on the total number of infections in each region relative to the total infections in all regions. Specifically, constraint (2.2) implies that the absolute value of the number of infected individuals in region r divided by the total number of infected individuals over all regions minus the ratio of the population of region r, u_r, over the total population over all regions should be

less than or equal to a specific value k.

Because the EVD case fatality rate is high [50% on average [WHO, 2020c]] and the EVD is highly contagious, having the lowest infections system-wide will lead to the lowest mortality for the EVD. Thus, we consider the number of infections instead of deaths as the main parameter for resource allocation in our equity metric. The number of infections in constraint (2) could also be adjusted to the number of fatalities.

Capacity Equity Constraint In the second formulation, we will formulate equity by limiting the absolute deviation between the proportion of treatment capacity established in a region and proportion of the population in a region relative to all regions while again, effectiveness corresponds to minimizing expected deaths and infections. The capacity equity constraint enforces allocating resources considering the proportionality based on the relative population and is formulated as follows:

$$\left|\frac{\sum_{j\in J}\sum_{\omega\in W} p^{\omega} C^{\omega}_{j,r}}{\sum_{j\in J}\sum_{r\in R}\sum_{\omega\in W} p^{\omega} C^{\omega}_{j,r}} - \frac{u_r}{\sum_{r\in R} u_r}\right| \leq k, \tag{2.3}$$

Similarly, we define the capacity equity constraint (2.3) to bound the absolute value of the difference between the proportion of the capacity at region r over the total capacity with the proportion of the population at region r over the total population with a predefined parameter k.

Prevalence Equity Constraint We also study a widely-used equity metric, known as prevalence [Lasry et al., 2008, Kedziora et al., 2019]. Here, we define the prevalence equity constraint to limit the absolute difference between the regional prevalence

(cases per population in a region) and the country prevalence (cases per population over all regions) by the parameter k, and formulate it as follows:

$$\left|\frac{\sum_{j\in J}\sum_{\omega\in W} p^{\omega} I^{\omega}_{j,r}}{u_r} - \frac{\sum_{j\in J}\sum_{r\in R}\sum_{\omega\in W} p^{\omega} I^{\omega}_{j,r}}{\sum_{r\in R} u_r}\right| \leq k \tag{2.4}$$

The prevalence equity constraint (2.4) bounds the proportion of infections in each region relative to the proportion of infections in all regions.

2.2.7 Mixed-Integer Linear Program (MIP) Model

In the mathematical formulation (2.1), we have two types of non-linearity. The first non-linear equation corresponds to the capacity-availability constraint (2.1o), and the second corresponds to the equity constraints (2.2) and (2.3) (see Appendix A.2 for linearization of (2.1o), (2.2), and (2.3)). The non-linear multi-stage stochastic programming epidemiclogistics model (2.1) is converted into an equivalent MIP formulation by replacing the non-linear capacity availability constraint (2.1o) with constraints (A.3), (A.4a)-(A.4d) and (A.5a)-(A.5d), the non-linear infection equity constraint (2.2) with constraints (A.7a) and (A.7b), and the non-linear capacity equity constraint (2.3) with constraints (A.8a) and (A.8b), as given in Appendix A.2.

We apply the MIP model to a case study involving the control of the 20142015 Ebola outbreak in the three most-affected West African countries, Guinea, Sierra Leone, and Liberia. The details of the 20142015 Ebola outbreak data used as an input into the mathematical model, including population and migration data, resource cost data, and epidemiological data are presented in Appendix A.3.

The MIP model is solved using CPLEX 12.7 on a desktop computer running with Intel i7 CPU and 64.0 GB of memory. A time limitation of 7,200 CPU seconds was imposed for solving the test instances without equity constraints, while the time limit is increased to 72,000 CPU seconds for the instances with equity constraints

due to their computational difficulty. The multi-stage stochastic model is solved over eight stages for the base case with each stage representing a 2-week period, thus for a total of the 16-week planning horizon. Since we consider three outcomes on each branch of the scenario tree, we solve for $3^8 = 6561$ scenarios in the mathematical model.

2.3 Results

In this section, we present computational results for the multi-stage stochastic MIP model presented in Section 2.2 for the considered case study instance in West Africa. Our goal in this section is to provide insights into the optimal and fair resource allocation for controlling the Ebola disease outbreak under the uncertainty of disease transmission.

2.3.1 Model Validation

In this subsection, we validate our model against the real outbreak data [WHO, 2016] in terms of the cumulative number of infections from August 30, 2014, to December 19, 2014. The values of parameters used in the model are obtained from the literature [Camacho et al., 2014, WHO E. R. Team, 2014, WHO, 2020c].

We fix the number of ETCs at each stage according to the number and timing of the ETCs established in reality [Büyüktahtakın et al., 2018a]. For instance, according to the outbreak data, one 50-bed ETC was established on September 15, 2014, in northern Liberia, and so the value of the related variable is fixed to one in stage one in the model. Once the ETCs are fixed in the model based on their opening time and the capacity throughout the planning horizon, the model is solved and validated by comparing the predicted number of infections with the real outbreak data given in the WHO database [WHO, 2016].

According to the visual comparison of the predicted results and real outbreak data in Figure 2.3, our model provides a good fit for the cumulative number of infected individuals in Guinea, Sierra Leone, and Liberia during the considered time period. In addition, we apply the paired t-test to analyze the difference between the pairs of weekly predicted cases and the actual data. As shown in Table 2.8, all p-values are greater than 0.05, indicating that our model provides statistically similar results to the real outbreak data from August 30, 2014, to December 19, 2014.

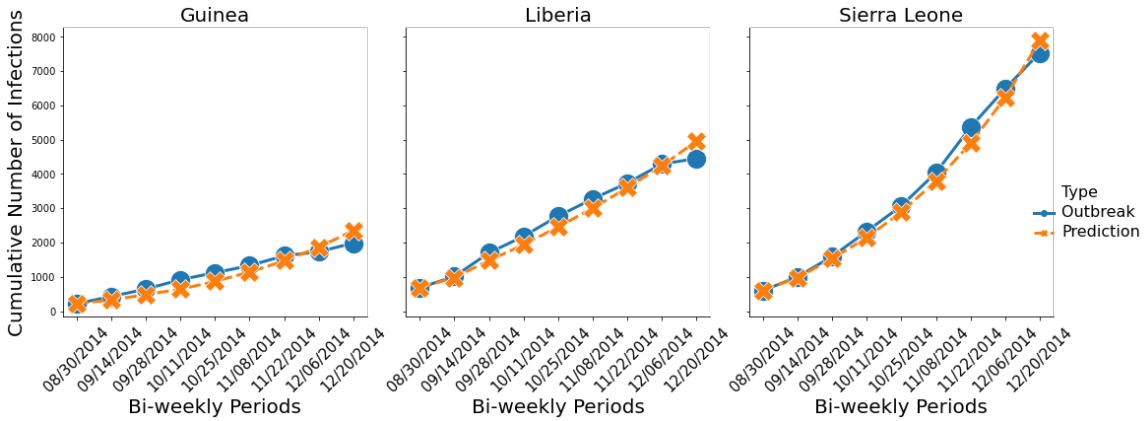

Figure 2.3 Comparison of predicted cases with real outbreak data for cumulative infections in Guinea, Liberia, and Sierra Leone.

Table 2.8 Statistical Analysis to Compare Bi-weekly Predicted Cases and Real Outbreak Data

	Country	Mean		Two-tailed paired t-test		
		Outbreak	Predicted	t-stat	t-critical	p-value
Infections	Guinea	221.0	266.8	0.41	1.89	0.65
	Sierra Leone	866.3	910.1	0.65		0.73
	Liberia	471.1	534.5	0.45		0.67

2.3.2 The Value of Stochastic Solution (VSS)

To demonstrate the value of using a stochastic program over a deterministic (expected value) model, we use a standard measure in stochastic programming, known as the value of stochastic solution (VSS) [Birge, 1982]. The VSS gives the expected gain from solving a stochastic model over its deterministic counterpart, in which random parameters are replaced by their expected values.

Two-Stage VSS WS is the wait-and-see problem objective value, which is the expected value of using the optimal solution for each scenario. EEV is the expected result of using the solution of the deterministic model (EV), which replaces all uncertain parameters by their expected values, and RP is the optimal value of our stochastic programming model, i.e., the minimization recourse problem. Then the following inequalities are satisfied for the minimization problems [Madansky, 1960]:

$$WS \leq RP \leq EEV$$

The VSS can then be formulated as follows:

$$VSS = EEV - RP$$

A large value of the VSS implies that incorporating uncertainty is important to represent the problem realistically, and the solution of the deterministic problem is not "so good." On the other hand, if the VSS value is small, replacing uncertain parameters with their expected values might be a good choice.

Multi-Stage VSS For the multi-stage problem, the value of the stochastic solution is introduced as a chain of values VSS_t for $t = 1, \ldots, T$, where T is the final period of the planning horizon [Escudero et al., 2007]. In order to calculate the VSS_t, the solution up to stage $t-1$ of the associated deterministic model is fixed in the stochastic

model resulting in the EEV_t value, and RP value is subtracted from EEV_t. Consider a stochastic model, which only contains decision variables x and recourse variables y, and let $(\hat{x}_t, \hat{y}_t)$ be the optimal solution of the corresponding EV model. The EEV_t can then be formulated as:

$$\begin{aligned} EEV_t : RP \qquad & \text{model} \\ \text{s.t.} \qquad & x_1^\omega = \hat{x}_1 \quad \forall \omega \in \Omega, \\ & \dots \\ & x_{t-1}^\omega = \hat{x}_{t-1} \quad \forall \omega \in \Omega. \end{aligned}$$

The VSS_t for each $t = 1, \dots, T$ is then given as:

$$VSS_t = EEV_t - RP$$

As an example, we calculate the VSS_t for an 8-stage problem for $t = 1, \dots, 4$. Since $EEV_1 = RP$, the value of the VSS_1 is zero. We solve the model under a \$24M budget and present the results in Table 2.9 below.

Table 2.9 VSS_t Values up to Four Stages for the 8-Stage Problem with EEV_t Values

$VSS_1(RP)$	VSS_2	VSS_3	VSS_4
0	41	65	69

The RP value for the 8-stage problem is 2207 individuals. The VSS_t value is increasing as the stage t increases, thus a multi-stage stochastic model is needed to obtain a better result compared to the deterministic problem. We notice that under the \$24M budget level, the model allocates almost all the ETCs in the first stage. Thus, the VSS_t value will not change significantly when $t \geq 3$. For varying budget cases or disease dynamics, we expect that the model will allocate ETCs in the stages

following the first stage, and thus the VSS_t values may become larger than the values in this instance. The results for solving the 8-stage model highlight the importance of using a multi-stage stochastic model for the epidemic-logistics problem over its deterministic counterpart.

2.3.3 Analysis of Budget Allocation

The columns of Table 2.10 present results for each **Budget** level ($12M, $24M, and $48M), each **Country** and **Region**, **Stage-1 Budget** allocated, **Total Budget** allocated, **Stage-1 ETC (50/100)** representing the number of 50- and 100-bed ETCs allocated in the first stage of the planning horizon, and **Total ETC (50/100)** indicating the total number of 50- and 100-bed ETCs allocated throughout the planning horizon. Here, expected values of the optimal budget and the number of ETCs allocated at the first stage and throughout the planning horizon over 6561 scenarios are presented for each budget level. Correspondingly, the expected values of the total number of infections and funerals for different budget levels are presented in Figure 2.6. The CPU time used to solve the model is $7230s$ for the $12M budget, $7232s$ for the $24M budget, and $7228s$ for the $48M budget. The optimality gaps for all the cases are 0.1%.

The fifth column of Table 2.10 and Figure 2.4 show the allocation of the total budget among three different countries. Due to the high initial number of infected individuals, Sierra Leone gets the most budget allocation under all different budget levels. Although the transmission rate of Guinea is higher than Liberia, the second highest budget goes to Liberia under the $48M budget case because the initial state of the infection in this country is high, and thus, the allocated budget will provide a more significant impact on Liberia compared to Guinea when the budget is ample. According to the results of ETC allocation at all budget levels, most of the beds are allocated in the first period (stage-1) of the planning horizon under tight budget

cases, as shown in Table 2.10. Figure 2.5 shows the total capacity allocation under different budget levels.

Figure 2.6 shows the total number of infections and funerals in those three countries under different budget levels. According to the result under the \$0M budget level, the case in which no intervention action is taken, the number of infections and funerals in Sierra Leone would be extremely large if we do not take any intervention action. As shown in Figure 2.6, the total number of infections and funerals in all three countries, especially in Liberia and Sierra Leone, drops significantly from \$12M to \$48M budget level.

Table 2.10 Budget and Bed Allocated under Different Budget Levels

Budget ($M)	**Country**	**Region**	**Stage-1 Budget ($M)**	**Total Budget ($M)**	**Stage-1 ETC (50/100)**	**Total ETC (50/100)**
12	Guinea	UG	0.06	0.13	1/1	1/1
		MG	0.01	0.02	1/0	1/0
		LG	0.03	0.06	1/0	1/0
	Sierra Leone	S	4.33	11.67	1/4	1/4
	Liberia	NL	0.04	0.09	1/1	1/1
		SL	0.01	0.03	1/1	1/1
Total			**4.47**	**11.99**	**6/7**	**6/7**
24	Guinea	UG	0.72	1.83	1/1	1/1
		MG	0.52	1.21	1/0	1/1
		LG	0.62	1.53	1/1	1/1
	Sierra Leone	S	5.35	15.50	1/5	1/5
	Liberia	NL	0.83	2.31	1/1	1/1
		SL	0.57	1.60	1/1	1/1
Total			**8.62**	**23.98**	**6/9**	**6/10**
48	Guinea	UG	1.11	2.52	1/1	1/1
		MG	0.91	1.91	1/1	1/1
		LG	1.01	2.32	1/1	1/1
	Sierra Leone	S	6.85	18.89	4/5	5/5
	Liberia	NL	3.94	10.42	3/3	3/3
		SL	2.40	6.03	2/2	2/2
Total			**16.22**	**42.09**	**12/13**	**13/13**

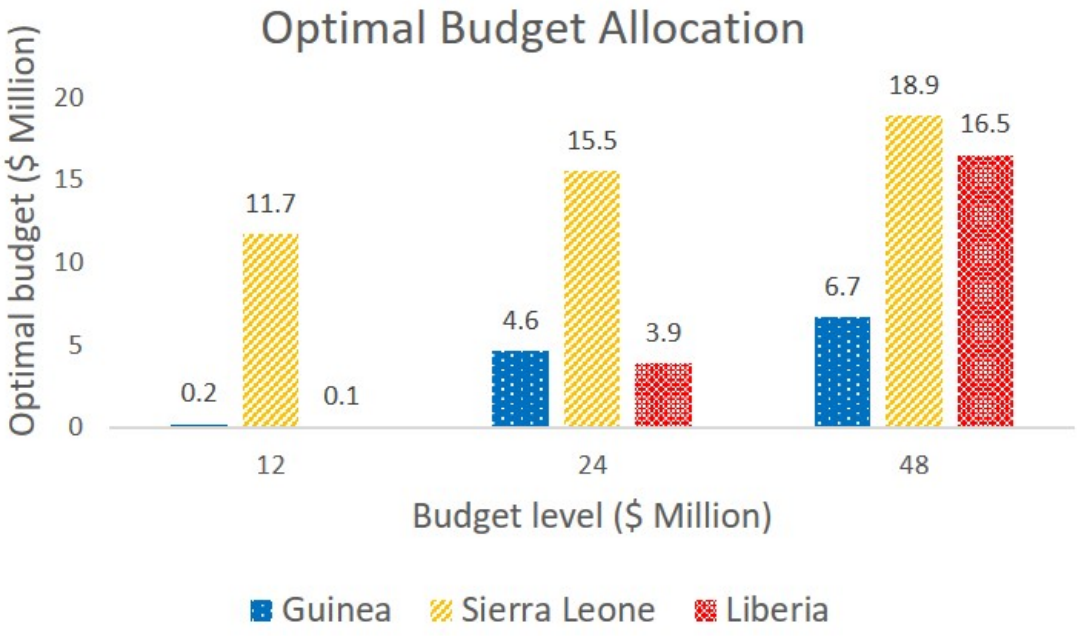

Figure 2.4 Total budget allocation under different budget levels.

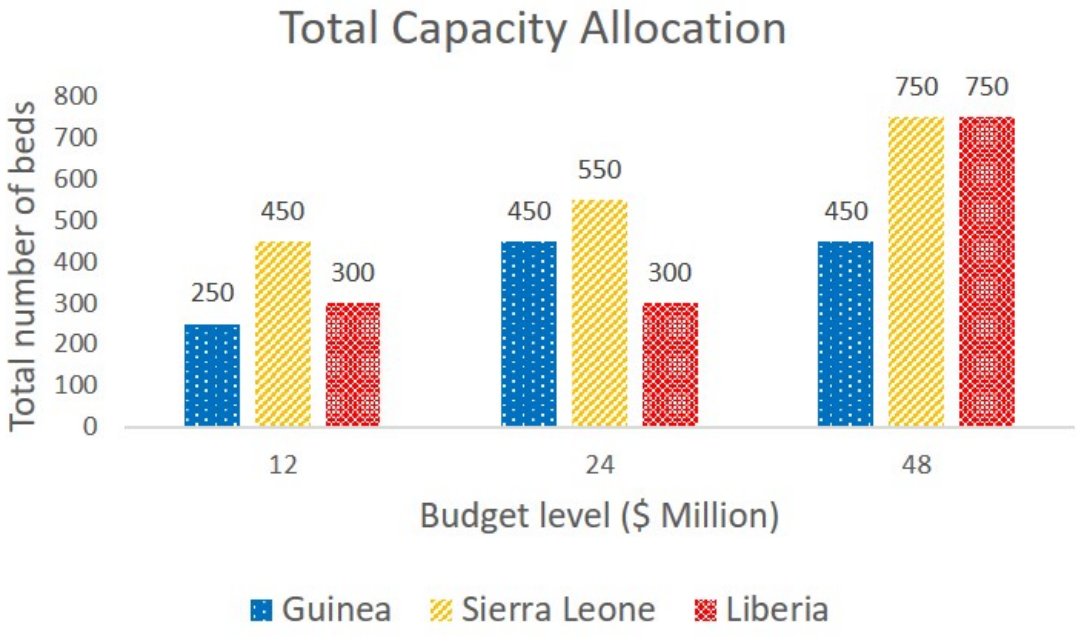

Figure 2.5 Total capacity allocation under different budget levels.

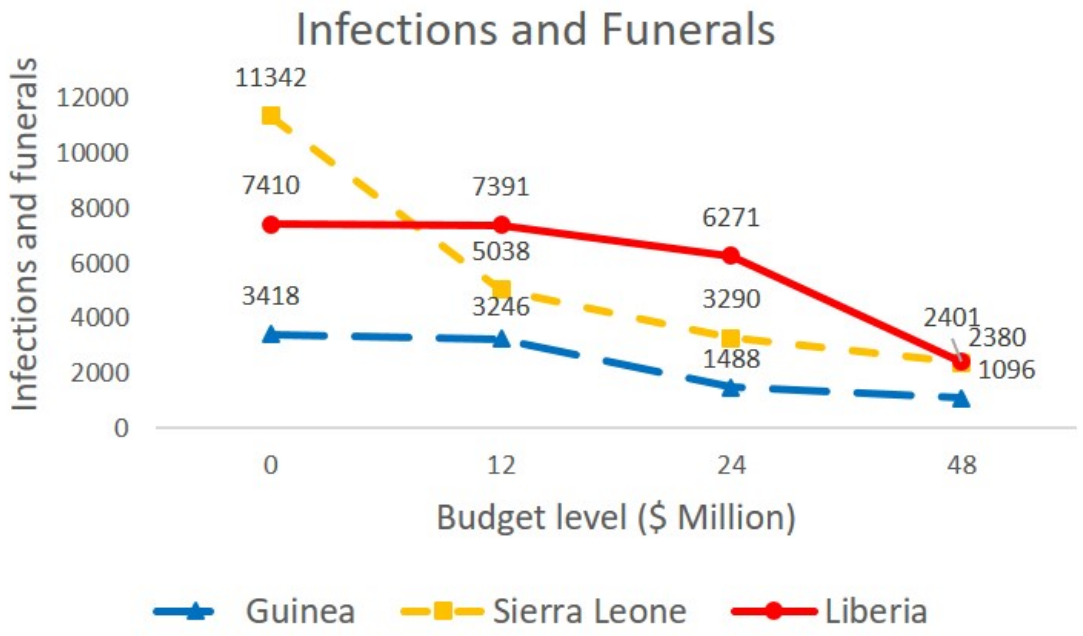

Figure 2.6 Total number of infections and funerals under different budget levels.

The results presented in this subsection represent the expected values over all scenarios. To perform a more detailed analysis, we picked 5 (five) out of 6561 scenarios and analyzed the corresponding results in the next subsection.

2.3.4 Analysis of Different Scenarios

In this subsection, we present results regarding the budget, and ETC allocation as well as the corresponding total number of infections and funerals for five specific scenarios under a budget level of $24M. Those four different scenarios are defined as follows. The first scenario is the "All Low" case that corresponds to the low realization of the uncertain community disease transmission rate from stages 1 to 8, the second scenario is the "All Medium" case that corresponds to the medium realization of the uncertain community disease transmission rate from stages 1 to 8, the third scenario is the "All High" case that represents the high realization of the community disease transmission rate from stages 1 to 8, the fourth scenario is the "Low-High" case that stands for

the low realization of the disease transmission rate from stages 1 to 4 followed by its high realization from stages 5 to 8, and the fifth scenario is the "High-Low" case that represents the high realization of the community disease transmission rate from stages 1 to 4 followed by a low transmission rate from stages 5 to 8. According to the results, we divided scenarios into two groups except for the "All Medium" case; the first one is called the better group, including "All Low" and "Low-High" cases, on the other hand, the second group is called the worse group, encompassing "All High" and "High-Low" cases. Similar to Table 2.10, Table 2.11 presents results for each **Scenario** defined above under the $24M budget level.

The first-stage budget allocation is presented in the fourth column of Table 2.11, while the total budget is presented in both the fifth column of Table 2.11 and Figure 2.7. In terms of bed allocation, all the regions have the same number of bed allocation for stage-1 and for the total stages under all scenarios. This result implies that it is optimal to open treatment centers early in all the locations, in particular, in the initial stages.

Figure 2.8 represents the total capacity allocation under different scenarios. According to the results, the total capacity allocated under the worse scenario group is higher than the capacity allocated for the better group. This result implies that under the worse scenario group, more budget is allocated to build new Ebola treatment centers. In addition, as shown in Figure 2.9, the total number of new infections and funerals under the "High-Low" case is much higher than the corresponding number under the "Low-High" case. Thus, a scenario where the disease starts with a low transmission rate and then progresses fast is better than a scenario in which the disease progression is fast and then slows down. This may be because diseases that initially progress less aggressively give us more time to get prepared, establish the ETCs and treatment resources, and thus reduce the number of infections immediately.

Table 2.11 Budget and Bed Allocated under Different Scenarios

Scenario ($M)	**Country**	**Region**	**Stage-1 Budget ($M)**	**Total Budget ($M)**	**Total Bed (50/100)**
All Low	Guinea	UG	0.60	1.15	2/0
		MG	0.60	1.02	2/0
		LG	0.60	1.13	2/0
	Sierra Leone	S	5.39	12.44	0/5
	Liberia	NL	2.15	5.46	0/2
		SL	1.08	2.79	0/2
Total			**10.41**	**24.00**	**6/9**
All Medium	Guinea	UG	0.60	1.64	2/0
		MG	0.60	1.43	2/0
		LG	0.60	1.64	2/0
	Sierra Leone	S	5.39	16.13	0/5
	Liberia	NL	0	0	0/0
		SL	1.08	3.16	0/2
Total			**8.26**	**24.00**	**6/7**
All High	Guinea	UG	1.08	2.75	0/2
		MG	0.60	1.51	2/0
		LG	1.08	2.23	0/2
	Sierra Leone	S	7.06	17.51	2/7
	Liberia	NL	0	0	0/0
		SL	0	0	0/0
Total			**9.82**	**24.00**	**4/11**
Low-High	Guinea	UG	0.60	1.44	2/0
		MG	0.60	1.18	2/0
		LG	0.60	1.34	2/0
	Sierra Leone	S	4.31	12.02	0/5
	Liberia	NL	1.68	4.91	2/2
		SL	1.08	3.11	0/2
Total			**8.86**	**24.00**	**8/9**
High-Low	Guinea	UG	1.08	2.44	0/2
		MG	0.60	1.29	2/0
		LG	1.08	2.23	0/2
	Sierra Leone	S	6.46	15.47	0/7
	Liberia	NL	1.08	2.56	0/2
		SL	0	0	0/0
Total			**10.29**	**24.00**	**2/13**

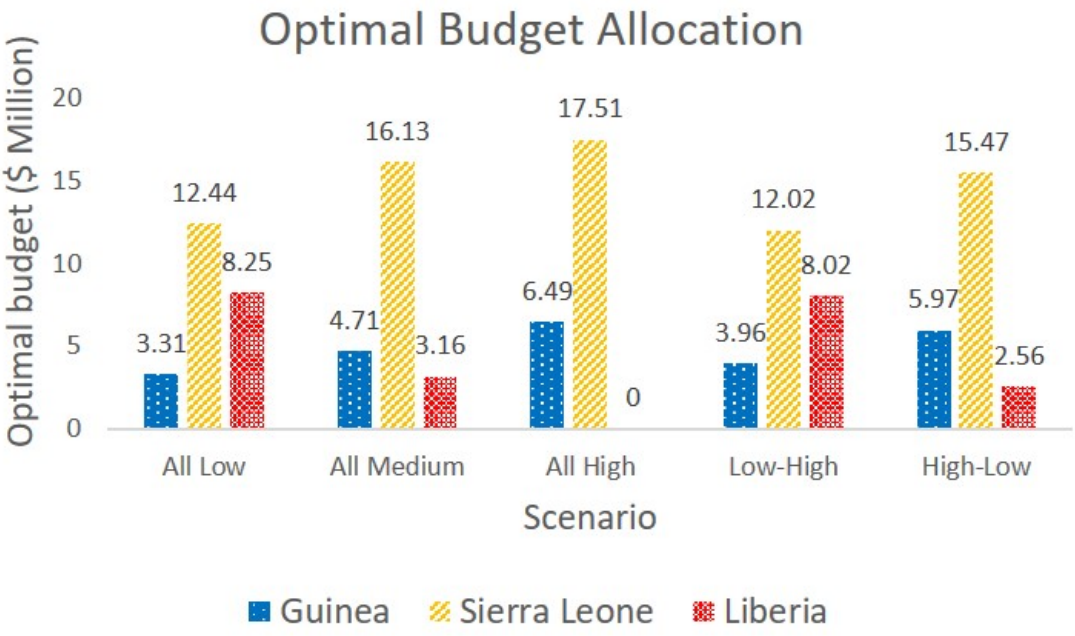

Figure 2.7 Total budget allocation under different scenarios.

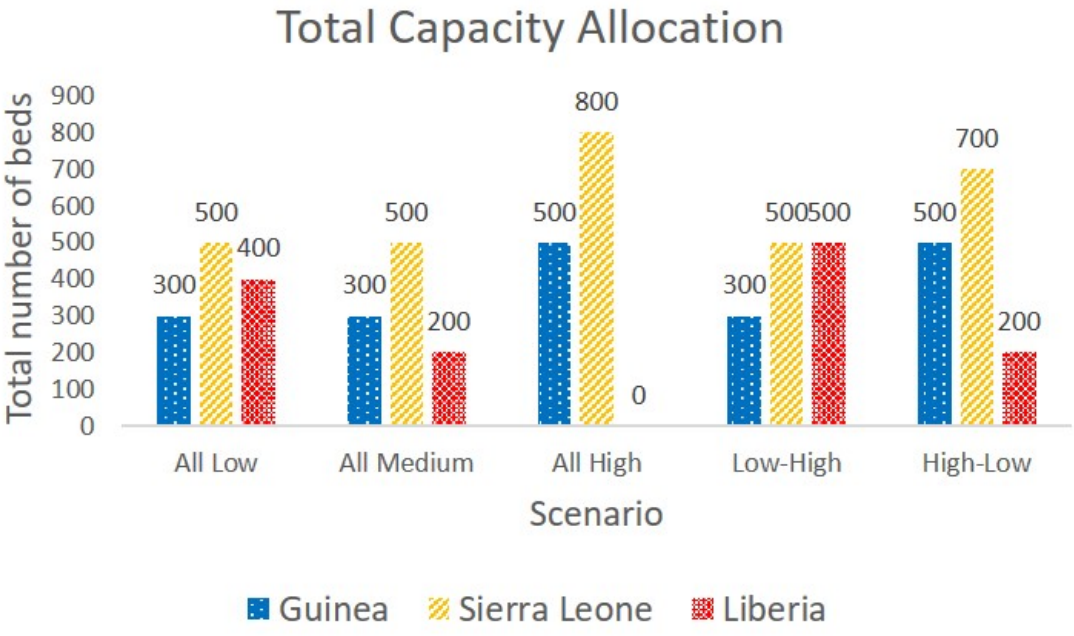

Figure 2.8 Total capacity allocation under different scenarios.

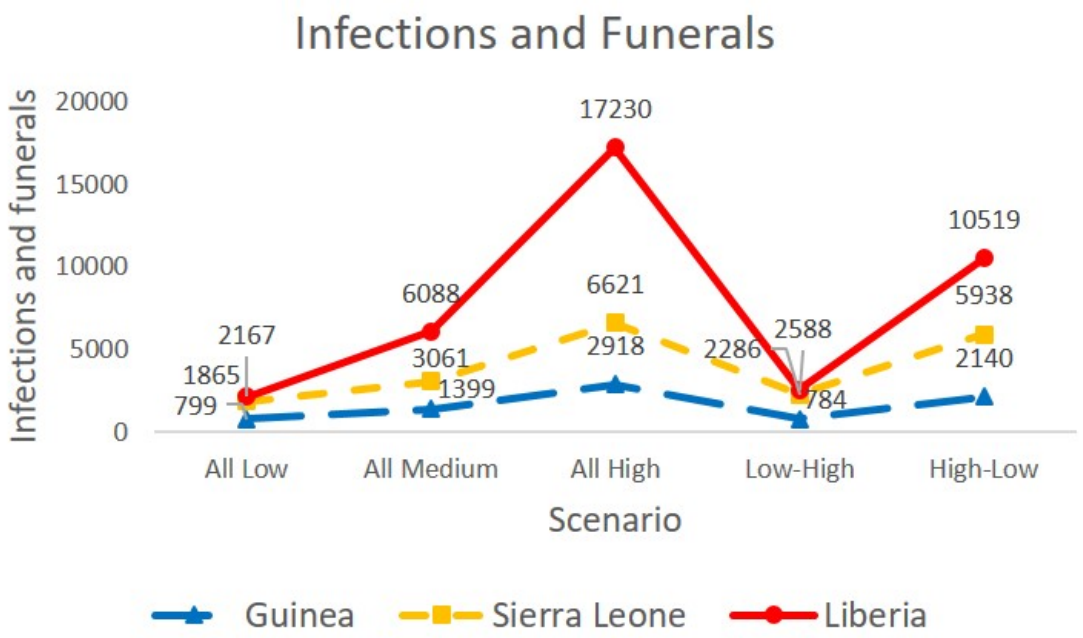

Figure 2.9 Total number of new infections and funerals under different scenarios.

The results above indicate that if the budget is tight or the disease moves fast, some countries or regions may not get the ETC allocation or treatment. For example, under the "All High" scenario, no budget is allocated to Liberia. Therefore, in the next subsection, we introduce the equity constraint to remedy the problem of not allocating any ETCs or treatment resources to a single country or some of the regions of a country.

2.3.5 Impacts of Equity Considerations

In this subsection, we present results by adding each of the three equity constraints (2.2), (2.3), and (2.4), as introduced in Subsection 2.2.6, separately into the linearized multi-stage stochastic programming epidemic-logistics model (2.1). Equity constraints impose a bound on the total number of infections in each region and thus enforcing that each region considered in West Africa receives a more equitable share

of resources, including ETCs and treatment funds, while minimizing the total number of infections and deaths.

According to the results, imposing the infection equity constraint (2.2) or the prevalence equity constraint (2.4) does not significantly change the optimal budget allocation or the total number of new infections and funerals (see Appendix A.4 for detailed results). Without introducing the infection equity constraint into the mathematical model (2.1), the absolute value of the difference between the infection ratio and the population ratio in Guinea, Sierra Leone, and Liberia is 0.42, 0.04, and 0.38, respectively, based on the optimal solution value similar to the k values considered here. This result implies that our model balances the total number of infections in each region with its population and population, even without the infection equity constraint.

Similar to the infection equity case, we introduce the capacity equity constraint (2.3) into the multi-stage stochastic programming epidemic-logistics model (2.1) for an 8-stage instance with the \$24M budget level under different values of k. Table 2.12 represents the run time specifics regarding the mathematical model (2.1) with the capacity equity constraint (2.3), while Figures 2.10 and 2.11 present the budget allocation and the total number of infections and funerals over the three considered countries for varying k values. When k is larger than 0.4, we observe no significant change in the results. However, a small k value can impact the results significantly. For example, when $k = 0.05$, all three regions have a similar budget allocation. If k increases from 0.05 to 0.2, the total number of infections and funerals in Guinea is slightly increased, but it is decreased when k is further increased. Thus, allocating the majority of resources to Guinea may not be necessary, and some of those resources would be wasted. As we relax the equity capacity constraint by increasing the k value from 0.05 to 0.4 and above, we observe a significant drop in the number of infected individuals and funerals in Sierra Leone. The total number of infected people

and funerals over all three countries is the largest (12,769) when the capacity equity constraint is strictly enforced, and it is the smallest (10,995) when the capacity equity constraint is relaxed. This result implies that enforcing a tight equity constraint might adversely impact the total number of infections and deaths, and thus resulting in a high cost that we have to pay for fairness.

Table 2.12 Model Run Specifics with the Capacity Equity Constraint (2.3)

k value	Solution Time (CPU sec)	Optimality Gap (%)
0.05	72,103	7
0.1	72,121	8
0.2	72,053	6
0.4	72,031	2
A large k value (no-equity-constraint case)	7,232	0

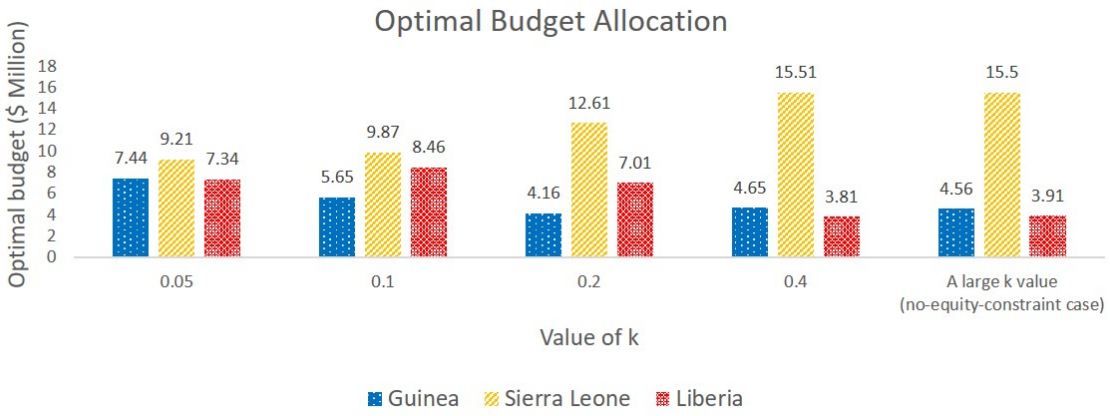

Figure 2.10 Optimal budget allocation under different k values for an 8-stage problem with \$24M budget.

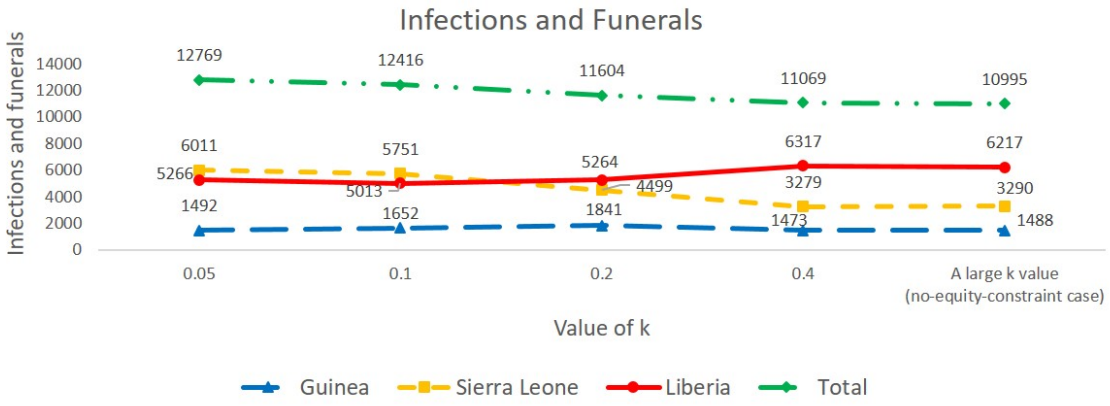

Figure 2.11 Total number of new infections and funerals under different k values for an 8-stage problem with \$24M budget.

2.4 Discussion and Future Research Directions

In this chapter, we extended the epidemic-logistics model of Büyüktahtakın et al. [2018a] to study an epidemic control problem in a large-scale population where the transmission rate of the disease is uncertain. To our knowledge, this is the first multi-stage stochastic epidemic-logistic model that takes into account both the uncertain disease growth and equitable resource allocation simultaneously. We consider various disease progression scenarios resulted from the realization of the community transmission rates. Our objective is to minimize the total expected number of infected individuals and funerals over all scenarios, all periods, and all regions considered. We study the value of the stochastic solution and introduce the equity constraints to analyze the fair resource allocation among different countries and multiple regions of a country. Our multi-stage VSS analysis suggests that the stochastic model considerably improves the solution of the deterministic model, and the consideration of uncertainty in a multi-stage disease-transmission model is necessary.

We define the infection level as the difference between the ratio of the number of infected people in a region to the total number of infected people over all regions

and the ratio of the population in a region to the total population over all regions. Under tight budget levels, most of the budget would be allocated to the region that has the highest initial infection level, while other regions would receive ETCs and treatment resources according to their infection level as the available budget increases. This indicates that the initial infection level is a key factor in resource allocation. Additionally, more 100-bed ETCs would be allocated to the country that has a high infection level since more capacity will be needed to treat infected people while saving from the fixed cost of opening new ETCs.

According to the results, our model allocated most of ETCs in the first stage to provide a quick response to the epidemic and reduce a large number of unnecessary infections and funerals. Our results showed that the number of untreated infections dropped quickly when early actions were taken with a sufficiently large budget, and the disease was controlled much faster than the report date of the World Health Organization (WHO). The uncertainty in disease transmission is a critical factor that makes it challenging to manage an outbreak in a real-life situation. To be more specific, the transmission rate might suddenly become high after a latent period, and the existing resources may not be sufficient to handle such unexpected situations. Consequently, a large number of unisolated and untreated individuals could stay in the community and continue to spread the disease, as in the case of the current outbreak of Coronavirus (COVID-19) disease [WHO, 2020e]. Thus, the preparedness and early action to handle the uncertain disease transmission are crucial, and we would rather "the beds waiting for people" than "people waiting for the beds." Our findings are consistent with several other articles that also report the importance of early action for epidemic control [Lekone and Finkenstädt, 2006, Jacobsen et al., 2016, Siedner et al., 2015]. The lessons learned from the EVD control in West Africa by WHO and Centers for Disease Control and Prevention (CDC) also indicate that

an early action will have a significant improvement in slowing down an epidemic and eventually stopping it [CDC, 2019b, WHO, 2020c].

Different than the former literature, the solutions of our multi-stage stochastic programming model show that the optimal timing of the resource allocation might vary if we have a relatively ample budget. For instance, in both \$24M and \$48M budget levels, some resources were allocated throughout the planning horizon in some locations, such as Guinea and Sierra Leone. This is because we have more budget to take action when the transmission of the disease gets worse. This result shows that the timing of the resource allocation should be decided dynamically and based on the predicted disease growth scenario and budget, and thus implying the superiority of a multi-stage stochastic programming model over a two-stage or static model again.

We analyze five specific disease growth scenarios and study resource allocation strategies under each scenario. Under the scenarios in which the disease moves faster, more number of ETCs are allocated compared to the scenarios in which the disease moves slower to treat more people. In addition, if the disease moves faster, the majority of the capacity is allocated to the region that has the highest initial infection level. If the disease consistently moves at a slow rate, the treatment capacity is allocated more equally among regions to help fight against the disease. In the "Low-High" case, in which the disease moves in a slow rate first and then starts to be more aggressive in the following time stages, the model allocates budget immediately to the regions with a high infection level and knocks down the number of infected individuals to low values, which will lessen the impacts of a high disease transmission rate later in the planning horizon. Because an initially slow-moving disease gives us more time to get prepared to control the disease spread, the "Low High" case can be considered as a better scenario compared to the "High-Low" case.

We introduced the infection and capacity equity constraints separately into our model to analyze the impact of enforcing fairness in resource allocation. Solutions

obtained with the infection equity constraint imply that the original optimal solution balances the resource allocation among multiple regions in a similar fashion to the infection equity constraint. Thus, our model takes into account the ratio of infection to the total infection level as well as the ratio of the population to the total population level over all three countries while making the resource allocation decision.

When a tight capacity equity constraint is enforced, the budget is allocated equally to the three regions. However, in this case, some of the budget may be wasted, and no obvious effects are brought out by providing additional capacity to a region based solely on its population. This result shows that allocating treatment resources proportional to population is sub-optimal, which is also consistent with the findings of Ren et al. [2013]. When the capacity equity constraint is relaxed, the number of infections and funerals in Guinea and Liberia is slightly changed, but this number decreased significantly for Sierra Leone, and the total three countries. For both tight and ample budget cases, the total number of infections and funerals is much higher when the capacity equity constraint is strictly forced, resulting in a heavy price we would have to pay for perfect equity in resource allocation. This result implies that the decision maker should be cautious about enforcing fairness when allocating resources to multiple regions.

There are several important future research directions that arise out of this study. For example, the impact of vaccinations currently used to prevent the spread of the disease could be analyzed in a future study. The influence of vaccination is group-specific, and thus susceptible individuals can be divided into different groups according to their age, sex, race, and health status. Due to the lack of available data, the transmission rate from susceptible individuals to infected individuals would be more difficult to predict under vaccination. Furthermore, different kinds of vaccines used, the amount of vaccine allocated to each region, and the time when vaccination becomes accessible might impact the disease transmission rate significantly. Our

model could be extended by adding a compartmental class named as "vaccinated" to study the various dimensions of vaccination.

Moreover, our multi-stage stochastic program only includes the expectation criterion in the objective function when it compares random variables to find the best decisions. Thus, our study provides a risk-neutral approach. In a future extension of this work, risk measures, such as Conditional Value at Risk ($CVaR$), could be incorporated into the objective function to reflect the perspectives of a risk-averse decision maker.

CHAPTER 3

RISK-AVERSE MULTI-STAGE STOCHASTIC PROGRAMMING TO OPTIMIZING VACCINE ALLOCATION AND TREATMENT LOGISTICS FOR EFFECTIVE EPIDEMIC RESPONSE

3.1 Introduction

Epidemics and pandemics have devastated humanity throughout its existence. One recent example is the Coronavirus (COVID-19), which has spread all over the world since its first detection in China at the end of 2019, causing over 33 million cases and 1 million deaths as of October 2020 [JHU, 2021]. The COVID-19 has also resulted in large economic losses, and the associated damage continues to escalate. For example, due to the pandemic, 400 million full-time jobs were lost across the world [CNBC, 2020], and consumer spending so far decreased by more than one trillion dollars only in the U.S. [Routley, 2020]. Another example is the 2014-16 Ebola Virus Disease (EVD), one of the deadliest viral infections, causing more than ten thousand deaths in West Africa. Other recent examples include the Severe Acute Respiratory Syndrome (SARS), which affected 26 countries since its discovery in South China in 2003, and the novel swine-origin influenza A (H1N1) virus that spread fast in the human population since its first appearance in 2009, causing tens of millions of cases and 12,469 deaths only in the U.S. [CDC, 2016, WHO, 2019b, CDC, 2019a]. Such viral diseases causing lower respiratory infections, such as pneumonia, have remained among the top causes of death globally including stroke and cancer [WHO, 2021b, Hasan et al., 2019].

Effective and timely allocation of limited resources, such as medical treatment and vaccination, plays a crucial role in alleviating the ravaging impacts of infectious disease outbreaks on the human population. This problem has attracted much attention from academics and practitioners. The vast majority of the research literature involves simulations and differential equations [Siettos et al., 2015, Ajelli et al., 2016, Craft et al., 2005, Kaplan et al., 2003] to estimate the transmission of

the disease and tackle the epidemic resource allocation problem. Other studies use network models and stochastic compartmental models to analyze various strategies on the control of an epidemic [Berman and Gavious, 2007, Longini Jr et al., 2007, Porco et al., 2004, Riley and Ferguson, 2006, Lekone and Finkenstädt, 2006, Tanner et al., 2008, Funk et al., 2017] as well as resource allocation analysis [Zaric et al., 2000, Tebbens and Thompson, 2009, Nguyen et al., 2017, Shaw and Schwartz, 2010].

Previous operations research models that study the epidemic diseases and resource allocation mainly focused on the logistics and operation management to control the disease in optimal ways [Zaric and Brandeau, 2001, Büyüktahtakın et al., 2018a, Ekici et al., 2013, Liu et al., 2019, Queiroz et al., 2020]. Only a few of those OR studies that integrate resource allocation with epidemics control consider the uncertain parameters for resource allocation to control the disease. Those mainly use stochastic and approximate dynamic programming [Coşgun and Büyüktahtakın, 2018, Long et al., 2018] and two-stage stochastic programming [Ren et al., 2013, Yarmand et al., 2014, Tanner et al., 2008]. Because the growth of an infectious disease dynamically changes over time, Yin and Büyüktahtakın [2021a] present a multi-stage stochastic programming model to capture the dynamics of an evolving disease for effective epidemic control under the uncertainty of disease transmission.

Multi-stage stochastic programs typically minimize an expectation criterion, which calculates the expected cost of all possible scenarios, each of which is mapped with a certain probability of occurrence. The expectation is the most widely-used objective criterion in stochastic programming [Ahmed, 2006]. However, it does not capture the variability in possible scenarios that could arise, in particular, the situations with high impact and low probability. If some extreme scenarios occur, there could be a significant loss when only the expected value is considered in resource allocation decision-making. For example, in a disastrous epidemic outbreak situation, non-repetitive decisions made at the beginning of the horizon, such as the placement

of treatment facilities, may result in capacity shortages and unmet demand under the realization of a severe disease spread scenario. At the beginning of an epidemic outbreak, disease characteristics, such as the infection or disease transmission rate, may be unknown, and the disease growth could be highly uncertain due to the lack of data. Thus a large number of infections and losses could happen in shorter time periods than expected, as in the case of COVID-19 [Lazzerini and Putoto, 2020, Li et al., 2020]. The former epidemics control multi-stage stochastic programming model of Yin and Büyüktahtakın [2021a] only considered an expectation criterion in the objective function. To alleviate the adverse impacts of experiencing a disastrous disease transmission scenario, we consider a risk measure in the objective function in addition to the expectation criterion.

Conditional value-at-risk (CVaR) is a coherent risk measure that can be used in an optimization model without losing convexity [Rockafellar and Uryasev, 2002]. Therefore, many previous studies considered mean-risk models with CVaR in stochastic programming models [Ahmed, 2006, Rockafellar and Uryasev, 2002, Schultz and Tiedemann, 2006, Miller and Ruszczyński, 2011]. CVaR-based mean-risk stochastic programming has been studied in various applications, such as supply chain management [Alem and Morabito, 2013], reverse logistic network design problem [Soleimani and Govindan, 2014], solid waste management system [Dai et al., 2014], water resources allocation [Zhang et al., 2016], and forestry invasive species control planning [Bushaj et al., 2020a].

In this chapter, we address the problem of building a mean-CVaR, multi-stage, stochastic mixed-integer programming epidemics-vaccination-logistics model. Our model evaluates various scenarios regarding the disease growth and the vaccine availability to optimize the distribution of treatment centers and vaccines while minimizing the total expected number of infections, funerals, and close contacts of infected people under a limited budget. Here, we consider the risk of experiencing

scenarios that lead to adverse outcomes in terms of the number of infected and dead people due to the epidemic. Combining the risk-neutral objective with a risk measure allows for a trade-off between the weighted expected impact of the outbreak and the expected risks associated with experiencing extremely disastrous scenarios.

For a newly-discovered disease, the invention of a new vaccine is difficult and typically takes a long time. Even if there is an approved vaccine available, its production will be short compared to the high demand in the early period of the outbreak, and thus the availability of the vaccines will be limited. In this study, we address the optimal distribution of limited vaccine supply in addition to the allocation of treatment resources to control an epidemic outbreak under the uncertainty in the vaccine supply and the transmission rate.

To incorporate human mobility within multiple regions of a country, we present a new formulation to estimate migration rates among various locations. We apply our model to the case of controlling the 2018-2020 EVD in the Democratic Republic of the Congo (DRC). We provide insights into the optimal resource allocation among different regions of DRC in a multi-period planning horizon with and without risk. We also analyze how risk-aversion affects decision-making, such as the budget allocated to treatment and vaccination and the number of infections and deaths, compared to the risk-neutral problem.

3.1.1 Key Contributions and Insights

Former studies on the logistics of epidemics have omitted the risk of experiencing extreme scenarios when formulating a stochastic optimization model. A risk-neutral stochastic programming approach, which does not consider variability in possible scenario outcomes, may perform poorly when there are outliers in the distribution of the scenarios. Also, existing mathematical programming studies on epidemic control have not incorporated vaccine allocation into a compartmental-logistics model.

Furthermore, due to the lack of data, the rates of migration among multiple regions of DRC are not known. The population is quite mobile within regions and countries in Africa [Flahaux and De Haas, 2016]. Thus, movement rates are difficult to estimate.

In this chapter, we address those aforementioned limitations existing in both the epidemiological modeling and healthcare operations research literature. Below, we present the modeling and applied contributions with key recommendations to decision makers.

Modeling Contributions. First, to our knowledge, we present the first risk-averse multi-stage stochastic programming model presented in the research field of infectious disease control. Different than the former literature, we formulate the uncertainty in the transmission rate from the close contacts of infected people to the infections compartment and the uncertainty in total vaccines available as two dependent random variables in a multi-stage stochastic scenario tree. We then incorporate a nested CVAR risk measure into the objective function of the formulation while defining risk-related constraints to alleviate the risk of experiencing scenarios that lead to adverse outcomes in terms of the number of infected and dead people due to the epidemic. We also provide insights on how the expected impact and expected risk in terms of deaths and infections change as the decision maker shifts from being risk-neutral to risk-averse at varying risk levels.

Second, we address the optimal allocation of vaccines to multiple regions within a country in addition to the allocation of Ebola Treatment Centers (ETCs) and treatment resources to control an epidemic outbreak in a multi-stage stochastic mean-risk model. Specifically, we have extended the Susceptible-Infected-Treated-Recovered-Funeral-Burial epidemics-logistics model of Büyüktahtakın et al. [2018a] into an epidemic-vaccination-logistics model by incorporating new ring vaccination compartment under uncertainty and risk.

Third, we develop a new formulation to estimate the migration rates between regions of a country and integrate the impacts of human mobility into our epidemic-vaccination-logistics model. Thus, our mathematical model captures the influence of human movement on the transmission of the disease.

Fourth, our risk-averse epidemic-vaccination-logistics model is general and thus could be adopted to study other epidemic diseases, such as influenza and H1N1, as well as pandemics, such as the COVID-19.

Applied Contributions and Key Recommendations to Decision Makers. We implement our multi-stage stochastic mean-risk model to study the case of the 2018-2020 EVD in the DRC. We collect and synthesize epidemiological, population, and economic data of Ebola infections in the provinces of DRC and organize them into regional data, using WHO Ebola situation reports [WHO, 2021a, 2020a]. We perform computational experiments to analyze the impact of treatment budget, risk parameters, uncertain vaccine availability, and vaccine acceptance and effectiveness rates on the allocation of resources, such as ETC and vaccines, during an epidemic. We drive several insights into the optimal resource allocation under various risk levels that the decision maker is willing to take for controlling an infectious disease. As such, our mathematical model could be used as a decision support tool to aid policymakers in determining the optimal risk-averse treatment and vaccine-allocation policies.

Based on our results, we provide the following recommendations to inform the resource allocation decision making under an epidemic situation:

(**i**) Regions with a high initial infection level ("the number of infected people in a region" / "the total number of infected people" - "population in a region" / "total population over all regions") get the majority of the resources. While the ETCs and treatment budget are mainly allocated to highly infected locations, the model allocates a budget for vaccination to most locations to prevent the disease's spread. Our findings also suggest using the budget for vaccination in regions where the disease has just started, while in regions with high initial

infections, the model gives priority to build new ETCs and treat infected people over vaccination.

(**ii**) The potential risk associated with regions with low or zero initial infection levels should also be taken into account when making resource allocation decisions. For instance, a non-infected region nearby a highly-infected location may also be severely affected by the disease due to human mobility among multiple regions. Thus, as the risk-averseness level increases, the budget allocated to areas with the highest initial infection level is decreased by moving the ETC and treatment budget to neighboring locations under the risk of getting infections.

(**iii**) A risk-averse decision-maker should expect a possible increase in the number of infections and deaths while trying to mitigate disastrous outbreak scenarios. Being risk-averse also increases the expected cost of treatment and vaccination.

(**iv**) For the considered case of the EVD in DRC, isolating and treating infected individuals are the most efficient ways to slow the disease's transmission. When the supplied vaccines are available but limited, the vaccination is supplementary to the primary interventions on reducing the number of infections.

(**v**) While vaccination is supplementary, its delay could cause an exponential increase in the number of infections and deaths, even under the main intervention measures, such as treatment and isolation. In particular, vaccination at earlier stages of an epidemic would also help control the disease faster than immunization at later stages. Thus, if available, vaccination should be applied as early as possible for effective epidemic response.

(**vi**) The number of vaccines supplied to Upper North Kivu and Middle North Kivu, the two most-impacted regions of DRC, has a complementary relationship. When the vaccine acceptance rate is fixed, the number of vaccines provided to these two regions only sightly fluctuates under different vaccine effectiveness rates. Also, the more effective the vaccine is, the fewer vaccines are needed in highly-impacted areas so that some remaining vaccines could be used in regions with lower infection.

(**vii**) When the vaccine effectiveness rate is fixed, vaccine acceptance rates affect vaccine allocation at the initial stages of the vaccine rollout. Under a very low vaccine acceptance rate, available vaccines are moved from highly impacted locations to less affected areas. However, vaccine acceptance rates do not impact the total number of vaccines distributed throughout the planning horizon under a limited vaccine supply.

3.2 Multi-Stage Risk and Time Consistency

Let $F_Z(\cdot)$ be the cumulative distribution function of a random variable Z. The α-quantile of the distribution, $\inf_\eta\{\eta \in \mathbb{R} : F_Z(\eta) \geq \alpha\}$, is defined as the value-at-risk (VaR) at the confidence level $\alpha \in [0, 1)$ and denoted by $\text{VaR}_\alpha(Z)$.

The mean excess loss or tail VaR, at level α, is called conditional value-at-risk (CVaR), defined as $\text{CVaR}_\alpha(Z) = \mathbb{E}(Z \mid Z \geq \text{VaR}_\alpha(Z))$. Specifically, CVaR is the conditional expected value that exceeds the VaR at the confidence level α. For a minimization problem, VaR_α is the α-quantile of the cost distribution, and it provides an upper bound on the cost that is exceeded only with a small probability of $1 - \alpha$. On the other hand, CVaR_α measures an expectation of the cost that is more than VaR_α, the α-quantile of the distribution of costs. The conditional value-at-risk can be calculated as an optimization problem as follows [Rockafellar and Uryasev, 2002]:

$$\text{CVaR}_\alpha(Z) = \inf_{\eta \in \mathbb{R}}\{\eta + \frac{1}{1-\alpha}\mathbb{E}([Z - \eta]_+)\},$$

where $(a)_+ := max(a, 0)$ for any $a \in \mathbb{R}$.

In this chapter, we study a mean-risk minimization problem, as first introduced in Markowitz [1991]:

$$\min_{x \in X}\{\mathbb{E}(f(x, \omega)) + \lambda \text{CVaR}_\alpha(f(x, \omega))\}, \tag{3.1}$$

where $\mathbb{E}(f(x, \omega))$ represents the expected cost function of the scenarios $\omega \in \Omega$, CVaR_α represents the conditional value-at-risk at $\alpha \in [0, 1)$, and $\lambda \in [0, 1]$ is a non-negative coefficient of the risk part. The risk preference parameter λ is the weight of the risk term in the objective function (3.1), and can be adjusted for a trade-off between optimizing an expectation value $[\mathbb{E}(f(x, \omega))]$ and the level of risk taken $[\text{CVaR}_\alpha(f(x, \omega))]$. The larger the λ, more risk-averse the decision maker is. The α parameter, on the other hand, gives the confidence level on the perceived risky scenarios that exceed the maximum acceptable loss, VaR_α. As α increases, the

probability of exceeding the VaR_α reduces, and thus the decision maker becomes more risk averse. The parameter $\alpha \in [0, 1)$ is typically set to a high value, e.g., 0.95. The parameters λ and α are set by the user to adjust the level of risk averseness and do not have a direct relationship.

Time Consistency. When modeling a risk-averse multi-stage stochastic program, time consistency is considered as a critical issue. Time consistency implies that if you solve a multi-stage stochastic programming model today and find solutions for each node of a tree, you should get the same solution if you resolve the problem tomorrow when you are given the information that is observed and decided today. For a multi-stage stochastic model, risk measures can be applied at every stage additively or to the complete scenario path or in a nested form similar to dynamic programming. The nested risk measures are shown to satisfy the time consistency of multi-stage stochastic programs in the study of [Homem-de Mello and Pagnoncelli, 2016].

We consider a nested risk measure, expected conditional value-at-risk ($\mathbb{E}$-CVaR), as defined in Homem-de Mello and Pagnoncelli [2016]. The $\mathbb{E}$-CVaR can be linearized and formulated as a linear stochastic programming model. In the next section, we will utilize the $\mathbb{E}$-CVaR as a risk measure to formulate our mean-risk multi-stage stochastic epidemics-vaccination-logistics model.

3.3 Problem Formulation

This section presents the compartmental model description and the mean-risk formulation of the multi-stage stochastic epidemics-vaccination-logistics model.

3.3.1 Notation

In this subsection, we describe the model notation that will be used throughout the rest of this chapter.

Sets and indices:

J : Set of time periods, $J = \{0, ..., \overline{J}\}$.

A : Set of ETC types, $A = \{1, ..., \overline{A}\}$.

R : Set of regions, $R = \{1, ..., \overline{R}\}$.

M_r : Set of all surrounding regions of region r.

Ω : Set of scenarios, $\Omega = \{1, ..., \overline{\Omega}\}$.

j : Index for time period, where $j \in J$.

r : Index for region where $r \in R$.

a : Index defining type of ETC, where $a \in A$.

ω : Index for scenario, where $\omega \in \Omega$.

Transition parameters used to describe the rate of movement between disease compartments:

$\chi_{1,r}$:Disease fatality rate without treatment in region r.

$\chi_{2,r}$:Disease fatality rate while receiving treatment in region r.

$\chi_{3,r}$:Disease survival rate without treatment in region r.

$\chi_{4,r}$:Disease survival rate with treatment in region r.

$\chi_{5,r}$:Safe burial rate of Ebola-related dead bodies in region r.

σ_r :Transmission rate per person in general community due to community interaction in region r.

$\theta^{\omega}_{1,r}$:Transmission rate per person of close contacts due to

interaction with infected individuals in region r under scenario ω.

$\theta_{2,r}$:Transmission rate per person of close contacts during a traditional funeral ceremony in region r.

f :Vaccine acceptance rate.

β_r :Vaccine effectiveness rate.

ε_r :Transmission rate per person from successfully vaccinated V (immune) to general community S (not immune anymore) in region r.

Other parameters:

$b_{j,r}$:Unit cost of treatment for an infected individual in region r at the end of period j.

$g_{aj,r}$:Fixed cost of establishing type a ETC in region r at the end of period j.

k_a :Capacity (number of beds) of type a ETC.

u_r :The population in region r.

$e_{j,r}$:Unit cost per vaccine in region r at the end of period j.

Δ :Total available budget for treatment.

π_r :Initial number of susceptible individuals in general community in region r.

ϕ_r :Initial number of close contacts of infected people in region r.

φ_r :Initial number of vaccinated individuals in region r.

ϖ_r :Initial number of infected individuals in region r.

κ_r :Initial number of treated individuals in region r.

ϑ_r :Initial number of recovered individuals in region r.

υ_r :Initial number of unburied dead bodies in region r.

τ_r :Initial number of buried dead bodies (funerals) in region r.

ς_r :Initial treatment capacity in terms of the number of ETC beds in region r.

$i_{l\to r}$:Migration rate of infected individuals from surrounding regions $l \in M_r$ to region r.

$h_{l\to r}$:Migration rate of close contacts from surrounding regions $l \in M_r$ to region r.

$i_{r\to l}$:Migration rate of infected individuals from region r to surrounding regions $l \in M_r$.

$h_{r\to l}$:Migration rate of close contacts from region r to surrounding regions $l \in M_r$.

$d^{\omega}_{j,r}$:Binary variable for linearization in region r at the end of period j under scenario ω.

$U^{\omega}_{j,r}$:Auxiliary variable to be substituted with $(C^{\omega}_{j,r} - T^{\omega}_{j,r})d^{\omega}_{j,r}$ in region r at the end of period j under scenario ω.

$W^{\omega}_{j,r}$:Auxiliary variable to be substituted with $I^{\omega}_{j,r}(1 - d^{\omega}_{j,r})$ in region r at the end of period j under scenario ω.

Q_{LB} :Lower bound for $C^{\omega}_{j,r} - T^{\omega}_{j,r}$.

Q_{UB} :Upper bound for $C^{\omega}_{j,r} - T^{\omega}_{j,r}$.

I_{LB} :Lower bound for $I^{\omega}_{j,r}$.

I_{UB} :Upper bound for $I^{\omega}_{j,r}$.

G^{ω}_{j} :Number of total supplied vaccines at the end of period j under scenario ω.

q :Average number of close contacts per each infected individual.

State variables:

$S^{\omega}_{j,r}$:Number of susceptible individuals in general community in region r at the end of period j under scenario ω.

$H^{\omega}_{j,r}$:Number of close contacts of infected people in region r at the end of period j under scenario ω.

$V^{\omega}_{j,r}$:Number of successfully vaccinated individuals, who are fully immunized to disease, in region r at the end of period j under scenario ω.

$I^{\omega}_{j,r}$:Number of infected individuals in region r at the end of period j under scenario ω.

$T^{\omega}_{j,r}$:Number of individuals receiving treatment in region r at the end of period j under scenario ω.

$R^{\omega}_{j,r}$:Number of recovered individuals in region r at the end of period j under scenario ω.

$F^{\omega}_{j,r}$:Number of deceased individuals due to the epidemic in region r at the end of period j under scenario ω.

$B^{\omega}_{j,r}$:Number of buried individuals in region r at the end of period j under scenario ω.

$\hat{H}^{\omega}_{j,r}$:Number of close contacts of infected people migrating into region r at the end of period j under scenario ω.

$\widetilde{H}^{\omega}_{j,r}$:Number of close contacts of infected people emigrating from region r at the end of period j under scenario ω.

$\hat{I}^{\omega}_{j,r}$:Number of infected individuals migrating into region r at the end of period j under scenario ω.

$\widetilde{I}^{\omega}_{j,r}$:Number of infected individuals emigrating from region r at the end of period j under scenario ω.

Decision variables:

$C^{\omega}_{j,r}$:Total capacity (number of beds) in ETCs to be established in region r at the end of period j under scenario ω.

$\overline{I}^{\omega}_{j,r}$:Number of infected individuals hospitalized (and quarantined) in region r at the end of period j under scenario ω.

$y^{\omega}_{aj,r}$:Number of type a ETCs established in region r at the end of period j under scenario ω.

$O^{\omega}_{j,r}$:Number of vaccines allocated to region r at the end of period j under scenario ω.

Risk parameters:

α :Confidence level of value-at-risk, where $\alpha \in [0, 1)$.

λ :Non-negative risk preference parameter or mean-risk trade-off coefficient.

Risk variables:

η_j^ω :Value at risk at the confidence level α for each stage j under scenario ω.

z_j^ω :Value exceeding the value-at-risk at the confidence level α (η_j^ω) at stage j under scenario ω.

Sets and Parameters related to non-anticipativity:

N :Set of nodes in the scenario tree.

n :The serial number of nodes in the stochastic decision tree.

$\beta(n)$:Set of scenarios that pass through node $n \in N$.

$t(n)$:The corresponding stage that node n marked in the decision tree.

3.3.2 Compartmental Disease Model Description

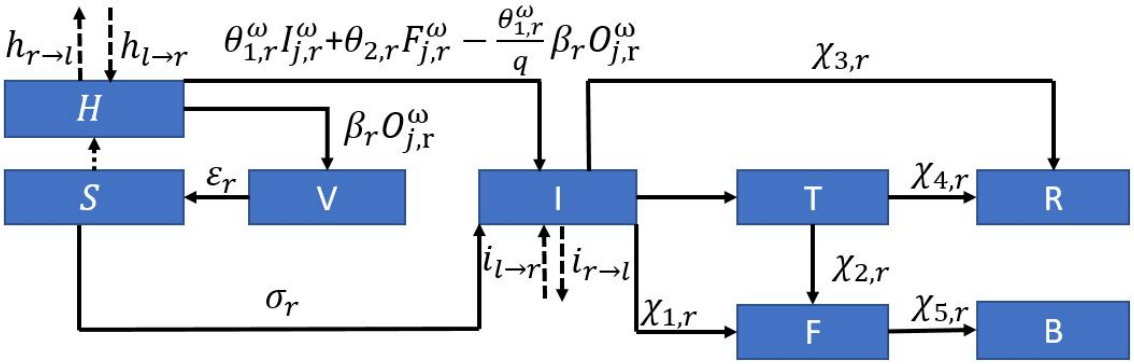

Figure 3.1 One-Step disease compartmental model.

Figure 3.1 shows the transmission dynamics of the EVD in a region r located in DRC for each period j. The disease spreads among susceptible individuals (S) as

well as close contacts of infected (H), by either person-to-person contact at a periodic rate of $\theta^{\omega}_{1,r}$ under scenario ω or through touching Ebola-related dead bodies that are not yet buried during traditional funerals at a periodic rate of $\theta_{2,r}$ in region r. Thus, once close contacts (H) or susceptible individuals (S) become infected, they move to the infected (I) compartment. However, individuals in the general community (S) are infected with a lower rate of σ_r compared to close contacts (H).

Here, we focus on modeling the ring vaccination, where only close contacts with infected people can be vaccinated. The quantity of vaccines allocated to region r under scenario ω at the end of period j under scenario ω is defined by the variable $O^{\omega}_{j,r}$. Given the effectiveness rate of vaccination, β_r, there will be $\beta_r O^{\omega}_{j,r}$ people who are moving from the (H) to (V) compartment in each period j, where (V) represents the successfully vaccinated individuals, who become fully immunized by vaccination. Next, due to the time effect, successfully vaccinated individuals (V) become no longer immune to the disease over time and move to the general community (S) with a rate of ε_r in region r. When the number of infected people increases, the close contacts of infected people will also increase. Thus, the dotted arrow from the general community (S) to close contacts (H) represent the movement of people from (S) to (H) as (I) increases. Furthermore, since people are getting vaccinated, the number of close contacts in (H) being infected and moving into the (I) compartment should be decreased by $\frac{\theta^{\omega}_{1,r}}{q}\beta_r O^{\omega}_{j,r}$, where q is the average number of close contacts for each infected individual. The term $\frac{\theta^{\omega}_{1,r}}{q}$ shows the proportion of close contacts that would be infected for each infected individual, and because $\beta_r O^{\omega}_{j,r}$ represents the number of successfully vaccinated close contacts who become fully immunized by vaccination, $\frac{\theta^{\omega}_{1,r}}{q}\beta_r O^{\omega}_{j,r}$ gives the number of close contacts saved by the vaccination.

Without treatment, some of the infected individuals in the compartment (I) will die and move to the funeral (F) compartment with the rate of $\chi_{1,r}$, while some of the infected individuals will recover with a rate of $\chi_{3,r}$, moving into the recovered

compartment (R). However, the number of individuals hospitalized for treatment (T) is based on the treatment capacity variable $C^{\omega}_{j,r}$, which gives the available number of beds in the ETCs in region r under scenario ω in period j. Thus, there is no constant transition rate from I to T. Meanwhile, individuals who did not receive treatment will remain in the community and spread the disease. In treated compartment (T), some individuals will recover with a periodic rate of $\chi_{4,r}$, and a fraction of them will die with a periodic rate of $\chi_{2,r}$. The deceased individuals in the funeral compartment are safely buried at a rate of $\chi_{5,r}$, moving into the buried compartment (B).

To describe the migration of infected individuals and close contacts within a given country, we define $i_{l\to r}$ and $i_{r\to l}$ as the rates of migration of infected individuals into and out of region r, as shown in dotted arrows going in and out of compartment (I). Similarly, we define $h_{l\to r}$ and $h_{r\to l}$ as the rates of migration of close contacts of infected people (H) into and out of region r.

3.3.3 Uncertainty and Model Assumptions

Modeling Uncertainty. In this chapter, we used a discrete set of scenarios $\omega \in \Omega$ to model the uncertainties related to the disease–the uncertainty in the transmission rate from the close contacts of the infected individuals to infections and the uncertainty in total vaccines supplied (available) at each stage j. Each scenario has a probability of p^{ω}, where $\sum_{\omega\in\Omega} p^{\omega} = 1$. We assume that the uncertainty of the transmission rate is highly dependent on the availability of vaccine supply. If the vaccine supply is high, we observe a low transmission rate from close contacts to infections, and if the vaccine supply is low, we will have a high transmission rate instead. For our multi-stage stochastic model, we have two branches in each node of the scenario tree, representing the two possible realizations in each stage j: low and high transmission rates $\theta^{\omega}_{1,r}$ corresponding to the high and low levels of vaccines supplied at time j under scenario ω, G^{ω}_{j}. The case study values of the uncertain transmission and the vaccine

availability parameters under two realizations at each branch of the scenario tree are presented in Table B.7 in Appendix B.1.4.

Assumptions on Model, Data, and Parameters. The transmission of the EVD is affected by many factors, including damaged public health infrastructures, cultural beliefs, behavioral practices, and violent events frequently happening in DRC [Wannier et al., 2019, WHO, 2015]. Due to these issues, data to calibrate some of the model parameters is either lacking or inaccurate. Data parameters, such as the transmission rate and the probability of scenarios, are quite difficult to estimate. Therefore, we make assumptions about some of the parameters used in the model formulation.

First, in our current model, each infected individual is assumed to have 100 close contacts, including direct close contacts and their close contacts (i.e., contacts of contacts) [CDC, 2015, Doshi et al., 2020]. Those close contacts (e.g., household and health care workers) are considered as the high-risk group to be infected. In contrast, the susceptible people in the general community are considered in the lower risk group compared to infected people's close contacts. Due to the nature of the ring vaccination, we assume that only the close contacts of infected people will get the vaccination.

Second, in our model, each node of the scenario tree has two realizations of the transmission rate and vaccine availability, as low and high. Former research has shown that violent events happening in DRC contribute to the increased transmission of EVD [Wannier et al., 2019]. During our planning horizon of 15 weeks, from June 25, 2019, to October 8, 2019, seven violent events were reported [Dickey, 2018]. Considering the likelihood of a violent event happening in each period, we assign a probability of 0.5 to each potential outcome (low and high) of disease transmission in our scenario tree in each time period. Disease transmission rates under no violent events are reported to vary between 0.81 and 1.08 [Wannier et al., 2019]. Thus, we

use a low transmission rate of 0.948 for North Kivu and 0.84 for Ituri based on the estimations reported in Camacho et al. [2014] and Wannier et al. [2019]. The mean value of the transmission rate in DRC is 1.11 [Wannier et al., 2019], and the highest transmission rate in history is 1.83 [Chowell et al., 2004]. In between those two values of transmission rates in DRC, we consider a high transmission rate of 1.422 for North Kivu and adjust it proportionally to a high transmission rate of 1.26 for Ituri based on the ratios of low transmission rates in both locations. Similar to their impacts on transmission rates, we assume that violent events lead to a low vaccine supply upper bound due to hindered humanitarian operations and lowered access to the infected population. Third, the transmission rate defined in our model represents how many new infections can be generated from the existed infected individuals through a certain time period. Under the situation of a small population, this value will be influenced by the total number of susceptible individuals since the total number of infected individuals will approach the maximum of population. However, our implementation regions have a large amount of population, it will not be influenced by the total number of susceptible individuals since the number of infections will never reach the total number of susceptible individuals under the interventions. In addition, the dependent relationship between general community and the number of newly infected individuals will cause a non-linear issue in the optimization model. Thus, the number of newly infected individuals in our model is independent with the general community size. Finally, current Ebola vaccines are shown to provide immunization for at least two years with high and stable levels of antibodies to the Ebola Zaire Virus in the blood of volunteers who are vaccinated [WHO, 2021a, Branswell, 2018]. Thus, we assume that recovered individuals will not get infected again within four months of vaccination or recovering from the disease, which is nearly the planning horizon we consider in our study.

3.3.4 Model Formulation

Using the notation defined in Appendix 3.3.1, the mean-risk multi-stage stochastic epidemic-vaccination-logistics model can be formulated as follows:

$$\min \quad \sum_{j\in J}(\sum_{\omega\in\Omega} p^{\omega}(\sum_{r\in R}(I^{\omega}_{j,r}+F^{\omega}_{j,r}+H^{\omega}_{j,r})+\lambda(\eta^{\omega}_{j}+\frac{1}{1-\alpha}z^{\omega}_{j})) \tag{3.2a}$$

$$\text{s.t.} \quad S^{\omega}_{0,r}=\pi_r, \quad I^{\omega}_{0,r}=\varpi_r, \quad T^{\omega}_{0,r}=\kappa_r, \quad R^{\omega}_{0,r}=\vartheta_r, \quad H^{\omega}_{0,r}=\phi_r,$$

$$F^{\omega}_{0,r}=\upsilon_r, \quad B^{\omega}_{0,r}=\tau_r, \quad V^{\omega}_{0,r}=\varphi_r, \quad C^{\omega}_{0,r}=\zeta_r, \quad \forall r\in R, \forall\omega\in\Omega, \tag{3.2b}$$

$$S^{\omega}_{(j+1),r}=S^{\omega}_{j,r}-\sigma_r I^{\omega}_{j,r}+\varepsilon_r V^{\omega}_{j,r}-q((\sigma_r+\theta^{\omega}_{1,r})I^{\omega}_{j,r}+\theta_{2,r}F^{\omega}_{j,r}-\frac{\theta^{\omega}_{1,r}}{q}\beta_r O^{\omega}_{j,r}),$$
$$j\in J\setminus\{\overline{J}\}, \forall r\in R, \forall\omega\in\Omega, \tag{3.2c}$$

$$I^{\omega}_{(j+1),r}=I^{\omega}_{j,r}+\hat{I}^{\omega}_{j,r}-\widetilde{I}^{\omega}_{j,r}+(\sigma_r+\theta^{\omega}_{1,r})I^{\omega}_{j,r}+\theta_{2,r}F^{\omega}_{j,r}-\frac{\theta^{\omega}_{1,r}}{q}\beta_r O^{\omega}_{j,r}$$
$$-(\chi_{1,r}+\chi_{3,r})I^{\omega}_{j,r}-\overline{I}^{\omega}_{j,r}, \qquad j\in J\setminus\{\overline{J}\}, \forall r\in R, \forall\omega\in\Omega, \tag{3.2d}$$

$$H^{\omega}_{(j+1),r}=H^{\omega}_{j,r}+\hat{H}^{\omega}_{j,r}-\widetilde{H}^{\omega}_{j,r}-\theta^{\omega}_{1,r}I^{\omega}_{j,r}-\theta_{2,r}F^{\omega}_{j,r}-\beta_r O^{\omega}_{j,r}+q((\sigma_r+\theta^{\omega}_{1,r})I^{\omega}_{j,r}$$
$$+\theta_{2,r}F^{\omega}_{j,r}-\frac{\theta^{\omega}_{1,r}}{q}\beta_r O^{\omega}_{j,r})+\frac{\theta^{\omega}_{1,r}}{q}\beta_r O^{\omega}_{j,r}, \qquad j\in J\setminus\{\overline{J}\}, \forall r\in R, \forall\omega\in\Omega, \tag{3.2e}$$

$$V^{\omega}_{(j+1),r}=V^{\omega}_{(j+1),r}+\beta_r O^{\omega}_{j,r}-\varepsilon_r V^{\omega}_{j,r},$$
$$j\in J\setminus\{\overline{J}\}, \forall r\in R, \forall\omega\in\Omega, \tag{3.2f}$$

$$T^{\omega}_{(j+1),r}=T^{\omega}_{j,r}+\overline{I}^{\omega}_{j,r}-(\chi_{2,r}+\chi_{4,r})T^{\omega}_{j,r},$$
$$j\in J\setminus\{\overline{J}\}, \forall r\in R, \forall\omega\in\Omega, \tag{3.2g}$$

$$R^{\omega}_{(j+1),r}=R^{\omega}_{j,r}+\chi_{3,r}I^{\omega}_{j,r}+\chi_{4,r}T^{\omega}_{j,r},$$
$$j\in J\setminus\{\overline{J}\}, \forall r\in R, \forall\omega\in\Omega, \tag{3.2h}$$

$$F^{\omega}_{(j+1),r}=F^{\omega}_{j,r}+\chi_{1,r}I^{\omega}_{j,r}+\chi_{2,r}T^{\omega}_{j,r}-\chi_{5,r}F^{\omega}_{j,r},$$
$$j\in J\setminus\{\overline{J}\}, \forall r\in R, \forall\omega\in\Omega, \tag{3.2i}$$

$$B^{\omega}_{(j+1),r}=B^{\omega}_{j,r}+\chi_{5,r}F^{\omega}_{j,r}, \qquad j\in J\setminus\{\overline{J}\}, \forall r\in R, \forall\omega\in\Omega, \tag{3.2j}$$

$$\hat{I}^{\omega}_{j,r}=\sum_{l\in M_r} i_{l\to r}I^{\omega}_{j,l}, \quad \hat{H}^{\omega}_{j,r}=\sum_{l\in M_r} h_{l\to r}H^{\omega}_{j,l},$$
$$j\in J, \forall r\in R, \forall\omega\in\Omega, \tag{3.2k}$$

$$\widetilde{I}^{\omega}_{j,r} = \sum_{l \in M_r} i_{r \to l} I^{\omega}_{j,r}, \quad \widetilde{H}^{\omega}_{j,r} = \sum_{l \in M_r} h_{r \to l} H^{\omega}_{j,r},$$
$$j \in J, \forall r \in R, \forall \omega \in \Omega, \tag{3.2l}$$

$$\sum_{r \in R} (\sum_{j \in J \setminus \{0, \overline{J}\}} \sum_{a \in A} g_{aj,r} y^{\omega}_{aj,r} + \sum_{j \in J} (b_{j,r} T^{\omega}_{j,r} + e_{j,r} O^{\omega}_{j,r})) \leq \Delta \quad \forall \omega \in \Omega, \tag{3.2m}$$

$$C^{\omega}_{j,r} = \sum_{m=1}^{j} \sum_{a \in A} k_a y^{\omega}_{am,r} + C_{0,r}, \qquad j \in J \setminus \{\overline{J}\}, \forall r \in R, \forall \omega \in \Omega, \tag{3.2n}$$

$$\overline{I}^{\omega}_{j,r} = U^{\omega}_{j,r} + W^{\omega}_{j,r}, \qquad j \in J \setminus \{\overline{J}\}, \forall r \in R, \forall \omega \in \Omega, \tag{3.2o}$$

$$U^{\omega}_{j,r} \leq Q_{UB} d^{\omega}_{j,r}, \quad U^{\omega}_{j,r} \geq Q_{LB} d^{\omega}_{j,r},$$

$$U^{\omega}_{j,r} \leq (C^{\omega}_{j,r} - T^{\omega}_{j,r}) - Q_{LB}(1 - d^{\omega}_{j,r}), \quad U^{\omega}_{j,r} \geq (C^{\omega}_{j,r} - T^{\omega}_{j,r}) - Q_{UB}(1 - d^{\omega}_{j,r}),$$

$$j \in J \setminus \{\overline{J}\}, \forall r \in R, \forall \omega \in \Omega, \tag{3.2p}$$

$$W^{\omega}_{j,r} \leq I_{UB}(1 - d^{\omega}_{j,r}), \quad W^{\omega}_{j,r} \geq I_{LB}(1 - d^{\omega}_{j,r}),$$

$$W^{\omega}_{j,r} \leq I^{\omega}_{j,r} - I_{LB} d^{\omega}_{j,r}, \quad W^{\omega}_{j,r} \geq I^{\omega}_{j,r} - I_{UB} d^{\omega}_{j,r}$$

$$j \in J \setminus \{\overline{J}\}, \forall r \in R, \forall \omega \in \Omega, \tag{3.2q}$$

$$O^{\omega}_{j,r} \leq H^{\omega}_{j,r}, \qquad j \in J, \forall r \in R, \forall \omega \in \Omega, \tag{3.2r}$$

$$\sum_{r \in R} O^{\omega}_{j,r} \leq G^{\omega}_{j} \qquad j \in J, \forall r \in R, \forall \omega \in \Omega, \tag{3.2s}$$

$$z^{\omega}_{j} \geq \sum_{r \in R} (I^{\omega}_{j,r} - I^{\omega}_{j-1,r} + F^{\omega}_{j,r} + H^{\omega}_{j,r}) - \eta^{\omega}_{j}, \qquad j \in J, \forall \omega \in \Omega, \tag{3.2t}$$

$$z^{\omega}_{j} \geq 0, \qquad j \in J, \forall \omega \in \Omega, \tag{3.2u}$$

$$y^{\omega}_{at(n),r} - y_{an,r} = 0, \quad \overline{I}^{\omega}_{t(n),r} - \overline{I}_{n,r} = 0, \quad C^{\omega}_{t(n),r} - C_{n,r} = 0,$$

$$O^{\omega}_{t(n),r} - O_{n,r} = 0, \quad z^{\omega}_{t(n),r} - z_{n,r} = 0, \quad \eta^{\omega}_{t(n)} - \eta_n = 0,$$

$$a \in A, \forall \omega \in \beta(n), \forall n \in N, \tag{3.2v}$$

$$S^{\omega}_{j,r}, \quad O^{\omega}_{j,r}, \quad H^{\omega}_{j,r}, \quad V^{\omega}_{j,r}, \quad I^{\omega}_{j,r}, \quad T^{\omega}_{j,r}, \quad R^{\omega}_{j,r}, \quad F^{\omega}_{j,r}, \quad B^{\omega}_{j,r}, \quad \overline{I}^{\omega}_{j,r} \geq 0,$$

$$j \in J, \forall r \in R, \forall \omega \in \Omega, \tag{3.2w}$$

$$y^{\omega}_{aj,r} \in \{0, 1, 2, \ldots\}; \quad y^{\omega}_{aj,r} \leq I^{\omega}_{j,r},$$

$$a \in A, j \in J \setminus \{\overline{J}\}, \forall r \in R, \forall \omega \in \Omega, \tag{3.2x}$$

$$d^{\omega}_{j,r} \in \{0, 1\}, \qquad \forall j \in J, \forall r \in R, \forall \omega \in \Omega. \tag{3.2y}$$

The objective function (3.2a) minimizes the total expected number of infected individuals, funerals, plus the close contacts of infected individuals, plus the conditional value-at-risk over all scenarios, in all regions throughout the planning horizon.

Initial Condition Constraints:

Constraints (3.2b) give the initial number of the general community, infected, treated, recovered, close contacts, funerals, buried, and vaccinated compartments, and the total ETC capacity, respectively, in each region r at the beginning of the planning horizon.

Population Dynamics Constraints:

Equations (3.2c)–(3.2j) represent the dynamics of the population in each disease compartment, which are shown in Figure 3.1. Constraint (3.2c) shows that the number of susceptible individuals in the community in region r at the end of period $j+1$ under scenario ω is equal to the number of susceptible individuals from the previous time period minus the number of newly infected individuals, plus the number of successfully vaccinated individuals who were no longer immune to the disease at the end of period j under scenario ω. Furthermore, the term $q((\sigma_r+\theta_{1,r})I^{\omega}_{j,r}+\theta_{2,r}F^{\omega}_{j,r}-\frac{\theta^{\omega}_{1,r}}{q}\beta_r O^{\omega}_{j,r})$ represents the number of susceptible individuals in the community (S) that transfer to close contacts (H) due to the newly infected individuals (I), where q is the average number of close contacts of each newly infected individual.

Constraint (3.2d) implies that the number of infected individuals at the end of period $j+1$ in region r under scenario ω is equal to the number of infected individuals from the previous time period plus the net migrated infected individuals, plus newly infected individuals from the close contacts, general community, and funerals, minus

individuals who were saved from infection by vaccination ($\frac{\theta^{\omega}_{1,r}}{q}\beta_r O^{\omega}_{j,r}$) minus recovered, died, and treated individuals at the end of period j under scenario ω.

Constraints (3.2e) define the number of close contacts at the end of time period $j+1$, which equals the number of close contacts from the previous time period plus the net migrated close contacts, minus the number of newly infected individuals from close contacts, minus the number of successfully vaccinated individuals during period j, and plus the new close contacts and the close contacts saved by the vaccination. Constraint (3.2f) ensures that the number of successfully vaccinated individuals at the end of period $j+1$ equals the number of successfully vaccinated individuals from the previous time period plus the number of new successfully vaccinated individuals and minus the number of individuals who are not immune to the virus anymore. Constraint (3.2g) describes the total number of treated individuals in region r at the end of time period $j+1$ under scenario ω, which is equal to the number of treated individuals at the end of period j plus infected individuals who were admitted to the hospital for treatment based on the availability of beds minus treated individuals who died or recovered. Constraint (3.2h) implies that the cumulative number of individuals who recover in region r at the end of the period $j+1$ under scenario ω is equal to the number of individuals who recover from the previous period plus newly recovered individuals. Constraint (3.2i) ensures the number of unburied funerals in region r at the end of time period $j+1$ under scenario ω is equal to the sum of infected and treated individuals who died, minus the buried dead people. Constraint (3.2j) gives the total number of buried dead bodies at the end of the period j under scenario ω.

Migration Constraints:

Constraints (3.2k) and (3.2l) formulate the number of net immigrated individuals in infected and close contact compartments, similar to the spatio-temporal reaction-

diffusion (RD) models [Kıbış and Büyüktahtakın, 2019]. Specifically, constraints (3.2k) show the number of infected individuals and close contacts migrating into region r from region $l \in M_r$ under scenario ω. Constraints (3.2l) represent the number of infected individuals and close contacts emigrating from region r into neighboring region $l \in M_r$ under scenario ω.

Logistics and Operation Management Constraints:

Constraints (3.2m)–(3.2s) show the restrictions regarding logistics and operations management. Specifically, the inequality (3.2m) represents the budget constraint on the sum of the fixed costs of opening ETCs and the variable cost of treating infected individuals, and the cost of allocating vaccines over all regions r in all periods j under scenario ω. Constraint (3.2n) denotes the total capacity in region r at the end of period j under scenario ω. Constraint (3.2o)–(3.2q) are linear constraints that ensure the number of available beds in ETCs limit the number of hospitalized individuals in region r. Particularly, linear equations (3.2o)–(3.2q) are equivalent to the non-linear constraints implying that the number of hospitalized individuals ($\overline{I}$) is equal to the minimum number of infected individuals and the capacity available at established ETCs after considering currently hospitalized individuals in ETCs (see Yin and Büyüktahtakın [2021a] for the details of the linearization). Constraint (3.2r) represents that the number of vaccines supplied to region r at period j under scenario ω is limited by the number of close contacts in region r at period j under scenario ω. Constraint (3.2s) ensures that the total number of vaccines allocated over all regions can not exceed the available supply at each time period.

Risk Measure Constraints:

Constraints (3.2t) and (3.2u) represent the risk measure limitations. Constraint (3.2t) calculates the difference between the objective function value and the value-at-risk

for each stage under each scenario. Constraint (3.2u) ensures that the loss value exceeding the value-at-risk is included in the CVaR calculation, and thus z_j^ω should be greater than or equal to 0.

Non-anticipativity Constraints:
Constraints (3.2v) are non-anticipativity restrictions stating that if two scenarios share the same path up to stage j, the corresponding decisions will be the same.

Non-negativity Constraints:
Constraints (3.2w) imply non-negativity restrictions on the number of individuals who are susceptible, being vaccinated, close contacts, successfully vaccinated, infected, total treated, recovered, funeral, buried, and treated, respectively, under scenario ω. Constraints (3.2x) represent the integer requirements on the number of type-a ETCs to be opened in region r at the end of period j under scenario ω. Additionally, if the number of infected individuals is less than 1 in a region r, the value of integer variable corresponding to opening an a-bed ETC is forced to be zero, and thus there will be no ETC opened in that region.

Constraint (3.2y) represents the binary variable $d_{j,r}^\omega$, which is 1 when the number of infected individuals to be hospitalized is restricted by the number of available beds in the ETCs, and 0 when all infected individuals are hospitalized for treatment in the ETCs due to the available capacity.

3.4 Case Study and Results

3.4.1 Implementation Details

We apply our model 3.2a–3.2y to the case of the 2018-2020 EVD in the Democratic Republic of the Congo (DRC). The North Kivu and Ituri provinces of the DRC are

affected by the EVD. We divided these two provinces into six different sub-regions: Upper (UNK), middle (MNK), and lower (LNK) North Kivu, and upper (UI), middle (MI), and lower (LI) Ituri. We describe the case study data used to formulate the model parameters, including population and migration data, resource cost data, and epidemiological data in Appendix B.1. The details of the mathematical formulation used to calculate the migration rates are presented in Appendix B.1.2.

We use a nested risk measure in multi-stage stochastic programming, known as the $\mathbb{E}$-CVaR, in the stochastic model, as described in Section 3.2. We assume that the vaccines' availability impacts the transmission rates in community contact, and thus uncertain transmission rates depend on the uncertain vaccine supply. Hence the high (low) availability of vaccines implies the low (high) realization of the uncertain transmission parameter. We present the value of the vaccine availability and uncertain transmission parameters under two realizations at each branch of the scenario tree, as shown in Table B.7 in Appendix B.1.4. We solve the model for a 5-stage time period, where each stage corresponds to three weeks (from June 25, 2019, to October 8, 2019, in total 15 weeks) with high and low vaccine supply under different budget levels. Because each node of the scenario tree has two branches, each corresponding to a possible realization of the random parameters, we have $2^5 = 32$ scenarios for $T = 5$ stages.

The mathematical model is solved using CPLEX 12.7 on the desktop running with Intel $i7$ CPU and 64.0GB of memory. For each run, the time limitation is set at 72,000 CPU seconds. In the following subsections, we present results from solving the mean-risk multi-stage stochastic epidemics-vaccination-logistics model.

3.4.2 Resource Allocation under Different Budget Levels

We test the formulation for each time period under different budget levels: Very Tight ($\$40M$), Tight ($\$70M$), Medium ($\$100M$), and Ample ($\$130M$). The mean-risk trade-off coefficient λ is set to be 1, and the confidence level α is set to be 0.5.

Figure 3.2 presents the optimal allocation of resources (budget, capacity [number of beds], and vaccine) for each region under each budget level. According to the results, the regions with the highest initial infestation levels receive most of the budget, as in the case of Upper North Kivu and Middle North Kivu (Figure 3.2a). When the budget increases from very tight to ample, other regions will also get their share of the budget depending on their initial infection levels and disease-growth scenarios in the model.

Similar to the total budget allocation, the total capacity is allocated based on the initial infection levels (Figure 3.2b). However, different from the total budget allocation, the majority of the ETCs are assigned in the first stage of the 5-stage planning horizon. For instance, under the $\$130M$ budget level, 1450 beds are allocated to Upper North Kivu in the first stage, while the total number of beds allocated to Upper North Kivu only increases by 150 by the end of stage five. Therefore, quick response in terms of allocating most of the treatment centers at the beginning of the outbreak will help to slow down the spread of the disease, while the majority of the budget should be allocated to treat infected people in ETCs and vaccine close contacts over multiple periods throughout the planning horizon.

When the budget level increases, the number of vaccines allocated to each region does not always increase (Figure 3.2c). For instance, under the $\$100M$ budget level, Lower North Kivu receives 177 vaccines, while this reduces to 128 vaccines under the $\$130M$ budget level. A possible reason for this is that vaccination can prevent more people from being infected, but it is not the most efficient way to reduce infections.

(a)

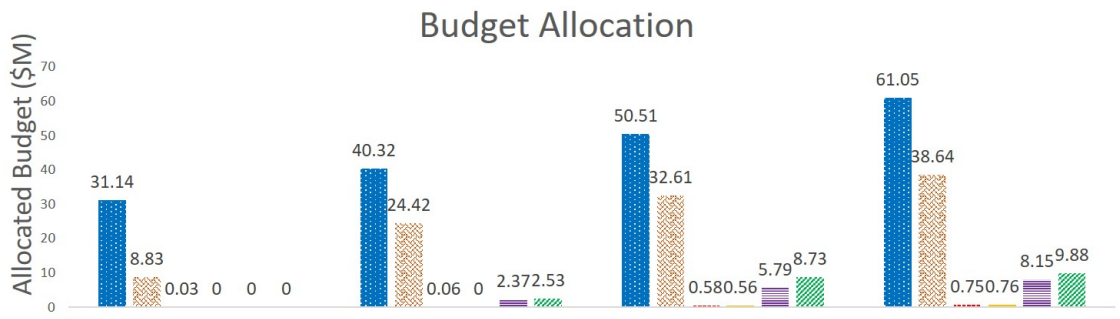

(b)

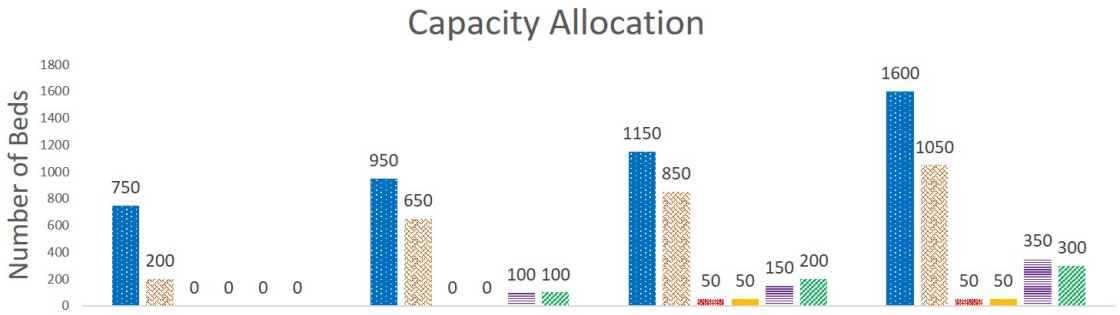

(c)

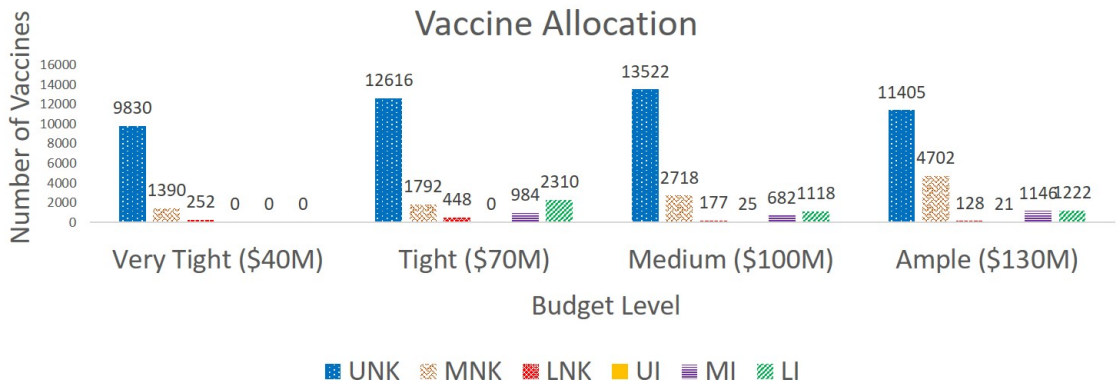

Figure 3.2 Budget, capacity (bed), and vaccine allocated to each region ($\lambda = 1$ and $\alpha = 0.5$).

Thus, the model gives priority to opening new ETCs and treating infected individuals and then uses the rest of the budget to allocate vaccines.

3.4.3 Analysis of the Risk Trade-off

We perform an analysis of the risk parameters λ and α in terms of their impact on the objective function values and the resource allocation strategies. Specifically, under the $\$70M$ budget level, we compare four different problems with respect to their risk-averseness level, adjusting λ and α values accordingly–risk-neutral ($\lambda = 0, \alpha = 0$), weak risk-aversion ($\lambda = 1, \alpha = 0.05$), mild risk-aversion ($\lambda = 10, \alpha = 0.5$) and strong risk-aversion ($\lambda = 100, \alpha = 0.95$).

Impact, Risk, and Cost under Risk-Neutral and Risk-Averse Policies In this subsection, we provide insights on the effect of risk parameters λ and α on the expected impact and expected risk and how those values change as the decision maker shifts from being risk-neutral to risk-averse at varying risk levels. To analyze the results with the risk trade-off coefficient, we decompose the objective function into the *expected impact* $[\mathbb{E}(f(x,\omega))]$ and the *expected risk* $[\lambda \text{CVaR}_\alpha(f(x,\omega))]$, as demonstrated in Equation (3.1). Specifically, the expected impact represents the expected value of the total number of infections, funerals, and close contacts of infected people, and the expected risk corresponds to the expected $CVaR_\alpha$ term in Eq. (3.2a). Table 3.1 presents results for the optimal objective function value for Eq. (3.2a), expected impact, expected risk, and the expected total cost over the four different risk-averseness levels described above. We also present values of the expected impact and expected risk for various combinations of $\lambda = \{0, 1, 10, 100\}$ and $\alpha = \{0.05, 0.5, 0.95\}$ under the $\$70M$ budget level in Table 3.2. In both Tables 3.1 and 3.2, the "Expected Risk" under the risk-neutral model, where $\lambda = 0$, is computed as the expected total number of infections, funerals, and close contacts of infected people over all periods for the $(1 - \alpha)$ worst scenarios.

Table 3.1 Comparison of Objective Value, Expected Impact, Expected Risk, and Expected Cost under Various Risk-Averseness Levels

Risk-aversion	**Risk Neutral**	**Weak**	**Mild**	**Strong**
(λ, α)	(0, 0.95)	(1, 0.05)	(10, 0.5)	(100, 0.95)
Objective Value [a]	3,881,046	7,771,744	44,365,553	409,005,446
Expected Impact	3,881,046	3,881,501	3,882,344	3,884,815
Expected Risk [b]	5,628,125	3,890,243	4,048,321	4,051,206
Expected Cost ($\$M$)	69.70	69.76	69.84	69.85

[a] *The calculation with units is represented as "Expected Impact" + λ * "Expected Risk"*
[b] *The Expected Risk is the $CVaR_\alpha$ and does not include preceding λ coefficient*

According to Table 3.1, the risk-neutral model has the smallest expected impact but the largest expected risk compared to all other risk-averseness levels. This indicates that the risk-neutral model provides the least expected number of infections, funerals, and close contacts over all scenarios, but once one of the worse-case scenarios happens, it gives much larger number of infections, funerals, and close contacts compared to the risk-averse model. When both λ and α increase, the level of risk-averseness increases. Consequently, the optimal objective function value significantly increases due to the additional values of risk that are added to the objective formulation. The expected impact also increases, implying that there is a price for being risk-averse in terms of the increased number of infections, funerals, and close contacts under a more risk-averse policy. Moreover, the total cost of allocated capacity, treatment, and vaccination increase slightly when the risk-averseness level increases, implying that more budget is needed as the decision maker becomes more risk-averse.

Table 3.2 Expected Impact and Expected Risk for Different Risk-averseness Levels

$\lambda \backslash \alpha$	**0.05**		**0.5**		**0.95**	
	Expected Impact	Expected Risk [a]	Expected Impact	Expected Risk [a]	Expected Impact	Expected Risk [a]
0	3,881,046	3,957,443	3,881,046	4,512,163	3,881,046	5,628,125
1	3,881,501	3,890,243	3,881,323	4,047,577	3,887,508	4,054,319
10	3,881,053	3,889,802	3,882,344	4,048,321	3,883,418	4,050,082
100	3,883,462	3,892,219	3,881,704	4,047,882	3,884,815	4,051,206

[a] *The Expected Risk is the* $CVaR_\alpha$ *and does not include preceding* λ *coefficient*

Each row of Table 3.2 shows the change of the expected impact and expected risk when we fix the value of one of the risk parameters ($\lambda = \{1, 10, 100\}$ and $\alpha = \{0.05, 0.5, 0.95\}$) and change the other. All optimality gaps for the computational results in Table 3.2 are between 0.51% and 1.26%. According to the results, the largest expected risk occurs when $\lambda = 0$ for each α value. Similar to Table 3.1, in Table 3.2 the expected risk is the highest and the expected impact is the lowest under the risk-neutral model. When we move from risk-neutral ($\lambda = 0$) to risk-averse ($\lambda = \{1, 10, 100\}$), the expected impact always increases. However, changing the λ parameter have a non-monotonous influence on the expected impact. When fixing the λ value and increasing the α value, the expected risk increases because we increase the confidence level for the impact of scenarios that is under the VaR value. When we increase α from 0.05 to 0.95, the risk-averseness level increases, and the expected impact also shows an increasing trend for all risk-averse policies ($\lambda \geq 1$).

Resource Allocation under different Risk-Averse Policies Table 3.3 presents the allocation of the budget over the five stages of the planning horizon. We observe that the majority of the budget is allocated under stages one, two, and four, while

as the risk-averseness increases, the budget under stage one is slightly decreased and moved further into the future to be used later. The total budget used over all stages increases as the decision-maker becomes more risk-averse.

Table 3.3 The Budget ($\$M$) Allocation at Each Stage over Four Different Risk-Averseness Levels

Risk-averseness Level	Stage 1	Stage 2	Stage 3	Stage 4	Stage 5	Total
Risk-neutral	14.0	20.6	8.9	20.6	5.6	69.7
Weak Risk-aversion	12.1	22.4	9.0	20.6	5.6	69.8
Mild Risk-aversion	13.0	22.0	8.8	20.9	5.3	69.8
Strong Risk-aversion	13.8	20.9	9.0	20.8	5.4	69.9

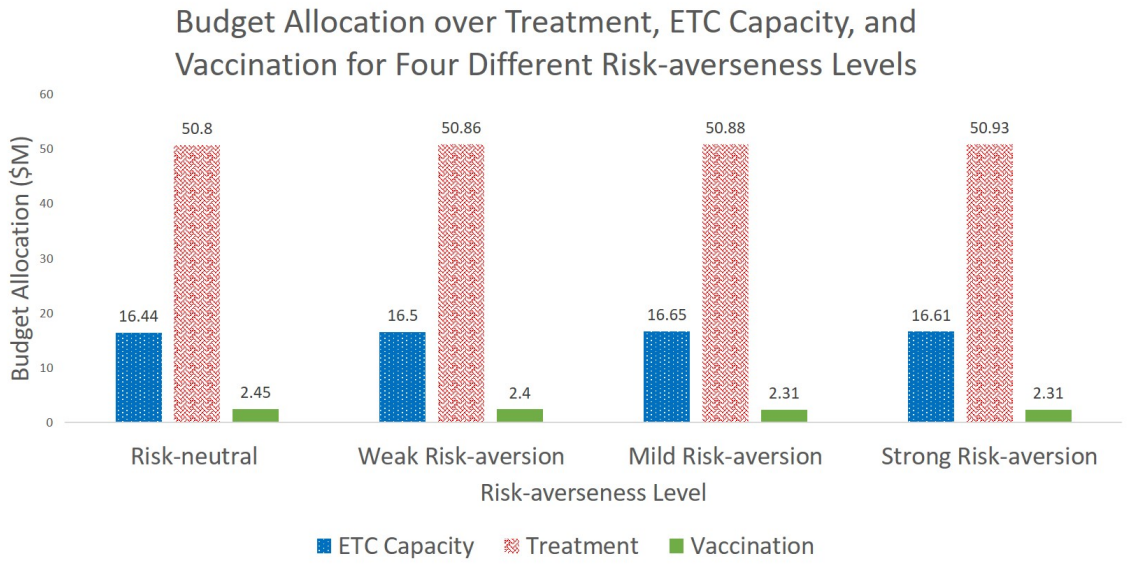

Figure 3.3 Budget allocation over treatment, ETC capacity, and vaccine for four different risk-averseness.

Figure 3.3 illustrates the budget allocation of treatment, ETC capacity, and vaccination for different risk-averseness levels. As shown here, the capacity and treatment budget shows an increasing trend, and the budget allocated to vaccination shows a decreasing trend when the risk-averseness level increases. This may imply

that as the decision-maker becomes more risk-averse, more investment is made on treatment rather than vaccination. It helps reduce variability in the set of scenarios that results in the highest number of infections and deaths.

The optimal allocation of treatment budget, ETC capacity, and vaccine allocation under different risk-averseness levels is presented in Figure 3.4. When the risk-averseness level increases, the budget allocated to Upper North Kivu, which has the highest initial infection level, is decreased by moving the budget to neighboring locations with a potential risk of getting infections from Upper North Kivu (Figure 3.4a). For example, under the strong risk-averseness level, the budget allocated to Middle Ituri and Lower Ituri increases because they are geographically close to Upper North Kivu and thus are under the risk of getting infections through the large migrant population from Upper North Kivu.

The total capacity allocation of 1700 beds over all regions under the risk-neutral and weak risk-averseness cases is increased to 1750 beds under the mild and strong risk-averseness levels to alleviate adverse outcomes under the worst-case scenarios exceeding the VaR value (Figure 3.4b). As the risk-averseness level increases, the model allocates more beds to some regions that have low infection levels, considering their proximity to highly-infected locations and the risk of getting more infections from those locations. For example, Lower Ituri, right above the Upper North Kivu, receives an increased number of beds under the strong risk-averseness level.

The number of vaccines allocated to each region varies under different risk-averseness levels (Figure 3.4c). The total number of allocated vaccines decreases when the risk-averseness level increases. Regions that initially have zero infections get zero bed capacity. However, they still get vaccination due to the migration impact and the expectation of the disease spread under the risk-neutral and all risk-aversion cases. Thus, in locations where the disease has just started, the model uses the budget for vaccination to stop or slow the epidemic's growth rather than building new ETCs.

(a)

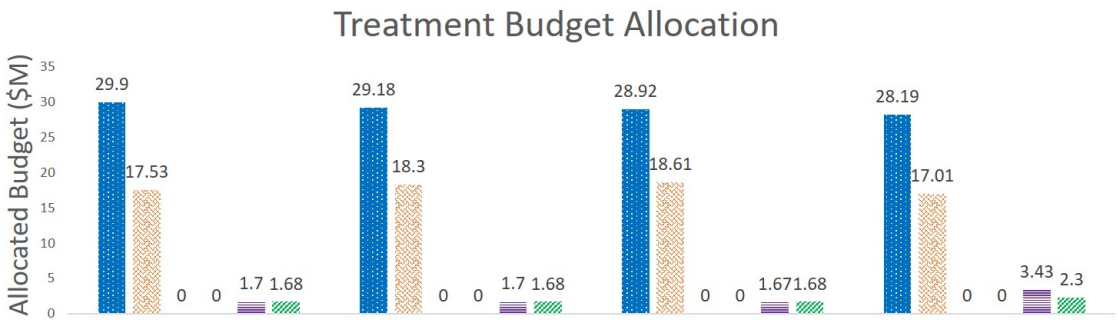

(b)

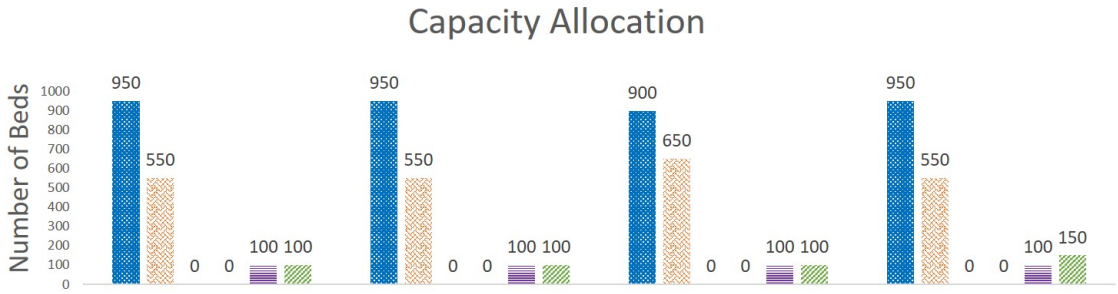

(c)

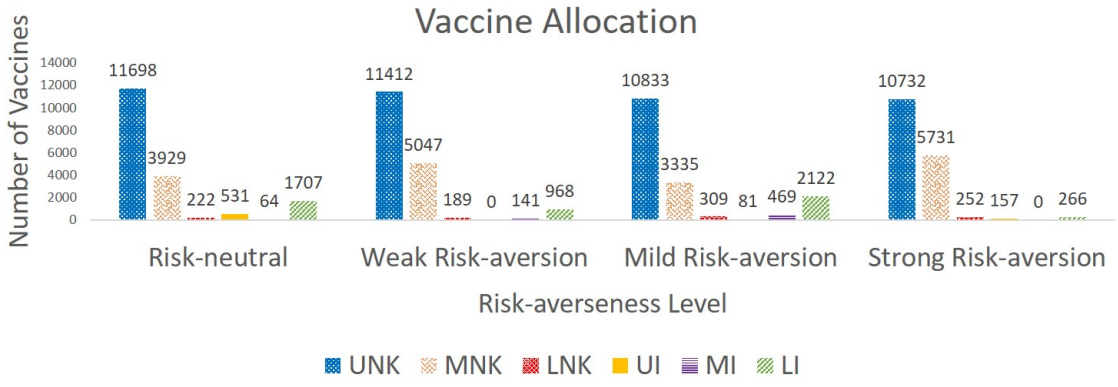

Figure 3.4 Treatment budget, capacity (bed), and vaccine allocation under different risk-averseness levels.

3.4.4 Analyzing the Impact of Delay in Vaccination

In this subsection, we compare the number of infections and funerals for each stage for the 5-stage planning horizon with respect to the delay of the vaccine application in the first stage (Delay 1), first two stages (Delay 2), first three stages (Delay 3), first four stages (Delay 4) and five stages (Delay 5) under the $\$70M$ budget level. For example, in "Delay 3", we fix the number of available vaccines in the first three stages to zero. In those first three stages, we assume a high transmission rate, which is equivalent to the low vaccine supply, and thus results presented here provide a lower bound on the number of infections and deaths. Here, we also consider a mild risk-averseness level by setting λ at 10 and α at 0.5.

The results of the cumulative number of infections and funerals in each type of delay in vaccines are shown in Figure 3.5, while Figure 3.6 demonstrates the non-cumulative infections and funerals for each delay option over no delay of vaccines for five stages. Both figures indicate that the number of infections and funerals increases exponentially over time for each delay type. The more the vaccination is delayed, the larger the infections and funerals are. Furthermore, the difference in the number of infections and funerals between "Delay 1" and "Delay 3" is larger than the difference between "Delay 3" and "Delay 5." A possible reason is that the vaccination at the initial stages of the disease transmission would decrease the transmission rate faster and cause fewer infections and funerals than vaccination at later stages. These results indicate that the vaccines should be supplied as soon as possible once the epidemic breaks out, given the vaccines' availability.

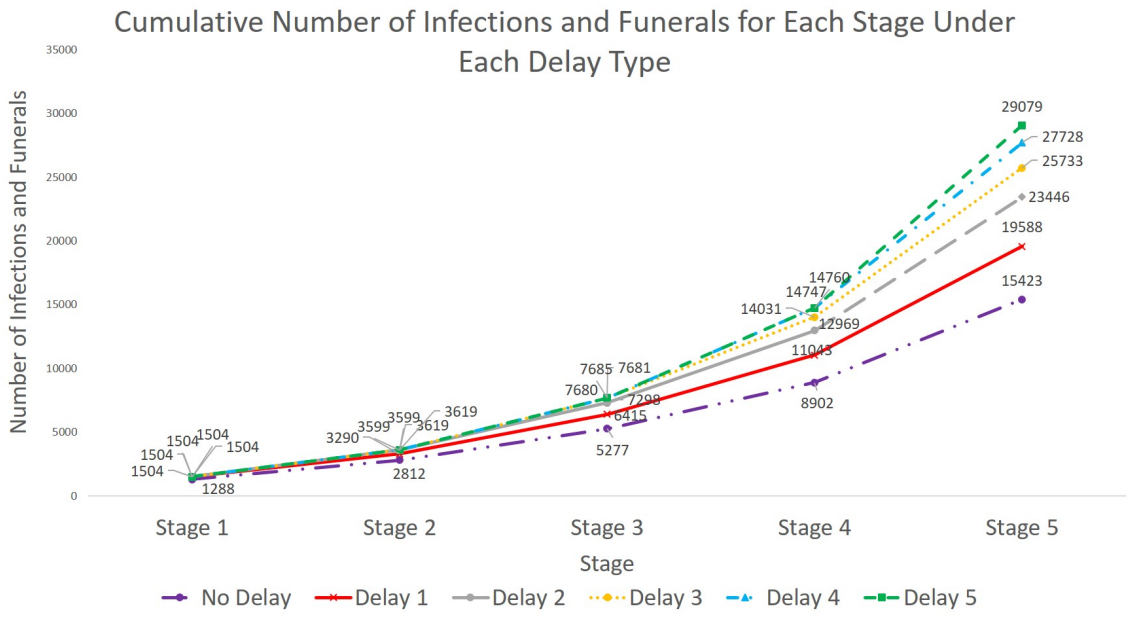

Figure 3.5 Cumulative number of infections and funerals for each stage under different types of delay ($\lambda = 10$ and $\alpha = 0.5$).

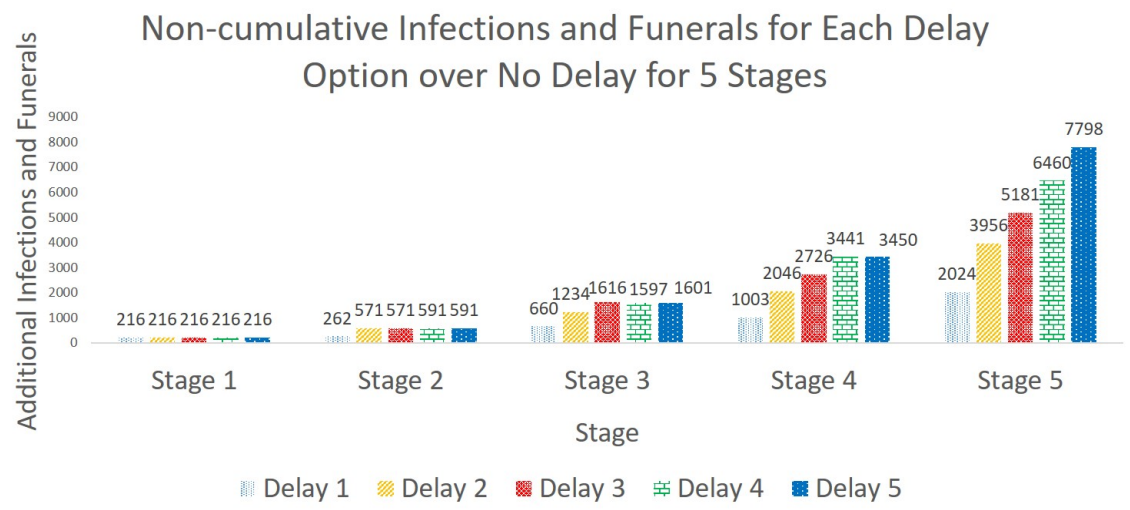

Figure 3.6 Non-cumulative number of infections and funerals for each delay option over no delay ($\lambda = 10$ and $\alpha = 0.5$).

3.5 Analyzing Vaccine Effectiveness and Acceptance Rates

In this section, we perform the sensitivity analysis on vaccination effectiveness and acceptance rates. Specifically, we adjust the vaccination effectiveness rate and the proportion of close contacts who are willing to get vaccinated. In WHO [2019c], the

vaccination effectiveness rate is estimated as 0.975. In our model, we test vaccination effectiveness rates varying from 0.7 to 0.975 in increments of 0.05. Specifically, we change the value of the parameter β_r from low to high to simulate the impact of varying vaccination effectiveness rates on the number and location of vaccines allocated.

Several papers study the willingness of people to be vaccinated. For instance, Kpanake et al. [2018] find that 38% of people always choose to be immunized for the Ebola Virus Disease. Mudatsir et al. [2019] conclude that 74% of the people who participate in the interview express their acceptance for an Ebola vaccine. In addition, Ughasoro et al. [2015] suggest that 80% of the respondents accept being vaccinated with the Ebola vaccine. Therefore, we consider four different vaccine acceptance rates in the sensitivity analysis, which are 0.01, 0.4, 0.8, and 1. In reality, the vaccine acceptance rate may not be as low as 0.01. However, considering that the vaccine supply is quite limited, even under a vaccine acceptance rate of 0.4, the number of people who are willing to get vaccinated is still more than the upper bound on the vaccine supply. Thus, we use a vaccine acceptance rate of 0.01 to observe the changes in the vaccine allocation when the upper bound of vaccine supply is larger than the number of people who are willing to get vaccinated. In particular, we use a new parameter f to represent the number of close contacts who are willing to be vaccinated. Thus, Constraint (3.2r) is replaced by:

$$O^{\omega}_{j,r} \leq H^{\omega}_{j,r} f, \qquad j \in J, \forall r \in R, \forall \omega \in \Omega. \tag{3.3}$$

Constraint (3.3) implies that the number of successfully vaccinated individuals at stage j in region r under scenario ω should be less than or equal to the number of close contacts who are willing to be vaccinated.

In this section, we assume that the amount of available vaccine supply changes with respect to the time period. For example, in the initial stages of an epidemic or a vaccine discovery, it is less likely to make sufficient vaccine supply available to all demand locations. As time progresses, the vaccine supply upper bound will also increase. In this section's analysis, the vaccine supply upper bound under each scenario is set to be 1000 at stage one, 2000 at stage two, 4000 at stage three, 5000 at stage four, and 6000 at stage five. The budget level for each test instance is set to be an ample level of $\$130M$. Since the number of people who are willing to get vaccinated at the initial stages is less than the number of available vaccines, the remaining vaccines can be allocated in the following stages. Thus, in this analysis, Constraint (3.2s) is replaced by:

$$\sum_{r\in R} O^{\omega}_{j,r} \leq \sum_{m=1}^{j} G^{\omega}_{m} - \sum_{m=1}^{j-1}\sum_{r\in R} O^{\omega}_{m,r}, \qquad j \in J, \forall \omega \in \Omega. \tag{3.4}$$

Constraint (3.4) ensures that the number of vaccines allocated to region r at stage j under scenario ω should be less than or equal to the total number of available vaccines up to stage j minus the total number of vaccines that are allocated to various regions from stage 1 until the end of stage $j-1$.

Figure 3.7 shows the optimal number and location of vaccines allocated under different vaccination effectiveness rates when the vaccine acceptance rate is fixed at 0.8. For all the cases, the Upper North Kivu has most of the vaccines allocated, followed by Middle North Kivu. Also, the number of vaccines allocated to these two regions has a complementary relationship. When Upper North Kivu receives more (fewer) vaccines, Middle North Kivu will get fewer (more) vaccines allocated. This is because these two regions suffer from Ebola the most. The total number of infections and deaths does not fluctuate much if the number of vaccines allocated to these two regions is in a range of 11,000 to 15,000 for Upper North Kivu and 2,000 to 6,000 for

Middle North Kivu. In addition, the total number of vaccines allocated under each case is close to the total supply upper bound of 18,000. Thus, we can conclude that, as long as the vaccine stays effective, no matter what vaccine effectiveness rate is, the total number of vaccines allocated will not significantly change under a limited supply of vaccines.

When the vaccination effectiveness rate increases, we also observe some of the vaccines that are allocated to regions with high levels of infections are moved to regions with fewer infections. Specifically, 17,670 vaccines allocated to Upper North Kivu and Middle North Kivu reduce to 16,113 vaccines when the vaccination effectiveness rate increases from 0.7 to 0.975. This result implies that the more effective the vaccine is, the fewer vaccines are needed in highly-impacted areas so that regions with lower infection could benefit from the remaining vaccines.

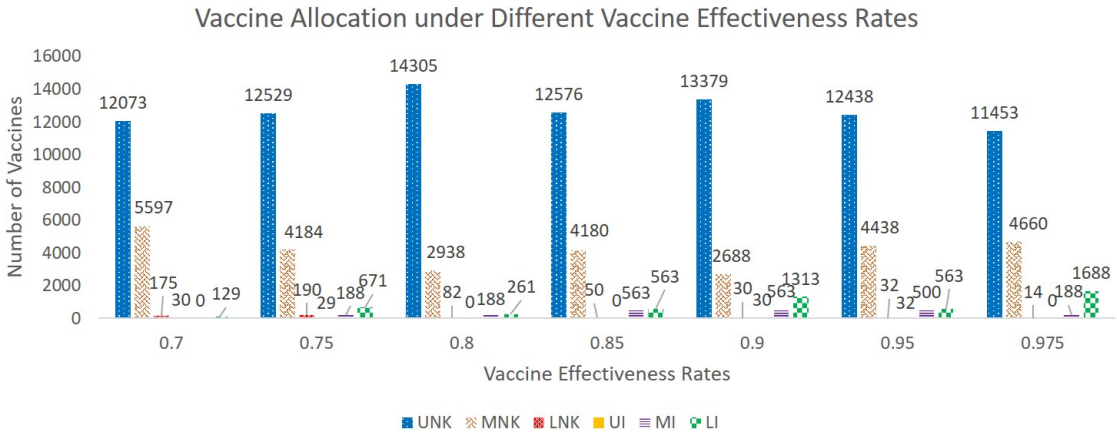

Figure 3.7 Vaccine allocation under different vaccine effectiveness rates ($\lambda = 10$ and $\alpha = 0.95$).

Figures 3.8a and 3.8b present the results for the first-stage and total vaccine allocation over all stages, respectively, under different vaccine acceptance rates when the vaccine effectiveness rate is fixed at 0.975. When the vaccine acceptance rate is 0.01, fewer vaccines are allocated in the first stage compared to the number of vaccines allocated under vaccine acceptance rates of 0.4, 0.8, and 1. Upper North

Kivu is the only region that receives vaccines at the first stage when the vaccine acceptance rate equals 0.4, 0.8, and 1 because it has the highest number of initial infections among all regions. However, under the vaccine acceptance rate of 0.01, the number of close contacts willing to get vaccinated in Upper North Kivu is less than the supplied vaccines in the first stage. Thus, some vaccines in hand are allocated to other regions.

Compared to the first stage vaccine allocation, the total vaccine allocation over all stages shows a similar trend under different vaccine acceptance rates. This is because as the number of infections increases in the following stages, the number of close contacts also significantly increases. Therefore, even under the vaccine acceptance rate of 0.01, the number of close contacts who are willing to get vaccinated is more than the vaccine supply upper bound when considering the planning horizon of five stages. Furthermore, remaining vaccines from previous time stages will be used in the following stages. The total number of vaccines allocated to Upper North Kivu under the 0.01 vaccine acceptance rate is less than those in other cases. This is because more vaccines become available under a quite low vaccine acceptance rate, and those available vaccines are allocated to other regions with infections lower than that of Upper North Kivu.

3.6 Discussion and Conclusions

This chapter presents a multi-stage mean-risk epidemics-vaccination-logistics model to address the optimal resource allocation challenges for epidemic control. We apply our model to the 2018-2020 EVD case in the Democratic Republic of the Congo (DRC). Because the information regarding the migration rates between regions in DRC is limited, we develop a method to estimate the transmission rate between each considered region. In our multi-stage stochastic programming model formulation, we use the CVaR in a nested form over multiple stages to minimize the total expected

(a)

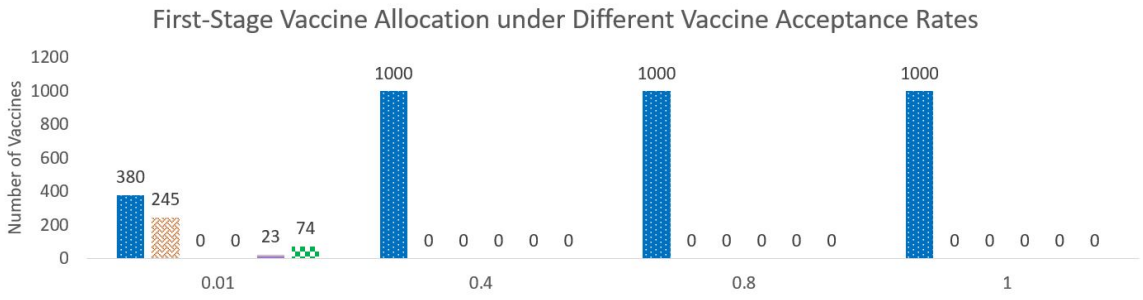

(b)

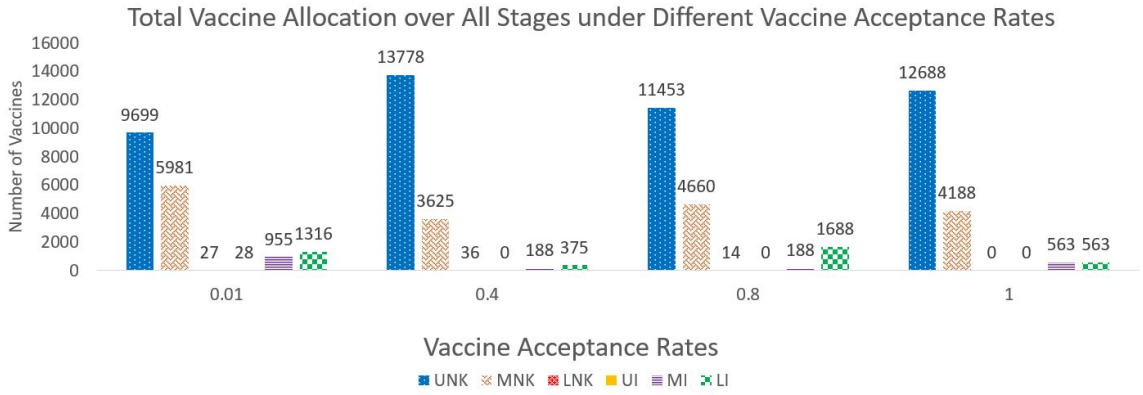

Figure 3.8 The first-stage and total vaccine allocation under different vaccine acceptance rates ($\lambda = 10$ and $\alpha = 0.95$).

number of infections, funerals, and close contacts of infected people, and a weighted risk in a five-stage planning horizon, including 15 weeks.

The results regarding the analysis of risk trade-off show that there is a price for being prepared for the worst set of disease-growth scenarios. In other words, a risk-averse decision-maker should expect a possible increase in the number of infections and deaths while trying to mitigate disastrous outbreak scenarios. Thus, when the mean-risk trade-off coefficient increases, the confidence level in a risk-averse model will improve while the expected impact on infections and deaths worsens. Furthermore, the total cost of treatment and vaccination increases as the decision-maker becomes more risk-averse.

Allocating the resources fully based on the initial infection level will increase the risk of experiencing more infections and deaths in some disease scenarios. For example, the initial infection level of Lower Ituri is not high. Still, the model considers the possible adverse scenarios that may happen in Lower Ituri and allocates more resources to Lower Ituri under the case of strong risk-aversion. Thus, the potential risk associated with the disease growth in regions that have low initial infection levels but are in close proximity to hot spots of infection should also be considered when making risk-averse decisions on epidemics resource allocation.

The analysis of resource allocation under different budget levels indicates that the initial infection level is the key parameter that influences the budget and capacity allocation among each region. The regions with high initial infection levels get more resources, similar to the findings in Yin and Büyüktahtakın [2021a]. Different from the former literature, we study the budget allocation trade-off between treatment and vaccination while also accounting for the disease transmission dynamics. The results of vaccine allocation under different budget levels suggest that priority must be given to treat and isolate infected individuals in ETCs, while vaccination is supplementary to treatment. This has also been justified by the study of Kucharski

et al. [2016], which states that ring vaccination might be insufficient to contain the outbreak if standard measures for controlling the transmission are not working, as in the EVD case in West Africa in early 2014. In another study, Kretzschmar et al. [2004] state that ring vaccination can contain the smallpox disease provided the intervention measures are very useful. Being risk-averse reinforces our findings on the resource-allocation priority of treatment over vaccination.

Our results also show that as the number of stages with no vaccines supplied increases, the number of infections, funerals, and close contacts exponentially increases even under other intervention measures, such as treatment and isolation. This result implies that vaccination is still quite effective when performed in addition to standard intervention measures, as shown in the studies of Kretzschmar et al. [2004], Ajelli et al. [2016], and Merler et al. [2016]. Under the same length of delay, the delay of the vaccine at the early stages will cause more infections and deaths compared to the delay in the late stages. This proves that when the vaccines are limited but available, we should supply them as early as possible to minimize the number of infections at the beginning of an outbreak. Similarly, Wells et al. [2019] mention that even modest delays in initiating vaccination could noticeably degrade the impact of the epidemic control.

Interestingly, the model allocates vaccination to regions that get no treatment resources under a limited budget because it estimates a disease spread to these locations due to human mobility. Specifically, the model uses the budget for vaccination in regions where the disease has just started to curb the growth of the epidemic, while in regions with high initial infections, the model gives priority to build new ETCs and treat infected people over vaccination.

The sensitivity analysis on the vaccine effectiveness and acceptance rates indicates that the number of vaccines supplied to Upper North Kivu and Middle North Kivu has a complementary relationship. The number of vaccines provided

to these two regions fluctuates under different vaccine effectiveness rates when the vaccine acceptance rate is fixed. This fluctuation does not influence the number of infections significantly.

When the vaccine effectiveness rate is fixed, vaccine acceptance rates affect vaccine allocation in the initial stages. Specifically, available vaccines are moved from highly impacted locations to less affected areas under a very low vaccine acceptance rate. In the early stages of an epidemic, there are fewer infections and close contacts, and the number of close contacts who are willing to get vaccinated is less than the number of vaccines supplied when the vaccine acceptance rate is very low. However, in the subsequent stages of an epidemic, the number of infections increases, thus significantly increasing close contacts. Therefore, even under a low vaccine acceptance rate, the number of close contacts who are willing to get vaccinated is much more than the available vaccine supply as the disease progresses over time. Consequently, those leftover and newly-supplied vaccines are allocated in the stages following the first stage to locations with both high and low infection levels. Thus, the total number of vaccines distributed over the whole planning horizon is similar under different vaccine acceptance rates.

This study leads to a number of important future directions. For example, the method we present for calculating the migration rate between each region could be further improved. Human behavior and social effects could be incorporated into the calculation of migration rates. For instance, Miami is not a metropolis compared to New York City. However, a substantial amount of people may travel to Miami for vacation. In our model, we only chose the metropolis of each region as the center of movement but did not consider other regions that may also have large short-term population migrations. This research could be extended by improving our estimation by considering more complicated environments to formulate the migration-estimation model.

In our epidemic-vaccination-logistics model, the term "logistics" represents the spatial and temporal allocation of ETCs, treatment budget used at ETCs as a function of T (treated) people, and the number of vaccines in region r at the end of period j under scenario ω. Here logistics do not involve details, such as distributing vaccines to certain locations within a region and its transportation specifics. A future extension of this work could investigate the transportation details of both vaccination and treatment resources, such as distributing those resources to specified locations within a region and its associated costs. Future work could also specify the transmission rate parameter, $\theta_{1,r}$, as a function of the vaccines allocated in region r, converting the model into a stochastic non-linear mixed-integer program. Both future directions would require the development of advanced solution algorithms, such as decomposition methods, global optimization, and cutting plane algorithms, to tackle the increased complexity of the mathematical model.

In this study, we present a general multi-stage mean-risk epidemics-vaccination-logistics model. This epidemic model could be adopted, for example, in the case of the COVID-19 pandemic. In such a model, the susceptible individuals can be divided into multiple sub-compartments based on their risk, demographics, and behaviors. For example, susceptible individuals can be divided into different sub-groups, such as people who wear masks and people under quarantine, with each group having a different infection rate, depending on the intervention measures applied. We can also analyze specific groups for vaccination, e.g., doctors, nurses, and volunteers to be injected. Increasing the number of compartments in a heterogenous-mixing epidemiological model will further complicate the epidemic-vaccination-logistics optimization model. Thus, the analysis of multiple specified groups can be studied in a more detailed agent-based simulation rather than a large-scale meta-population model as in our case.

For the pandemic control, we should also consider the international imported infections for the selected regions. Also, the travel patterns of people during the pandemic might influence the transmission of the disease. Therefore, our future research would present new mathematical models that will control a pandemic and help optimize resource allocation decisions.

CHAPTER 4

COVID-19: OPTIMAL ALLOCATION OF VENTILATOR SUPPLY UNDER UNCERTAINTY AND RISK

4.1 Introduction

The world is undergoing a major health crisis, which has now eventually turned into a pandemic. The Coronavirus Disease 2019 (COVID-19), first detected in Wuhan city of China at the end of 2019, has been creating havoc on human life and economies in all parts of the world. Countries worldwide enforce lockdown and quarantine rules to slow down the spread of the virus. The lockdown, imposing travel restrictions, and social distancing have severely affected the economy, from small-scale industries to stock prices and international trading. The virus has such a high transmission rate, causing more than 104.7 million cases globally, out of which 2.3 million people have succumbed to death by mid-February 2021 [JHU, 2021]. The continuous increase seen in coronavirus cases has made a worldwide scarcity of essential resources, such as ventilators, Intensive Care Unit (ICU) beds, Personal Protective Equipment (PPE), and masks. Effective, sufficient, and timely delivery of those critical resources to serve the COVID-19 patients has been a major challenge faced by the world countries during the pandemic.

COVID-19 is primarily an acute respiratory disease. Ventilator incubation delivers high oxygen concentrations while removing carbon dioxide and reduces the risk of hypoxia for COVID-19 patients [Meng et al., 2020]. The standard Acute Respiratory Distress Syndrome protocol mandates that the most severe COVID-19 patients, who constitute 5% of all COVID-19 patients, should receive ventilator support [Bein et al., 2016]. As a result, the life of many COVID-19 patients depends on the use of ventilators. The shortage of supplies and uncertainty in disease transmission has affected the proper allocation of ventilators, causing immense distress on the

healthcare system. Due to ventilator shortages worldwide during the pandemic's peak times, hospital officials have had to make life-altering resource allocation decisions and prioritized the care of COVID-19 patients [Ranney et al., 2020]. To tackle ventilator shortages and reduce the number of COVID-related deaths, studies have come up with new approaches for ventilator distribution. For example, Ranney et al. [2020] suggest that the demand for ventilators can be fulfilled by the government by allowing other industries to come together and help medical industries to cater to the needs of the ventilators. Another study by Castro et al. [2020] suggests that the government in Brazil should start thinking about expanding the resource capacity rather than only focusing on the allocation of the available resources for controlling COVID-19. White and Lo [2020] develop a framework for the distribution of ICU beds and ventilators depending on the priority scores using a scale of 1 to 8 based on patients' likelihood of survival and ethical considerations.

Operations Research (OR) methods have been widely used to determine optimal resource allocation strategies to control an epidemic or pandemic. Several studies have used multi-period OR models to optimize the allocation and redistribution of ventilators (see, e.g., Mehrotra et al. [2020], Bertsimas et al. [2020], and Blanco et al. [2020]). Other OR research models that study the epidemic diseases and resource allocation mainly focus on the logistics and operation management to control the disease in optimal ways [Büyüktahtakın et al., 2018a, Zaric and Brandeau, 2001, Yin and Büyüktahtakın, 2021a, Kaplan et al., 2003, Tanner et al., 2008, Coşgun and Büyüktahtakın, 2018]. We refer the reader to excellent reviews of Dasaklis et al. [2012] and Queiroz et al. [2020] for a discussion of OR models for epidemic resource allocation.

While OR has been an extremely useful tool for effective and timely allocation of resources as a response to epidemics, none of the former work has considered the ventilator allocation problem using a risk-averse spatio-temporal stochastic

programming model under uncertainty of asymptomatic infections. People move between regions, states, and countries, which aggravates the disease transmission to the other areas. Evaluating undetected or asymptomatic individuals is critical for determining disease dynamics because asymptomatic individuals move around and unknowingly infect other individuals [McCrimmon, 2021]. Thus, the short-term migration of people is a critical factor that needs to be considered to forecast the transmission of the COVID-19 realistically. However, the short-term migration rate is hard to predict and is affected by interventions and human behaviors. Furthermore, disease transmission rates are not constant and rather evolve over time with government interventions, such as the lockdown or social distancing measures. This change in the transmission rates also should be considered in a realistic model. To our knowledge, none of the former OR ventilator allocation models have integrated the epidemiological aspects of the disease and resource allocation challenges in one optimization model.

In this chapter, we address the limitation of realistically forecasting the transmission of COVID-19 and build a risk-averse multi-stage stochastic epidemics-ventilator-logistics programming model to study the ventilator allocation for the treatment of severe COVID-19 patients. Our model considers the uncertainty of untested asymptomatic individuals during the transmission of COVID19 and involves various pandemic scenarios for the proportion of untested infections during each time stage of the planning horizon. Our model also incorporates the short-term migration between the highly-impacted regions while using changing transmission rates under various non-pharmaceutical intervention measures. The model optimizes the distribution of ventilators while minimizing the total expected number of infected and deceased people. We calibrate, validate, and test our epidemiological ventilator allocation model using COVID-19 data collected during the pandemic's early stages.

4.1.1 Key Contributions and Insights

In summary, former stochastic programming approaches on ventilator allocation in a pandemic situation have involved a time domain of only two stages, and have not integrated an epidemic model within the stochastic program. Furthermore, the mathematical models on the forecast of the COVID-19 do not include the uncertainty of untested asymptomatic infections. They do not incorporate the impact of short-term migrations on COVID-19 transmission in an epidemiological model. Also, former studies on the COVID-19 modeling and logistics have omitted the time consistency of the risk for making decisions over multiple stages of a stochastic program under extreme pandemic scenarios.

Our modeling and applied contributions to the epidemiology and OR literature are summarized below.

Modeling contributions: First, to our knowledge, this is the first study that addresses the optimal distribution of ventilators to control a pandemic in a multi-stage stochastic mean-Conditional Value at Risk (CVaR) model. Considering multiple stages is essential to capture uncertain disease dynamic over multiple time periods. This model includes many realistic effects critical in the COVID-19 pandemic, including untested asymptomatic infections, human movement among multiple regions, and evolving transmission rates under non-pharmaceutical intervention measures. Second, we consider the uncertainty of the proportion of untested asymptomatic infections at each stage and integrate this unknown dimension of the pandemic by generating a multi-stage scenario tree. Third, we present a new susceptible (S)- tested infected (I)- untested asymptomatic (X)- hospitalized (H)- ICU (C)- recovered (R)- death (D) compartmental disease model specialized for the COVID-19, and also incorporate the short-term human migration among multiple regions into this epidemiological model. Fourth, we derive a new time- and space-varying disease transmission formulation, which takes into account the

impact of government interventions on transmission rates. Fifth, we formulate a budget-constrained ventilator allocation logistics model. Sixth, we incorporate a time-consistent CVaR risk-measure and the expectation criterion in the objective function to alleviate the impacts of extreme pandemic scenarios. Lastly, we integrate all those elements into one epidemics-ventilator-logistics mathematical formulation, which minimizes the number of infections and deceased individuals under different intervention strategies while determining the optimal timing and location of resources (ventilators) allocated. Our model combines the forecast of the transmission of COVID-19 and the determination of optimal ventilator allocation strategies in one formulation. Accordingly, the decision-maker can evaluate possible outcomes of wait-and-see decisions while foreseeing how the disease could progress in each time period.

Applied Contributions: We apply our general multi-stage mean-risk epidemics-ventilator-logistics model to the case of controlling the COVID-19 in highly-impacted counties of New York and New Jersey. We collect real data from various resources and provide researchers with compact epidemiological, population and logistics-capacity data for COVID-19. Using this data, we calibrate, validate, and test our model, which could be used as a decision support tool for fighting against the COVID-19. Our model can also be adapted to study other similar diseases transmission dynamics and logistics.

Key Recommendations to Decision Makers. This study provides optimal risk-averse ventilator allocation policies under different risk levels that the decision-maker can take to control the COVID-19. Based on our results, we offer the following recommendations to inform resource allocation policies under a pandemic:

(**i**) The short-term movement of people influences the number of new infections even if the disease transmission rate stays the same.

(**ii**) The number of treated people in the ICU may stay at the capacity limit under different intervention strategies because this value depends on the minimum number of patients who require a ventilator for treatment and the scarce ventilator supply. There is also a lag time to observe the impacts of government non-pharmaceutical interventions on the number of hospitalized, ICU and deceased individuals.

(**iii**) "Lockdown" is the best strategy to control the COVID-19. However, the "Mask and Social Distance" intervention following a certain period of "Lockdown" is the second-best choice, considering the need for opening facilities and businesses.

(**iv**) The region with a high initial transmission rate and low initial ICU capacity will have more ventilators allocated under a limited budget and low or high transmission scenarios. Independent from the budget level, the region with a low initial transmission rate and low initial ICU capacity gets more ventilators allocated under a medium transmission scenario.

(**v**) Under a medium and ample budget level, the model allocates more capacity to the regions with a higher population and a larger initial number of infections but with a lower transmission rate. A large-enough budget also provides some flexibility in delaying ventilator allocation to some regions. In contrast, all of the ventilators are allocated at the first two stages under a limited budget.

(**vi**) Considering risk in decision-making improves the confidence level for reducing the loss of lives under risky pandemic scenarios. However, a risk-averse decision-maker should also expect a possible increase in the number of infections and deaths while mitigating disastrous outbreak scenarios.

4.2 Problem Formulation

This section presents the description of the notations, compartmental disease model, the formulation for transmission rates, uncertainty and scenario tree generation scheme, specific features and assumptions made in the mathematical model, a brief description of the CVaR, and the formulation for our epidemics-ventilator-logistics model.

4.2.1 Model Notation and Formulation

Below we provide notations used for the rest of the paper.

Sets and Indices:

J: Set of time periods, $J = \{0, ..., \overline{J}\}$.

R: Set of regions, $R = \{1, ..., \overline{R}\}$.

Ω: Set of scenarios, $\Omega = \{1, ..., \overline{\Omega}\}$.

N: Set of nodes in the scenario tree, where $n \in N$.

j: Index for time period, where $j \in J$.

r: Index for region where $r \in R$.

ω: Index for scenario, where $\omega \in \Omega$.

State Variables:

$S^{\omega}_{j,r}$: Susceptible individuals in region r at stage j under scenario ω.

$I^{\omega}_{j,r}$: Tested symptomatic infected individuals in region r at stage j under scenario ω.

$X^{\omega}_{j,r}$: Untested asymptomatic infected individuals in region r at stage j under scenario ω.

$H^{\omega}_{j,r}$: Hospitalized individuals in region r at stage j under scenario ω.

$C^{\omega}_{j,r}$: Individuals treated in the intensive care unit (ICU) in region r at stage j under scenario ω.

$R^{\omega}_{j,r}$: Recovered individuals in region r at stage j under scenario ω.

$F^{\omega}_{j,r}$: Deceased individuals in region r at stage j under scenario ω.

$O^{\omega}_{j,r}$: Number of tested symptomatic infected individuals admitted to the hospital in region r at stage j under scenario ω.

$\overline{I}^{\omega}_{j,r}$: Number of tested symptomatic infected individuals who cannot be admitted to the hospital due to limited capacity in region r at stage j under scenario ω.

$\overline{C}^{\omega}_{j,r}$: Number of individuals admitted to ICU in region r at stage j under scenario ω.

$K^{\omega}_{j,r}$: Number of hospitalized individuals not admitted to the ICU due to the limited availability of ventilators in region r at stage j under scenario ω.

$U^{\omega}_{j,r}$: Number of cumulative ventilators (ICU capacity) in region r at stage j under scenario ω.

$\breve{I}^{\omega}_{j,r}$: Number of infections caused by short-term migration in region r at stage j under scenario ω.

Parameters:

λ_1: Recovery rate of tested symptomatic infected individuals in region r.

λ_2: The death rate of tested symptomatic infected individuals in region r.

λ_3: Hospitalization requirement rate of tested symptomatic infected individuals in region r.

λ_4: Recovery rate of the hospitalized individuals in region r.

λ_5: Death rate of hospitalized individuals in region r.

λ_6: Ventilator requirement rate of hospitalized individuals in region r.

λ_7: Recovery rate of ICU patients in region r.

λ_8: Death rate of ICU patients in region r.

λ_9: Recovery rate of untested asymptomatic individuals in region r.

$\sigma_{1,j,r}$: Transmission rate of tested symptomatic infected individuals in region r at stage j.

$\sigma^{\omega}_{2,j,r}$: Proportion of untested asymptomatic infections in region r at stage j under scenario ω.

$T^{\omega}_{j,r}$: Hospital capacity in region r at stage j under scenario ω.

$U_{0,r}$: Initial number of ventilators (ICU capacity) in region r.

e_1: Cost of each ventilator.

Δ: Total budget for ventilators.

Risk parameters:

α: Confidence level of value-at-risk, where $\alpha \in [0, 1)$.

λ: Non-negative risk preference parameter or mean-risk trade-off coefficient.

Risk variables:

η^{ω}_{j}: Value at risk for each stage j under scenario ω.

z^{ω}_{j}: Value exceeding the value-at-risk at the confidence level α at stage j under scenario ω.

Non-anticipativity parameters:

n: The serial number of nodes in the scenario tree, where $n \in N$.

$t(n)$: The corresponding stage that node n marked in the scenario tree.

$\beta(n)$: The set of scenarios that pass through node n.

Decision variables:

$y^{\omega}_{j,r}$: Number of ventilators allocated to region r at the end of stage j under scenario ω.

4.2.2 Compartmental Disease Model Description

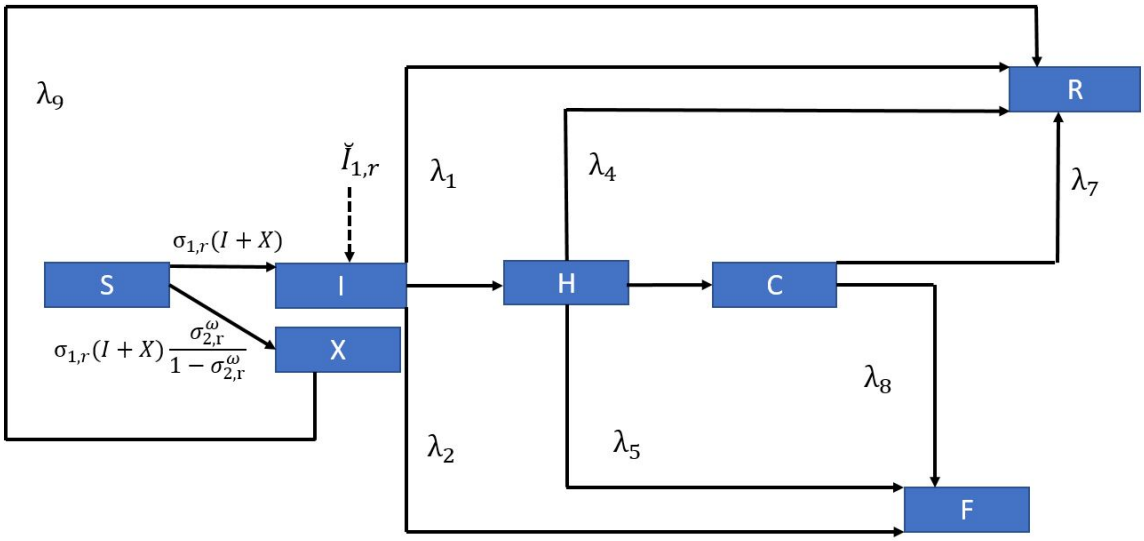

Figure 4.1 One-step COVID-19 compartmental model.

Figure 4.1 shows the transmission dynamics of COVID-19 in each region r at each time period j for a particular scenario ω. In this figure, susceptible individuals (S) can be infected and become infected (either symptomatic or asymptomatic). Asymptomatic infections (X) may have slight or no symptoms throughout the infection period and will recover with a rate of λ_9. Tested symptomatic infections (I) may recover or die with rates of λ_1 and λ_2, respectively, if they are not treated in the hospital (H). Note that $\breve{I}^{\omega}_{j,r}$ with an incoming dashed arc to the I compartment represents the number of infected people coming into the region r at stage j under scenario ω from neighboring regions. Tested infected individuals (I) move to the hospital (H) compartment, depending on the number of tested infections (I) and available hospital capacity. Some of the treated infected people in the hospital (H) will recover with a rate of λ_4. The situations of some patients in the hospital (H) may get worsen, and thus they may be transferred into the intensive care unit (we use C to represent ICU), and those individuals need ventilators for the treatment.

Similar to the case of admittance into the hospital, the number of hospitalized patients transferred into ICU at each time period is equal to the minimum of the number of patients who need to be transferred into ICU and the number of available ventilators. The patients who are not able to receive the treatment in the ICU due to the limitation on the number of available ventilators may die at a rate of λ_5. After being treated in the ICU, some of the patients may recover with a rate of λ_7, while others may die with a rate of λ_8. Different from a typical compartmental model, the transfer rate from I to H and H to C is not a constant, and it depends on the available capacity in the H and C compartments, respectively, as discussed previously.

4.2.3 Time- and Space-Varying Transmission Rate

In this subsection, we formulate the transmission rate $\sigma_{1,j,r}$ as a time- and space-varying parameter, which depends on the government interventions taken at time j and region r. Since the onset of the COVID-19, many governments have imposed different intervention strategies to reduce the transmission rate. At a certain stage, each intervention has a different impact on the transmission rate for the next stage. In this chapter, we incorporate three main non-pharmaceutical interventions to formulate the time-varying transmission rate — none, mask and social distancing, and lockdown.

Let $x^1_{j,r}$, $x^2_{j,r}$, and $x^3_{j,r}$ be binary decision variables that correspond to none ($i = 1$), mask and social distancing ($i = 2$), and lockdown ($i = 3$) interventions, respectively, taken at stage j and region r. If $x^i_{j,r}$ takes a value 1, then intervention i is employed; otherwise, it is not employed, at stage j and region r. The transmission rate at stage $j + 1$ in region r is a function of the transmission rate and specific intervention employed at stage j in the same region, as given in the below equations:

$$\sigma_{1,j+1,r} = \sigma_{1,j,r}(m^1_{j,t}x^1_{j,r} + m^2_{j,t}x^2_{j,r} + m^3_{j,t}x^3_{j,r}) \quad \forall j \in J \setminus \{\overline{J}\},\ r \in R, \tag{4.1}$$

$$x^1_{j,r} + x^2_{j,r} + x^3_{j,r} = 1 \quad \forall j \in J,\ r \in R, \tag{4.2}$$

$$x^1_{j,r}, x^2_{j,r}, x^3_{j,r} \in \{0, 1\} \quad \forall j \in J,\ r \in R, \tag{4.3}$$

where $m^i_{j,t}$ represents the percent change in the transmission rate with respect to the binary decision variable $x^i_{j,r}$ for intervention $i = 1, 2, 3$ taken at stage j in region r. Equation (4.1) shows that the transmission rate at stage $j + 1$ is a function of the transmission rate at stage j and the intervention strategy i taken at stage j. Equation (4.2) indicates that only one intervention measure can be taken at each stage j. Equation (4.3) describes the binary nature of intervention decisions.

The transmission rate in our model is not equal to the basic reproduction number, R_0. It shows how many new tested infections will be caused by the symptomatic and asymptomatic infections from the previous stage. Since the number of new asymptomatic infections is uncertain, the number of new infections (both symptomatic and asymptomatic) changes under different scenarios even if the transmission rates at each stage j stay the same.

There is a delay in the impact of the government' interventions on the number of infections and the reaction to the test results is also slow. Therefore, we calculate the transmission rate for the first two stages directly using the real data from JHU [2020], independent from the intervention type. Based on the first two-stage transmission rates, we calculate the transmission rates from stages three to five using the formulation (4.1)–(4.3) for each intervention strategy. Also, the values of $m^i_{j,t}$ are trained using the real data obtained from JHU [2020]. As an example, the initial transmission rates for the first two stages in New York and New Jersey and the impacts of government intervention strategies $m^i_{j,t}$ are shown in Table 4.5 under Subsection 4.3.2.

4.2.4 Uncertainty and Multi-period Scenario Tree

Data regarding undetected or untested asymptomatic cases is lacking and uncertain. Therefore, we model the uncertainty regarding the proportion of untested asymptomatic infections ($\sigma^{\omega}_{2,r}$) by generating a set of scenarios $\omega \in \Omega$, each representing a specific realization of the uncertain proportion of untested asymptomatic individuals over multiple time periods. Our scenario generation approach is similar to Alonso-Ayuso et al. [2018]'s method developed to model the demand uncertainty in forestry management. Each scenario has a probability of p^{ω} and $\sum_{\omega \in \Omega} p^{\omega} = 1$. Since data is not available to describe the probability distribution of the uncertain variable ($\sigma^{\omega}_{2,r}$), we assume that the uncertain parameter follows a normal distribution. The lower and upper bounds for the proportion of asymptomatic infections are obtained from the study of Meller [2020]. The lower bound value for the random variable is considered as the value of 0.001-quantile and the upper bound is considered as the value of 0.999-quantile of the normal distribution.

As an example, Figure 4.2 shows a particular scenario tree for the proportion of untested asymptomatic infections ($\sigma^{\omega}_{2,r}$) for a two-stage problem. We consider three realizations at each node of the scenario tree by dividing its normal distribution into three discrete parts [low (L), medium (M), high (H)]. The low and high realizations have a probability of 0.3, and the medium realization has a probability of 0.4. Each path from the root node to the leaf node of the scenario tree represents a scenario ω. The probability of a scenario ω, p^{ω}, is calculated as the multiplication of probabilities on the path for scenario ω. For two stages, 9 (3^2) scenarios will be generated in this instance. The non-anticipativity constraints indicate that two scenarios are inseparable at a stage j if they share the same scenario path up to that stage. This means that the corresponding decision made at this stage for those two scenarios should also be the same.

The value of the proportion of asymptomatic infections has a mean μ_r^j and standard deviation σ_r^j at stage j. We use Q_h to represent the value of h-quantile in the normal distribution. For each node n in the scenario tree, the mean value of the low realization is the value of 0.15-quantile ($E(\mu_{r,low}^n | Q_{0.001} \leq \mu_{r,low}^n \leq Q_{0.30}) = Q_{0.15}$), the mean value of medium realization is the value of 0.50-quantile ($E(\mu_{r,medium}^n | Q_{0.30} \leq \mu_{r,medium}^n \leq Q_{0.70}) = Q_{0.50}$), and the mean value of high realization is the value of 0.85-quantile ($E(\mu_{r,high}^n | Q_{0.70} \leq \mu_{r,high}^n \leq Q_{0.999}) = Q_{0.85}$). For node 0 in our example, the proportion of untested asymptomatic infections at stage $j = 0$ has $\mu_r^0 = 0.26$ and $\sigma_r^0 = 0.05$. The low, medium, and high realizations at node 0 in stage $j = 0$ and nodes 1 and 3 in stage $j = 1$ are given in Table 4.1 below. According to the distributions presented in Table 4.1, the proportion of untested asymptomatic infections in stage 1 is realized as 0.21 (Low) at node 1, 0.26 (Medium) at node 2, and 0.31 (High) at node 3.

Table 4.1 The 0.15-, 0.50-, 0.85-Quantiles of the Normal Distribution at Nodes 0, 1, and 3 of the Scenario Tree in Figure 4.2 and the Associated Node of the Uncertain Parameter Realization.

	Low (realized node)	Medium (realized node)	High (realized node)
	$Q_{0.15}$	$Q_{0.50}$	$Q_{0.85}$
Node 0	0.21 (node 1)	0.26 (node 2)	0.31 (node 3)
Node 1	0.17 (node 4)	0.21 (node 5)	0.25 (node 6)
Node 3	0.12 (node 10)	0.31 (node 11)	0.50 (node 12)

4.2.5 Model Features and Assumptions

Since the transmission of COVID-19 is affected by many factors, data to calibrate some of the model parameters, such as the impact of human mobility, is either lacking or inaccurate. Therefore, we incorporate some important features and make some

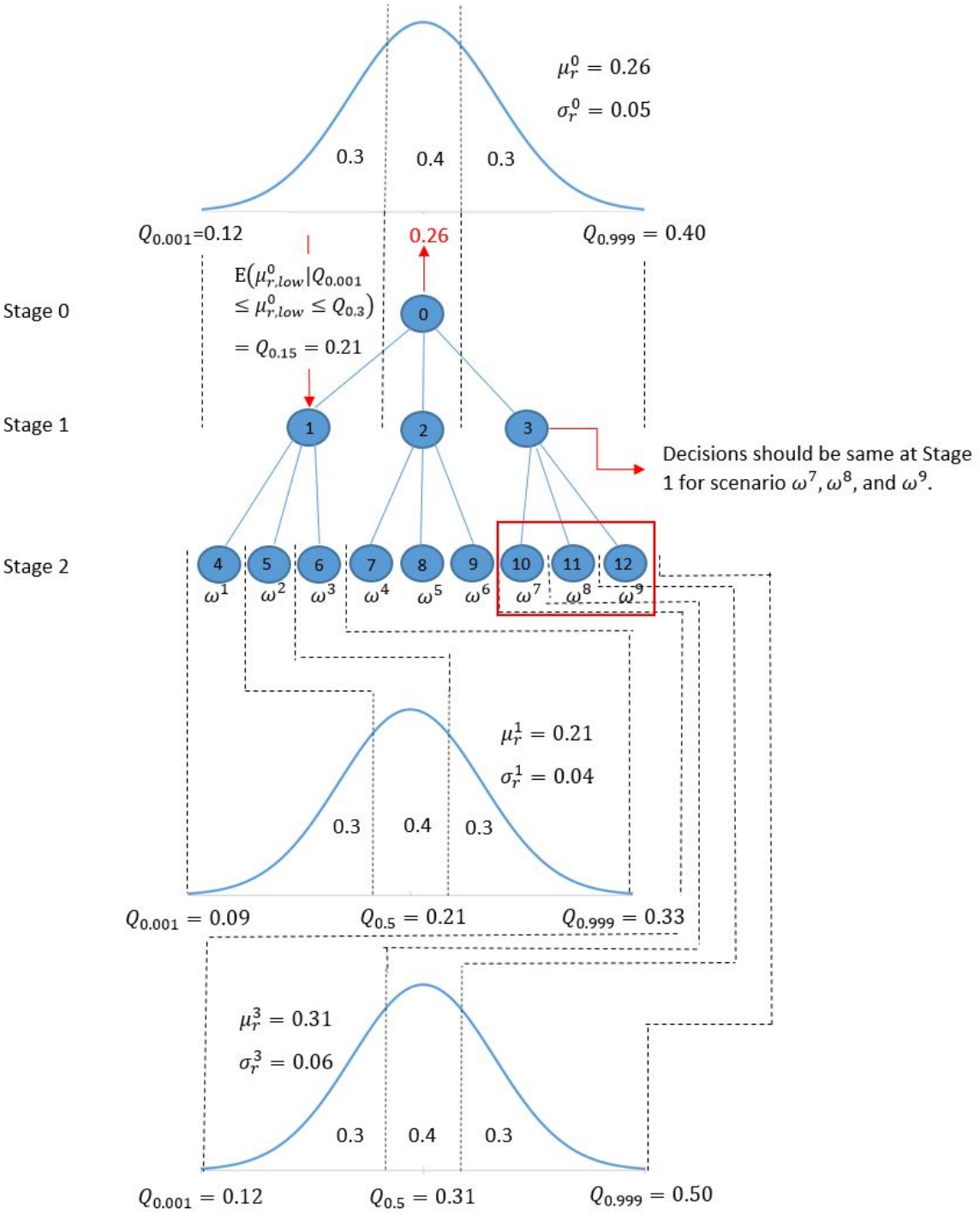

Figure 4.2 Multi-stage scenario tree generation example for the uncertain proportion of untested asymptomatic infections ($\sigma_{2,r}^{\omega}$).

assumptions in the model formulation.

Important features. First, we consider the impact of different intervention strategies on the disease transmission rate and adjust the short-term migration population depending on the intervention strategy. For instance, under the lockdown strategy, we assume that the short-term migration among each county is zero. Under mask and social distancing strategies, the short-term migration population among each county is reduced to 60% of the original value, as estimated from the study of Lee et al. [2020]. Second, we incorporate the cost for purchasing ventilators to provide a capacity limitation on the total number of ventilators that could be allocated for treating COVID-19 patients. Since there are significant fluctuations in the ventilator prices [Glass, 2020], we consider the minimum purchase price for each ventilator acquired. Third, we train the real data to determine the impact rate of each intervention strategy on the disease transmission rate. The trained value of the impact of interventions can only be used in the regions considered in our case study since all the selected counties in New York and New Jersey are geographically close to each other, and thus interventions have similar social effects. However, for example, the impact of intervention strategies in a rural area may be different from those taken in a city. To estimate the COVID-19 transmission in other regions of the United States, the model should be re-trained using the associated data.

Assumptions. First, since studied counties in New Jersey and New York are geographically close to each other, the proportions of untested asymptomatic infections at each stage j under scenario ω are set to be the same for each region r. Second, the model considers allocating newly purchased ventilators for the treatment of COVID-19 patients instead of re-allocating existing ventilators from other counties or states since the demand for ventilators during the disease's peak periods is high for all the counties and states, and there is a lead time for transfer of the ventilators between the states that are far from each other. Here, we also assume a central

decision maker entitled to allocate a given supply of ventilators to multiple regions. Third, the infected individuals who cannot be treated in the hospital (both severe and less severe) due to the limited capacity have the same death rate as the ICU patients because some of those infections may worsen without professional treatment. Fourth, we assume that all symptomatic individuals are tested, and asymptomatic infected individuals are untested. Fifth, we assume that people react to the pandemic by anticipating the government's interventions and may start social distancing and quarantining days or weeks before an intervention is imposed [Zhang et al., 2020b, Fischer et al., 2020]. Thus, the transmission rate with either doing nothing or mask and social distancing shows a decreasing trend in later stages of the pandemic due to physical distancing among people. Lastly, we use each county's ICU capacity from JHU [2020] as the initial ventilator availability. We assume that non-COVID-19 patients use 60% of this capacity [Mehrotra et al., 2020]. Thus, only 40% of the initial ICUs are available for treating the COVID-19 patients.

4.2.6 Multi-Stage Risk and Time Consistency

The α-quantile of the cumulative distribution of a random variable z, $\inf_\eta\{\eta \in \mathbb{R} : F_z(\eta) \geq \alpha\}$, is defined as the value-at-risk (VaR) at the confidence level $\alpha \in \{0, 1\}$ and denoted by $\text{VaR}_\alpha(z)$. The conditional expected value that exceeds the VaR at the confidence level α is called conditional value-at-risk (CVaR), defined as $\text{CVaR}_\alpha(z) = \mathbb{E}(z \mid z \geq \text{VaR}_\alpha(z))$. For a minimization problem, VaR_α is the α-quantile of the distribution of the cost, and it provides an upper bound on the cost that is exceeded only with a small probability of $1 - \alpha$. CVaR_α measures an expectation of the cost that is more than VaR_α, and can be calculated as an optimization problem as follows [Rockafellar and Uryasev, 2002]:

$$\text{CVaR}_\alpha(z) = \inf_{\eta \in \mathbb{R}} \{\eta + \frac{1}{1-\alpha}\mathbb{E}([z - \eta]_+)\},$$

where $(a)_+ := max(a, 0)$ for any $a \in \mathbb{R}$.

We formulate our model as a mean-risk minimization problem:

$$\min_{x \in X} \{\mathbb{E}(f(x, \omega)) + \lambda \text{CVaR}_\alpha(f(x, \omega))\}, \tag{4.4}$$

where $\mathbb{E}(f(x, \omega))$ is the expected cost function over the scenarios $\omega \in \Omega$, CVaR_α represents the conditional value-at-risk at α, and $\lambda \in [0, 1]$ is a non-negative weighted risk coefficient and it can be adjusted for a trade-off between optimizing an expectation value and the level of risk taken.

Time Consistency. Time consistency is considered as a critical issue when modeling a risk-averse multi-stage stochastic program. Time consistency means that if you solve a multi-stage stochastic programming model today, you should get the same solution if you resolve the problem tomorrow given the information that is observed and decided today. We consider a nested risk measure, expected conditional value-at-risk ($\mathbb{E}$-CVaR), as defined in Homem-de Mello and Pagnoncelli [2016] since it is shown to satisfy the time consistency of multi-stage stochastic programs. The $\mathbb{E}$-CVaR can be linearized and formulated as a linear stochastic programming model. In the following subsection, we will utilize the $\mathbb{E}$-CVaR as a risk measure in our formulation.

4.2.7 Mathematical Model Formulation and Description

The mathematical formulation for our risk-averse multi-stage stochastic epidemics-ventilator-logistics model is given below.

Epidemics-Ventilator-Logistics Model Formulation:

$$\min \quad \sum_{j \in J} \sum_{\omega \in \Omega} p^\omega \left(\sum_{r \in R} (I^\omega_{j,r} + F^\omega_{j,r}) + \lambda(\eta^\omega_j + \frac{1}{1-\alpha} z^\omega_j) \right) \tag{4.5a}$$

s.t. $$S^{\omega}_{j+1,r} = S^{\omega}_{j,r} - \sigma_{1,r}(I^{\omega}_{j,r} + X^{\omega}_{j,r}) - \sigma_{1,r}(I^{\omega}_{j,r} + X^{\omega}_{j,r})\frac{\sigma^{\omega}_{2,r}}{1-\sigma^{\omega}_{2,r}}$$

$$j \in J \setminus \{\overline{J}\}, r \in R, \forall \omega \in \Omega, \tag{4.5b}$$

$$I^{\omega}_{(j+1),r} = I^{\omega}_{j,r} + \breve{I}^{\omega}_{1,j,r} + \sigma_{1,r}(I^{\omega}_{j,r} + X^{\omega}_{j,r}) - \lambda_1 I^{\omega}_{j,r} - \lambda_2 \overline{I}^{\omega}_{j,r} - O^{\omega}_{j,r}$$

$$j \in J \setminus \{\overline{J}\}, r \in R, \forall \omega \in \Omega, \tag{4.5c}$$

$$X^{\omega}_{(j+1),r} = X^{\omega}_{j,r} + \sigma_{1,r}(I^{\omega}_{j,r} + X^{\omega}_{j,r})\frac{\sigma^{\omega}_{2,r}}{1-\sigma^{\omega}_{2,r}} - \lambda_9 X^{\omega}_{j,r}$$

$$j \in J \setminus \{\overline{J}\}, r \in R, \forall \omega \in \Omega, \tag{4.5d}$$

$$H^{\omega}_{(j+1),r} = H^{\omega}_{j,r} + O^{\omega}_{j,r} - \lambda_4 H^{\omega}_{j,r} - \lambda_5 K^{\omega}_{j,r} - \overline{C}^{\omega}_{j,r}$$

$$j \in J \setminus \{\overline{J}\}, r \in R, \forall \omega \in \Omega, \tag{4.5e}$$

$$C^{\omega}_{(j+1),r} = C^{\omega}_{j,r} + \overline{C}^{\omega}_{j,r} - \lambda_7 C^{\omega}_{j,r} - \lambda_8 C^{\omega}_{j,r} \qquad j \in J \setminus \{\overline{J}\}, r \in R, \forall \omega \in \Omega, \tag{4.5f}$$

$$R^{\omega}_{(j+1),r} = R^{\omega}_{j,r} + \lambda_1 I^{\omega}_{j,r} + \lambda_9 X^{\omega}_{j,r} + \lambda_4 H^{\omega}_{j,r} + \lambda_7 C^{\omega}_{j,r}$$

$$j \in J \setminus \{\overline{J}\}, r \in R, \forall \omega \in \Omega, \tag{4.5g}$$

$$F^{\omega}_{(j+1),r} = F^{\omega}_{j,r} + \lambda_2 \overline{I}^{\omega}_{j,r} + \lambda_5 K^{\omega}_{j,r} + \lambda_8 C^{\omega}_{j,r}$$

$$j \in J \setminus \{\overline{J}\}, r \in R, \forall \omega \in \Omega, \tag{4.5h}$$

$$O^{\omega}_{j,r} = min\{\lambda_{3,r} I^{\omega}_{j,r}, T^{\omega}_{j,r} - H^{\omega}_{j,r}\} \qquad j \in J, r \in R, \forall \omega \in \Omega, \tag{4.5i}$$

$$\overline{C}^{\omega}_{j,r} = min\{\lambda_{6,r} H^{\omega}_{j,r}, U^{\omega}_{j,r} - C^{\omega}_{j,r}\} \qquad j \in J, r \in R, \forall \omega \in \Omega, \tag{4.5j}$$

$$U^{\omega}_{j,r} = U_{0,r} + \sum_{l=1}^{j} y^{\omega}_{l,r}, \qquad j \in J, r \in R, \forall \omega \in \Omega, \tag{4.5k}$$

$$\overline{I}^{\omega}_{j,r} \geq \lambda_3 I^{\omega}_{j,r} - (T^{\omega}_{j,r} - H^{\omega}_{j,r}) \qquad j \in J, r \in R, \forall \omega \in \Omega, \tag{4.5l}$$

$$\overline{I}^{\omega}_{j,r} \geq 0 \qquad j \in J, r \in R, \forall \omega \in \Omega, \tag{4.5m}$$

$$K^{\omega}_{j,r} \geq \lambda_6 H^{\omega}_{j,r} - (U^{\omega}_{j,r} - C^{\omega}_{j,r}) \qquad j \in J, r \in R, \forall \omega \in \Omega, \tag{4.5n}$$

$$K^{\omega}_{j,r} \geq 0 \qquad j \in J, r \in R, \forall \omega \in \Omega, \tag{4.5o}$$

$$\sum_{j \in J} \sum_{r \in R} y^{\omega}_{j,r} e_1 \leq \Delta \qquad \forall \omega \in \Omega, \tag{4.5p}$$

$$z^{\omega}_{j} \geq \sum_{r \in R} (I^{\omega}_{j,r} + F^{\omega}_{j,r}) - \eta^{\omega}_{j} \qquad j \in J, \forall \omega \in \Omega, \tag{4.5q}$$

$$z^{\omega}_{j} \geq 0 \qquad j \in J, r \in R, \forall \omega \in \Omega, \tag{4.5r}$$

$$y^{\omega}_{t(n),r} - y_{n,r} = 0, \quad z^{\omega}_{t(n)} - z_n = 0, \quad \eta^{\omega}_{t(n)} - \eta_n = 0,$$
$$\forall \omega \in \beta(n), \forall n \in N, \tag{4.5s}$$
$$S^{\omega}_{j,r}, \quad I^{\omega}_{j,r}, \quad T^{\omega}_{j,r}, \quad H^{\omega}_{j,r}, \quad C^{\omega}_{j,r}, \quad R^{\omega}_{j,r}, \quad F^{\omega}_{j,r}, \quad B^{\omega}_{j,r}, \quad \overline{C}^{\omega}_{j,r}, \quad O^{\omega}_{j,r} \geq 0,$$
$$j \in J, r \in R, \forall \omega \in \Omega, \tag{4.5t}$$
$$y^{\omega}_{j,r} \in \{0, 1, 2, \ldots, \frac{\Delta}{e_1}\} \qquad j \in J \setminus \{\overline{J}\}, r \in R, \forall \omega \in \Omega. \tag{4.5u}$$

Objective Function (4.5a)**.** The objective function (4.5a) minimizes the total expected number of tested infected individuals and deaths and the conditional value-at-risk over all stages j and scenarios ω.

Population Infection Dynamics Constraints (4.5b) **-** (4.5h)**.** Constraint (4.5b) represents that the number of susceptible individuals in region r at stage $j+1$ under scenario ω equals the number of susceptible individuals at stage j minus the number of susceptible individuals who become either tested infected or untested asymptomatic infected at stage j. In this equation, the number of untested asymptomatic infections equals the number of tested infections multiplied by the proportion of the untested asymptomatic infections to the tested infections. Constraint (4.5c) shows that the number of tested infected individuals in region r at stage $j+1$ under scenario ω equals the number of tested infected individuals at stage j plus the infected individuals caused by short-term migration, plus the newly tested infections at time j, minus the recovered and deceased infections of tested individuals at stage j, minus the hospitalized individuals at stage j. Constraint (4.5d) implies that the number of untested asymptomatic infections in region r at stage $j+1$ under scenario ω equals the number of untested asymptomatic infections at stage j plus new, untested asymptomatic infections, minus the recovered untested asymptomatic infections at stage j. Constraint (4.5e) shows that the hospitalized individuals in region r at stage $j+1$ under scenario ω equals the number of hospitalized individuals at stage j

plus the newly hospitalized individuals at stage j, minus the recovered and deceased individuals at stage j, minus the individuals who move to the intensive care unit (ICU) at stage j. Constraint (4.5f) indicates that the total number of individuals in ICU in region r at stage $j+1$ under scenario ω equals the total number of individuals in ICU at stage j plus the individuals who moved to ICU at stage j, minus the individuals who are recovered or died at the ICU at stage j. Constraint (4.5g) shows that the number of recovered individuals in region r at stage j under scenario ω equals the number of recovered individuals at stage j plus the recovered individuals from tested infected, untested asymptomatic infected and hospitalized individuals, and ICU patients at stage j. Constraint (4.5h) indicates that the number of deceased individuals in region r at stage $j+1$ under scenario ω equals the number of deceased individuals at stage j plus the deceased individuals from tested infected and hospitalized individuals and ICU patients at stage j.

Ventilator Logistics and Capacity Constraints (4.5i) **-** (4.5p)**.** Constraint (4.5i) ensures that the number of individuals admitted to the hospital in region r at stage j under scenario ω equals the minimum number of individuals who require hospitalization and the available hospital capacity at stage j. Constraint (4.5j) implies that the number of individuals admitted to ICU in region r at stage j under scenario ω equals the minimum number of individuals who require treatment in ICU and the number of available ventilators at stage j. Constraint (4.5k) represents that the cumulative number of ICU beds (equivalent to ventilators) in region r at stage j under scenario ω equals the initial number of ICU beds plus the cumulative number of ICU beds (new ventilators) allocated from stage 1 to stage j. Constraints (4.5l) - (4.5o) show that the number of individuals who can not be admitted to the hospital or the ICU due to limited capacity should be greater than or equal to zero. Constraint (4.5p) represents that the cost of ventilators allocated over all regions and time stages under

scenario ω cannot exceed the total budget allocated for ventilators. The budget here also represents the maximum total ventilator supply that could be available throughout the planning horizon.

Risk Measure Constraints (4.5q) **and** (4.5r)**.** Constraint (4.5q) indicates the difference between the objective function value and the value-at-risk for each stage j under each scenario ω. Constraint (4.5r) ensures that the loss value exceeding the value-at-risk is included in the CVaR calculation, and thus z_j^ω should be greater than or equal to zero.

Non-Anticipativity, Non-Negativity and Integrality Constraints (4.5s) **-** (4.5u)**.** Constraint (4.5s) is the non-anticipativity constraint, indicating that the scenarios that share the same path up to stage j should also have the same corresponding decisions. Constraint (4.5t) indicates that the number of individuals in each compartment in region r at stage j under scenario ω should be greater or equal to zero. Constraint (4.5u) implies that the number of allocated ventilators should be an integer.

Remark 1. Both (4.5i) and (4.5j) are non-linear, and thus we replace them with equivalent linear constraints with additional linearization variables, using the method presented in Yin and Büyüktahtakın [2021a]. Hence, the non-linear multi-stage stochastic programming epidemics-ventilator-logistics model (4.5a)–(4.5u) is converted into an equivalent mixed-integer linear programming (MIP) formulation. We implement this MIP formulation for the rest of the paper.

4.2.8 Scenario Sub-Problem and Bounds

We implement the scenario sub-problems and lower and upper bounds proposed by Büyüktahtakın [2020] to reduce the optimality gap of solving our risk-averse multi-stage stochastic programming problem (4.5a)–(4.5u), while referring to Büyüktahtakın [2020] for the proofs of those bounds originally driven for the general multi-stage stochastic programs. The scenario sub-problem and bounds are described below.

Definition 4.2.1 *The scenario-ω problem (P^ω) is formulated as follows:*

$$Z^\omega = \min \quad \sum_{j\in J} p^\omega \left(\sum_{r\in R} (I^\omega_{j,r} + F^\omega_{j,r}) + \lambda(\eta^\omega_j + \frac{1}{1-\alpha} z^\omega_j) \right) \tag{4.6a}$$

$$s.t. \quad \textit{Constraints} \quad (4.5b) - (4.5u). \tag{4.6b}$$

Specifically, in P^ω we minimize the objective function value only under scenario ω while keeping all the variables and the constraints from the original problem (4.5a)–(4.5u).

Proposition 1 *(**Lower Bound**) Let Z^* represent the objective function of the original problem* (4.5a)–(4.5u)*, P. Then we have:*

$$Z^* \geq \sum_{\omega\in\Omega} Z^\omega. \tag{4.7}$$

Proposition 2 *(**Upper Bound**) Let $\dot{x}^\omega$ be the optimal solution of scenario-ω problem, P^ω, and $Z(\dot{x}^\omega)$ be the objective value of original problem* (4.5a)–(4.5u) *where $\dot{x}^\omega$ is substituted in the original problem objective function* (4.5a)*. Then we have:*

$$Z^* \leq \min_{\omega\in\Omega} Z(\dot{x}^\omega). \tag{4.8}$$

4.3 Case Study Data

This section provides the data used to calibrate model parameters and formulate the model, including population and short-term migration data, transmission parameters,

as well as the cost of a ventilator. As shown in Figure 4.3, we select eight counties that are most impacted by the pandemic in the states of New York and New Jersey for our case study. They are New York County, Kings County, Queens County, Bronx County, Richmond County, Hudson County, Bergen County, and Essex County. In our multi-stage model, each stage represents a two-week period. Thus, all the data regarding the transmission and migration are bi-weekly.

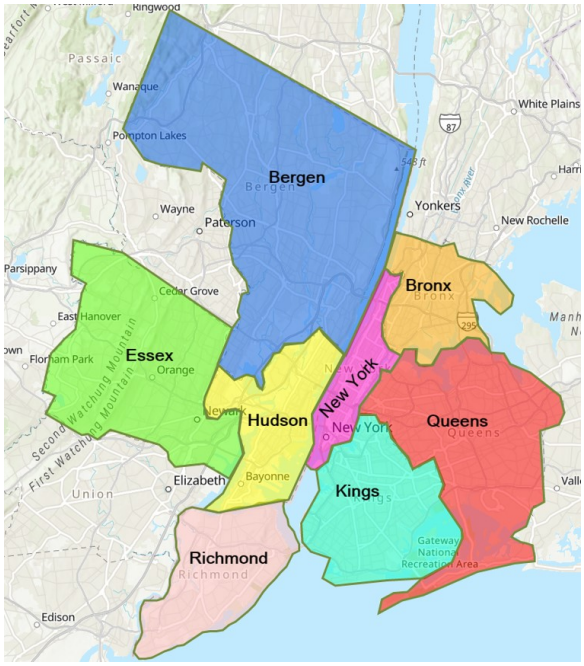

Source: [ESRI, 2020]

Figure 4.3 Counties in New York and New Jersey.

4.3.1 Population and Migration Data

Table 4.2 shows the population data for each considered county in New York and New Jersey. Population data is obtained from JHU [2020]. The migration rates among the considered counties, estimated from the data on CENSUS [2020], are presented in Table 4.3. The blank areas in Table 4.3 represent a zero short-term migration because the movement among those counties is too small to make an impact on the model results.

Table 4.2 Counties and Population Sizes in New York and New Jersey

New York	Population	New Jersey	Population
New York	1,632,480	Hudson	668,631
Kings	2,600,747	Bergen	929,999
Queens	2,298,513	Essex	793,555
Bronx	1,437,872		
Richmond	474,101		
Total	**8,443,713**		**2,392,185**

Table 4.3 Migration Rate Among Counties in New York and New Jersey

To From	New York	Kings	Queens	Bronx	Richmond	Hudson	Bergen	Essex
New York		0.015	0.012	0.009	0.006	0.007	0.007	0.007
Kings	0.192		0.038	0.004	0.004			
Queens	0.218	0.044		0.009	0.002			
Bronx	0.209	0.014	0.028			0.003		0.003
Richmond	0.105	0.105						
Hudson	0.040				0.001		0.040	0.040
Bergen	0.126					0.039		0.039
Essex	0.079				0.001	0.057	0.057	

4.3.2 Epidemiological Data

Table 4.4 presents the data values for transmission parameters for the studied counties in New York and New Jersey. The data contains the proportion of untested asymptomatic infections, recovery rate, and the death rate for tested infections,

hospitalized infections, and ICU patients. Table 4.5 shows the transmission rate of each county at the first two stages and the impacts of applying different intervention strategies, as discussed in Subsection 4.2.3.

Table 4.4 Transmission Parameters and Bi-weekly Rates for the COVID-19

Parameter	Description	Data		Reference
		NY	NJ	
$\sigma_{2,r}$	Proportion of untested asymptomatic infections	0.15-0.4	0.15-0.4	Meller [2020]
λ_1	Recovery rate without hospitalization	0.69-0.79	0.69-0.79	Hogan [2020]
λ_2	Death rate without hospitalization	0.4	0.4	JHU [2020]*
λ_3	Hospitalization rate	0.21-0.31	0.21-0.31	Hogan [2020]
λ_4	Recovery rate with hospitalization	0.88	0.88	Hogan [2020]
λ_5	Death rate with hospitalization (No ventilators)	0.4	0.4	JHU [2020]*
λ_6	Ventilator requirement rate of hospitalized	0.12	0.12	Hogan [2020]
λ_7	Recovery rate with ventilator	0.643	0.643	Bernstein [2020]
λ_8	Death rate with ventilator	0.357	0.357	Bernstein [2020]
λ_9	Recovery rate with asymptomatic infections	1	1	Bertsimas et al. [2020]

* Trained using real data.

Table 4.5 Transmission Rate ($\sigma_{1,r}$) in New York and New Jersey and Impact of Interventions

County	Transmission Rate at Stage 1	Transmission Rate at Stage 2	Impact of None	Impact of Mask	Impact of Lockdown
New York	4.5	0.9855	1	0.4	0.6
Kings	9	0.9855	1	0.4	0.6
Queens	10	1.095	1	0.4	0.6
Bronx	12	1.314	1	0.4	0.6
Richmond	12	1.314	1	0.4	0.6
Hudson	22	2.409	1	0.3	0.6
Bergen	11	1.408	1	0.3	0.6
Essex	22	2.409	1	0.3	0.6

4.3.3 Initial Infection, Capacity and Cost Data

Table 4.6 shows the initial number of infections, hospital capacity, and ICU capacity for each county. The data is obtained from JHU [2020].

Table 4.6 Initial Number of Infections, Hospital Capacity, and ICU Capacity for Each County

County	Initial Infections	Initial Hospital Capacity	Initial ICU Capacity
New York	1200	8650	944
Kings	1300	5838	282
Queens	1100	3210	146
Bronx	554	2816	274
Richmond	206	1177	72
Hudson	66	1764	89
Bergen	249	2874	122
Essex	73	3541	226

Ventilator Cost. The cost of each ventilator ranges from \$5000 to \$50000 [Glass, 2020]. In our case, we consider a cost of \$5000 for each ventilator, and different budget levels are set to impose different upper bounds on the ventilator supply.

4.4 Results

4.4.1 Model Validation

This subsection presents the validation results of the mathematical model in Equations (4.5a)–(4.5u) as presented in Subsection 4.2.7 for the 8-stage time period from April 3, 2020, to July 10, 2020. We consider a medium realization of the uncertain asymptomatic proportions at each stage of the planning horizon and compare the number of infections forecasted by our model to the real outbreak data.

The government applied a lockdown strategy from April 3, 2020, to July 10, 2020, at those considered locations in New York and New Jersey. Thus, we use the lockdown strategy and the corresponding transmission rate at each stage in our model for validation.

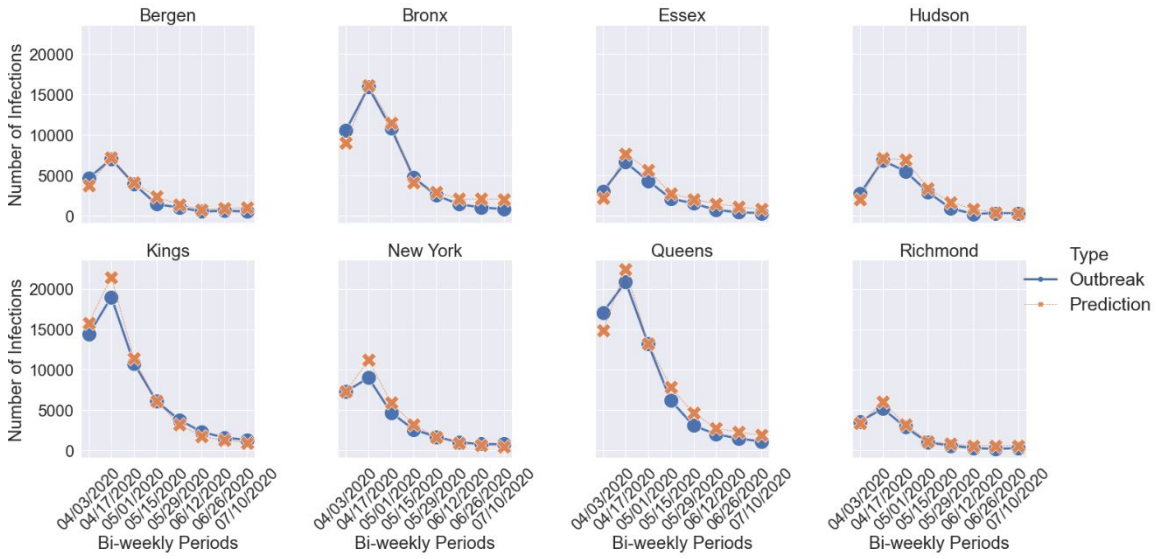

Figure 4.4 Comparison of predicted cases with real outbreak data for new infections in New York and New Jersey.

Figure 4.4 shows the comparison between the predicted infections and real outbreak data. The model's predictions provide a visually good fit for the actual number of new infections in each region, implying that the model can capture the disease transmission dynamics under a lockdown intervention strategy. We also perform a paired-t-test to analyze the difference between the pairs of predicted new infections and the actual data in each period. As shown in Table 4.7, all p-values are greater than 0.05, and thus our model provides statistically similar predictions with the real outbreak data from April 3, 2020, to July 10, 2020, for each considered county.

Table 4.7 Statistical Analysis to Compare the Bi-Weekly Predicted New Cases and Real Outbreak Data

County	Mean		Two-tailed paired-t-test		
	Outbreak	Predicted	t-stat	t-critical	p-value
New York	7300	7299	0.20	2.36	0.58
Kings	7413	7754	0.41		0.65
Queens	8138	8751	0.21		0.58
Bronx	5956	6214	0.46		0.67
Richmond	1762	2040	0.04		0.51
Hudson	2455	2806	0.16		0.56
Bergen	2444	2656	0.30		0.61
Essex	2366	2948	0.04		0.51

4.4.2 Case Study Implementation Details

We apply our model described in Section 4.2 to the selected counties in New York and New Jersey. We first solve the risk-neutral model. We incorporate the uncertainty of the proportion of untested asymptomatic infections as well as the short-term migration in the disease transmission and forecast the number of new infections, deceased individuals, hospitalized individuals, and ICU patients under different intervention strategies. Also, we solve the model to determine the optimal location and number of ventilators allocated under different budget levels and scenarios to provide insights into resource allocation over multiple jurisdictions under uncertainty. Due to the high complexity of the mathematical formulation, we solve it for a 5-stage time period. Each stage corresponds to two weeks, resulting in a planning horizon of ten weeks from March 20, 2020, to May 29, 2020. Because each node of the scenario

tree has three possible realizations of the random parameters, we solved 243 (3^5) scenarios simultaneously.

The mathematical model is solved using CPLEX 12.7.1 on a desktop computer running with Intel i7 CPU and 64.0 GB of memory. We set the time limit at 7200 CPU seconds to solve each test instance. We extend running time for specific budget levels ($30 Million) and interventions ("Lockdown") due to the large optimality gap. In the following subsections, we present results from solving the multi-stage stochastic epidemics-ventilator-logistics model with an application to the case of COVID-19 using the data presented in Section 4.3.

4.4.3 Transmission Forecast under Different Intervention Strategies

Here, we present results of our formulation for each time period under different intervention strategies: No intervention ("None"), mask and social distancing for all stages ("Mask and Social Distance"), lockdown for all stages ("Lockdown"), mask and social distancing for the first three stages and lockdown for the following two stages ("Mask + Lockdown"), lockdown for the first three stages and mask and social distancing for the following two stages ("Lockdown + Mask"). The model is solved under the $30 million budget level. The model with the "Lockdown" strategy gives a 4.54% optimality gap after a run time of 43,241 CPU seconds, while the model solved for all other strategies has a zero optimality gap within 7,200 CPU seconds.

Figure 4.5 presents the number of infections and deceased individuals at each stage under different intervention strategies. According to the results, short-term migration influences the number of new infections even under constant transmission rates. As in the first stage, within the same initial transmission rate, the number of infections under different intervention strategies is different from each other. When the stage increases, the difference in the number of new infections among each intervention strategy becomes more and more significant. The "None" strategy

has the most infections at each stage, followed by the "Mask and Social Distance" strategy. The "Lockdown" strategy results in the lowest number of new infections compared to those under other strategies at each stage. The "Lockdown" strategy provides a little higher number of infections compared to the actual infection data since our model slightly (but statistically insignificantly) overestimates the number of infections. Compared to the "Mask + Lockdown" strategy, the "Lockdown + Mask" intervention leads to fewer infections. This implies that applying the "Lockdown" strategy immediately at the onset of the pandemic followed by the "Mask and Social Distance" intervention is a better strategy than enforcing "Mask and Social Distance" first and delaying the lockdown.

The intervention strategy does not influence the number of deceased individuals as quickly as it does impact the number of infections, as shown in Figure 4.5. Here, the number of deceased individuals at the first two stages is much lower than that of the last three stages. Starting from stage three, the number of deceased individuals under different intervention strategies shows a similar trend with the number of new infections. The influence of interventions is further delayed for those confirmed infections to be treated in the hospital and ICU (Figure 4.6).

To reduce both the number of new infections and deaths, "Lockdown" is the best strategy. As shown in Figure 4.5b, the "Lockdown" strategy with the optimal ventilator allocation further reduces the actual number of deaths. Due to the negative impact of COVID-19 on employment and its economic burden, governments are often forced to stop the lockdown and reopen businesses. In such cases, applying "Mask and Social Distance" after a certain period of "Lockdown" will be the best choice.

Figure 4.6 shows the number of hospitalized individuals and ICU patients at each stage under different intervention strategies. Similar to the number of deceased individuals, there are delays in the impact of government interventions on the number of hospitalized individuals and ICU patients. An infected person may have mild

symptoms for about one week, then worsen rapidly (School [2021]). Thus, it may take some time for patients to be admitted to the ICU, so the impact of interventions on the number of ICU patients is delayed one more stage compared to the hospitalized cases. As shown in Figure 4.6, more number of hospitalized individuals at stage j will lead to more ICU patients at stage $j+1$.

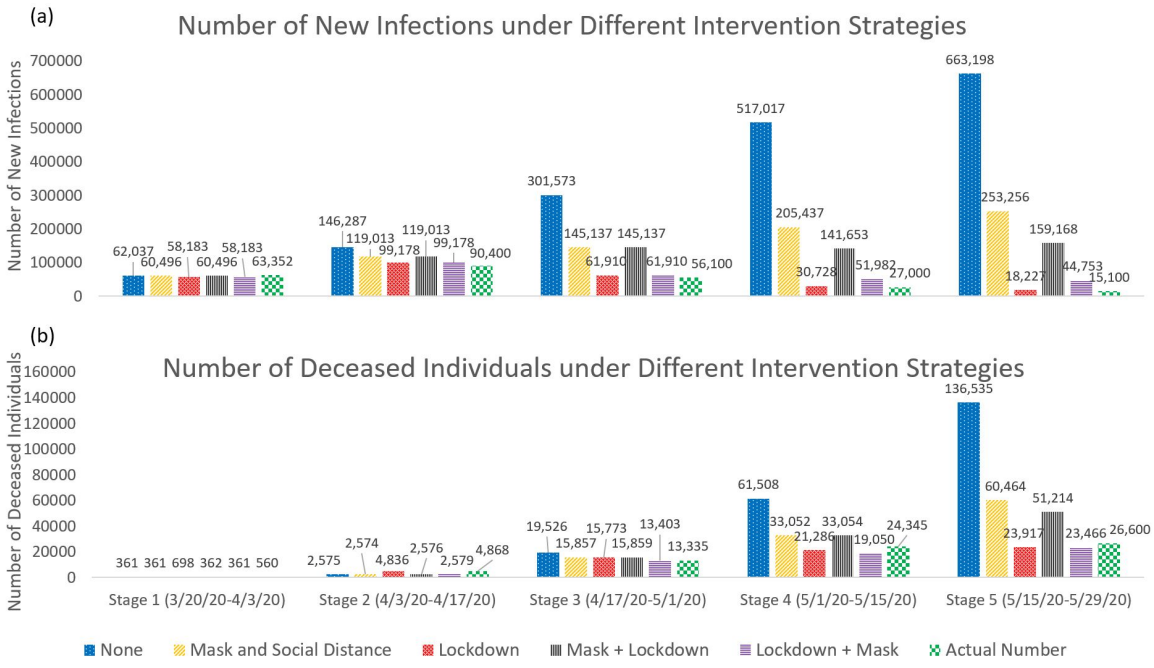

Figure 4.5 Number of new infections and deaths under different intervention strategies and actual numbers.

For all the stages, the "Lockdown" strategy has the least number of hospitalized individuals and the ICU patients, followed by the "Lockdown + Mask" intervention. The ICU patients of "None," "Mask and Social Distance," and "Mask + Lockdown" are almost the same at stages three to five. This is because under those, the need for ventilators is large, and the number of treated individuals in ICUs depends on the minimum number of patients who require ventilators and the ventilator supply in those ICUs. Thus, the number of treated patients in ICUs is limited by the tight ventilator availability.

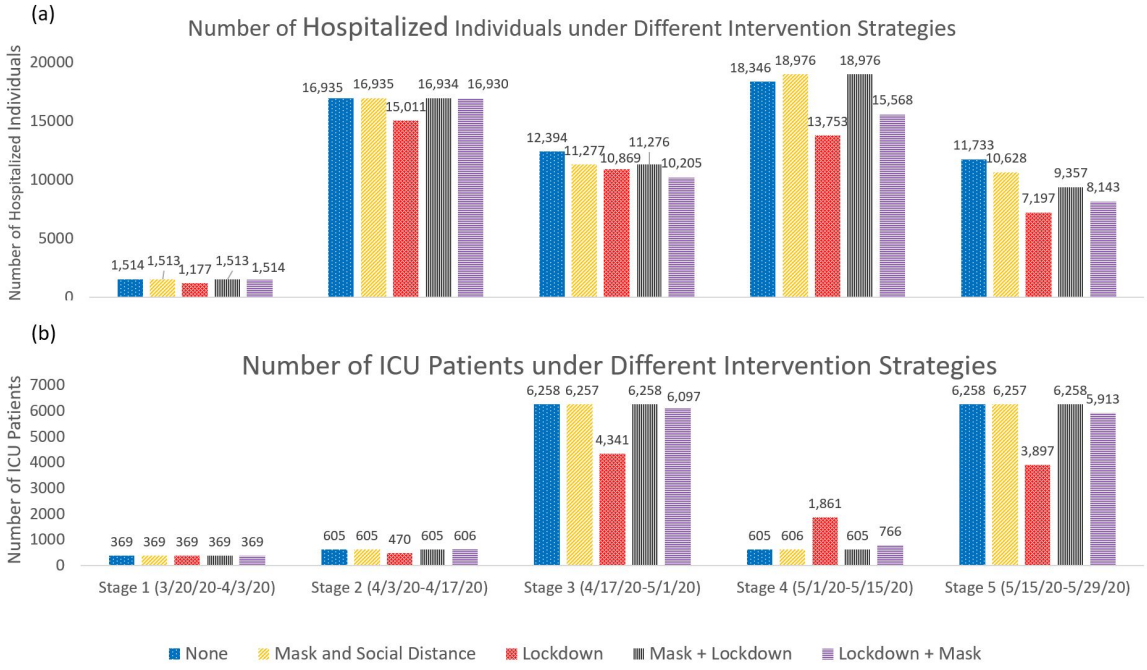

Figure 4.6 Number of hospitalized individuals and ICU patients under different intervention strategies.

4.4.4 Optimal Ventilator Allocation

Table 4.8 shows the number of ventilators allocated to each region at stages one and two and the total number of ventilators allocated throughout the planning horizon under different budget levels and three select scenarios. The "All Low," "All Medium," and "All High" scenarios represent low, medium, and high realization of the proportion of untested asymptomatic infections at each stage of a five-stage planning horizon, respectively. To analyze the impact of budget on the optimal ventilator allocation decisions, we select \$10M as the limited budget level, \$20M as the medium budget level, and \$30M as the ample budget level. The model has zero optimality gap under the \$10M budget level, 4.54% optimality gap under the \$20M budget level and 7.77% optimality gap under the \$30M budget level within two hours of solution time.

The results in Table 4.8 demonstrate that the location and number of ventilators allocated depend on several factors, including the initial and evolving disease

transmission rates, the population and the number of initial infections in a region, and the existing ventilator capacity. Thus, the optimal ventilator allocation should be determined case-by-case.

According to the results, the total number of ventilators allocated increases in the budget level due to the high need for ventilators. As shown in Table 4.8, under the limited budget level, some regions with many initial infections, e.g., the New York County, do not receive ventilators. This situation is because the initial ventilator capacity of those regions is higher than in other counties. Also, results suggest that more ventilators should be distributed to other areas with a higher initial transmission rate than the New York County, such as Kings, Hudson, and Essex, under a very tight budget. Kings, Queens, and Hudson have higher initial transmission rates and lower initial ICU capacity than New York. Thus, these regions get more ventilators allocated under a limited budget level and "All Low" scenario. Also, regions with a relatively smaller population, such as Hudson and Essex in New Jersey, get a large share of ventilators with a very tight budget under the "All Low" and "All Medium" scenarios due to their high transmission rates at the beginning of the pandemic.

Independent from the budget level, some regions with low initial infections and low initial ICU capacity (e.g., Bronx) will get more ventilators allocated under the "All Medium" scenario. Under this scenario, the number of infections in regions with a high initial transmission rate (e.g., Kings and Queens) will not significantly increase even if they receive a smaller number of ventilators. These regions usually have much more initial ICU capacity for the treatment because of their large population. On the contrary, the areas with a lower initial transmission rate but less initial ICU capacity may benefit more if they receive more ventilators. As a comparison with the "All Medium" scenario, the number of infections in the region with a low initial transmission rate will be much smaller under the "All Low" scenario, and the number of infections in the regions with a high initial transmission rate will be much larger

under the "All High" scenario. The model gives priority to allocate more ventilators to the regions with high initial transmission rates for both of the "All Low" and "All High" scenarios because the benefit of giving resources to those regions is higher than the regions with low initial disease transmission.

Moreover, the model is forced to make difficult decisions, and some of the regions may not have any ventilator allocated under a limited ventilator supply. When the budget is too tight, the regions with a high transmission rate gets the priority. As the budget increases to medium and ample, the model allocates more capacity to the regions with a higher population and a larger initial number of infections but with a lower transmission rate. Also, the stage-wise distribution of ventilators has a high relationship with the available budget. If the budget is tight, all ventilators are distributed within the first two stages. As we increase the budget, some of the ventilators are allocated in stages three and four in addition to stages one and two. Thus, a higher budget level also provides some flexibility in delaying the ventilator allocation to some regions.

4.4.5 Risk Analysis

In this subsection, we perform an analysis of the risk parameters λ and α in terms of their impact on the expected number of infected and deceased people as well as the CVaR of the impact. Specifically, under the $\$30M$ budget level, we compare four different problems with respect to their risk-averseness level, adjusting λ and α values accordinglyrisk-neutral ($\lambda = 0, \alpha = 0$), weak risk-aversion ($\lambda = 1, \alpha = 0.3$), mild risk-aversion ($\lambda = 10, \alpha = 0.6$), and strong risk-aversion ($\lambda = 10, \alpha = 0.95$). The model under the mild risk-aversion results in a high optimality gap (13%) within 7200 CPU seconds running time. Therefore, we solve the scenario-ω problems described in Subsection 4.2.8 and obtain the lower and upper bounds for the original problem. For our problem, we select five representative scenarios, and add bounds based on

the results of those select scenarios in the risk-averse model. After implementing the scenario bounds, the optimality gaps over all of the risk-averseness levels reduce to less than 9.13%.

We decompose the objective function (4.5a) into the *Expected Impact* $[\mathbb{E}(f(x,\omega))]$ and the *Expected Risk* $[\text{CVaR}_\alpha(f(x,\omega))]$, as demonstrated in Equation (4.4), to analyze the impact of risk trade-off on the results. Table 4.9 presents the value of the objective function (4.5a), expected impact, and expected risk (without λ) under different risk-averseness levels. Specifically, the expected impact represents the expected total number of infections and deceased individuals, and the expected risk corresponds to the expected CVaR term in Equation (4.5a) without the λ value. According to Table 4.9, when both λ and α increase, the level of risk-averseness and the expected risk increase. The optimal objective function value increases due to the additional risk term added into the objective formulation. The expected impact also increases, implying the cost of being risk-averse, which is the increased number of infections and deceased individuals while trying to mitigate specific disastrous scenarios.

Table 4.9 Comparison of Objective Value, Expected Impact, and Expected Risk under Various Risk-Averseness Levels

	Risk Neutral ($\lambda = 0$, $\alpha = 0$)	**Weak Risk-aversion** ($\lambda = 1$, $\alpha = 0.3$)	**Mild Risk-aversion** ($\lambda = 10$, $\alpha = 0.6$)	**Strong Risk-aversion** ($\lambda = 10$, $\alpha = 0.95$)
Objective Value	347,395	721,710	3,997,129	4,011,964
Expected Impact	347,395	360,438	362,559	363,526
Expected Risk	-	361,272	363,457	364,844

The expected impact and expected risk (without λ) for various combinations of $\lambda = \{0, 1, 10\}$ and $\alpha = \{0.3, 0.6, 0.95\}$ under the $\$30M$ budget level are presented in Table 4.10. We observe the change of the expected impact and expected risk when changing one of the risk parameters and fixing all others' original values. According

to the results, fixing the α value, both expected impact and expected risk show an increasing trend due to the increase of λ. When we move from risk-neutral ($\lambda = 0$) to risk-averse ($\lambda = \{1, 10\}$), the expected impact always increases. Similarly, $\lambda = \{1, 10\}$ increases the expected impact compared to the risk-neutral model. Besides, when fixing the λ value and increasing the α value, the expected risk increases because we increase the confidence level for reducing the risk of having an extremely large number of infections and big losses of lives.

Table 4.10 Expected Impact and Risk for Different Risk-Averseness Levels

$\boldsymbol{\lambda \backslash \alpha}$	**0.3**		**0.6**		**0.95**	
	Expected Impact	Expected Risk	Expected Impact	Expected Risk	Expected Impact	Expected Risk
0	347,395	0	347,395	0	347,395	0
1	360,438	361,272	361,950	363,251	363,882	365,236
10	360,880	361,341	362,559	363,457	363,526	364,844

4.5 Discussion and Future Directions

In this chapter, we present a general multi-stage mean-risk epidemics-ventilator-logistics model and apply this model to control the COVID-19 in select counties of New York and New Jersey. We first explicitly formulate the uncertainty of the proportion of untested asymptomatic infections at each stage, generating a multi-stage scenario tree. We then develop a compartmental disease model and integrate the short-term human movement among multiple regions into this model. We also derive a time- and space-varying disease transmission formulation and a logistics sub-model. We then integrate all those components into one mathematical formulation, which minimizes the number of infections and deceased individuals under different intervention strategies.

We solve the epidemics-ventilator-logistics model under different budget levels to determine the ventilator-distribution optimal timing and location under various pandemic scenarios. Next, we apply the CVaR in a nested form over a five-stage planning horizon to minimize the total expected number of infections and deceased individuals, as well as the weighted risk of the loss. Finally, we solve the scenario sub-problems under various scenarios to generate the lower and upper bounds for the original problem, reducing the optimality gap. Our results provide key insights into the resource-allocation decisions for controlling the COVID-19 and can be adapted to study the transmission and logistics of other similar diseases.

According to the results, the number of infections, deceased individuals, hospitalized individuals, and ICU patients indicates that short-term migration influences the number of infections, even if the transmission rate is constant over time. The impacts of government interventions on the number of deceased individuals, hospitalized individuals, and ICU patients are delayed because deaths and hospitalization have a lag period compared to zero or a small lag phase in the growth of infections. Furthermore, the number of ICU patients at each time period depends on the minimum number of patients who require the ICU and the available ventilators. Thus, the number of ICU patients might be at the capacity limit even under different intervention strategies at a particular stage. The "Lockdown" strategy is the best way to control disease transmission. Nevertheless, "Mask and Social Distance" applied after the several stages of "Lockdown" is the second-best strategy to optimistically alleviate the pandemic's economic impacts.

The ventilator allocation under different budget levels and scenarios indicates that the number of ventilators allocated to each region depends on various factors, such as the number of initial infections, initial disease transmission rates, initial ICU capacity, and the population of a geographical location. The region with a high initial transmission rate and low initial ICU capacity receives more ventilators under a low

disease transmission scenario and a limited budget level. This is because, under a low disease transmission scenario, other regions with low initial transmission rates have fewer infections, even if they have smaller initial ICU capacity. Independent from the budget level, the area with a low initial transmission rate and low initial ICU capacity has more ventilators allocated under the medium transmission scenario. This is because the number of infections in the region with a high initial transmission rate and high initial ICU capacity does not significantly increase even if they receive fewer ventilators under a mild disease transmission scenario. Under a medium and ample budget level, the model allocates more capacity to the regions with a higher population and a larger initial number of infections but with a lower transmission rate. Moreover, when the budget is limited, all of the ventilators are allocated at the first two stages. When the budget becomes ample, decision-makers would have some flexibility in delaying ventilator allocation to later stages of the planning horizon.

The increase in the mean-risk trade-off coefficients in the risk-averse model improves the confidence level, reducing the loss in the right tail of the objective function values (the number of infected and deceased individuals over highly-adverse scenarios). However, we should expect more infections and deceased individuals on average considering all possible scenarios when we want to decrease the impact of adverse scenarios by increasing the risk-averseness level.

This study leads to several future directions for research. For instance, vaccine allocation is also essential as it can potentially protect people from being infected. The combination of vaccine allocation and other interventions will provide more flexible strategies to prevent and control the disease. For example, for the region with a low transmission rate and high vaccine coverage, decision-makers could consider lifting the "Lockdown" earlier to stimulate the economy. Furthermore, the mathematical model cannot allocate ventilators to some regions under a very tight budget, and so future research could investigate ethical and fair resource allocation strategies during

a pandemic. Also, some of the assumptions and inferences made in our model could be updated in a future study as more data are available.

Table 4.8 Optimal Ventilators Allocated under Different Scenarios for Budget Levels

Scenario	County	Stage 1	Stage 2	Total Ventilator	Stage 1	Stage 2	Total Ventilator	Stage 1	Stage 2	Total Ventilator
		(Budget=$10M)			(Budget=$20M)			(Budget=$30M)		
All Low	New York	0	0	0	721	1	**802***	2100	0	2100
	Kings	119	0	119	1734	0	**1736***	2222	0	2222
	Queens	107	1069	1176	0	0	0	0	0	0
	Bronx	28	0	28	1016	1	1017	1016	1	1017
	Richmond	18	0	18	0	0	0	0	0	0
	Hudson	0	250	250	0	0	0	0	0	**2***
	Bergen	187	0	187	12	433	445	0	0	**165***
	Essex	218	0	218	0	0	0	0	0	**174***
Total		**677**	**1323**	**2000**	**3483**	**435**	**4000***	**5338**	**1**	**5680***
All Medium	New York	0	0	0	721	0	721	2100	0	**2101***
	Kings	119	0	119	1734	76	1810	2222	1	2223
	Queens	107	0	107	0	0	**3***	0	0	**69***
	Bronx	28	809	837	1016	0	1016	1016	0	**1017***
	Richmond	18	0	18	0	0	0	0	0	**35***
	Hudson	0	250	250	0	0	0	0	0	**53***
	Bergen	187	264	451	12	435	447	0	0	0
	Essex	218	0	218	0	0	**3***	0	0	**349***
Total		**677**	**1323**	**2000**	**3483**	**511**	**4000***	**5338**	**1**	**5847***
All High	New York	0	0	0	721	0	721	2100	1	**2190***
	Kings	119	0	119	1734	0	1734	2222	0	2222
	Queens	107	1055	1162	0	0	**2***	0	0	**451***
	Bronx	28	4	32	1016	0	1016	1016	0	**1017***
	Richmond	18	0	18	0	0	**78***	0	0	0
	Hudson	0	0	0	0	0	0	0	0	0
	Bergen	187	264	451	12	437	449	0	0	**93***
	Essex	218	0	218	0	0	0	0	0	**27***
Total		**677**	**1323**	**2000**	**3483**	**437**	**4000***	**5338**	**1**	**6000***

* Some of the ventilators are allocated at stages three and four.

CHAPTER 5

AN AGENT-BASED SIMULATION-OPTIMIZATION VACCINE CENTER LOCATION VACCINE ALLOCATION APPROACH TO CONTROLLING COVID-19

5.1 Introduction

The Coronavirus Disease 2019 (COVID-19) has caused around 4 million deaths worldwide by mid-July 2021 [JHU, 2021] and 607 thousand only in the United States with the largest death toll in the world (15%). Fast disease spread caused the collapse of the healthcare system in many countries, forcing them to use other intervention strategies to slow down the virus spread, such as lockdown, quarantine, and mandatory mask [Zhang et al., 2020a, Eikenberry et al., 2020]. In some countries, where people can strictly follow the rules, these strategies are very effective, and the cases have been reduced significantly. However, for some countries where people have more social activities, these strategies could not lessen the increasing number of cases and deaths in the long term.

The most effective way to stop this health crisis is to produce effective vaccines and let most people be vaccinated [Peter Loftus, 2021b]. On March 11, 2020, World Health Organization (WHO) declared the COVID-19 as a pandemic making it a global threat. All countries felt the urgency to invest in the research and development of a vaccine, especially the Group of Twenty (G20), which has the most to lose from the COVID-19. The Pfizer/BioNTech (Pfizer) vaccine was the first vaccine listed for WHO Emergency Use Listing (EUL) on December 31, 2020. On February 16, 2021, the SII/Covishield and AstraZeneca vaccines were given EUL. The Janssen developed by Johnson & Johnson was listed for EUL on March 12, 2021. The Moderna vaccine was listed for EUL on 30 April 2021. The Sinopharm vaccine is produced by China National Biotec Group (CNBG) and was listed on May 7, 2021. The Sinovac-CoronaVac was listed for EUL on June 1, 2021 [WHO, 2021d]. Among these, we

consider mainly three vaccines used in the United States, PfizerBioNTech, Moderna, and Johnson & Johnson (Janssen), in our model.

With more and more people getting vaccinated, the number of cases and deaths decreased significantly. Until July 2021, there were about 332 million doses administered in the United States. About 55.3% of US people got at least one dose, and about 47.8% of people were fully vaccinated by July 2021 [CDC, 2021]. Since December 2020, when people started to get vaccinated, the number of daily deaths in the United States has decreased from about 4,000 to only 300, and the number of daily cases has dropped from about 200,000 to 20,000 by July 9, 2021 [JHU, 2020]. The dramatic drop in both the number of deaths and the total infections shows that the vaccines are very effective for controlling the epidemic. Despite this, the vaccination process differs based on the vaccines available, the total budget, and the logistic processes. This study aims to develop a mathematical model to use the available resources under different budgets effectively and provide insights into optimal vaccine allocation achieving the lowest infection rate.

Human behavior has a significant influence on COVID-19 transmission. If we can model human interactions and disease transmission realistically, we can accurately estimate how vaccines reduce the infection numbers. This aspect is also quite essential to decide where to locate vaccination centers and find the optimal vaccine allocation. Kerr et al. [2021] propose an agent-based model (Covasim) that simulates person-to-person contact among different communities. In their Covasim project, each individual has the probability of being infected in a complicated environment for the agent-based simulation. For instance, the kids of the family may go to school, and adults may go to work. Both activities give them a chance to contact infected individuals. People may also spend time together with their family members and friends in the community and get infected. We extend the Covasim agent-based model and incorporate it with an optimization model to optimize vaccine allocation.

In this chapter, we formulate an optimization model to determine the COVID-19 optimal vaccine allocation strategies under budget and population dynamics constraints. Our model extends the agent-based simulation presented by Kerr et al. [2021] to incorporate different types of vaccines with one or two shots. We incorporate service center location and service decision for each center, including the nearby regions served by the center in the optimization model, and the number of vaccines allocated to each region. We integrate all those elements into one simulation-optimization model. The optimization model uses the simulation results as input to generate the optimal vaccine allocation decisions and transfers the optimal decisions into the simulation model, which populates health states, such as the number of infections, in the following period. We calibrate, validate, and test our simulation-optimization vaccine allocation model using JHU [2020] COVID-19 data collected during the middle stages of the pandemic.

5.2 Key Contributions and Insights

The majority of existing studies only use the simulation or optimization model separately. In addition, most researches only focus on one side of the epidemic control, either transmission forecasting or optimizing the resource allocation strategies. To our best knowledge, none of them consider the agent-based simulation of disease transmission with the optimal vaccination center location and vaccine allocation problem together. To address the limitation of the resource allocation and logistic planning problem on epidemic control, we formulate our model with the following contributions:

(**i**) We formulate an optimization model to determine the COVID-19 optimal vaccine allocation strategies. Besides the simulation model, the optimization model includes the population dynamics constraints on the susceptible individuals, infections, vaccinated individuals to project disease growth, and impacts of optimization decisions under a limited budget.

(**ii**) We extend the agent-based simulation presented by Kerr et al. [2021] to incorporate vaccination compartments and different types of vaccines with one or two shots.

(**iii**) In the optimization model, we incorporate service center location and service decision for each center, including the nearby regions served by the center and the number of vaccines allocated to each region. We use exponential functions to generate the lower bound of the number of vaccines allocated, and the vaccine acceptance rate provides the upper bound of vaccine supply.

(**iv**) We integrate all those elements mentioned above into one simulation-optimization model. The optimization model applies the simulation results as the inputs to generate the optimal vaccine allocation decisions. Then the decision results are imported into the simulation model, which populates very detailed health states, such as the number of infections, hospitalized, and deaths, in the following period.

(**v**) Our results suggest that the vaccine with a lower cost is recommended to be allocated more under a limited budget level. Under an ample budget level, the vaccine with a higher efficiency should be administered more. In addition, the region that has a high population or initial infections should have more vaccines allocated.

5.3 Model Description

5.3.1 Agent-based Simulation Model

In this section, we discuss the agent-based simulation and optimization models and their integration in more detail.

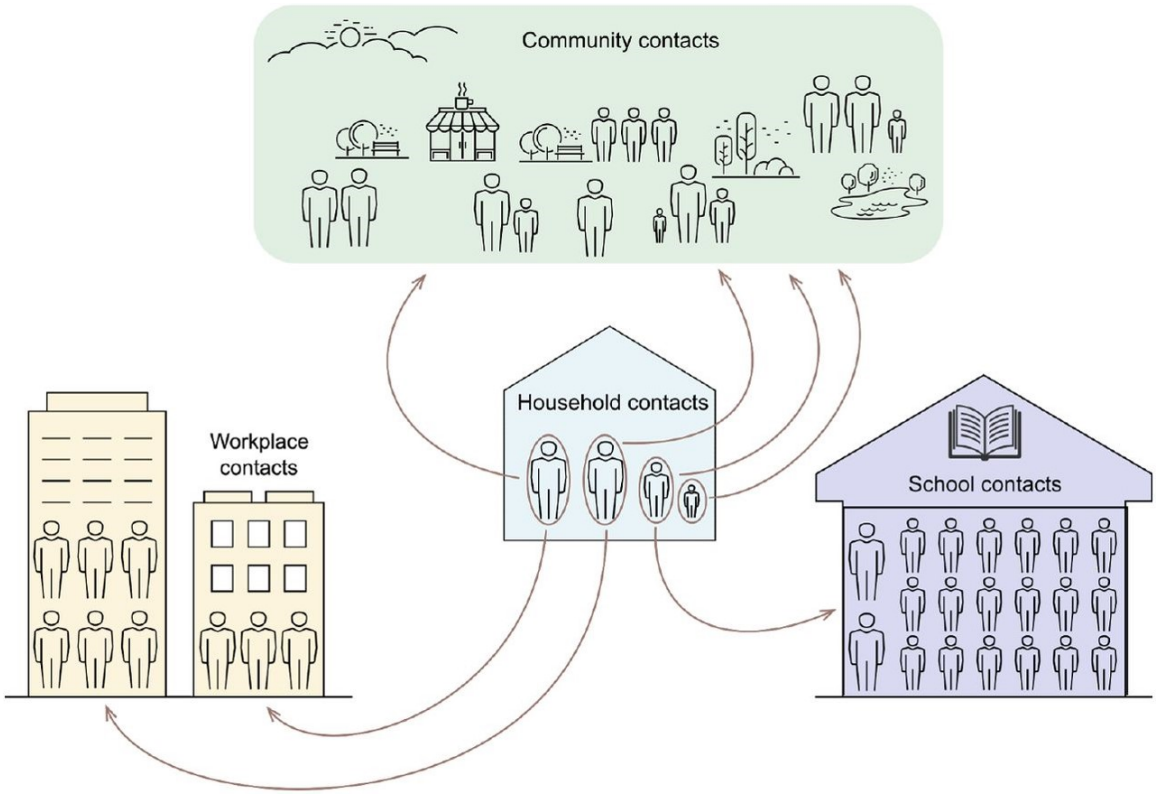

Source: [Kerr et al., 2021]

Figure 5.1 Covasim simulation.

The Covasim agent-based simulation process is presented in Figure 5.1. Here, individuals interact with each other increasing the probability of being infected. For instance, the student of the family may go to school and contact their classmate, and adults may go to workplaces and contact their colleagues. People may also go to a public place during daily activities or hang out with their family members and friends in the community. Both behaviors increase the risks of contracting infections and being sick.

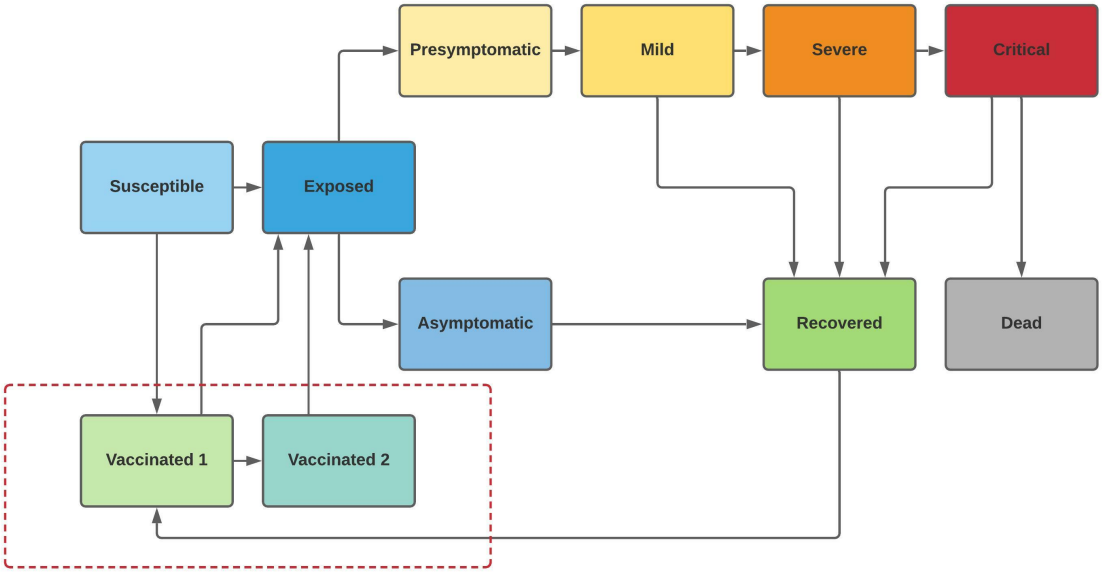

Figure 5.2 Compartment model of simulation.

For each individual, the health status can be described in Figure 5.2. In the Covasim simulation, each individual has the following health statuses: the *Susceptible* compartment represents people who can potentially be infected. The *Exposed* compartment represents the group of people who are exposed to the virus. The *Asymptomatic* compartment denotes the infected people who never develop symptoms, while the *Presymptomatic* compartment represents people who are not yet displaying symptoms of an illness or disease. The *Mild* compartment indicates people who have minor symptoms. The *Severe* compartment means that people have severe symptoms. The *Critical* compartment represents people who have even more severe symptoms and need to be treated in the intensive care unit. The *Recovered* compartment shows the recovered people, and the *Dead* compartment represents people who are dead from the critical symptoms.

Susceptible individuals can contact the infections and be exposed to the virus. On the one hand, a proportion of exposed individuals shows no symptoms and thus become asymptomatic. The asymptomatic infections recover from the disease

automatically. On the other hand, part of the exposed individuals develops symptoms. The symptoms can vary from mild to severe and then to critical. The majority of the people with every degree of symptoms recover. However, some individuals with critical symptoms may die due to their weak immunity or the delayed treatment process.

In our model, we extend the compartment model presented by Kerr et al. [2021] by adding two vaccine compartments. As shown in Figure 5.2, *Vaccinated 1* represents the individuals that have received the first shot of the vaccine, and *Vaccinated 2* represents the individuals that have received the second shot of the vaccine. We incorporate three types of vaccines in the model, which are Pfizer, Moderna, and Janssen. The Pfizer and Moderna vaccines include two shots, and the Janssen vaccine only requires one shot. Thus, a proportion of susceptible and recovered individuals receives the first shot of the vaccine at each period. The individuals who choose the Pfizer and Moderna vaccines receive the second shot after a few weeks of their first shot. The people who have received the vaccine can still be infected, but the probability of being infected is much smaller than the general susceptible individuals.

5.4 Optimization Model Formulation

This section provides the essential features and assumptions of the optimization model, the notations used in the optimization model, and the mathematical formulation of the optimization model.

5.4.1 Important Features and Model Assumptions

A few assumptions are made in the formulation of the optimization model. To begin with, the optimization model includes three types of vaccines, where Pfizer and Moderna vaccines require two shots and Janssen vaccines come with only one shot. Second, the Pfizer vaccination center has a 6,000 daily vaccine capacity due to the high

number of supplies [NJIT, 2021], while the Moderna and Janssen vaccination centers have 2,000 vaccine capacity [Heffernan, 2021a]. Third, since the human behavior for the vaccination is hard to predict, we assume the people in each region are served only by the vaccine centers in the closest nearby region. Fourth, for the new vaccine centers, we calculate the distribution cost from the warehouse to them. For the existing local pharmacies and small vaccine sites, since the detailed location and transportation cost information is limited, we only solve an overall vaccine capacity for each county and do not specify the vaccine capacity for each small site and the associated transportation cost. According to the data on Heffernan [2021b], the daily vaccine supply capacity for local pharmacies and small vaccination sites is set to 10,000, and we assume an ample total vaccine supply availability at each stage. In addition, we add \$1.41 to each of the vaccines allocated to the local pharmacies and small vaccination sites as a unit cost for delivery, according to the information obtained from WHO [2021c]. Fifth, the exact location of the supply warehouse for each type of vaccine is unknown. According to Pfizer [2021] and Peter Loftus [2021a], the Pfizer and Moderna vaccine manufacturing center is far from New Jersey. Thus, we assume that the Pfizer and Moderna vaccines are transported from the manufacturing center to the supply warehouse by air. The largest port of New Jersey locates in Essex County (Newark Airport), so we assume the Pfizer and Moderna supply warehouses for New Jersey are in Essex County. In addition, we observe that the Janssen supply warehouse locates in Somerset County. Sixth, the vaccine willingness rate is estimated as 0.3% per day using the information obtained from NJ.GOV [2021]. Seventh, we simulate the compartment flow in the optimization model in each region at each stage. As shown in Figure 5.3, S includes the *Susceptible* compartment in Figure 5.2, which means the susceptible individuals. People in S can be infected and become infected individuals I, which includes *Asymptomatic* and *Presymptomatic* compartments in Figure 5.2. *V1* and *V2* represent the individuals who received the first-dose and second-dose of different

types of vaccines, which represent *Vaccinated 1* and *Vaccinated 2* compartments in Figure 5.2, respectively. The susceptible individuals can be vaccinated and transfer to *V1* and *V2*. People in both *V1* and *V2* can transfer to recovered individuals R depending on the vaccine type. The results for each compartment in each region at each stage are only used in the optimization model to generate the vaccine center location and vaccine allocation decisions, and they will not influence the results of the agent-based simulation.

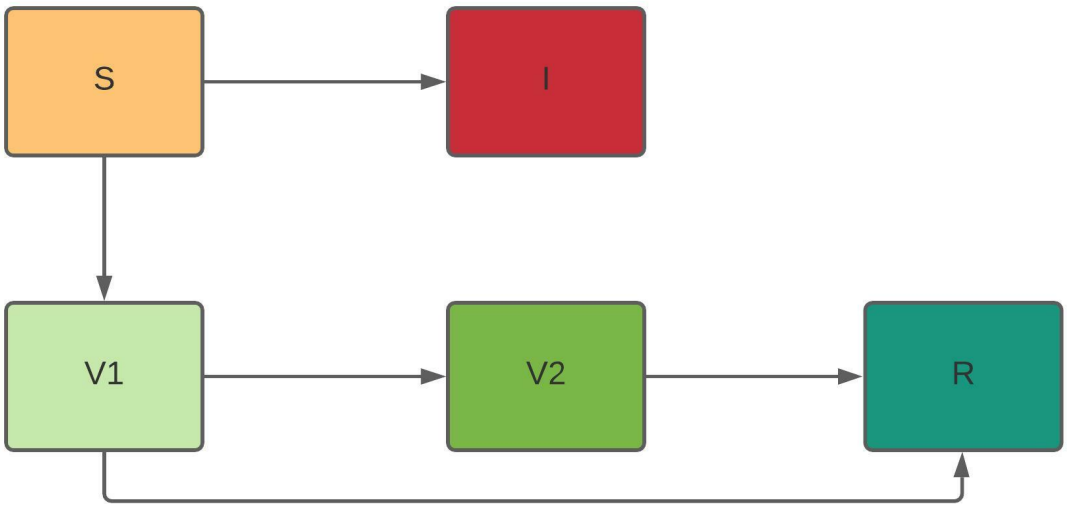

Figure 5.3 Compartment model of optimization.

5.4.2 Notation

Below we provide the notations used for the rest of the chapter.

Sets and Indices

J : Set of time periods, $J = \{0, \ldots, \overline{J}\}$.

R : Set of regions, $R = \{0, \ldots, \overline{R}\}$.

P : Set of vaccine supply warehouse, $P = \{1, 2, 3\}$.

N : Set of the number of the days between the first and second shot

of type i vaccine, $N = \{21, 28\}$.

j : Index for time period, where $j \in J$.

r : Index for region, where $r \in R$.

i : Index for vaccine, where $i \in \{1, 2, 3\}$.

p : Index for vaccine supply warehouse, where $p \in P$.

n : Index for the number of the days between the first and second shot of type i vaccine, $n \in N$.

State Variables

$S_{j,r}$: Susceptible individuals in region r at stage j.

$I_{j,r}$: Infected individuals including both symptomatic and asymptomatic individuals in region r at stage j.

$V^1_{j,r}$: Number of people get the first dose of type i ($i \in \{1, 2\}$) vaccine and a single dose of type i ($i \in \{3\}$) vaccine in region r at stage j.

$V^2_{j,r}$: Number of people who get the second dose of type i ($i \in \{1, 2\}$) vaccine in region r at stage j.

Other Parameters

b^i_r : Cost of building type i vaccination center in region r.

c^i : Purchase cost for each type i vaccine.

$d_{r,l}$: The distance from the highest populated city in region r to the highest populated city in region l.

$d_{p,r}$: The distance from vaccine supply warehouse p to the highest populated city in region r.

t : Unit transportation cost of vaccines with a truck from the vaccine supply warehouse to a region.

$G^i_{j,r}$: Vaccination capacity for type i vaccination center at stage j in region r.

H_j^i : Vaccine supply upper bound for type i vaccine at stage j.

$C_{j,r}^i$: Total existing capacity of the local pharmacies and small vaccination sites for type i vaccine at stage j in region r.

β_r^1 : The first shot vaccine acceptance rate, i.e., willingness to get vaccinated, for a two-dose vaccine in region r.

β_r^2 : The lower bound of the second shot vaccine acceptance rate for a two-dose vaccine in region r.

β_r : The vaccine acceptance rate for the one-dose vaccine in region r.

$\alpha_r^{1,i}$: Proportion of individuals who get immunization by the first shot of type i two-dose vaccine.

$\alpha_r^{2,i}$: Proportion of individuals who get immunization by the second shot of type i two-dose vaccine.

α_r : Proportion of individuals immune by the one-shot vaccines.

n_r : The total number of vaccine centers allocated in region r.

e : Euler's number.

m : Parameter that is used to change the value of equations (5.1q) and (5.1r).

k : Parameter used to change the value of equations (5.1q) and (5.1r).

π_r : The initial number of susceptible individuals in region r, inputted from the simulation model.

ϖ_r : The initial number of infections in region r, inputted from the simulation model.

θ_r^i : The initial number of the individuals who have received the first-dose type i ($i \in \{1, 2\}$) vaccine shot in region r.

ϑ_r^i : The initial number of the individuals who have received the second-dose type i ($i \in \{1, 2\}$) vaccine shot in region r.

σ_r^i : The initial number of the individuals who have received the first-dose type i ($i \in \{3\}$) vaccine shot in region r.

Decision variables:

x_r^i :Whether to build type i vaccination center in region r ($x_r^i \in \{0,1\}$).

$y_{r,l}$:Whether vaccination center in region r serves people in region l ($y_{r,l} \in \{0,1\}$).

$o_{j,r}^{i,1}$:Number of type i ($i \in \{1,2\}$) first-dose vaccines allocated to region r at end of period j for a newly established center.

$o_{j,r}^{i,2}$:Number of type i ($i \in \{1,2\}$) second-dose vaccines allocated to region r at end of period j for a newly established center.

$o_{j,r}^{i}$:Number of type i ($i \in \{3\}$) vaccines allocated to region r at end of period j for a newly established center.

$z_{j,r}^{i,1}$:Number of type i ($i \in \{1,2\}$) first-dose vaccines allocated to region r at end of period j for existing pharmacies and small vaccination sites.

$z_{j,r}^{i,2}$:Number of type i ($i \in \{1,2\}$) second-dose vaccines allocated to region r at end of period j for existing pharmacies and small vaccination sites.

$z_{j,r}^{i}$:Number of type i ($i \in \{3\}$) vaccines allocated to region r at end of period j for existing pharmacies and small vaccination sites.

5.4.3 Optimization Model Formulation

The mathematical formulation for the optimization model is given below.

$$\min \quad \sum_{j\in J}\sum_{r\in R} I_{j,r} \tag{5.1a}$$

$$\text{s.t.} \quad y_{r,l} \le x_r^i \qquad r \in R, i \in \{1,2\}, \tag{5.1b}$$

$$\sum_{r\in R} y_{r,l} = 1 \qquad \forall l \in R, \tag{5.1c}$$

$$x_k^i + y_{r,l} \le 1 \qquad \forall k,r,l \in R, i \in \{1,2\}$$

$$(\text{s.t.} \quad d_{k,l} \le d_{r,l}), \tag{5.1d}$$

$$\sum_{i=1}^{3} x_r^i \le n_r \qquad \forall r \in R, \tag{5.1e}$$

$$S^{\omega}_{0,r} = \pi_r, \quad I^{\omega}_{0,r} = \varpi_r, \quad V^{i,1}_{0,r} = \theta^i_r, \quad V^{i,2}_{0,r} = \vartheta^i_r \quad r \in R, i \in \{1,2\},$$

$$V^i_{0,r} = \sigma^i_r \quad r \in R, i \in \{3\}, \tag{5.1f}$$

$$S_{j+1,r} = S_{j,r} - \hat{I}_{j,r} - \sum_{i\in\{1,2\}} (o^{i,1}_{j,l} + z^{i,1}_{j,l}) - (o^3_{j,l} + z^3_{j,l})$$
$$j \in J \setminus \{\overline{J}\}, r \in R, \tag{5.1g}$$

$$I_{j+1,r} = I_{j,r} + \hat{I}_{j,r} - \sum_{i\in\{1,2\}} (o^{i,1}_{j,l} + z^{i,1}_{j,l})\alpha^{1,i}_r - \sum_{i\in\{1,2\}} (o^{i,2}_{j,l} + z^{i,2}_{j,l})\alpha^{2,i}_r$$
$$-(o^3_{j,l} + z^3_{j,l})\alpha_r \qquad j \in J \setminus \{\overline{J}\}, r \in R, \tag{5.1h}$$

$$V^1_{j+1,r} = V^{i,1}_{j,r} + \sum_{i\in\{1,2\}} (o^{i,1}_{j,r} + z^{i,1}_{j,r} - o^{i,2}_{j,r} - z^{i,2}_{j,r}) + (o^3_{j,r} + z^3_{j,r})$$
$$j \in J \setminus \{\overline{J}\}, r \in R, \tag{5.1i}$$

$$V^2_{j+1,r} = V^{i,2}_{j,r} + o^{i,2}_{j,r}, \qquad j \in J \setminus \{\overline{J}\}, r \in R, i \in \{1,2\}, \tag{5.1j}$$

$$\sum_{l\in R} (o^{i,1}_{j,l} + o^{i,2}_{j,l}) y_{r,l} \le G^i_{j,r} \qquad j \in J, r \in R, i \in \{1,2\}, \tag{5.1k}$$

$$\sum_{l\in R} o^i_{j,l} y_{r,l} \le G^i_{j,r} \qquad j \in J, r \in R, i \in \{3\}, \tag{5.1l}$$

$$\sum_{l\in R} (z^{i,1}_{j,l} + z^{i,2}_{j,l}) \le C^i_{j,r} \qquad j \in J, r \in R, i \in \{1,2\}, \tag{5.1m}$$

$$\sum_{l\in R} z^i_{j,l} \le C^i_{j,r} \qquad j \in J, r \in R, i \in \{3\}, \tag{5.1n}$$

$$\sum_{l\in R} (o^{i,1}_{j,l} + o^{i,2}_{j,l} + z^{i,1}_{j,l} + z^{i,2}_{j,l}) \le H^i_j \qquad \forall j \in J, i \in \{1,2\}, \tag{5.1o}$$

$$\sum_{l\in R} (o^i_{j,l} + z_{j,l}) \le H^i_j \qquad \forall j \in J, i \in \{3\}, \tag{5.1p}$$

$$\sum_{l\in R} (o^{i,1}_{j,l} + o^{i,2}_{j,l} + z^{i,1}_{j,l} + z^{i,2}_{j,l}) \ge \frac{m}{1+e^{kj}} \qquad \forall j \in J, i \in \{1,2\}, \tag{5.1q}$$

$$\sum_{l\in R} (o^i_{j,l} + z_{j,l}) \ge \frac{m}{1+e^{kj}} \qquad \forall j \in J, i \in \{3\}, \tag{5.1r}$$

$$o^{i,1}_{j,l} + z^{i,1}_{j,l} \le S_{j,r}\beta^1_r \qquad j \in J, \quad r,l \in R, i \in \{1,2\}, \tag{5.1s}$$

$$\beta^2_r o^{i,1}_{j-n,l} \le o^{i,2}_{j,l} \le o^{i,1}_{j-n,l} \qquad j \in J, \quad r,l \in R, i \in \{1,2\}, n \in N, \tag{5.1t}$$

$$o^i_{j,l} + z^i_{j,l} \le S_{j,r}\beta_r \qquad j \in J, \quad r,l \in R, i \in \{3\}, \tag{5.1u}$$

$$\sum_{r\in R} b^i_r x^i_r + \sum_{j\in J}\sum_{l\in R}\sum_{i\in\{1,2\}} c^i (o^{i,1}_{j,l} + o^{i,2}_{j,l}) + \sum_{j\in J}\sum_{l\in R}\sum_{i\in\{3\}} c^i o^i_{j,r}$$

$$+\sum_{j\in J}\sum_{l\in R}\sum_{i\in\{1,2\}} c^i(z^{i,1}_{j,l}+z^{i,2}_{j,l})+\sum_{j\in J}\sum_{l\in R}\sum_{i\in\{3\}} c^i z^i_{j,r}$$

$$+\sum_{i\in\{1,2,3\}}\sum_{p\in P}\sum_{r\in R} td_{p,r}x^i_r \le \Delta \tag{5.1v}$$

$$x^i_r, y_{r,l}\in\{0,1\} \qquad i\in I, j\in J, r\in R, \tag{5.1w}$$

$$S_{j,r},\quad G_{j,r},\quad C_{j,r},\quad I_{j,r},\quad \hat{I}_{j,r},\quad o^{i,1}_{j,r},\quad o^{i,2}_{j,r},\quad o^i_{j,r},\quad z^{i,1}_{j,r},\quad z^{i,2}_{j,r},\quad z^i_{j,r}\ge 0,$$

$$i\in I, \in J, r\in R. \tag{5.1x}$$

Objective Function (5.1a)**.** The objective function (5.1a) minimizes the total number of infections over all the regions throughout the planning horizon.

Vaccination Center Location and Service Constraints (5.1b) **-** (5.1e)**.** Constraint (5.1b) ensures that region r cannot serve region l if there is no vaccination center build in region r. Constraint (5.1c) represents that only one region with a vaccination center can serve region l. Constraint (5.1d) ensures that the nearest region with a vaccination center serves region l. Constraint (5.1e) limits the total number of different types of vaccine centers allocated to region r.

Population Infection Dynamics Constraints (5.1f) **-** (5.1j)**.** Constraint (5.1f) gives the initial number of susceptible individuals and infections generated from the simulation model and the initial number of individuals who have received the first-dose of type i vaccine, as well as the initial number of individuals who have received the second-dose of type i ($i\in\{1,2\}$) vaccine. Constraint (5.1g) shows that the number of susceptible individuals in region r at stage $j+1$ equals the number of susceptible individuals from the previous stage minus the number of infected individuals in region r at stage j and minus the number of susceptible individuals who have received the first-dose of type i ($i\in\{1,2\}$) vaccine in region r at stage j, and minus the number

of susceptible individuals who have received a single dose of type i ($i \in \{3\}$) vaccine in region r at stage j.

Constraint (5.1h) represents that the number of infected individuals in region r at stage $j+1$ equals the number of infected individuals from the previous stage plus newly infected individuals, minus the number of individuals saved by the vaccines. Constraint (5.1i) indicates that the number of people who have received the first-dose of type i ($i \in \{1, 2, \}$) vaccine and a single dose of type i ($i \in \{3\}$) vaccine in region r at stage $j+1$ equals the number of people who have received the first-dose of type i ($i \in \{1, 2\}$) vaccine and a single dose of type i ($i \in \{3\}$) vaccine from the previous stage plus the newly vaccinated people (first dose and single dose) minus the number people who have taken the second dose of type i ($i \in \{1, 2, \}$) vaccine. Constraint (5.1j) indicates that the number of people who have received the second-dose of type i ($i \in \{1, 2\}$) vaccine in region r at stage $j+1$ equals the number of people who have received the second-dose of type i ($i \in \{1, 2\}$) vaccine from previous stage plus the newly vaccinated people (second dose).

Vaccines Logistics and Capacity Constraints (5.1k) **-** (5.1v)**.** Constraints (5.1k) and (5.1l) ensure that the total number of each type of vaccine allocated to the new vaccine centers in region r at stage j should be smaller or equal to the vaccine capacity upper bound of the vaccination center in region r. Constraints (5.1m) and (5.1n) ensure that the total number of each type of vaccine allocated to local pharmacies and small vaccine sites in region r at stage j should be smaller than or equal to the vaccine capacity upper bound (obtained from Heffernan [2021b]). Constraints (5.1o) and (5.1p) ensure that the total number of each type of vaccine supplied to the new vaccine centers and local pharmacies (and small vaccination sites) over all regions at each stage j should be smaller than or equal to the vaccine supply upper bound at stage j. Constraints (5.1q) and (5.1r) indicate that the total number of each type

of vaccine supplied to the new vaccine centers and the existed vaccine locations over all regions at each stage j should be greater than or equal to the vaccination lower bound at stage j. The vaccination lower bound at each stage j is represented by an exponential function reaching an asymptote over time. Constraint (5.1s) indicates that the total number of people who have received the first shot of type i ($i \in \{1, 2\}$) vaccine should be smaller than or equal to the people who are willing to be vaccinated. Constraint (5.1t) implies that the total number of people vaccinated by the second shot of type i ($i \in \{1, 2\}$) vaccine should be greater than or equal to the lower bound of the people who are willing to be vaccinated but smaller than or equal to the people who have received the first shot n ($n \in N$) days before the second shot. Constraint (5.1u) represents that the total number of people vaccinated by type i ($i \in \{3\}$) vaccine should be smaller than or equal to the people who are willing to be vaccinated.

Constraint (5.1v) represents the budget limitations. Specifically, constraint (5.1v) ensures that the total vaccination center building cost, plus the cost of vaccines that are distributed to the newly established vaccine centers and existing pharmacies and small vaccination sites, plus the logistics distribution cost from the vaccine supply warehouses to vaccine centers, over all regions throughout the whole planning horizon, should be smaller than or equal to a certain budget level.

Integrality and Non-Negativity Constraints (5.1w) **-** (5.1x)**.** Constraints (5.1w) and (5.1x) are the variable's restrictions. Specifically, constraint (5.1w) indicates that x_r^i and $y_{r,l}$ are binary variables. Constraint (5.1x) implies that the number of susceptible individuals, the vaccine upper bounds, the number of existed infected and newly infected individuals, the number of each type of vaccine should be greater than or equals to 0.

5.4.4 Linearization

Constraint (5.1l) is non-linear. We define two variables $U^i_{j,r,l}$ and $o^{i,UB}_{j,r}$, where $U^i_{j,r,l} = y_{r,l}o^i_{j,r}$ and $o^{i,UB}_{j,r}$ is the upper bound of parameter $o^i_{j,r}$. Thus, constraint (5.1l) can be linearized by the following equations:

$$U^i_{j,r,l} \leq o^{i,UB}_{j,r} y_{r,l} \qquad j \in J, \quad r,l \in R, i \in \{3\}, \tag{5.2}$$

$$U^i_{j,r,l} \leq o^i_{j,r} \qquad j \in J, \quad r,l \in R, i \in \{3\}, \tag{5.3}$$

$$U^i_{j,r,l} \geq o^i_{j,r} - o^{i,UB}_{j,r}(1 - y_{r,l}) \qquad j \in J, \quad r,l \in R, i \in \{3\}, \tag{5.4}$$

$$0 \leq U^i_{j,r,l} \leq o^{i,UB}_{j,r} \qquad j \in J, \quad r,l \in R, i \in \{3\}. \tag{5.5}$$

Constraint (5.1k) can be linearized by using a similar method.

5.4.5 Simulation-Optimization Model

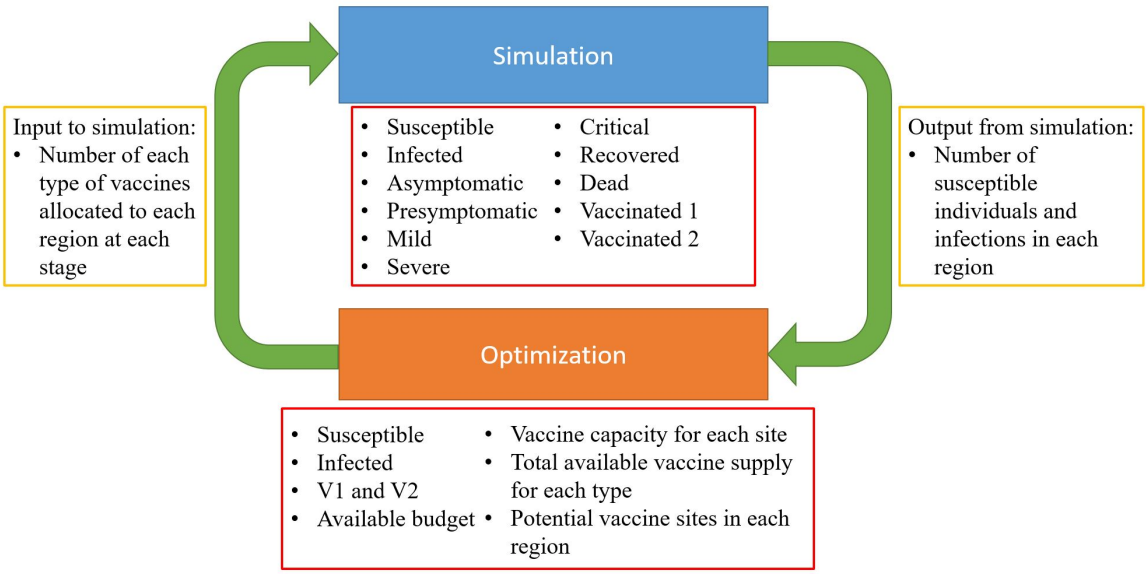

Figure 5.4 The loop of simulation-optimization model.

In this chapter, we introduce a simulation-optimization approach to address the vaccination facility location and vaccine allocation challenges of the COVID-19. We extend the Covasim agent-based model of the COVID-19 and incorporate it with

a new vaccination center and vaccine-allocation optimization model. As shown in Figure 5.4, the integrated model runs in a loop, where the simulation model forecasts the disease transmission and import the results into the optimization model. The optimization model minimizes the total number of infections throughout the planning horizon by choosing the optimal vaccination center locations and vaccine allocation among each region and sends the results back to the simulation model to estimate the number of infections in the future. Specifically, the simulation model uses the number of initial susceptible and infected individuals to forecast the number of susceptible and infected individuals, presymptomatic and asymptomatic individuals, as well as the mild, severe, critical, recovered, and dead individuals for each stage in the current planning horizon. The forecast numbers of susceptible and infected individuals are imported into the optimization model. The optimization model incorporates the available budget, potential vaccine sites in each region, vaccine capacity for each site, and total available vaccine supply for each vaccine type to generate the optimal vaccination center location and vaccine allocation while minimizing the total number of infections in the considered regions. The optimization results include the number of people that are supposed to be vaccinated in vaccination centers and local pharmacies (and small vaccination sites) at each future stage in each region. Then these parameters are fed into the simulation model to simulate the number of susceptible and infected individuals for the next periods.

We implement our model to the New Jersey state in the United States; each stage in the model represents a one-day period. We run the simulation optimization in three steps. In the first step, the number of initial susceptible individuals and infections from JHU [2020] is imported into the optimization model to generate the vaccination center locations and vaccine allocations for the first 30-days period. Then the results are input in the simulation model to simulate the number of susceptible individuals and infections for the first 30-days period. In the second step, the

simulation results of the first 30-days are input into the optimization model, and the optimization model generates the optimal vaccination center locations and vaccine allocation decisions for the second 30-days period. The optimization model results for the second 30-days are combined with the first 30-days together and then imported into the simulation model to estimate the total number of susceptible individuals and infections for the first 60-days. In the last step, we repeat the second step and combine the 90-days vaccine allocation results. Thus, we solve the model for a total 90-days time period. For step 2 and step 3, the vaccination center allocation variable x_r^i is fixed to be the same as the solution of step 1. This indicates that the model generates the vaccine allocation decisions under the same x_r^i values in each loop.

5.5 Case Study Data

Source: [Aparadinar, 2021]

Figure 5.5 All the counties in New Jersey.

This section presents the data used to formulate and test the model. The data includes the population for each county in New Jersey State, the number of infections over time for each county in New Jersey State, the logistics cost, and the cost of vaccines. In our model, each stage represents a one-day period. In total, we consider a 90-day planning horizon, which is equal to three months.

5.5.1 Population and Infection Data

Table 5.1 shows the population and the cumulative number of infections data for each county in New Jersey state, which is obtained from JHU [2020]. For the number of infections, we only present three specific days of the total 90 day period, which are March 1, April 12, and May 24, 2021. The numbers of cumulative infections are rounded in thousands.

Table 5.1 Populations and the Number of Infections (in Thousands) for Each County in New Jersey

County	Population	March 1, 2021	April 12, 2021	May 24, 2021
Atlantic	274.5	24.9	29.7	31.5
Bergen	905.1	78	96.4	104.1
Burlington	448.7	35.5	41.9	44.1
Camden	513.5	44.3	51.1	55.4
Cape May	97.3	7.3	8.6	9.1
Cumberland	156.6	14.3	15.8	17
Essex	783.9	74	90.1	93.8
Gloucester	288.8	24.2	28.2	30.4
Hudson	634.3	69.6	83.7	87.8
Hunterdon	127.4	7	9	9.8
Mercer	367.5	27.9	32.1	33.8
Middlesex	810.0	72.8	87.8	91.9
Monmouth	630.4	57.2	71.5	75.3
Morris	492.3	37.7	47.4	50
Ocean	576.5	58.9	71.9	75.6
Passaic	501.6	57	67.5	72.7
Salem	66.1	4.7	5.5	6.1
Somerset	323.5	22.9	28.1	30
Sussex	148.9	9.2	12.7	13.9
Union	536.5	57	67.4	71.2
Warren	108.6	7.1	9	9.9

5.5.2 Logistics and Operations Cost Data

Table 5.2 presents the vaccine cost and efficiency data for Pfizer, Moderna, and Janssen. Table 5.3 shows the logistic and operations cost data. The fixed cost of

the vaccination center includes planning and coordination cost, training cost, social mobilization cost, cold chain equipment cost, pharmacovigilance cost, as well as hand hygiene cost. The recurring cost contains cold chain recurrent cost, vaccination certificates cost, personal protective equipment (PPE) cost, Hand hygiene cost, and waste management cost.

Table 5.2 COVID-19 Vaccine Cost ($) and Efficiency [Seladi-Schulman, 2021]

Vaccine Category	Cost per dose	First Dose Efficiency	Second Dose Efficiency
Pfizer	19.5	80%	95%
Moderna	15	80%	94.1%
Janssen	10	74.4%	-

Table 5.3 Logistics Cost ($) for the COVID-19 Vaccines [WHO, 2021c]

Cost Category	Fixed	Recurring	Total
Planning and coordination	30,513	-	30,513
Training	7,629	-	7,629
Social mobilization	137,308	-	137,308
Cold chain equipment	61,026	-	61,026
Cold chain recurrent	-	1,447	1,447
Pharmacovigilance	15,257	-	15,257
Vaccination certificates	-	4,495	4,495
PPE	-	9,745	9,745
Hand hygiene	2,247	13,955	16,202
Waste management	-	5,944	5,944

5.6 Model Validation

In this section, we present the validation results of the simulation-optimization model shown in Section 5.3. The government set up one Pfizer vaccination center in March at the New Jersey Institute of Technology in Essex County. The vaccination center can vaccinate up to 6,000 people each day. Thus, we use this actual vaccination center location in our model for validation. The number of Pfizer vaccine centers in our model is set to 1, and the location is in Essex County, while other types of vaccine centers are set to be 0 in the validation experiments. The optimization model decides on how many vaccines of each type are allocated to each region and uses these values as inputs in the simulation model. We present the number of estimated infections throughout the 90-days planning horizon and compare it with the real outbreak data. The results of nine counties are shown in Figure 5.6 (the validation results of all the counties in New Jersey are shown in Figures C.1, C.2, and C.3 in Appendix C).

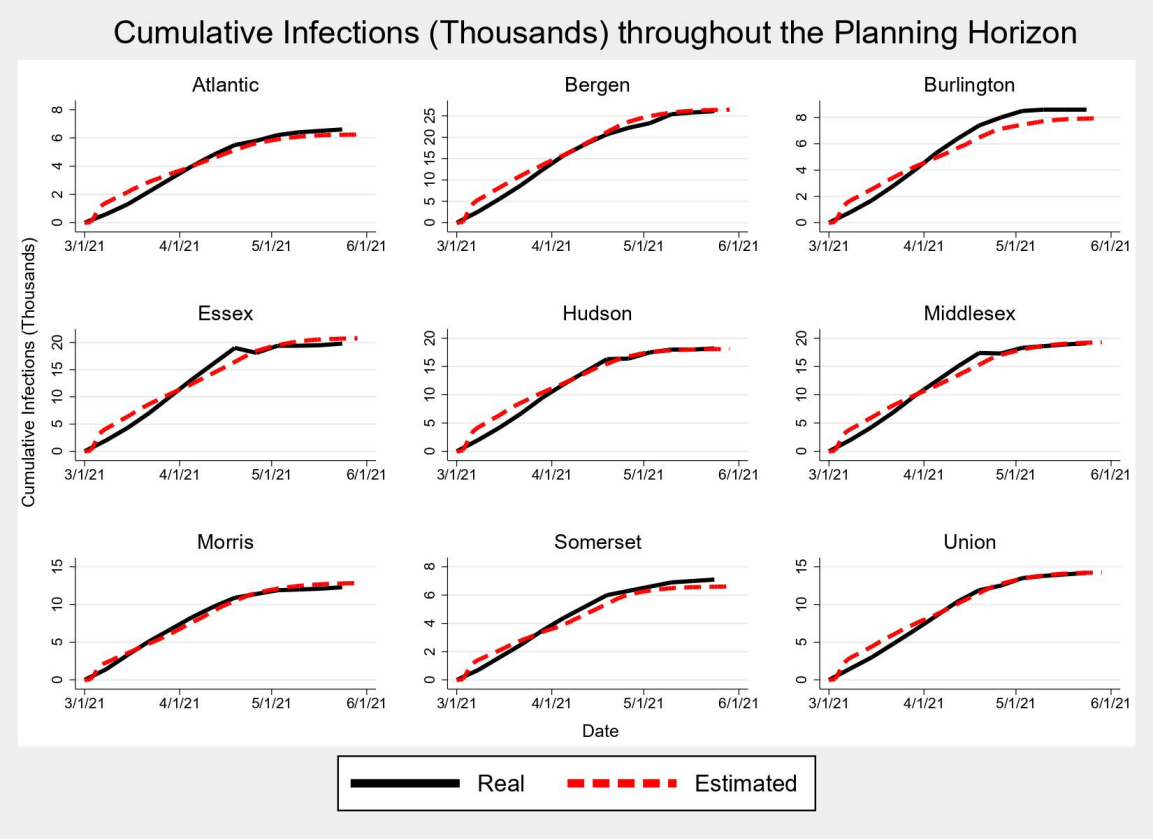

Figure 5.6 Model validation against real outbreak data in New Jersey.

Table 5.4 Statistical Analysis to Compare the Weekly Predicted New Cases and Real Outbreak Data

County	Mean		Two-tailed paired-t-test		
	Outbreak	Predicted	t-stat	t-critical	p-value
Atlantic	508	479	0.21	2.20	0.73
Bergen	2008	2030	0.04		0.94
Burlington	662	609	0.28		0.61
Camden	854	860	0.03		0.96
Cape May	138	167	0.60		0.27
Cumberland	208	183	0.46		0.59
Essex	1523	1593	0.14		0.84
Gloucester	477	402	0.69		0.25
Hudson	1400	1391	0.02		0.97
Hunterdon	215	193	0.40		0.56
Mercer	454	449	0.03		0.95
Middlesex	1469	1477	0.02		0.98
Monmouth	1392	1405	0.03		0.96
Morris	946	984	0.14		0.74
Ocean	1285	1318	0.08		0.86
Passaic	1208	1300	0.33		0.62
Salem	108	117	0.40		0.54
Somerset	546	507	0.26		0.64
Sussex	362	484	1.24		0.27
Union	1092	1093	0.00		0.99
Warren	215	188	0.52		0.35

According to the results, since the model starts from zero infections, but the real data is in the middle of the pandemic, the model predicts a greater number of infections at the beginning of the time period than the predicted number becomes less than the real data in the later periods. Overall, the estimation fits the real data well. In addition, we perform a paired-t-test to analyze the difference between the pairs of predicted new infections and the actual data in each period. As shown in Table 5.4, all p-values are greater than 0.05, and thus our model provides statistically similar predictions with the real outbreak data from March 1 to May 30, 2021, for each considered county.

5.7 Case Study Results

We apply our model described in Section 5.3 to all the counties in New Jersey. We solve the optimization model to generate the results of the optimal vaccination center locations and vaccines' allocation, including Pfizer, Moderna, and Janssen. Then we use the results generated by the optimization model as the inputs of the simulation model. We incorporate vaccination in the Covasim model. The vaccination includes the first and second shots for Pfizer and Moderna vaccines and a single shot for the Janssen vaccine. We solve the model for a 90-days period, a planning horizon from March 1, 2021, to May 30, 2021. The optimization model is solved using CPLEX 20.1 on a desktop computer running with Intel i7 CPU and 64.0 GB of memory. The simulation model is run on the same desktop computer in PyCharm Edu (using python language).

5.7.1 The Number of Cumulative Infections under Different Budget Levels

We fix only one Pfizer vaccination center in Essex county, similar to the validation experiments and test our model under different budget levels (from limited to ample).

We use $\$5M$ as a limited budget level, $\$10M$ as a medium budget level, and we do not put a budget restriction under the ample budget scenario. However, under the ample budget scenario, the number of people being vaccinated is bounded by the number of people willing to be vaccinated in each region.

Figure 5.7 shows the number of cumulative infections under different budget levels for nine counties in New Jersey (the number of cumulative infections under different budget levels for all the counties in New Jersey are shown in Figures C.4, C.5, and C.6 in Appendix C). According to the results, the number of cumulative infections stays the same under different budget levels at the initial stages. This is because it takes time for people to be exposed and develop symptoms after their being infected. Thus, the difference in the number of cumulative infections becomes more significant after a certain time period. For almost all the counties shown in Figure 5.7, the ample budget level generates the least number of cumulative infections due to the high number of vaccines allocated, followed by the medium budget level. However, for some of the counties, the cumulative number of infected individuals under different budget levels are similar, especially for the medium and ample budget levels. Not surprisingly, we find that these counties either have high populations or high initial infections. Thus, the model gives priority to allocate more vaccines to these counties when the budget is not ample. Therefore, the total number of vaccines that these counties receive under the medium budget level is similar to the number under the ample budget level, leading to a similar number of cumulative infections.

We find that some counties do not have the lower number of infections under the ample budget level (e.g., CapeMay and Salem County). This is because we randomly vaccinate susceptible and recovered individuals in the agent-based simulation model. Although more people are vaccinated under the medium and ample budget levels, more recovered people could be vaccinated than susceptible people. Thus, the

number of cumulative infections may be higher under medium and ample budget levels compared with the limited budget level.

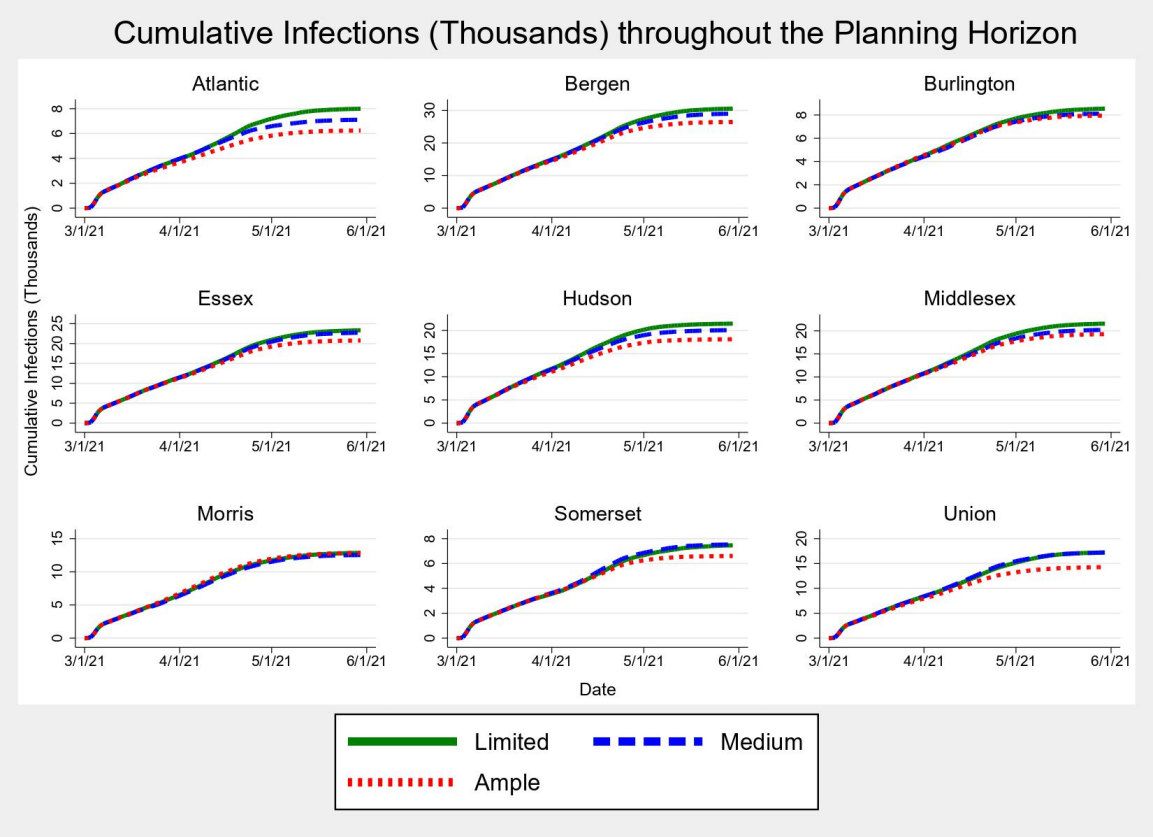

Figure 5.7 New Jersey cumulative infections under different budget levels.

5.7.2 The Number of Vaccines Allocated to Each County under Different Budget Levels

The number of vaccines allocated to each county under different budget levels is presented in Tables 5.5, 5.6, and 5.7, respectively. Each table presents the population proportion of each county, the total vaccines allocated to each county, the proportion of the vaccines allocated to each county, and the number of first and second doses of each type of vaccine allocated to each county. Figure 5.8 shows the proportion of each type of vaccine allocated under different budget levels.

Table 5.5 Vaccine Allocation under Limited Budget Level

County	Population Proportion	Vaccine Proportion	Total Vaccine	Pfizer First Dose	Pfizer Second Dose	Moderna First Dose	Moderna Second Dose	Janssen
Atlantic	3.1%	3.6%	38,789	4,500	1,083	6,493	2,676	24,037
Bergen	10.3%	9.5%	103,971	4,500	1,082	12,072	7,138	79,179
Burlington	5.1%	5.1%	56,034	4,502	1,080	6,862	2,970	40,620
Camden	5.8%	5.9%	63,752	4,500	1,080	8,640	4,392	45,140
Cape May	1.1%	1.8%	20,085	4,500	1,080	4,500	1,080	8,925
Cumberland	1.8%	2.4%	25,848	4,500	1,080	4,500	1,080	14,688
Essex	8.9%	7.9%	86,335	4,500	1,080	4,500	1,080	75,175
Gloucester	3.3%	3.6%	38,654	4,500	1,080	4,500	1,080	27,494
Hudson	7.2%	6.6%	71,729	4,500	1,080	4,500	1,080	60,569
Hunterdon	1.4%	2.1%	23,024	4,500	1,080	4,515	1,093	11,836
Mercer	4.2%	4.3%	46,304	4,500	1,080	4,500	1,080	35,144
Middlesex	9.2%	8.2%	88,937	4,500	1,080	4,500	1,080	77,777
Monmouth	7.2%	6.6%	71,448	4,500	1,080	4,500	1,080	60,288
Morris	5.6%	5.3%	58,236	4,500	1,080	4,500	1,080	47,076
Ocean	6.6%	6.1%	66,165	4,500	1,080	4,500	1,080	55,005
Passaic	5.7%	5.4%	59,113	4,500	1,080	4,500	1,080	47,953
Salem	0.8%	1.6%	17,099	4,500	1,080	4,500	1,080	5,939
Somerset	3.7%	4.0%	43,294	4,500	1,080	6,118	2,378	29,218
Sussex	1.7%	2.3%	25,086	4,500	1,080	4,500	1,080	13,926
Union	6.1%	5.8%	63,450	4,500	1,080	5,782	2,106	49,982
Warren	1.2%	2.0%	21,463	4,500	1,080	4,842	1,354	9,687
Total	**100.0%**	**100.0%**	**1,088,816**	**94,502**	**22,685**	**113,824**	**38,147**	**819,658**

According to the results, the total number of vaccines allocated increases when the budget level increases. Under a limited budget level, the majority of the vaccines are allocated in Janssen, followed by Moderna, while Pfizer has the least number

of vaccines allocated (Figure 5.8). On the contrary, Pfizer has the highest vaccine efficiency. This is because the insufficient budget limits the total number of vaccines purchased. Although Pfizer has the highest efficiency, the cost of each dose of the Pfizer vaccine is much higher than the others. On the contrary, the Janssen vaccine has the lowest price, followed by Moderna. Therefore, under the limited budget level (Table 5.5), the model considers purchasing more doses of vaccines rather than purchasing the vaccines with the highest efficiency. Thus under a limited budget, the model chooses to vaccine more people with mainly cheaper vaccines and the vaccines with a single dose. Compared with the population proportion and vaccine proportion, the counties with a bigger population are more likely to receive more vaccines. However, some counties may receive more (or less) vaccines compared with their population proportion due to their high (or low) number of initial infections.

Table 5.6 Vaccine Allocation under Medium Budget Level

County	Population Proportion	Vaccine Proportion	Total Vaccine	Pfizer First Dose	Pfizer Second Dose	Moderna First Dose	Moderna Second Dose	Janssen
Atlantic	3.1%	3.2%	61,169	4,500	1,080	26,005	13,683	15,901
Bergen	10.3%	9.9%	188,279	4,500	1,080	84,927	47,770	50,002
Burlington	5.1%	5.2%	98,378	4,500	1,080	41,796	22,671	28,331
Camden	5.8%	5.9%	112,200	4,501	1,081	49,253	27,279	30,086
Cape May	1.1%	1.3%	24,961	4,504	1,084	8,905	3,680	6,788
Cumberland	1.8%	1.9%	36,933	4,501	1,080	14,368	6,814	10,170
Essex	8.9%	8.6%	163,455	4,500	1,080	72,965	40,689	44,221
Gloucester	3.3%	3.4%	65,606	4,504	1,084	27,469	14,543	18,006
Hudson	7.2%	7.0%	134,295	4,500	1,080	60,535	33,883	34,297
Hunterdon	1.4%	1.6%	31,162	4,500	1,080	11,837	5,398	8,347
Mercer	4.2%	4.3%	82,226	4,500	1,080	35,112	19,013	22,521
Middlesex	9.2%	9.0%	170,680	4,504	1,084	77,708	43,924	43,460
Monmouth	7.2%	7.0%	133,654	4,500	1,080	60,232	33,703	34,139
Morris	5.6%	5.5%	105,676	4,500	1,080	46,992	25,992	27,112
Ocean	6.6%	6.4%	122,502	4,500	1,080	54,960	30,630	31,332
Passaic	5.7%	5.6%	107,558	4,500	1,080	47,909	26,496	27,573
Salem	0.8%	1.0%	18,657	4,500	1,080	5,932	1,946	5,199
Somerset	3.7%	3.7%	71,320	4,500	1,080	30,800	16,489	18,451
Sussex	1.7%	1.9%	35,542	4,504	1,084	13,902	6,600	9,452
Union	6.1%	6.0%	114,559	4,500	1,080	51,216	28,433	29,330
Warren	1.2%	1.4%	27,316	4,500	1,080	10,020	4,334	7,382
Total	**100.0%**	**100.0%**	**1,906,128**	**94,518**	**22,697**	**832,843**	**453,970**	**502,100**

Under the medium budget level (Table 5.6), the total number of Janssen vaccines allocated is decreased, while more Moderna vaccines are allocated (which is also shown in Figure 5.8). This is because the model starts to consider the vaccine efficiency when

the budget increases, and the expected number of people saved by the vaccines with higher efficiency is more than the number of people saved by the vaccines with lower efficiency. Nevertheless, since Pfizer is still much more expensive than Moderna and Janssen, the model allocates more Moderna vaccines instead of Pfizer. Compared with the population proportion with the vaccine allocation proportion, the counties with a higher population receive even more vaccines. This is because the total number of vaccines allocated is still not enough to satisfy the people's vaccination need, and the model gives priority to distribute more vaccines to the regions with high population and initial infections.

Table 5.7 Vaccine Allocation under Ample Budget Level

County	Population Proportion	Vaccine Proportion	Total Vaccine	Pfizer First Dose	Pfizer Second Dose	Moderna First Dose	Moderna Second Dose	Janssen
Atlantic	3.1%	3.1%	88,854	34,143	17,744	29,833	2,634	4,500
Bergen	10.3%	10.3%	294,610	161,094	66,391	58,775	3,850	4,500
Burlington	5.1%	5.1%	145,735	70,577	31,296	36,846	2,514	4,502
Camden	5.8%	5.9%	167,620	104,750	38,124	18,890	1,352	4,504
Cape May	1.1%	1.1%	30,842	13,383	4,596	6,619	1,744	4,500
Cumberland	1.8%	1.8%	50,308	21,690	9,031	13,131	1,956	4,500
Essex	8.9%	8.9%	254,718	136,864	55,362	53,241	4,751	4,500
Gloucester	3.3%	3.3%	93,755	56,344	20,229	11,328	1,352	4,502
Hudson	7.2%	7.2%	205,278	101,315	45,020	51,386	3,057	4,500
Hunterdon	1.4%	1.4%	40,817	18,793	6,749	8,766	2,009	4,500
Mercer	4.2%	4.2%	119,530	56,846	24,608	30,394	3,178	4,504
Middlesex	9.2%	9.3%	264,130	136,834	61,506	59,940	1,350	4,500
Monmouth	7.2%	7.2%	204,867	104,985	42,127	46,883	6,372	4,500
Morris	5.6%	5.6%	160,023	70,210	33,748	47,679	3,886	4,500
Ocean	6.6%	6.5%	186,872	95,527	38,248	42,705	5,892	4,500
Passaic	5.7%	5.7%	162,595	76,867	35,180	43,377	2,671	4,500
Salem	0.8%	0.7%	20,749	6,852	2,420	5,502	1,475	4,500
Somerset	3.7%	3.7%	105,050	47,109	20,604	29,120	3,717	4,500
Sussex	1.7%	1.7%	47,786	19,483	8,233	13,374	2,196	4,500
Union	6.1%	6.1%	174,383	86,554	36,975	42,214	4,140	4,500
Warren	1.2%	1.2%	34,624	13,765	5,579	9,104	1,676	4,500
Total	**100.0%**	**100.0%**	**2,853,146**	**1,433,985**	**603,770**	**659,107**	**61,772**	**94,512**

As shown in Table 5.7 and Figure 5.8, the total number of Pfizer vaccines allocated under the ample budget level increases significantly. Compared with Moderna and Janssen vaccines, the model gives priority to allocate as many Pfizer

vaccines as possible. When there is no budget limitation on the vaccine allocation, vaccine efficiency is the only consideration for the vaccine administration. Thus, Pfizer vaccines have the priority to be allocated compared with Moderna and Janssen. Moreover, under the ample budget level, the vaccine allocation proportion is almost the same as the population proportion. This is because we assume the same vaccine acceptance rate in each county of New Jersey. Under the ample budget level, the number of people who receive vaccines reaches the upper bound on the vaccine supply available. This implies that all the people who are willing to be vaccinated receive the vaccine shots when the budget is ample and as long as there is sufficient vaccine supply. Thus, the vaccine allocation proportion is the same as the population proportion for each county in New Jersey.

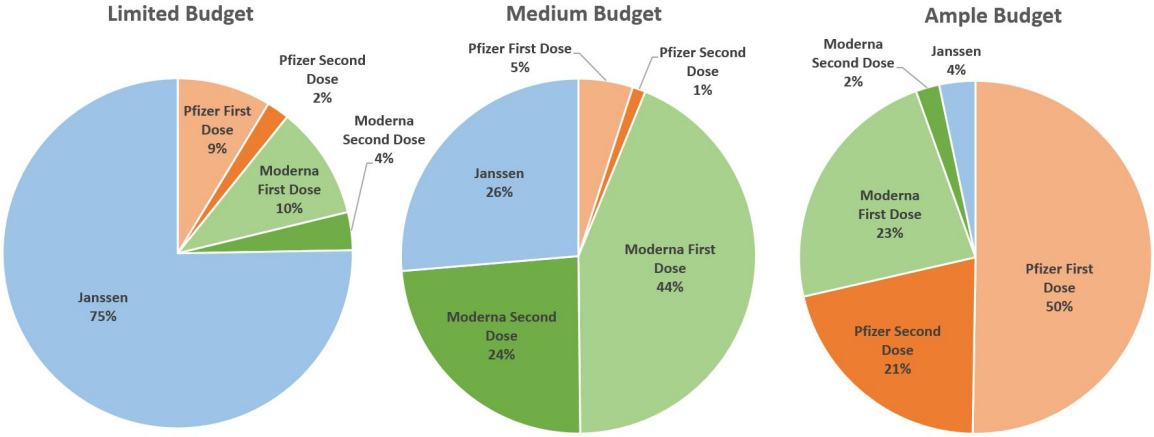

Figure 5.8 Proportion of each type of vaccine under different budget levels.

For all the budget levels, the number of the second dose of Pfizer and Moderna vaccines is much smaller than that of the first dose. This is because when the total number of vaccine supply is bounded even if the purchasing budget is ample, the model gives priority to administer as many as the first shots of those vaccines since the effectiveness of the first shot is high and more people can benefit from the vaccination.

5.7.3 Vaccination Center Location Decision under Medium Budget Levels and Number Restrictions

In this subsection, we present the vaccination center location decisions generated by the model. Specifically, we change the number of vaccine centers that can be allocated for each type of vaccine and then generate the vaccination center locations and service decisions for those vaccine centers under medium budget level.

Vaccination Center Locations for Pfizer We fix the Pfizer vaccination center to one while keeping Moderna and Janssen centers to zero, as shown on the left side of Figure 5.9. The model allocates the Pfizer center to Essex county, which is the same decision the government has taken in the real situation.

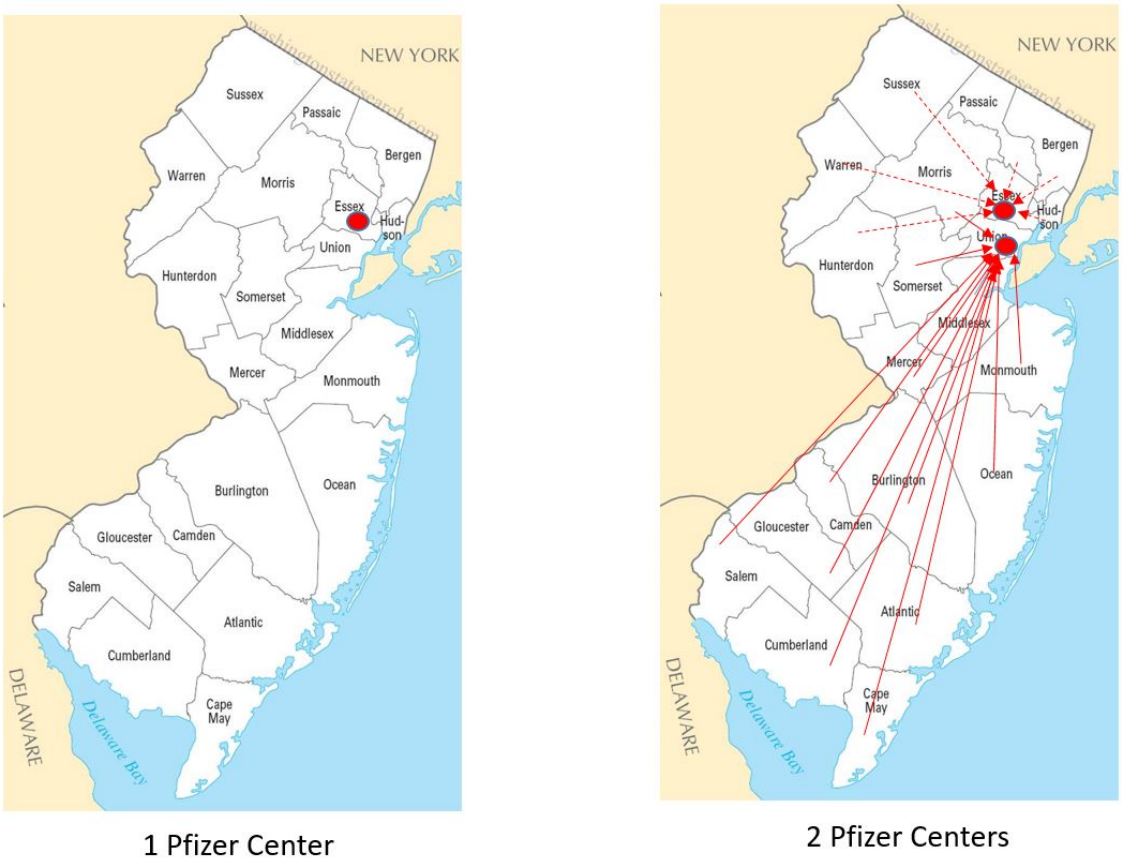

Figure 5.9 Vaccination center locations for Pfizer.

We then increase the number of Pfizer vaccine centers to two, and the vaccination center decision is changed. The right side of Figure 5.9 shows that one

of the vaccination centers is allocated in Essex County, and the other is allocated in Union County. The vaccination center in Essex County serves Bergen County, Hudson County, Passaic County, Sussex County, Warren County, and Hunterdon County. The Union County vaccination center serves the rest of the counties in New Jersey.

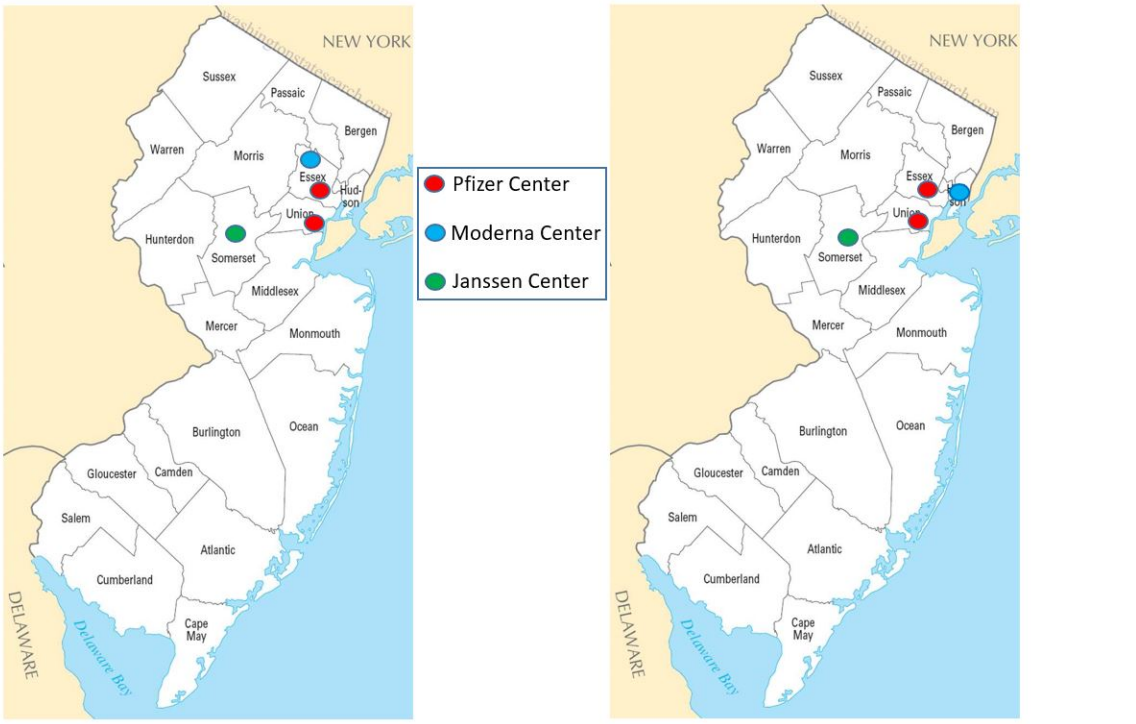

Figure 5.10 Vaccination center locations for all types of vaccines.

Vaccination Center Locations for Multiple Types of Vaccines Vaccination center locations for multiple types of vaccines are studied. Figure 5.10 presents the vaccination center locations when the numbers of Moderna centers and Janssen centers are set to one, while the number of Pfizer centers remains to be two. On the left side of Figure 5.10, we allow each county to have different types of vaccine centers. On the right side of Figure 5.10, each region can only have one type of vaccine center. For the first case, Essex County has the Pfizer and Moderna centers allocated, while Union County has another Pfizer center allocated. This is because the vaccine

warehouses for Pfizer and Moderna are located in Essex County. Somerset County has the Janssen vaccination center allocated. When only considering the transportation cost from the warehouse to the vaccination centers, the distance from the warehouse to the vaccination centers is the only factor that can influence the vaccination center locations. Therefore, the model chooses the closest county to the supply warehouse for each type of vaccine as the corresponding vaccination center. For the second case, the Moderna vaccination center is moved to Hudson County since each county can only have one vaccination center and Hudson County is the third closest county to the warehouse after Essex County and Union County. We do not show the vaccine centers service decision in Figure 5.10 because the service decision for the Pfizer center is the same as Figure 5.9. We find that Union County is geographically the closest county to Essex County, where the Pfizer and Moderna vaccine warehouses are allocated. Thus, the vaccination center locations for the counties in New Jersey are ordered by their distance from the warehouse from low to high.

5.7.4 Vaccine Allocation between Vaccination Centers and Local Pharmacies (and Small Vaccination Sites)

In this subsection, we compare the vaccine allocation between vaccination centers and local pharmacies (and small vaccination sites) under different budget levels ($\$5M$ as the limited, $\$10M$ as the medium, and no budget limitation as to be ample).

Table 5.8 presents the results of vaccine allocation between the vaccination centers and local pharmacies (and small vaccination sites) when only one Pfizer center is located. Under the limited budget level, the model allocates all the Pfizer vaccines to the vaccination centers. This is because vaccines allocated to the vaccination center cost lower than those allocated to local pharmacies and small vaccination sites. Under the limited budget level, the model chooses to distribute vaccines to the vaccination centers because more people benefit from the vaccination. Under the medium budget

level, the number of vaccines allocated to the vaccination center decreases. However, the total number of vaccines allocated to the vaccination center is much more than the local pharmacies and small vaccination sites. Under an ample budget level, the model allocates the majority of the vaccines to local pharmacies and small vaccination sites since there is no budget limitation on purchasing vaccines and the vaccination capacity provided over pharmacies and small vaccination sites in total is larger than that of the vaccination centers.

Table 5.8 Vaccine Allocation between Vaccination Centers and Local Pharmacies (and small vaccination sites) with Only One Pfizer Center

Budget		Limit		Medium		Ample	
Pfizer	Center	117,180	100.0%	141,959	73.2%	310,134	15.2%
	Pharmacy	0	0.0%	51,916	26.8%	1,727,621	84.8%
	Total	117,180	100.0%	193,875	100.0%	2,037,755	100.0%

Table 5.9 shows the vaccine allocation results between vaccination centers and local pharmacies (and small vaccination sites) with different types of vaccination centers. In this case, the number of Pfizer vaccination centers is fixed to two, and the number of Moderna and Janssen vaccination centers is set to one each. Similar to Table 5.8, the number of vaccines allocated to the vaccination centers shows a decreasing trend for each type of vaccine when the budget is increased from limited to ample. For the Janssen vaccine, the proportion of the vaccines allocated to the vaccination center increases under the medium budget level compared with the limited budget level. One possible reason might be that the total number of Janssen vaccines allocated decreases significantly under the medium budget level, as we discussed in Section 5.7.2.

Table 5.9 Vaccine Allocation between Vaccination Centers and Local Pharmacies (and small vaccination sites) with Different Types of Vaccination Centers When Vaccine Center Types and Locations are Fixed a Priori in the Model

Budget		Limit		Medium		Ample	
Pfizer	Center	117,180	100.0%	117,173	100.0%	5,310	0.3%
	Pharmacy	0	0.0%	19	0.0%	1,657,658	99.7%
	Total	117,180	100.0%	117,192	100.0%	1,662,968	100.0%
Moderna	Center	117,180	100.0%	150,834	13.7%	0	0.0%
	Pharmacy	0	0.0%	949,523	86.3%	1,098,128	100.0%
	Total	117,180	100.0%	1,100,357	100.0%	1,098,128	100.0%
Janssen	Center	120,156	17.9%	122,988	21.4%	0	0.0%
	Pharmacy	550,425	82.1%	452,209	78.6%	94,500	100.0%
	Total	670,581	100.0%	575,197	100.0%	94,500	100.0%

5.8 Discussion and Future Direction

In this study, we formulate a simulation-optimization model to generate the vaccination center locations for different types of vaccines and the optimal vaccine allocation strategies among different regions. We extend the simulation model presented by Kerr et al. [2021] by adding two vaccination compartments. The simulation model is able to incorporate the vaccination for the three types of vaccines, which are the first and second shots for Pfizer and Moderna, and the first shot for Janssen. The simulation model simulates the number of susceptible individuals and infections for a certain time period and imports the results into the optimization model. The optimization model incorporates the available budgets and potential vaccination center locations as well as the total number of vaccines available to generate the optimal vaccination center location and vaccine allocation strategies for each county in the future planning horizon. Then the generated results are used

as the inputs of the simulation model to estimate the number of infections and various disease compartmental values with the vaccination strategies for the same period. We apply our model to the case of vaccine allocation among all the counties in New Jersey State.

First, we validate our model with the real outbreak data by fixing one Pfizer vaccination center at Essex County and keep the number of other types of vaccine centers to zero as in the real-life case. The predicted results fit the real outbreak data well, and the paired-t-test shows that our predicted results have no significant difference from the real outbreak data.

We test our model on the cumulative number of infections under different budget levels. The results indicate that there is at least a month to see the difference in the number of infections under different budget levels since it takes time for the disease transmission and infects people. In addition, the county with a high population and initial infections receives more vaccines allocated.

The number of vaccines allocated to each county under different budget levels shows that the total number of vaccines allocated increases with the increase in the available budget. Under a limited budget level, more vaccines with a lower unit cost should be allocated because the limited budget reduces the number of people being vaccinated compared with other budget levels. Using a low-cost vaccine, more people are vaccinated, and the number of infections is minimized. In addition, the counties with higher population proportions are more likely to have higher vaccine allocation proportions since the model gives priority to vaccinate people in these regions. Under the medium budget level, more vaccines with higher costs and higher efficiency are allocated. The model has the flexibility to allocate those highly efficient vaccines due to the increased budget, but there is still a limitation on the number of vaccines distributed since the budget is still not ample enough. The counties with a higher population will receive even more vaccines due to the high number of infections. Under

the ample budget level, there is no limitation on the vaccine cost. Two main factors that can influence vaccine allocation are the vaccine acceptance rate by people and the available vaccine supply. In this case, the model allocates as many high-efficiency vaccines as possible to minimize the total number of infections. The population proportion of each county is almost the same as the vaccine allocation proportion because the vaccine acceptance rate in our model is the same for each county. The total number of people being vaccinated under an ample budget level is bounded by the people who are willing to be vaccinated since the vaccine supply is also relatively abundant. For all the budget levels, the model allocates more first doses than second doses for Pfizer and Moderna vaccines. This is because more people benefit from taking the first shot of the vaccines.

The results of vaccination center locations show that the model gives priority to allocate vaccine centers to the region that has the closest distance to the vaccine supply warehouse. When more vaccine centers are included, the centers are located by order of distance to the vaccine warehouse from the shortest to the longest. When tightening the center's location constraint and only allowing one type of vaccination center allocated in each county, the model prioritizes the type of center with higher vaccine efficiency and then centers with lower efficiency.

The results of vaccine allocation between the vaccination centers and local pharmacies (and small vaccination sites) indicate that more vaccines are allocated to the vaccination centers than local pharmacies under the limited budget level due to reduced vaccine and logistics costs. When the budget level increases, the proportion of the vaccines allocated to the local pharmacies and small vaccination sites also increases to benefit more people from vaccination.

The future work of this model can be described in the following ways. First, our model considers the potential vaccination center locations and the overall local pharmacy capacity. The distribution specifics from the warehouse to the local

pharmacies are not included. In a future study, local pharmacy supply chain can be incorporated, and the vaccine allocation strategies can be defined with more detailed information. In addition, our model assumes that the people in each county can only be served by the vaccine centers located in the closest county. In the real situation, human behavior is hard to capture, and some of the people may go to further places to receive the vaccines due to the complex environment. Thus, various human behaviors on how to take the vaccines could be incorporated into the model. Moreover, we want to study the specific vaccination strategies in a real application. For instance, one may fix the number of vaccines but compare vaccination strategies targeting random people or age-based groups.

CHAPTER 6

SUMMARY AND FUTURE DIRECTIONS

In summary, this dissertation presents new multi-stage stochastic models and agent-based simulation-optimization models to simulate the transmission of the disease (e.g., Ebola Virus Disease (EVD), COVID-19) and determine the corresponding optimal resource allocation decisions among different regions of the considered geographical location. Each integrates models that can simulate the transmission of the disease and generate the optimal resource allocation over all the regions. In the first study, we develop a multi-stage stochastic model to simulate the transmission of EVD and provide corresponding treatment resource allocations. The model considers the equity of the resource allocation when different budgets are obtained. The second study extends the previous model to a mean-risk multi-stage stochastic model. The provided model uses Conditional-value-at-risk to alleviate the impact of the extreme epidemic scenarios. In addition, the model incorporates the ring vaccination to prevent people from being infected, which is applied to study the EVD control in the Democratic Republic of the Congo (DRC). The third study presents a new compartment model to simulate the transmission of COVID-19 under uncertainty of untested asymptomatic infections. The proposed multi-stage-mean-risk model addresses the optimal ventilator allocation during the COVID-19 pandemic. The fourth study defines a simulation-optimization model to address the location of vaccine centers and vaccine allocations for the COVID-19 pandemic. The simulation model estimates the number of infections in the future planning horizon and import the estimated values into the optimization model. The optimization model generates the vaccine center location and vaccine allocation decisions and applies them back to the simulation model to forecast the number of infections for the next period.

This dissertation opens up many future research directions. The studies on vaccine allocation provide an overall decision on where to allocate the vaccines to minimize the total number of infections throughout the planning horizon. When applying to the vaccine allocations, a more detailed strategy could be performed. For instance, whether to apply the ring or mass vaccination is dependent on how many vaccines are allocated to the studied region. Which group of people should be given priority to vaccinate, and how can we define the group of vaccination candidates (e.g., age, sex, and race) is another critical problem in this area.

Moreover, the proposed simulation-optimization model considers the vaccine center location and local pharmacy capacity, but the distribution of vaccine supply from the warehouse to the local pharmacy is not included. The transportation of vaccines to the local pharmacy could contain many problems, including the supply chain capacity and vehicle routing problem during the supply. Thus, the proposed model in the last study could be extended to include vaccine distribution specifics. In addition, the health care problem is not limited to epidemic control but also involves many treatment processes of different types of diseases. We want to continue our research on how to optimize the treatment process of those infectious diseases. For instance, simulating the cells migration of cancer and defining the optimal treatment process would be one of the future research topics. Last but not least, another topic could be finding the optimal efficient antibiotics for some diseases. Many diseases have developed resistance to antibiotics. For example, the gonorrhea treatment process is a hot topic in recent years. There are different antibiotics that can treat gonorrhea, but the efficiency of those antibiotics is decreasing over time since the virus has developed resistance to them. Thus, the treatment of gonorrhea includes the combination of different antibiotics to alleviate the impact on the virus's resistance. Therefore, defining the optimal treatment process of antibiotics on gonorrhea is another example of potential future directions.

APPENDIX A

A MULTI-STAGE STOCHASTIC PROGRAMMING APPROACH TO EPIDEMIC RESOURCE ALLOCATION WITH EQUITY CONSIDERATIONS

A.1 Non-Anticipativity

Two scenarios should have the same decision variables at a stage j if they share the same scenario path up to that stage. Corresponding decisions up to stage j of two inseparable scenarios should be the same. These implications are named as non-anticipativity constraints, and can be formulated as follows. Consider the node marked n in the scenario tree, and denote the corresponding stage as $t(n)$. Let the set of scenarios that pass through node n be $\beta(n)$. We must ensure that decision variables at stage $t(n)$ that are associated with node n (for example: $x^{\omega}_{t(n)}$) have identical values for $\omega \in \beta(n)$. One way to do this is to add the non-anticipativity constraint as in the following form:

$$x^{\omega}_{t(n)} - x_n = 0 \qquad \forall \omega \in \beta(n).$$

As an example, consider the first three stages of the multi-stage problem shown in Figure 2.2. The set of nodes of this scenario tree is given by $N = \{0, 1, 2, 3, ..., 13, 14\}$, where $t(0) = 0, t(1) = 1, t(2) = 1, t(3) = 2, t(4) = 2, t(5) = 2, t(6) = 2, t(7) = t(8) = t(9) = t(10) = t(11) = t(12) = t(13) = 3$. The set of scenarios that share node $n = 2$ is given by $\beta(2) = \{5, 6, 7, 8\}$. Let $x^{\omega}_{t(2)}$ represent decision variables for $\omega \in \beta(2)$. The non-anticipativity constraint for those variables can be written as:

$$x^{\omega}_{t(2)} - x_2 = 0 \qquad \forall \omega \in \beta(2).$$

A.2 Linearization

We first linearize the logical constraint that describes the number of hospitalized individuals in equation (2.1o). Following the method of Kıbış and Büyüktahtakın [2017], for each $j \in J \setminus \overline{J}$, $r \in R$, and $\omega \in \Omega$, constraint (2.1o) can be written as:

$$\overline{I}^{\omega}_{j,r} = (C^{\omega}_{j,r} - T^{\omega}_{j,r}) z^{\omega}_{j,r} + I^{\omega}_{j,r}(1 - z^{\omega}_{j,r}), \tag{A.1}$$

where $z^{\omega}_{j,r}$ is a binary variable, which takes the value 1 if the number of infected individuals to be hospitalized is restricted by the number of available beds in ETCs, and the value 0 if the number of beds in ETCs is sufficiently large to hospitalize all infected individuals. In order to ensure that $\overline{I}^{\omega}_{j,r}$ takes the minimum value of $(C^{\omega}_{j,r} - T^{\omega}_{j,r})$ and $I^{\omega}_{j,r}$, we should have the following inequalities satisfied for each $j \in J \setminus \overline{J}$, $r \in R$, and $\omega \in \Omega$:

$$\overline{I}^{\omega}_{j,r} \leq C^{\omega}_{j,r} - T^{\omega}_{j,r} \tag{A.2a}$$

$$\overline{I}^{\omega}_{j,r} \leq I^{\omega}_{j,r}. \tag{A.2b}$$

However, constraint (A.1) is still non-linear due to quadratic terms. Therefore, two auxiliary variables $U^{\omega}_{j,r}$ and $W^{\omega}_{j,r}$ are introduced to be substituted with $(C^{\omega}_{j,r} - T^{\omega}_{j,r})z^{\omega}_{j,r}$ and $I^{\omega}_{j,r}(1 - z^{\omega}_{j,r})$, respectively. In this case, for each $j \in J \setminus \overline{J}$, $r \in R$, and $\omega \in \Omega$, constraint (A.1) can be written as:

$$\overline{I}^{\omega}_{j,r} = U^{\omega}_{j,r} + W^{\omega}_{j,r} \tag{A.3}$$

We then introduce a lower bound (H_{LB}) and upper bound (H_{UB}) for $C^{\omega}_{j,r} - T^{\omega}_{j,r}$, such that $H_{LB} \leq C^{\omega}_{j,r} - T^{\omega}_{j} \leq H_{UB}$ and add the following constraints to the model for each $j \in J \setminus \overline{J}$, $r \in R$, and $\omega \in \Omega$:

$$U^{\omega}_{j,r} \leq H_{UB} z^{\omega}_{j,r} \tag{A.4a}$$
$$U^{\omega}_{j,r} \geq H_{LB} z^{\omega}_{j,r} \tag{A.4b}$$
$$U^{\omega}_{j,r} \leq (C^{\omega}_{j,r} - T^{\omega}_{j,r}) - H_{LB}(1 - z^{\omega}_{j,r}) \tag{A.4c}$$
$$U^{\omega}_{j,r} \geq (C^{\omega}_{j,r} - T^{\omega}_{j,r}) - H_{UB}(1 - z^{\omega}_{j,r}). \tag{A.4d}$$

Similarly, we introduce a lower bound (I_{LB}) and an upper bound (I_{UB}) for $I^{\omega}_{j,r}$, such that $I_{LB} \leq I^{\omega}_{j,r} \leq I_{UB}$, and add the following four constraints for each $j \in J \setminus \overline{J}$, $r \in R$, and $\omega \in \Omega$ to the model:

$$W^{\omega}_{j,r} \leq I_{UB}(1 - z^{\omega}_{j,r}) \tag{A.5a}$$
$$W^{\omega}_{j,r} \geq I_{LB}(1 - z^{\omega}_{j,r}) \tag{A.5b}$$
$$W^{\omega}_{j,r} \leq I^{\omega}_{j,r} - I_{LB} z^{\omega}_{j,r} \tag{A.5c}$$
$$W^{\omega}_{j,r} \geq I^{\omega}_{j,r} - I_{UB} z^{\omega}_{j,r}. \tag{A.5d}$$

Thus the constraint (2.1o) can be equivalently linearized by replacing it with constraints (A.3), (A.4a)-(A.4d) and (A.5a)-(A.5d).

We then linearize the equity constraint given by equation (2.2). By multiplying the two denominators on the left side of (2.2) by each other and multiplying the right side of (2.2) by $\sum_{r \in R} u_r \sum_{j \in J} \sum_{r \in R} \sum_{\omega \in W} P^{\omega} I^{\omega}_{j,r}$, we obtain the following inequality:

$$\left| \sum_{r \in R} u_r \sum_{j \in J} \sum_{\omega \in W} P^{\omega} I^{\omega}_{j,r} - u_r \sum_{j \in J} \sum_{r \in R} \sum_{\omega \in W} P^{\omega} I^{\omega}_{j,r} \right| \leq k \sum_{r \in R} u_r \sum_{j \in J} \sum_{r \in R} \sum_{\omega \in W} P^{\omega} I^{\omega}_{j,r} \tag{A.6}$$

The absolute value in inequality (A.6) could be linearized using the following two constraints:

$$\begin{aligned} &\sum_{r \in R} u_r \sum_{j \in J} \sum_{\omega \in W} P^{\omega} I^{\omega}_{j,r} - u_r \sum_{j \in J} \sum_{r \in R} \sum_{\omega \in W} P^{\omega} I^{\omega}_{j,r} \\ &-k \sum_{r \in R} u_r \sum_{j \in J} \sum_{r \in R} \sum_{\omega \in W} P^{\omega} I^{\omega}_{j,r} \leq 0 \\ &\sum_{r \in R} u_r \sum_{j \in J} \sum_{\omega \in W} P^{\omega} I^{\omega}_{j,r} - u_r \sum_{j \in J} \sum_{r \in R} \sum_{\omega \in W} P^{\omega} I^{\omega}_{j,r} \end{aligned} \tag{A.7a}$$

$$+k \sum_{r \in R} u_r \sum_{j \in J} \sum_{r \in R} \sum_{\omega \in W} P^{\omega} I^{\omega}_{j,r} \geq 0 \tag{A.7b}$$

Therefore, the constraint (2.2) can be equivalently linearized by replacing it with constraints (A.7a) and (A.7b).

Similarly, we have replaced the non-linear capacity equity constraint (2.3) with the following two linear constraints:

$$\sum_{r \in R} u_r \sum_{j \in J} \sum_{\omega \in W} P^{\omega} C^{\omega}_{j,r} - u_r \sum_{j \in J} \sum_{r \in R} \sum_{\omega \in W} P^{\omega} C^{\omega}_{j,r}$$
$$-k \sum_{r \in R} u_r \sum_{j \in J} \sum_{r \in R} \sum_{\omega \in W} P^{\omega} C^{\omega}_{j,r} \leq 0 \tag{A.8a}$$
$$\sum_{r \in R} u_r \sum_{j \in J} \sum_{\omega \in W} P^{\omega} C^{\omega}_{j,r} - u_r \sum_{j \in J} \sum_{r \in R} \sum_{\omega \in W} P^{\omega} C^{\omega}_{j,r}$$
$$+k \sum_{r \in R} u_r \sum_{j \in J} \sum_{r \in R} \sum_{\omega \in W} P^{\omega} C^{\omega}_{j,r} \geq 0 \tag{A.8b}$$

The non-linear multi-stage stochastic programming epidemiclogistics model (2.1) is converted into an equivalent MIP formulation by replacing the non-linear capacity availability constraint (2.1o) with constraints (A.3), (A.4a)-(A.4d) and (A.5a)-(A.5d), the non-linear infection equity constraint (2.2) with constraints (A.7a) and (A.7b), and the non-linear capacity equity constraint (2.3) with constraints (A.8a) and (A.8b). In the next section, we present a case study involving the control of the 20142015 Ebola outbreak in the three most-affected West African countries, Guinea, Sierra Leone, and Liberia.

A.3 Ebola Case Study Data

This section presents the data used to formulate the model, including population and migration data, resource cost data, and epidemiological data. All data provided in this section was collected using literature resources and given bi-weekly. Data pertaining to the 2014-2015 Ebola outbreak and the deterministic epidemics-logistics model have been validated by Büyüktahtakın et al. [2018a].

A.3.1 Population and Migration Data

Table A.1 presents the distribution of the population in Guinea, Liberia, and Sierra Leone, all located in West Africa. We consider six regions: three of them are located in Guinea (Upper Guinea (UG), Middle Guinea (MG), and Lower Guinea (LG)), two of them are in Liberia (Northern Liberia (NL) and Southern Liberia (SL)) and the last one, Sierra Leone, is a county itself (S). Table A.2 shows the total number of initial infections in each country. Table A.3 gives the migration rates from each of the five regions (UG,MG,LG,NL,SL) to the other four regions. There is no migration in Sierra Leone because it is considered as a region by itself. Rapidly after the initial recognition of the Ebola outbreak, those three countries closed the national borders, so we only consider the migration within a country.

Table A.1 Regions, Population Size and Rate in West Africa

Guinea	Population (millions)	Ratio	Liberia	Population (millions)	Ratio	Sierra Leone	Population (millions)	Ratio
UG	4,3	0.41	NL	2,2	0.64	S	4,9	1.00
MG	2,7	0.25	SL	1,2	0.36			
LG	3,7	0.34						
Total	**10,7**	1.00		**3,4**	1.00		**4,9**	1.00

Table A.2 The Number of Infected People at the Beginning of the Planning Horizon (August 30, 2014) in West Africa

Guinea	Sierra Leone	Liberia
218	604	685

Table A.3 Bi-weekly Migration Rate between Regions of Guinea and Liberia, Original Data Acquired from the study of Wesolowski et al. [2014]

From \ To	UG	MG	LG	NL	SL
UG		0.0032	0.0010		
MG	0.0052		0.0025		
LG	0.0012	0.0018			
NL					0.0007
SL				0.0011	

A.3.2 Resource Allocation Cost Data

The fixed cost of locating Ebola treatment centers (ETCs) and the per-person cost of Ebola treatment for either 50 or 100-bed ETC are given below in Table A.4. The treatment cost includes the fixed cost for establishing each type of ETCs, isolation unit center, and laboratory diagnosis. Additionally, each facility has a variable running cost mainly composed of treating infected people and contact tracing of the infected individuals. There is also a safe burial cost for safely burying infected dead bodies. Fixed costs are one-time; however, all other costs are given for a 2-week period in Table A.4. For example, the variable cost of the Ebola treatment center represents the cost of treating one infected individual over two weeks.

Table A.4 Summary of Ebola Treatment Cost for 50 (100)-bed ETC

Cost description	Fixed Cost	Variable cost*
Ebola treatment center	$386,000 ($694,800)	$8,810
Isolation unit center (IUC)	$112,500	$1,133
Laboratory diagnosis	$100,000	$540
Subnational technical services		$2,250
Contact tracing		$1,128
Safe burial		
Total	**$598,500 ($1,077,300)**	**$13,860**

* Variable and safe burial costs are bi-weekly.

A.3.3 Epidemiological Data

Table A.5 presents the data values for transmission parameters for each of the three considered countries in West Africa. The data contains the fatality rate with and without treatment, recovery rate with and without treatment, safe burial rate, and transmission rates. Because the transmission rate in the community is an uncertain parameter, we present its value under each of the two realizations as low and high. Moreover, we considered the expected value of the transmission rate at a traditional funeral for each country.

Table A.5 Transmission Parameters and Bi-weekly Rates for the Ebola Outbreak

Parameter	Description	Data			Reference
		Guinea	Sierra Leone	Liberia	
λ_1	Rate of fatality without treatment	0.428	0.124	0.176	WHO [2020c] WHO E. R. Team [2014]
λ_2	Rate of fatality with treatment	0.350	0.096	0.128	WHO [2020c] WHO E. R. Team [2014]
λ_3	Rate of recovery without treatment	0.240	0.242	0.232	WHO [2020c] WHO E. R. Team [2014]
λ_4	Rate of recovery with treatment	0.416	0.327	0.312	WHO [2020c] WHO E. R. Team [2014]
λ_5	Safe burial rate	0.730	0.710	0.740	WHO [2020c] WHO E. R. Team [2014]
$\chi^l_{1,r}$	Transmission rate in community (Low)	0.660	0.632	0.560	Camacho et al. [2014]
$\chi^h_{1,r}$	Transmission rate in community (High)	0.990	0.940	0.840	Camacho et al. [2014]
$\chi_{2,r}$	Transmission rate at traditional funeral	1.460	1.420	1.480	Camacho et al. [2014]

A.4 Analysis of Infection and Prevalence Equity Constraints

The infection equity constraint (2.2) limits the difference between the proportion of infections in each region over the total number of infections and the proportion of the population at each region over the total population with a specific k value. Introducing the infection equity constraint to the mathematical model with 8 stages increased the average CPU solution time from 7200 seconds to 10 hours when $k = 0.2$,

and the average optimality gap from 1% to 29%. Table A.6 gives the run time specifics regarding the mathematical model (2.1) with eight stages and the infection equity constraint (2.2). As seen in Table A.6, for k values between 0.2 and 0.4, the computational complexity significantly increases compared to the case where the infection equity constraint is relaxed, i.e., k is set to a large number.

Figures A.1 and A.2 show the budget allocation and the total number of infections and funerals over the three considered countries for different k values. According to the results, varying k values does not significantly change the optimal budget allocation and the total number of infections and funerals. Without introducing the infection equity constraint into the mathematical model (2.1), the absolute value of the difference between the infection ratio and the population ratio in Guinea, Sierra Leone, and Liberia is 0.42, 0.04, and 0.38, respectively, based on the optimal solution value similar to the k values considered here.

Table A.6 Model Run Specifics with the Infection Equity Constraint (2.2)

k value	Solution Time (CPU sec)	Optimality Gap (%)
0.2	36,068	29
0.3	7,213	1
0.4	7,214	1
A large k value (no-equity-constraint case)	7232	0

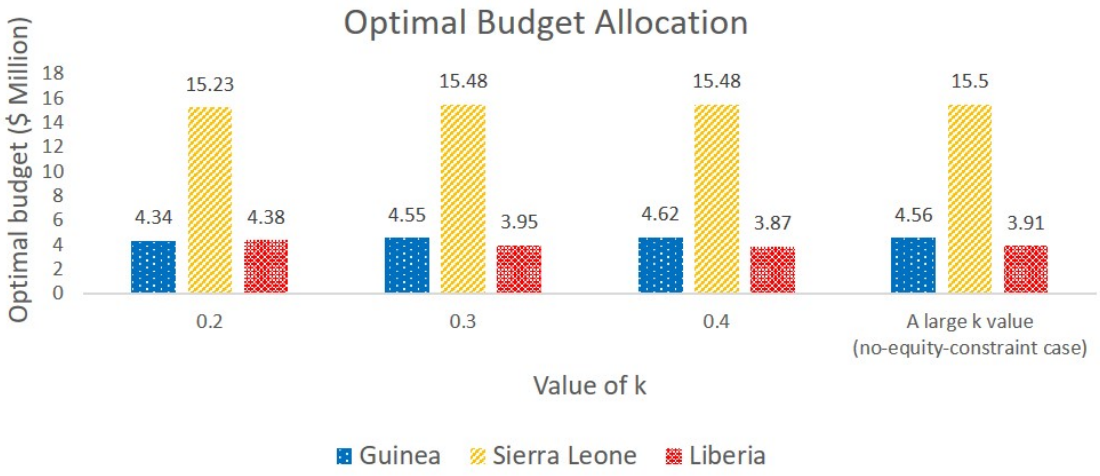

Figure A.1 Optimal budget allocation under different k values for an 8-stage problem with \$24M budget.

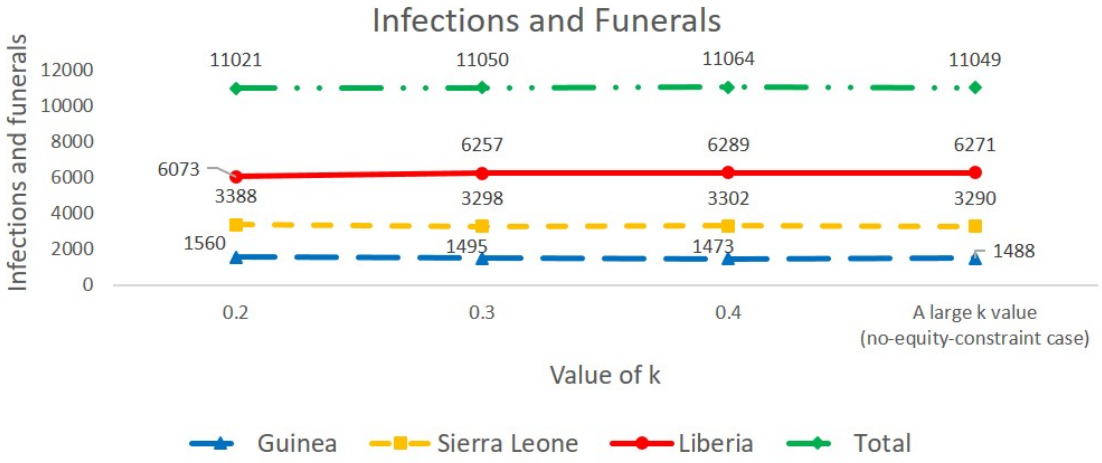

Figure A.2 Total number of new infections and funerals under different k values for an 8-stage problem with \$24M budget.

As a comparison, we also test the prevalence equity constraint (2.4) and compare it to the infection equity constraint (2.2). The prevalence equity constraint bounds the absolute difference between the regional prevalence (cases per population in a region) and the country prevalence (cases per population over all regions). Without the prevalence equity constraint (2.4) constraint, the absolute value of the difference between the infection ratio over a region and the infection ratio over all regions in Guinea, Sierra Leone, and Liberia is 4.4×10^{-4}, 8.2×10^{-5}, and 1.2×10^{-3}, respectively, based on the optimal solution value.

We test the prevalence equity constraint under the \$24M budget level. Table A.7 presents the run-time and optimality gap specifics for each k value in inequality (2.4) . Figures A.3 and A.4 show the optimal budget allocation and the number of infections and funerals under different k values, respectively. Note that the k values used in the prevalence equity constraint (2.4) are much smaller than the k values used in the infection equity constraint (2.2). Similar to the infection equity constraint, the optimal budget allocation does not show any significant difference among each k value, but the number of infections and funerals slightly reduces when we relax the prevalence equity constraint. These results imply that our model balances the proportion of infections in each region, even without imposing the infection equity (2.2) or (2.4) prevalence equity constraints.

Table A.7 Model Run Specifics with the Prevalence Equity Constraint

k value	Solution Time (CPU sec)	Optimality Gap (%)
3×10^{-9}	36,041	1
5×10^{-9}	7,204	1
1×10^{-8}	7,232	1
2×10^{-8}	7,231	1
A large k value (no-equity-constraint case)	7,232	0

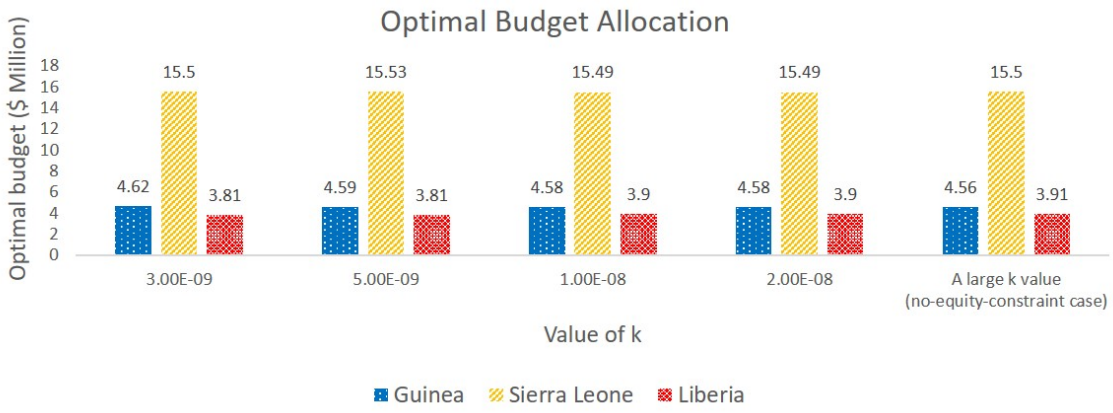

Figure A.3 Optimal budget allocation under different k values for an 8-stage problem with \$24M budget.

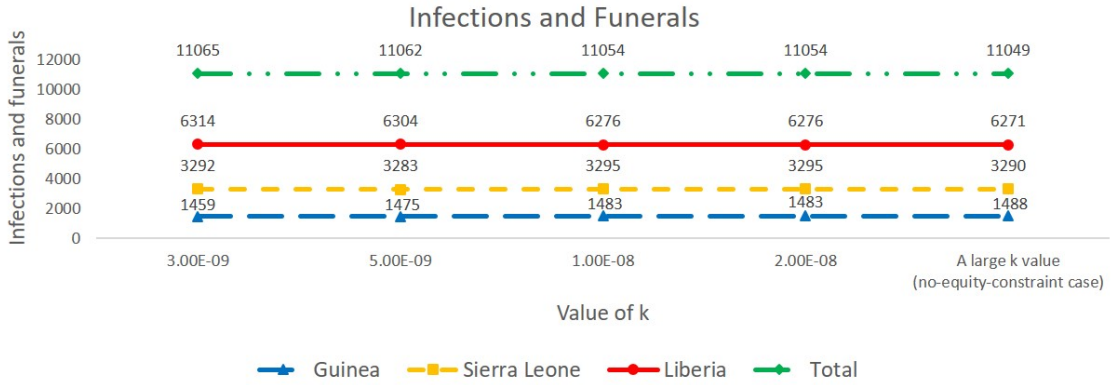

Figure A.4 Total number of new infections and funerals under different k values for an 8-stage problem with \$24M budget.

APPENDIX B

RISK-AVERSE MULTI-STAGE STOCHASTIC PROGRAMMING TO OPTIMIZING VACCINE ALLOCATION AND TREATMENT LOGISTICS FOR EFFECTIVE EPIDEMIC RESPONSE

B.1 Ebola Case Study Data

This section presents the data used to formulate the model parameters, including population and migration data, resource cost data, and epidemiological data, and the mathematical formulation for estimating the migration rate.

B.1.1 Regional and Population Data

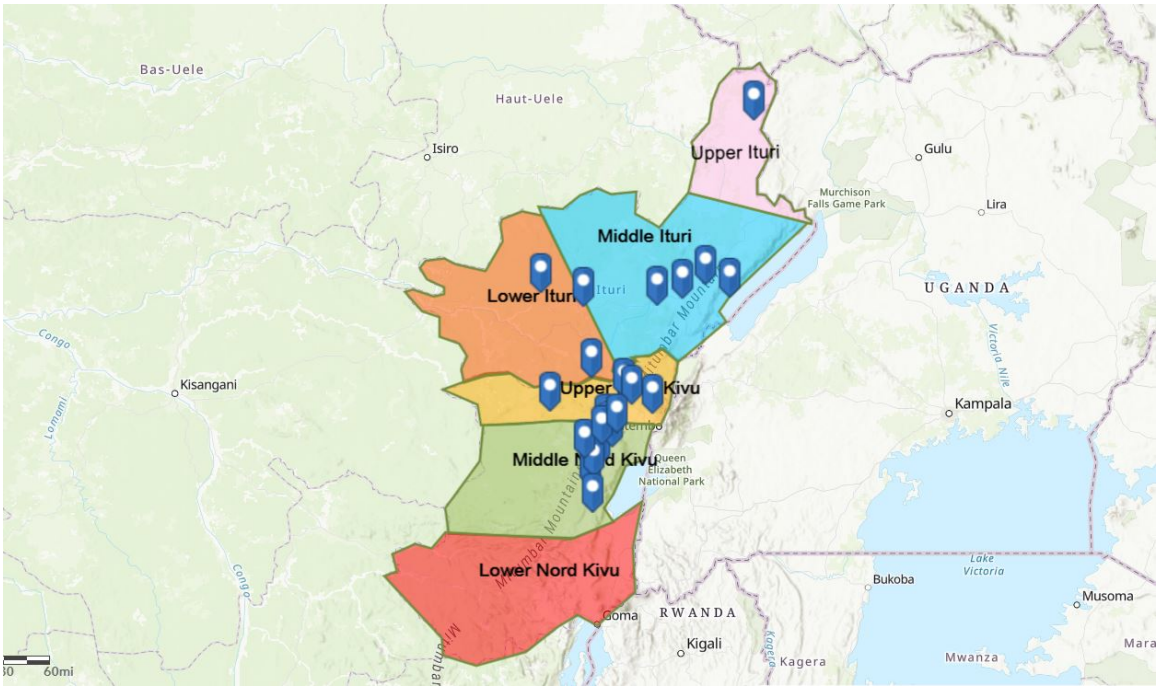

Figure B.1 Region division in North Kivu and Ituri. The map is constructed using ESRI [2020].

Based on the World Health Organization (WHO) Ebola situation report [WHO, 2020a], we divided North Kivu and Ituri provinces of the Democratic Republic of Congo that are affected by the EVD into six different sub-regions: Upper (UNK), middle (MNK), lower (LNK) North Kivu and Upper (UI), middle (MI), lower (LI) Ituri. In the report of June 25th, 2019, there were almost no cases confirmed in Upper Ituri and Lower North Kivu; however, in the latest report of December 17th, 2019, some cases were confirmed in these regions. We consider the migration of people among multiple regions in our model and include these regions to analyze the influence of immigration on transmitting the disease.

Table B.1 presents the population as well as the population ratio of each sub-region presented in Figure B.1, while Table B.2 shows the number of initial infections in each region on June 25, 2019.

Table B.1 Regions, Population Size, and Rate in West Africa

North Kivu	Population (millions)	Ratio	Ituri	Population (millions)	Ratio
UNK	1,9	0.19	UI	2,3	0.42
MNK	2,3	0.23	MI	2,8	0.51
LNK	5,7	0.58	LI	0,4	0.07
Total	**9,9**	1.00		**5,5**	1.00

Table B.2 The Number of Infected People at the Beginning of the Planning Horizon (June 25, 2019)

	Upper	Middle	Lower
North Kivu	380	260	0
Ituri	0	23	74

B.1.2 Migration Estimation Model and Data for Migration Rates

Migration plays a crucial role in disease transmission between regions of a country and among multiple countries. Because the data regarding the migration of the population among each region of North Kivu and Ituri is not available, we have driven a new formula to estimate the rate of movement among multiple regions as described below. The logical sequence to derive the migration formulation is presented in Figure B.2 and described below.

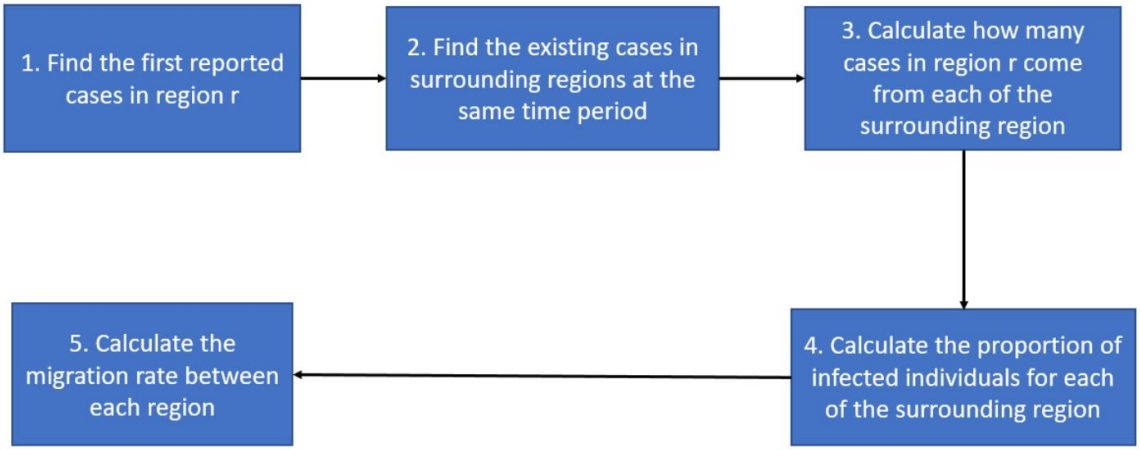

Figure B.2 Steps of calculating the migration rate.

If no border closure is imposed, some of the infected individuals from the regions where the disease has originated migrate to other regions during the incubation period of the virus. When disease symptoms begin to appear, they are discovered as the first cases in the new region. The Ebola virus average incubation period is around

2 to 21 days [WHO, 2020c]. Thus, we estimate the migration rate using a cycle of three weeks, and the migration rate presented below is three-weekly. Let $r \in R$ represents a newly infected region, and $l \in L = \{1, \ldots, \bar{R}\}$ stands for the region where the disease has already existed, and $\bar{R}$ is the upper bound for the number of infected regions. Suppose we have a total of six regions as shown in Figure B.1, $r \in R = \{UNK, MNK, LNK, UI, MI, LI\}$. For each region r, denote the number of infections detected in the first period (the first set of infected people) by I_r.

1. Find the First Reported Cases in Region r We first check the WHO case situation report [WHO, 2020a] and determine the first group of cases discovered in each defined region.

2. Find Existing Cases in Surrounding Regions at the Same Time Period We assume that the first group of infected individuals discovered in region r might have only come from the regions that already have infections at the same time period or before. Thus, using the WHO situation report [WHO, 2020a], we choose a subset of regions $l \in L$ surrounding region r, which have discovered infections before region r, as the possible emigration regions, where $I_l \neq 0$. Specifically, since the average time from infected to either recovered and funeral, with or without treatment, is from one week to three weeks, we calculate the total confirmed cases in region l within the three-week interval of the time period where the first infection is seen in region r, I_l.

3. Calculate How Many Cases in Region r **Might Have Come from Each of the Surrounding Region** In this step, we calculate the distance D_{rl} between each main region considered in Figure B.1 using Google Maps (Table B.3). We assume that the number of infected cases migrated from a possible emigration region l to region r is negatively correlated with D_{rl}. Therefore, we compute the ratio of D_{rl} and the sum of the distances from region r to all possible emigration regions, and multiply it with the total migrated infected cases I_r, to calculate the infected population in region r that resulted from people moving from region l to r, denoted by $\hat{I}_{l \to r}$, as given in below equation:

$$\hat{I}_{l \to r} = \frac{D_{rl}}{\sum_{l \in L} D_{rl}} I_r, \qquad \forall r \in R, \forall l \in L. \tag{B.1}$$

4. Calculate the Proportion of Infected Individuals for Each of the Surrounding Region In this step, we calculate the infection ratio at region l, $i = I_l / U_l$, where U_l is the population of area l. We also assume that we should have the same ratio i for the people who immigrate from region l to region r. Then we have:

$$i = \frac{I_l}{U_l} = \frac{\hat{I}_{l \to r}}{\hat{U}_{l \to r}}. \tag{B.2}$$

where $\hat{I}_{l \to r}$ represents the infected people who immigrate from region l to region r, as given in Equation (B.1), and $\hat{U}_{l \to r}$ stands for the migration population from l to r, which is the parameter that we want to estimate to calculate the migration rate.

5. Calculate the Migration Rate Between Each Region Substituting Equation (B.1) in Equation (B.2) and re-organizing it, the number of people that migrate from l to r can be calculated by the following equation:

$$\hat{U}_{l\to r} = \frac{D_{rl}}{\sum\limits_{l\in L} D_{rl}} I_r \frac{U_l}{I_l}. \tag{B.3}$$

Since we formulate the model based on the short-term migration, we assume that those migration population is temporary (for business travel, cargo delivery, etc.) and migrated population will come back to the original region. Thus, the number of immigrated people from new infection regions r to the emigration regions l is estimated the same as the number of people moving from emigration regions l to the new infection regions r, i.e., $\hat{U}_{l\to r} = \hat{U}_{r\to l}$.

Finally, the migration rate from region l to region r is calculated by dividing the immigration population from l to r with the total population of each region l, as given below:

$$i_{l\to r} = \frac{\hat{U}_{l\to r}}{U_l}. \tag{B.4}$$

Because we have $\hat{U}_{l\to r} = \hat{U}_{r\to l}$, similar to Equation (B.4), the migration rate from region r to region l is calculated by

$$i_{r\to l} = \frac{\hat{U}_{r\to l}}{U_r}. \tag{B.5}$$

Additionally, suppose a considered region $b \in R$ does not have any existed infections. In that case, we can estimate the migration rate based on the distance between region l and region r, for which the migration population from l to r is defined. Specifically, the migration between region b and region r can be estimated as:

$$\hat{U}_{l\to b} = \hat{U}_{l\to r} \frac{D_{lr}}{D_{lb}}. \tag{B.6}$$

Then we can use Equations (B.4) and (B.5) to calculate the migration rate between region b and region r.

Here, we note that the estimation of the migration rate based on the distance between each region may not be accurate in some cases due to the popularity of a region and social effects. For instance, larger short-term migrations occur between cities rather than a city and a village because of the greater opportunities in urban locations and the corresponding social behavior. Therefore, to calculate the migration rates, the locations that have similar social environments should be selected from each region to minimize the impact of social effects on human mobility. In our case, each location selected from a region is a metropolitan of that region.

Example. As an example, consider the case of MNK. The WHO report [WHO, 2020a] shows that MNK discovered the first three cases on September 11th, 2018,

and at this time, only UNK and LI had infected cases. Thus, we assume that newly infected cases in MNK come from these two regions. The proportion of the distance from the main cities of UNK and LI to the main city in MNK is 57.5/145. So we assume that 71.6% (1.86) of the three cases in MNK come from UNK, and 29.4% (1.14) of them come from LI. The proportion of infections in UNK and LI is 0.00001 (21 over 1861730) and 0.00001 (2 over 148, 387). Using Equation (B.3), the migration population of UNK and LI to MNK is estimated as $\hat{U}_{UNK\to MNK} = 164,896$ and $\hat{U}_{LI\to MNK} = 84,581$. Then the migration rate from UNK to MNK is calculated as $i_{UNK\to MNK} = 0.0886$, and the migration rate from LI to MNK is computed as $i_{LI\to MNK} = 0.5700$. On the other hand, because we assume that $\hat{U}_{MNK\to UNK} = \hat{U}_{UNK\to MNK} = 164,896$, the migration rate from MNK to UNK is calculated as $i_{MNK\to UNK} = 0.0685$, and the migration rate from MNK to LI is given as $i_{MNK\to LI} = 0.0351$.

The estimated migration rates between each region (Figure B.1) are presented in Table B.4.

Table B.3 Geographical Distance between Regions (KM)

From \ To	UNK	MNK	LNK	UI	MI	LI
UNK		57.5	358	467	202	92.6
MNK			301	523	258	145
MNK				823	558	445
UI					267	483
MI						217
LI						

Table B.4 Migration Rate between Regions of North Kivu and Ituri

From \ To	UNK	MNK	LNK	UI	MI	LI
UNK		0.0886	0.0012	0.0016	0.0424	0.0345
MNK	0.0685		0.0059	0.0025	0.0851	0.0351
LNK	0.0081	0.0511		0.0935	0.0062	0.0023
UI	0.0138	0.0283	0.1200		0.0795	0.0088
MI	0.1254	0.0735	0.0050	0.0273		0.0167
LI	0.1456	0.5700	0.0044	0.0129	0.0711	

B.1.3 Resource Allocation Cost Data

Table B.5 gives the fixed cost of locating Ebola treatment centers (ETCs) and the variable or per-person cost of the Ebola treatment. The treatment cost includes the fixed cost for establishing each type of ETCs (either 50 or 100-bed ETC), isolation unit center, and laboratory diagnosis. Additionally, each facility has a variable running cost mainly composed of treating infected people and contact tracing of the infected individuals. Safe burial cost is also included for safely burying infected dead bodies. Fixed costs are one-time; however, all other cost values given in Table B.5 are presented for a three-week period. For example, an Ebola treatment center's variable cost represents the cost of treating one infected individual over three weeks.

Table B.5 Summary of Fixed and Variable Treatment Costs in 50 (100)-Bed ETC

Cost description	Fixed Cost	Variable cost*
Ebola treatment center	$386,000 ($694,800)	$13,215
Isolation unit center (IUC)	$112,500	$1,699
Laboratory diagnosis	$100,000	$810
Subnational technical services		$3,375
Contact tracing		$1,692
Safe burial		
Total	**$598,500 ($1,077,300)**	**$20,791**

* Variable and safe burial costs are given for a period of three weeks.

B.1.4 Epidemiological Data

In this subsection, we present the values of the parameters that describe the disease transmission among compartments of the EVD that were described in Section 3.3.2 in North Kivu and Ituri of DRC.

Table B.6 Transmission Parameters and Three-Weekly Rates for the Ebola Outbreak

Parameter	Description	Data		Reference
		North Kivu	Ituri	
χ_1	Rate of fatality without treatment	0.527	0.372	WHO [2020c], WHO E. R. Team [2014]
χ_2	Rate of fatality with treatment	0.383	0.288	WHO [2020c], WHO E. R. Team [2014]
χ_3	Rate of recovery without treatment	0.695	0.725	WHO [2020c], WHO E. R. Team [2014]
χ_4	Rate of recovery with treatment	0.937	0.98	WHO [2020c], WHO E. R. Team [2014]
χ_5	Safe burial rate	2.22	2.13	WHO [2020c], WHO E. R. Team [2014]
σ_r	Transmission rate in the community	0.648	0.54	Camacho et al. [2014]
$\theta_{2,r}$	Transmission rate at a traditional funeral	2.04	2.19	Camacho et al. [2014]
β_r	Vaccination effectiveness rate	0.975	0.975	WHO [2019c]
ε_r	Probability of transition from vaccinated to susceptibles	0.06	0.06	WHO [2018]

Table B.7 Three-Weekly Values for Vaccine Supply Upper-Bound (G_j^ω) and the Uncertain Transmission Rate ($\theta_{1,r}^\omega$) for the Ebola Outbreak(High (Low) Realization for G_j^ω Implies Low (High) Realization for $\theta_{1,r}^\omega$)

Parameter	Scenario tree branch	Realization Value		Reference
		North Kivu	Ituri	
$(G_j^\omega, \theta_{1,r}^\omega)$	High	(4500, 0.948)	(4500, 0.84)	Camacho et al. [2014], WHO [2019a]
	Low	(3000, 1.422)	(3000, 1.26)	Camacho et al. [2014] WHO [2019a]

APPENDIX C

AN AGENT-BASED VACCINE ALLOCATION MODEL FOR CONTROLLING COVID-19

Figures C.1, C.2, and C.3 show the results of model validation against the real outbreak data for all the counties in New Jersey.

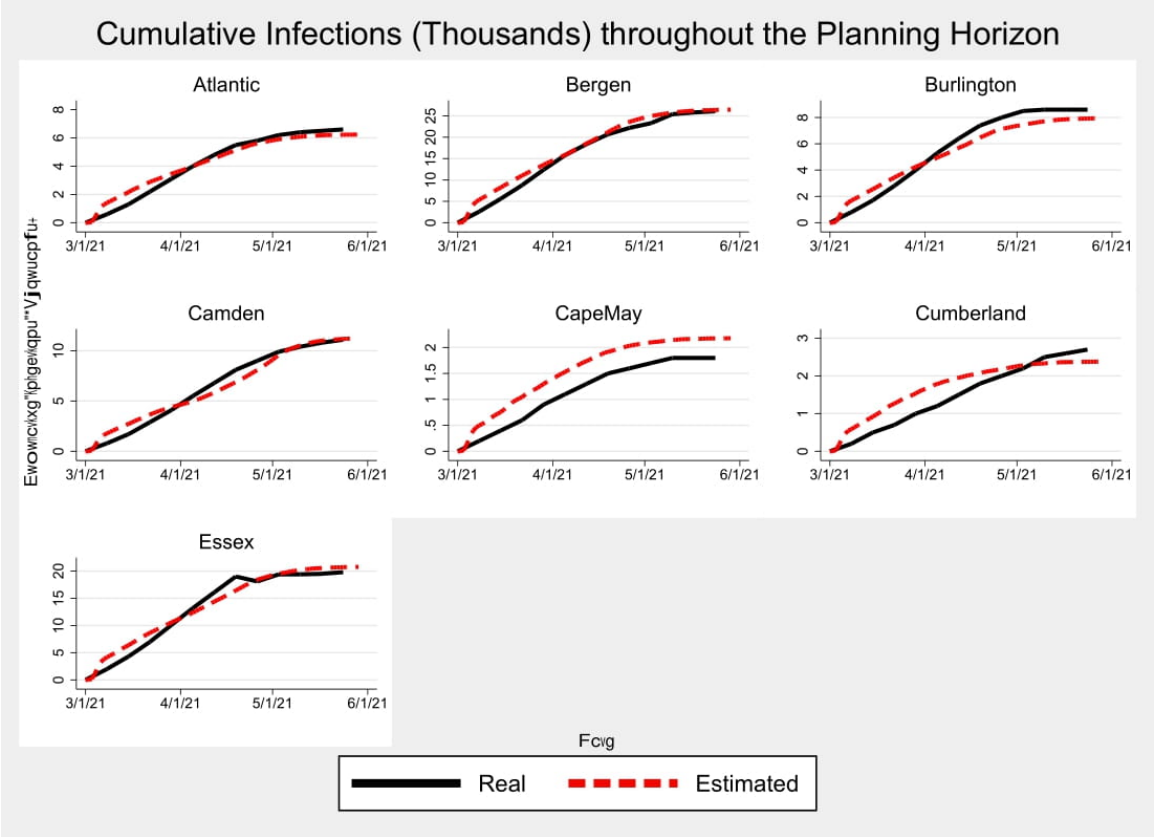

Figure C.1 Cumulative infections (thousands) throughout the planning horizon for New Jersey counties - 1.

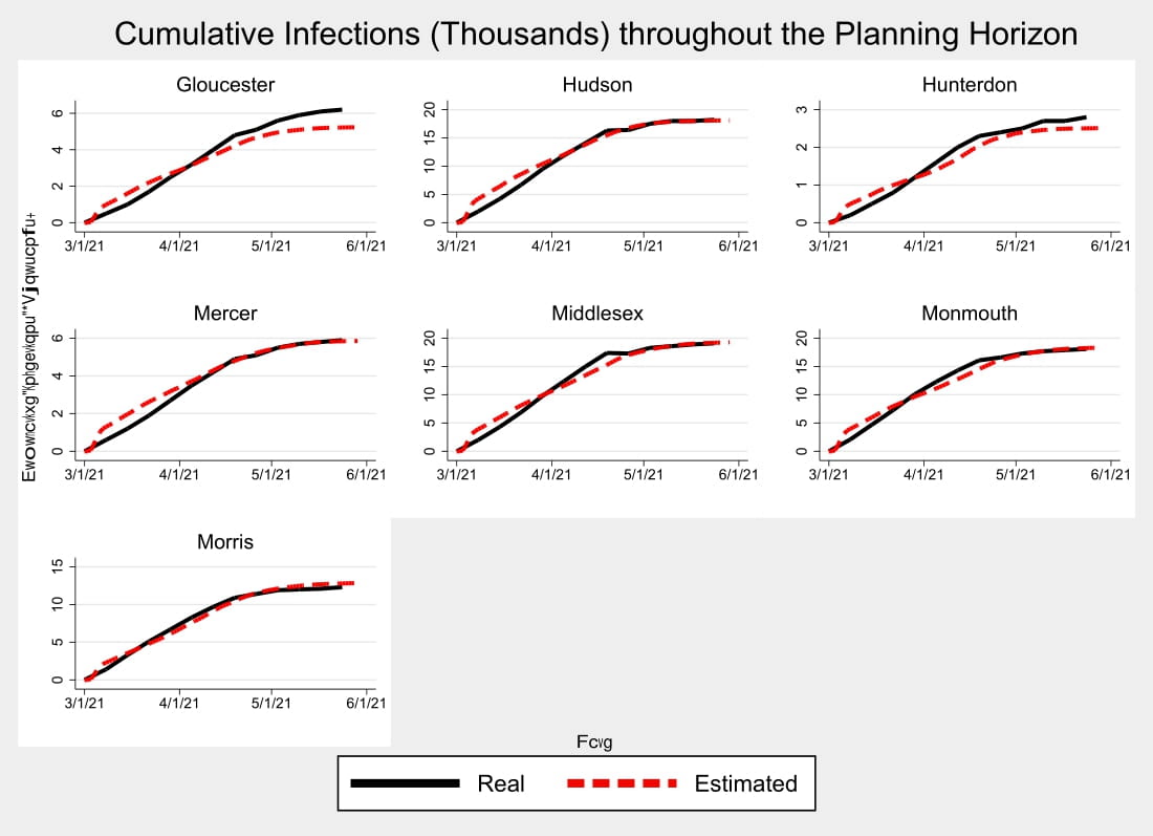

Figure C.2 Cumulative infections (thousands) throughout the planning horizon for New Jersey counties - 2.

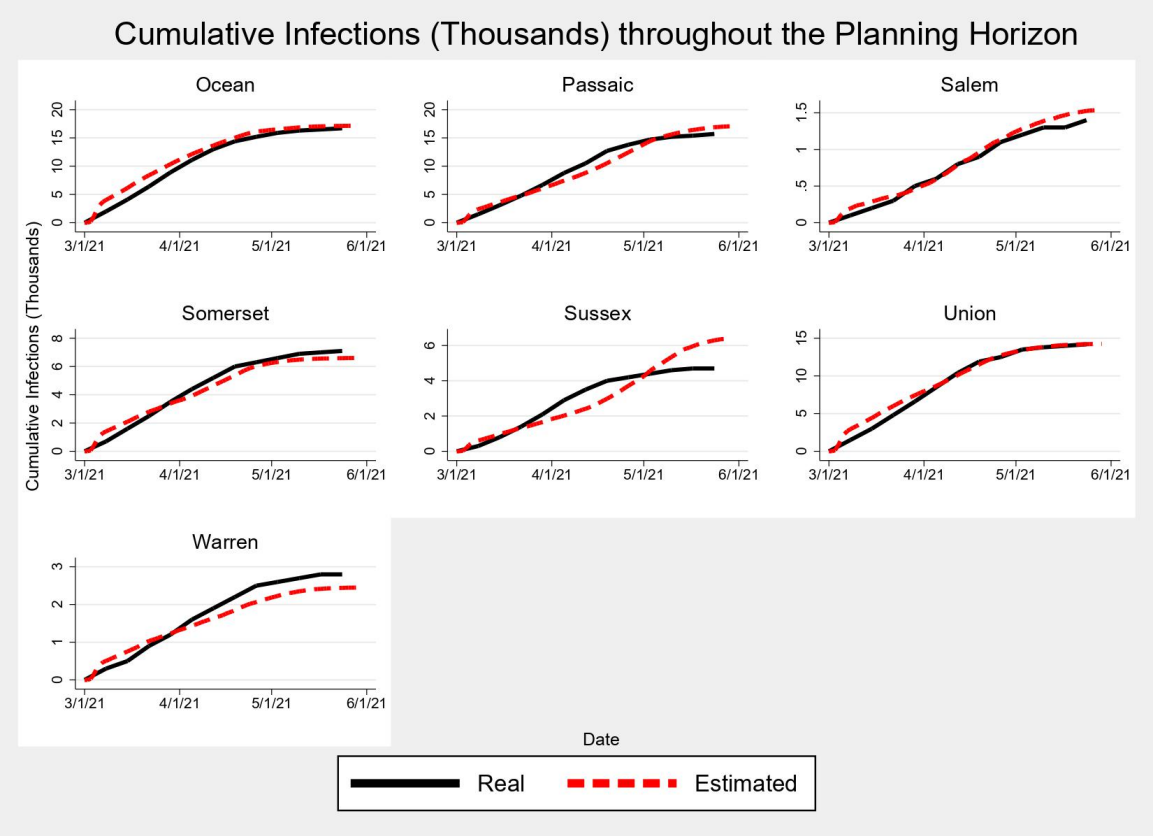

Figure C.3 Cumulative infections (thousands) throughout the planning horizon for New Jersey counties - 3.

Figures C.4, C.5, and C.6 show the results of the cumulative number of infections under different budget levels for all the counties in New Jersey.

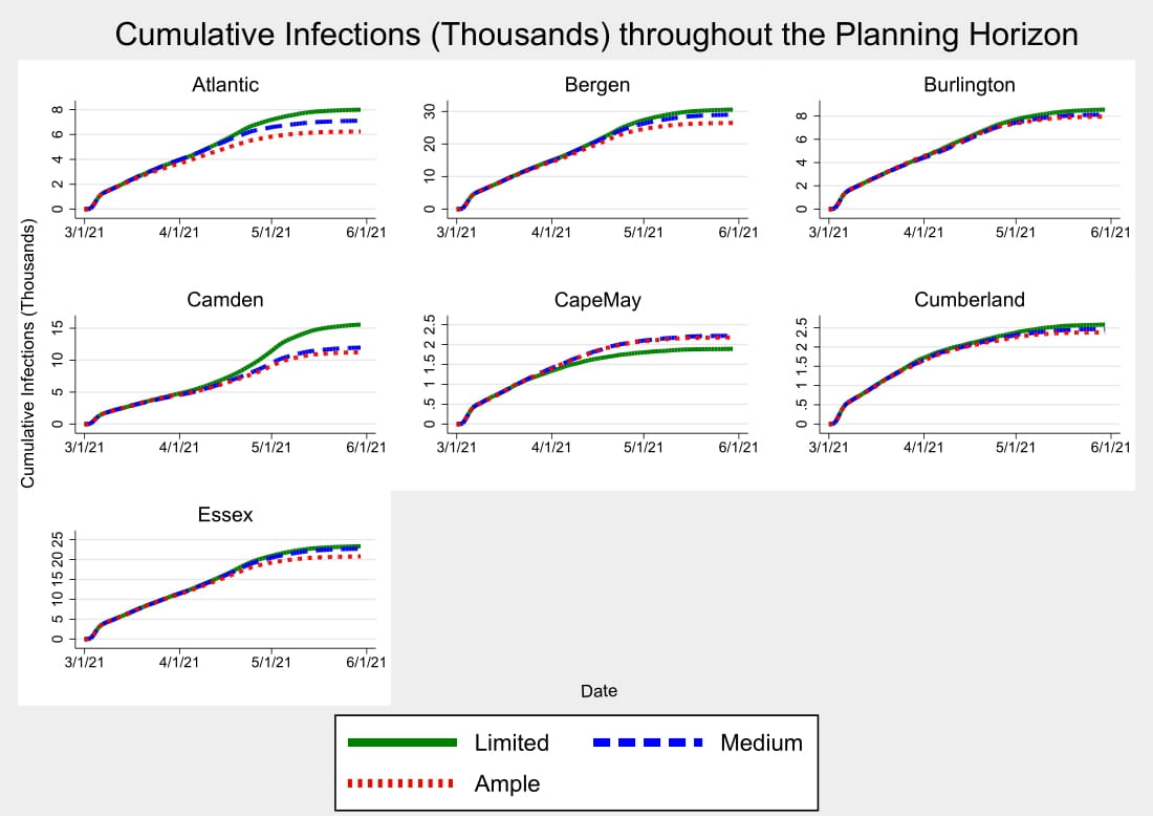

Figure C.4 New Jersey cumulative infections under different budget levels - 1.

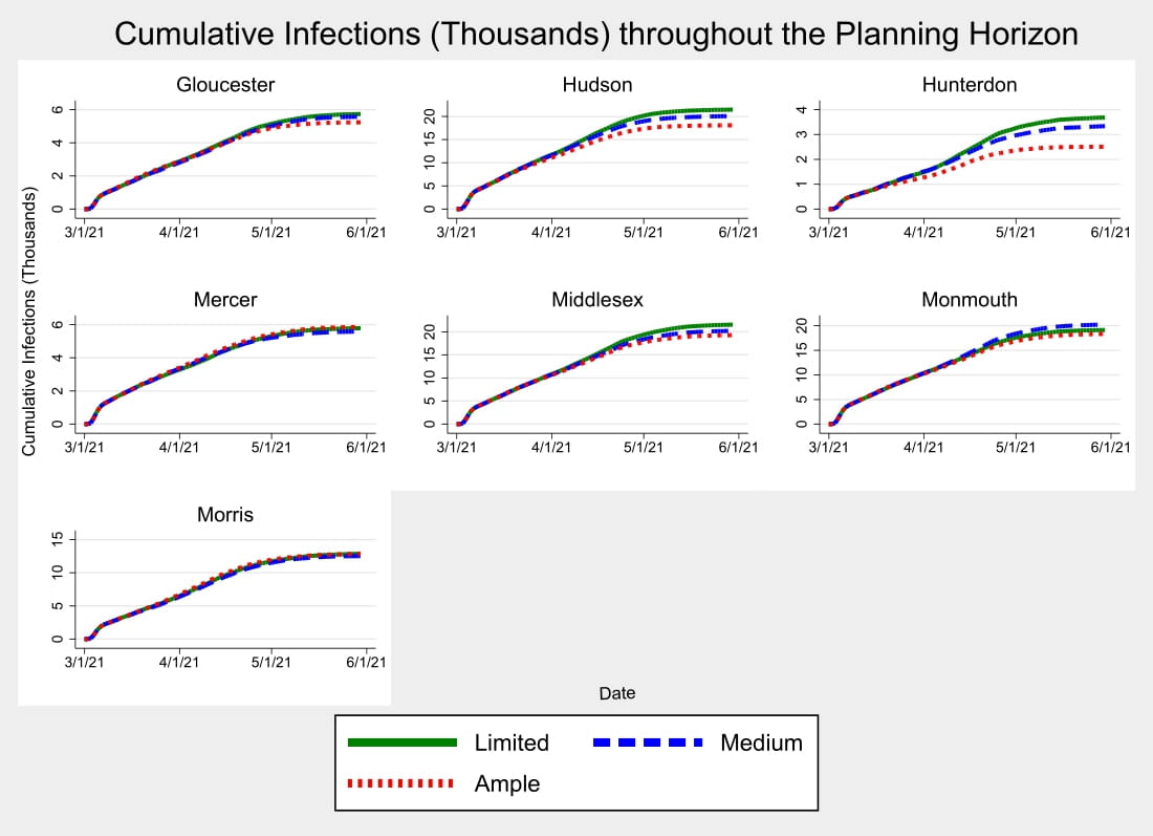

Figure C.5 New Jersey cumulative infections under different budget levels - 2.

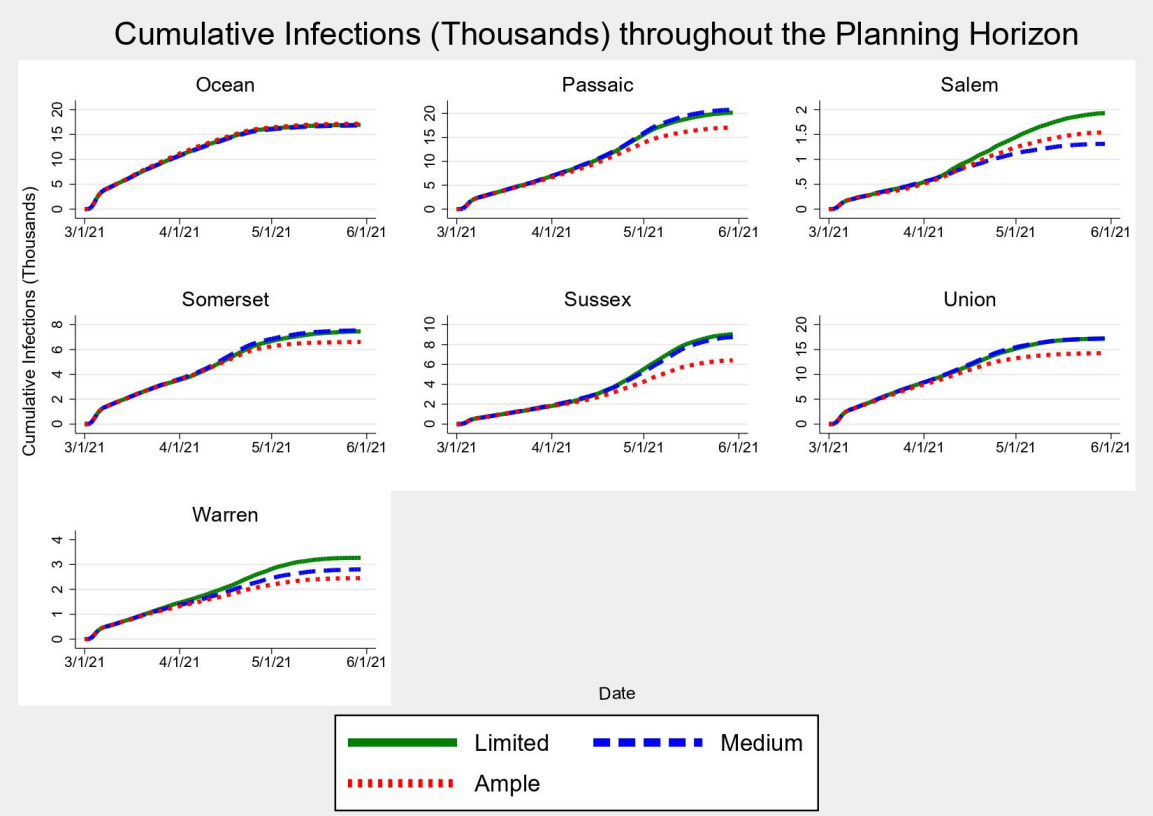

Figure C.6 New Jersey cumulative infections under different budget levels - 3.

REFERENCES

Shabbir Ahmed. Convexity and decomposition of mean-risk stochastic programs. *Mathematical Programming*, 106(3):433–446, 2006.

Marco Ajelli, Stefano Merler, Laura Fumanelli, Ana Pastore y Piontti, Natalie E Dean, Ira M Longini, M Elizabeth Halloran, and Alessandro Vespignani. Spatiotemporal dynamics of the Ebola epidemic in Guinea and implications for vaccination and disease elimination: A computational modeling analysis. *BioMed Central (BMC) Medicine*, 14(1):130, 2016.

Douglas Alem and Reinaldo Morabito. Risk-averse two-stage stochastic programs in furniture plants. *Operations Research (OR) Spectrum*, 35(4):773–806, 2013.

Antonio Alonso-Ayuso, Laureano F Escudero, Monique Guignard, and Andres Weintraub. Risk management for forestry planning under uncertainty in demand and prices. *European Journal of Operational Research*, 267(3): 1051–1074, 2018.

Christian L Althaus. Estimating the reproduction number of Ebola virus (EBOV) during the 2014 outbreak in West Africa. *PLoS Currents*, 6, 2014.

Bakiya Ambikapathy and Kamalanand Krishnamurthy. Mathematical modelling to assess the impact of lockdown on COVID-19 transmission in India: Model development and validation. *Journal of Medical Internet Research (JMIR) Public Health and Surveillance*, 6(2):e19368, 2020.

Aparadinar. NJ us map. https://5thworldadventures.blogspot.com/2018/07/nj-us-map.html, 2021. Accessed July 10, 2021.

Jay April, Fred Glover, James P Kelly, and Manuel Laguna. Practical introduction to simulation optimization. In *Proceedings of the 35th Conference on Winter Simulation: Driving Innovation*, pages 71–78. Citeseer, 2003.

IvÁn Area, FaÏÇal NdaÏrou, Juan J Nieto, Cristiana J Silva, and Delfim FM Torres. Ebola model and optimal control with vaccination constraints. *ArXiv Preprint ArXiv:1703.01368*, 2017.

José Núñez Ares, Harwin De Vries, and Dennis Huisman. A column generation approach for locating roadside clinics in Africa based on effectiveness and equity. *European Journal of Operational Research*, 254(3):1002–1016, 2016.

Frank Ball, Denis Mollison, and Gianpaolo Scalia-Tomba. Epidemics with two levels of mixing. *The Annals of Applied Probability*, pages 46–89, 1997.

Thomas Bein, Salvatore Grasso, Onnen Moerer, Michael Quintel, Claude Guerin, Maria Deja, Anita Brondani, and Sangeeta Mehta. The standard of care of patients with ARDS: Ventilatory settings and rescue therapies for refractory hypoxemia. *Intensive Care Medicine*, 42(5):699–711, 2016.

Oded Berman and Arieh Gavious. Location of terror response facilities: A game between state and terrorist. *European Journal of Operational Research*, 177 (2):1113–1133, 2007.

Lenny Bernstein. More COVID-19 patients are surviving ventilators in the ICU. https://www.washingtonpost.com/health/more-covid-19-patients-are-surviving-ventilators-in-the-icu/2020/07/03/2e3c3534-bbca-11ea-8cf5-9c1b8d7f84c6_story.html, 2020. Accessed November 30, 2020.

Dimitris Bertsimas, Vivek F Farias, and Nikolaos Trichakis. Fairness, efficiency, and flexibility in organ allocation for kidney transplantation. *Operations Research*, 61(1):73–87, 2013.

Dimitris Bertsimas, Leonard Boussioux, Ryan Cory Wright, Arthur Delarue, Vassilis Digalakis Jr, Alexandre Jacquillat, Driss Lahlou Kitane, Galit Lukin, Michael Lingzhi Li, Luca Mingardi, et al. From predictions to prescriptions: A data-driven response to COVID-19. *arXiv preprint arXiv:2006.16509*, 2020.

Samuel Billingham, Rebecca Widrick, Nathan J Edwards, and Sybil Klaus. COVID-19 (SARS-CoV-2) ventilator resource management using a network optimization model and predictive system demand. *MedRxiv*, 2020.

John R Birge. The value of the stochastic solution in stochastic linear programs with fixed recourse. *Mathematical Programming*, 24(1):314–325, 1982.

John R Birge and Francois Louveaux. *Introduction to Stochastic Programming*. Springer Science & Business Media, 2011.

Víctor Blanco, Ricardo Gázquez, and Marina Leal. Reallocating and sharing health equipments in sanitary emergency situations: The COVID-19 case in Spain. *arXiv preprint arXiv:2012.02062*, 2020.

Helen Branswell. Ebola vaccine appears to provide long-lasting protection. https://www.scientificamerican.com/article/ebola-vaccine-appears-to-provide-long-lasting-protection/, 2018. Accessed March 28, 2021.

Andrew Brettin, Rosa Rossi-Goldthorpe, Kyle Weishaar, and Igor V Erovenko. Ebola could be eradicated through voluntary vaccination. *Royal Society Open Science*, 5(1):171591, 2018.

Sabah Bushaj, İ Esra Büyüktahtakın, and Robert G Haight. Risk-averse multi-stage stochastic optimization for surveillance and operations planning of a forest insect infestation. *Under Review*, 2020a.

Sabah Bushaj, İ Esra Büyüktahtakın, Robert G. Haight, and Denys Yemshanov. Optimizing surveillance and management of emerald ash borer in urban environments. *Natural Resource Modeling*, 2020b.

İ Esra Büyüktahtakın. Introducing the concept of scenario-dominance for multi-stage stochastic mixed-integer programs. *Under Review*, 2020.

İ Esra Büyüktahtakın and Robert G Haight. A review of operations research models in invasive species management: State-of-the-art, challenges, and future directions. *Annals of Operations Research*, 271(2):357–403, 2018.

İ Esra Büyüktahtakın and Joseph C Hartman. A mixed-integer programming approach to the parallel replacement problem under technological change. *International Journal of Production Research*, 54(3):680–695, 2016.

İ Esra Büyüktahtakın and Ning Liu. Dynamic programming approximation algorithms for the capacitated lot-sizing problem. *Journal of Global Optimization*, 65(2):231–259, 2016.

İ Esra Büyüktahtakın, Zhuo Feng, George Frisvold, Ferenc Szidarovszky, and Aaryn Olsson. A dynamic model of controlling invasive species. *Computers & Mathematics with Applications*, 62(9):3326–3333, 2011.

İ Esra Büyüktahtakin, Zhuo Feng, Aaryn D Olsson, George Frisvold, and Ferenc Szidarovszky. Invasive species control optimization as a dynamic spatial process: an application to buffelgrass (pennisetum ciliare) in arizona. *Invasive Plant Science and Management*, 7(1):132–146, 2014.

İ Esra Büyüktahtakın, Zhuo Feng, and Ferenc Szidarovszky. A multi-objective optimization approach for invasive species control. *Journal of the Operational Research Society*, 65(11):1625–1635, 2014a.

İ Esra Büyüktahtakın, J Cole Smith, Joseph C Hartman, and Shangyuan Luo. Parallel asset replacement problem under economies of scale with multiple challengers. *The Engineering Economist*, 59(4):237–258, 2014b.

İ Esra Büyüktahtakın, Eyyüb Y Kıbış, Halil I Cobuloglu, Gregory R Houseman, and J Tanner Lampe. An age-structured bio-economic model of invasive species management: Insights and strategies for optimal control. *Biological Invasions*, 17(9):2545–2563, 2015.

İ Esra Büyüktahtakın, Emmanuel des Bordes, and Eyyüb Y Kıbış. A new epidemics–logistics model: Insights into controlling the Ebola Virus Disease in West Africa. *European Journal of Operational Research*, 265(3):1046–1063, 2018a.

İ Esra Büyüktahtakın, J Cole Smith, and Joseph C Hartman. Partial objective inequalities for the multi-item capacitated lot-sizing problem. *Computers & Operations Research*, 91:132–144, 2018b.

Anton Camacho, AJ Kucharski, S Funk, J Breman, P Piot, and WJ Edmunds. Potential for large outbreaks of Ebola Virus Disease. *Epidemics*, 9:70–78, 2014.

Yolanda Carson and Anu Maria. Simulation optimization: methods and applications. In *Proceedings of the 29th Conference on Winter Simulation*, pages 118–126, 1997.

Rebecca Mary Casey, Lee McCalla Hampton, Blanche-philomene Melanga Anya, Marta Gacic-Dobo, Mamadou Saliou Diallo, and Aaron Stuart Wallace. State of equity: childhood immunization in the world health organization African region. *The Pan African Medical Journal*, 27(Suppl 3), 2017.

Marcia C Castro, Lucas Resende de Carvalho, Taylor Chin, Rebecca Kahn, Giovanny VA Franca, Eduardo Marques Macario, and Wanderson Kleber de Oliveira. Demand for hospitalization services for COVID-19 patients in Brazil. *MedRxiv*, 2020.

CDC. Ebola report: Tracing contacts. https://www.cdc.gov/about/ebola/tracing-contacts.html, 2015. Accessed March 28, 2021.

CDC. CDC releases detailed history of the 2014-2016 Ebola response in MMWR. https://www.cdc.gov/media/releases/2016/p0707-history-ebola-response.html, 2016. Accessed November 20, 2019.

CDC. 2009 H1N1 pandemic (H1N1pdm09 virus). https://www.cdc.gov/flu/pandemic-resources/2009-h1n1-pandemic.html, 2019a. Accessed November 20, 2019.

CDC. Covid-19 vaccinations in the United States. https://covid.cdc.gov/covid-data-tracker/#vaccinations, 2021. Accessed July 10, 2021.

Ebola CDC. 2014-2016 Ebola outbreak in West Africa. https://www.cdc.gov/vhf/ebola/history/2014-2016-outbreak/index.html, 2019b. Accessed May 30, 2019.

CENSUS. Datasets. https://www.census.gov/data/datasets.html, 2020. Accessed November 30, 2020.

Gerardo Chowell, Nick W Hengartner, Carlos Castillo-Chavez, Paul W Fenimore, and Jim Michael Hyman. The basic reproductive number of Ebola and the effects of public health measures: the cases of Congo and Uganda. *Journal of Theoretical Biology*, 229(1):119–126, 2004.

Gerardo Chowell, Amna Tariq, and Maria Kiskowski. Vaccination strategies to control Ebola epidemics in the context of variable household inaccessibility levels. *ArXiv Preprint ArXiv:1906.04590*, 2019.

CNBC. Vicky McKeever,CNBC.the coronavirus is expected to have cost 400 million jobs in the second quarter, un labor agency estimates. https://www.cnbc.com/2020/06/30/coronavirus-expected-to-cost-400-million-jobs-in-the-second-quarter.html, 2020. Accessed September 10, 2020.

Halil I Cobuloglu and İ Esra Büyüktahtakın. Food vs. biofuel: An optimization approach to the spatio-temporal analysis of land-use competition and environmental impacts. *Applied Energy*, 140:418–434, 2015.

Halil I Cobuloglu and İ Esra Büyüktahtakın. A two-stage stochastic mixed-integer programming approach to the competition of biofuel and food production. *Computers & Industrial Engineering*, 107:251–263, 2017.

Halil Ibrahim Cobuloglu and İ Esra Büyüktahtakın. A mixed-integer optimization model for the economic and environmental analysis of biomass production. *Biomass and Bioenergy*, 67:8–23, 2014.

Özlem Coşgun and İ Esra Büyüktahtakın. Stochastic dynamic resource allocation for HIV prevention and treatment: An approximate dynamic programming approach. *Computers & Industrial Engineering*, 118:423–439, 2018.

David L Craft, Lawrence M Wein, and Alexander H Wilkins. Analyzing bioterror response logistics: The case of Anthrax. *Management Science*, 51(5):679–694, 2005.

Anthony J Culyer. Equity-some theory and its policy implications. *Journal of Medical Ethics*, 27(4):275–283, 2001.

Anthony J Culyer and Adam Wagstaff. Equity and equality in health and health care. *Journal of Health Economics*, 12(4):431–457, 1993.

Chao Dai, XH Cai, YP Cai, Q Huo, Y Lv, and GH Huang. An interval-parameter mean-CVaR two-stage stochastic programming approach for waste management under uncertainty. *Stochastic Environmental Research and Risk Assessment*, 28(2):167–187, 2014.

Benjamin D Dalziel, Max SY Lau, Amanda Tiffany, Amanda McClelland, Jon Zelner, Jessica R Bliss, and Bryan T Grenfell. Unreported cases in the 2014-2016 Ebola epidemic: Spatiotemporal variation, and implications for estimating transmission. *PLoS Neglected Tropical Diseases*, 12(1):e0006161, 2018.

Thomas K Dasaklis, Costas P Pappis, and Nikolaos P Rachaniotis. Epidemics control and logistics operations: A review. *International Journal of Production Economics*, 139(2):393–410, 2012.

Thomas K Dasaklis, Nikolaos Rachaniotis, and Costas Pappis. Emergency supply chain management for controlling a Smallpox outbreak: The case for regional mass vaccination. *International Journal of Systems Science: Operations & Logistics*, 4(1):27–40, 2017.

Ashley E Davis, Sanjay Mehrotra, John J Friedewald, Mark S Daskin, Anton I Skaro, Michael M Abecassis, and Daniela P Ladner. Improving geographic equity in kidney transplantation using alternative kidney sharing and optimization modeling. *Medical Decision Making*, 35(6):797–807, 2015.

Jan de Mooij, Davide DellAnna, Parantapa Bhattacharya, Mehdi Dastani, Brian Logan, and Samarth Swarup. Quantifying the effects of norms on COVID-19 cases using an agent-based simulation. In *Proceedings of the The 22nd International Workshop on Multi-Agent-Based Simulation (MABS)*, 2021.

Boris Defourny, Damien Ernst, and Louis Wehenkel. Multistage stochastic programming: A scenario tree based approach to planning under uncertainty. In *Decision Theory Models for Applications in Artificial Intelligence: Concepts and Solutions*, pages 97–143. IGI Global, 2012.

Emmanuel des Bordes and İ Esra Büyüktahtakın. Optimizing capital investments under technological change and deterioration: A case study on mri machine replacement. *The Engineering Economist*, 62(2):105–131, 2017.

Christopher Dickey. Whats worse than Ebola? Fighting it in a war zone. https://www.thedailybeast.com/whats-worse-than-ebola-fighting-it-in-a-war-zone, 2018. Accessed March 28, 2021.

Reena H Doshi, Monica Fleming, Arsene Kabwaya Mukoka, Rosalind J Carter, Terri B Hyde, Mary Choi, Michel Kabamba Nzaji, Stephane Hans Bateyi, Athalia Christie, Stuart T Nichol, et al. Vaccination of contacts of Ebola Virus Disease survivors to prevent further transmission. *The Lancet Global Health*, 8(12):e1455–e1456, 2020.

Lotty E Duijzer, Willem L van Jaarsveld, Jacco Wallinga, and Rommert Dekker. Dose-optimal vaccine allocation over multiple populations. *Production and Operations Management*, 27(1):143–159, 2018.

Stephanie R Earnshaw, Katherine Hicks, Anke Richter, and Amanda Honeycutt. A linear programming model for allocating HIV prevention funds with state agencies: a pilot study. *Health Care Management Science*, 10(3):239–252, 2007.

Steffen E Eikenberry, Marina Mancuso, Enahoro Iboi, Tin Phan, Keenan Eikenberry, Yang Kuang, Eric Kostelich, and Abba B Gumel. To mask or not to mask: Modeling the potential for face mask use by the general public to curtail the covid-19 pandemic. *Infectious Disease Modelling*, 5:293–308, 2020.

Ali Ekici, Pınar Keskinocak, and Julie L Swann. Modeling influenza pandemic and planning food distribution. *Manufacturing & Service Operations Management*, 16(1):11–27, 2013.

Özgün Elçi and Nilay Noyan. A chance-constrained two-stage stochastic programming model for humanitarian relief network design. *Transportation Research Part B: Methodological*, 108:55–83, 2018.

Shakiba Enayati and Osman Y Özaltın. Optimal influenza vaccine distribution with equity. *European Journal of Operational Research*, 283(2):714–725, 2020.

Laureano F Escudero, Araceli Garín, María Merino, and Gloria Pérez. The value of the stochastic solution in multistage problems. *Top*, 15(1):48–64, 2007.

ESRI. ArcGIS Online. https://www.arcgis.com/index.html, 2020. Accessed November 25, 2019.

Maddalena Ferranna, Daniel Cadarette, and David E Bloom. Covid-19 vaccine allocation: Modeling health outcomes and equity implications of alternative strategies. *Engineering*, 2021.

Ilan Fischer, Shacked Avrashi, Tomer Oz, Rabab Fadul, Koral Gutman, Daniel Rubenstein, Gregory Kroliczak, Sebastian Goerg, and Andreas Glöckner. The behavioural challenge of the COVID-19 pandemic: Indirect measurements and personalized attitude changing treatments (impact). *Royal Society Open Science*, 7(8):201131, 2020.

David N Fisman, Amy L Greer, and Ashleigh R Tuite. Bidirectional impact of imperfect mask use on reproduction number of covid-19: A next generation matrix approach. *Infectious Disease Modelling*, 5:405–408, 2020.

Marie-Laurence Flahaux and Hein De Haas. African migration: trends, patterns, drivers. *Comparative Migration Studies*, 4(1):1–25, 2016.

Brody H Foy, Brian Wahl, Kayur Mehta, Anita Shet, Gautam I Menon, and Carl Britto. Comparing covid-19 vaccine allocation strategies in india: A mathematical modelling study. *International Journal of Infectious Diseases*, 103:431–438, 2021.

Sebastian Funk, Iza Ciglenecki, Amanda Tiffany, Etienne Gignoux, Anton Camacho, Rosalind M Eggo, Adam J Kucharski, W John Edmunds, Josephus Bolongei, Phillip Azuma, et al. The impact of control strategies and behavioural changes on the elimination of Ebola from Lofa County, Liberia. *Philosophical Transactions of the Royal Society B: Biological Sciences*, 372(1721):20160302, 2017.

Salah Ghamizi, Renaud Rwemalika, Maxime Cordy, Lisa Veiber, Tegawendé F Bissyandé, Mike Papadakis, Jacques Klein, and Yves Le Traon. Data-driven simulation and optimization for covid-19 exit strategies. In *Proceedings of the 26th ACM SIGKDD International Conference on Knowledge Discovery & Data Mining*, pages 3434–3442, 2020.

Heather Glass. High-acuity ventilator cost guide. https://hcpresources.medtronic.com/blog/high-acuity-ventilator-cost-guide, 2020. Accessed November 30, 2020.

Maria Goddard and Peter Smith. Equity of access to health care services:: Theory and evidence from the uk. *Social Science & Medicine*, 53(9):1149–1162, 2001.

Kannan Govindan, Hassan Mina, and Behrouz Alavi. A decision support system for demand management in healthcare supply chains considering the epidemic outbreaks: A case study of Coronavirus Disease 2019 (covid-19). *Transportation Research Part E: Logistics and Transportation Review*, 138: 101967, 2020.

Haccp. A review of the whole process of fighting against SARS in 2003. https://www.sohu.com/a/368331721_614718, 2020. Accessed June 10, 2021.

William Hart, Leonhard Hochfilzer, Nik Cunniffe, Hyojung Lee, Hiroshi Nishiura, and Robin N Thompson. Accurate forecasts of the effectiveness of interventions against Ebola may require models that account for variations in symptoms during infection. *BioRxiv*, page 592030, 2019.

Joseph C Hartman, İ Esra Büyüktahtakin, and J Cole Smith. Dynamic-programming-based inequalities for the capacitated lot-sizing problem. *The Institute of Industrial Engineers (IIE) Transactions*, 42(12):915–930, 2010.

Mostafa Hasan, İ Esra Büyüktahtakın, and Elshami Elamin. A multi-criteria ranking algorithm (MCRA) for determining breast cancer therapy. *Omega*, 82:83–101, 2019.

Erin Heffernan. St. Luke's to open vaccine clinic at chesterfield mall with 2,000 dose daily capacity. https://www.stltoday.com/news/local/metro/st-lukes-to-open-vaccine-clinic-at-chesterfield-mall-with-2-000-dose-daily-capacity/article_5589924e-1d25-5836-9fd9-04c7f4460a4f.html, 2021a. Accessed June 10, 2021.

Erin Heffernan. Covid-19 vaccine distribution allocations by jurisdiction - Pfizer. https://data.cdc.gov/Vaccinations/COVID-19-Vaccine-Distribution-Allocations-by-Juris/saz5-9hgg, 2021b. Accessed June 10, 2021.

Holger Heitsch and Werner Römisch. Scenario tree reduction for multistage stochastic programs. *Computational Management Science*, 6(2):117–133, 2009.

Alex Hogan. Watch: Ventilators are in high demand for COVID-19 patients. How do they work? https://www.statnews.com/2020/03/30/covid-19-ventilators-how-they-work/, 2020. Accessed November 30, 2020.

Tito Homem-de Mello and Bernardo K Pagnoncelli. Risk aversion in multistage stochastic programming: A modeling and algorithmic perspective. *European Journal of Operational Research*, 249(1):188–199, 2016.

Hsin-Chan Huang, Ozgur M Araz, David P Morton, Gregory P Johnson, Paul Damien, Bruce Clements, and Lauren Ancel Meyers. Stockpiling ventilators for influenza pandemics. *Emerging Infectious Diseases*, 23(6):914, 2017.

Kathryn H Jacobsen, A Alonso Aguirre, Charles L Bailey, Ancha V Baranova, Andrew T Crooks, Arie Croitoru, Paul L Delamater, Jhumka Gupta, Kylene Kehn-Hall, Aarthi Narayanan, et al. Lessons from the ebola outbreak: action items for emerging infectious disease preparedness and response. *Ecohealth*, 13(1):200–212, 2016.

Beate Jahn, Gaby Sroczynski, Martin Bicher, Claire Rippinger, Nikolai Mühlberger, Júlia Santamaria, Christoph Urach, Michael Schomaker, Igor Stojkov, Daniela Schmid, et al. Targeted COVID-19 vaccination (tav-covid) considering limited vaccination capacitiesan agent-based modeling evaluation. *Vaccines*, 9(5):434, 2021.

Alien W Jalvingh, Mirjam Nielen, Huibert Maurice, Arjan J Stegeman, Armin RW Elbers, and Aalt A Dijkhuizen. Spatial and stochastic simulation to evaluate the impact of events and control measures on the 1997–1998 classical Swine Fever epidemic in the Netherlands.: I. description of simulation model. *Preventive Veterinary Medicine*, 42(3-4):271–295, 1999.

JHU. COVID-19 United States Cases by County. https://coronavirus.jhu.edu/us-map, 2020. Accessed November 30, 2020.

JHU. COVID-19 dashboard. https://coronavirus.jhu.edu/map.html, 2021. Accessed July 10, 2021.

Shuo Jiang, Kaiqin Wang, Chaoqun Li, Guangbin Hong, Xuan Zhang, Menglin Shan, Hongbin Li, and Jin Wang. Mathematical models for devising the optimal Ebola Virus Disease eradication. *Journal of Translational Medicine*, 15(1): 124, 2017.

Alperen Burak Kantas, Halil I Cobuloglu, and İ Esra Büyüktahtakın. Multi-source capacitated lot-sizing for economically viable and clean biofuel production. *Journal of Cleaner Production*, 94:116–129, 2015.

Edward H Kaplan and Michael H Merson. Allocating HIV-prevention resources: balancing efficiency and equity. *American Journal of Public Health*, 92(12): 1905–1907, 2002.

Edward H Kaplan, David L Craft, and Lawrence M Wein. Analyzing bioterror response logistics: the case of Smallpox. *Mathematical Biosciences*, 185(1): 33–72, 2003.

Parastu Kasaie and W David Kelton. Resource allocation for controlling epidemics: Calibrating, analyzing, and optimizing an agent-based simulation. *IIE Transactions on Healthcare Systems Engineering*, 3(2):94–109, 2013a.

Parastu Kasaie and W David Kelton. Simulation optimization for allocation of epidemic-control resources. *IIE Transactions on Healthcare Systems Engineering*, 3(2):78–93, 2013b.

Parastu Kasaie, W David Kelton, Abolfazl Vaghefi, and SGR Jalali Naini. Toward optimal resource-allocation for control of epidemics: an agent-based-simulation approach. In *Proceedings of the 2010 Winter Simulation Conference*, pages 2237–2248. IEEE, 2010.

Parastu Kasaie, David W Dowdy, and W David Kelton. An agent-based simulation of a tuberculosis epidemic: understanding the timing of transmission. In *Proceedings of the 2013 Winter Simulations Conference (WSC)*, pages 2227–2238. IEEE, 2013.

David J Kedziora, Robyn M Stuart, Jonathan Pearson, Alisher Latypov, Rhodri Dierst-Davies, Maksym Duda, Nata Avaliani, David P Wilson, and Cliff C Kerr. Optimal allocation of HIV resources among geographical regions. *BMC Public Health*, 19(1):1–15, 2019.

Matt J Keeling, Mark EJ Woolhouse, Darren J Shaw, Louise Matthews, Margo Chase-Topping, Dan T Haydon, Stephen J Cornell, Jens Kappey, John Wilesmith, and Bryan T Grenfell. Dynamics of the 2001 UK Foot and Mouth Epidemic: Stochastic dispersal in a heterogeneous landscape. *Science*, 294(5543):813–817, 2001.

Daniel Kelly, Junhyung Park, Ryan J Harrigan, Nicole A Hoff, Sarita D Lee, Rae Wannier, Bernice Selo, Mathias Mossoko, Bathe Njoloko, Emile Okitolonda-Wemakoy, et al. Real-time predictions of the 2018–2019 Ebola Virus Disease outbreak in the Democratic Republic of the Congo using Hawkes point process models. *Epidemics*, 28:100354, 2019a.

Daniel Kelly, Lee Worden, S Rae Wannier, Nicole A Hoff, Patrick Mukadi, Cyrus Sinai, Sarah Ackley, Xianyun Chen, Daozhou Gao, Bernice Selo, et al. Projections of Ebola outbreak size and duration with and without vaccine use in Équateur, Democratic Republic of Congo, as of May 27, 2018. *PloS One*, 14(3):e0213190, 2019b.

Cliff C Kerr, Robyn M Stuart, Dina Mistry, Romesh G Abeysuriya, Gregory Hart, Katherine Rosenfeld, Prashanth Selvaraj, Rafael C Nunez, Brittany Hagedorn, Lauren George, et al. Covasim: an agent-based model of COVID-19 dynamics and interventions. *MedRxiv*, 2021.

Eyyub Kibis, İ. Esra Büyüktahtakın, Robert G. Haight, Najmaddin Akhundov, Kathleen Knight, and Charlie Flower. A new multi-stage stochastic programming model and cutting planes for the optimal surveillance and control of emerald ash borer in cities. *Published online ahead of print in INFORMS Journal on Computing*, 2021.

Eyyüb Y Kıbış and İ Esra Büyüktahtakın. Optimizing invasive species management: A mixed-integer linear programming approach. *European Journal of Operational Research*, 259(1):308–321, 2017.

Eyyüb Y Kıbış and İ Esra Büyüktahtakın. Optimizing multi-modal cancer treatment under 3D spatio-temporal tumor growth. *Mathematical Biosciences*, 307:53–69, 2019.

Lonzozou Kpanake, Paul Clay Sorum, and Étienne Mullet. Willingness to get vaccinated against ebola: A mapping of Guinean people positions. *Human Vaccines & Immunotherapeutics*, 14(10):2391–2396, 2018.

Mirjam Kretzschmar, Susan Van den Hof, Jacco Wallinga, and Jan Van Wijngaarden. Ring vaccination and Smallpox control. *Emerging Infectious Diseases*, 10(5): 832, 2004.

Adam J Kucharski, Rosalind M Eggo, Conall H Watson, Anton Camacho, Sebastian Funk, and W John Edmunds. Effectiveness of ring vaccination as control strategy for Ebola Virus Disease. *Emerging Infectious Diseases*, 22(1):105, 2016.

Setsuya Kurahashi and Takao Terano. A health policy simulation model of Smallpox and Ebola haemorrhagic fever. In *Agent and Multi-agent Systems: Technologies and Applications*, pages 405–415. Springer, 2015.

Lucas Lacasa, Robert Challen, Ellen Brooks-Pollock, and Leon Danon. A flexible method for optimising sharing of healthcare resources and demand in the context of the COVID-19 pandemic. *Plos One*, 15(10):e0241027, 2020.

Haylee Lane, Mitchell Sarkies, Jennifer Martin, and Terry Haines. Equity in healthcare resource allocation decision making: A systematic review. *Social Science & Medicine*, 175:11–27, 2017.

Arielle Lasry, Michael W Carter, and Gregory S Zaric. S4HARA: System for HIV/AIDS resource allocation. *Cost Effectiveness and Resource Allocation*, 6(1):7, 2008.

Marzia Lazzerini and Giovanni Putoto. Covid-19 in Italy: momentous decisions and many uncertainties. *The Lancet Global Health*, 8(5):e641–e642, 2020.

Bruce Y Lee, Shawn T Brown, George W Korch, Philip C Cooley, Richard K Zimmerman, William D Wheaton, Shanta M Zimmer, John J Grefenstette, Rachel R Bailey, Tina-Marie Assi, et al. A computer simulation of vaccine prioritization, allocation, and rationing during the 2009 H1N1 influenza pandemic. *Vaccine*, 28(31):4875–4879, 2010.

Minha Lee, Jun Zhao, Qianqian Sun, Yixuan Pan, Weiyi Zhou, Chenfeng Xiong, and Lei Zhang. Human mobility trends during the early stage of the COVID-19 pandemic in the United States. *PLoS One*, 15(11):e0241468, 2020.

Judith Legrand, Rebecca Freeman Grais, Pierre-Yves Boelle, Alain-Jacques Valleron, and Antoine Flahault. Understanding the dynamics of Ebola epidemics. *Epidemiology & Infection*, 135(4):610–621, 2007.

Neele Leithaeuser, Johanna Schneider, Sebastian Johann, Sven Krumke, Manuel Streicher, Eva Schmidt, and Stefan Scholz. Quantifying COVID-19-vaccine location strategies for germany. *MedRxiv*, 2020.

Phenyo E Lekone and Bärbel F Finkenstädt. Statistical inference in a stochastic epidemic SEIR model with control intervention: Ebola as a case study. *Biometrics*, 62(4):1170–1177, 2006.

Hernan Leövey and Werner Römisch. Quasi-Monte Carlo methods for linear two-stage stochastic programming problems. *Mathematical Programming*, 151(1): 315–345, 2015.

Junjiang Li, Philippe Giabbanelli, et al. Returning to a normal life via COVID-19 vaccines in the united states: A large-scale agent-based simulation study. *JMIR Medical Informatics*, 9(4):e27419, 2021.

Ruiyun Li, Sen Pei, Bin Chen, Yimeng Song, Tao Zhang, Wan Yang, and Jeffrey Shaman. Substantial undocumented infection facilitates the rapid dissemination of novel coronavirus (sars-cov-2). *Science*, 368(6490):489–493, 2020.

Ming Liu, Xifen Xu, Jie Cao, and Ding Zhang. Integrated planning for public health emergencies: A modified model for controlling H1N1 pandemic. *Journal of the Operational Research Society*, pages 1–14, 2019.

Xianning Liu, Yasuhiro Takeuchi, and Shingo Iwami. Svir epidemic models with vaccination strategies. *Journal of Theoretical Biology*, 253(1):1–11, 2008.

Elisa F Long, Eike Nohdurft, and Stefan Spinler. Spatial resource allocation for emerging epidemics: A Comparison of Greedy, Myopic, and Dynamic Policies. *Manufacturing & Service Operations Management*, 20(2):181–198, 2018.

Ira M Longini Jr, M Elizabeth Halloran, Azhar Nizam, Yang Yang, Shufu Xu, Donald S Burke, Derek AT Cummings, and Joshua M Epstein. Containing a large bioterrorist Smallpox attack: A computer simulation approach. *International Journal of Infectious Diseases*, 11(2):98–108, 2007.

James Love-Koh, Susan Griffin, Edward Kataika, Paul Revill, Sibusiso Sibandze, and Simon Walker. Methods to promote equity in health resource allocation in low-and middle-income countries: an overview. *Globalization and Health*, 16 (1):6, 2020.

Albert Madansky. Inequalities for stochastic linear programming problems. *Management Science*, 6(2):197–204, 1960.

Harry M Markowitz. Foundations of portfolio theory. *The Journal of Finance*, 46(2): 469–477, 1991.

Michael T Marsh and David A Schilling. Equity measurement in facility location analysis: A review and framework. *European Journal of Operational Research*, 74(1):1–17, 1994.

Ardeshir Raihanian Mashhadi, Sara Behdad, and Jun Zhuang. Agent based simulation optimization of waste electrical and electronics equipment recovery. *Journal of Manufacturing Science and Engineering*, 138(10), 2016.

Martial L Ndeffo Mbah and Christopher A Gilligan. Resource allocation for epidemic control in metapopulations. *PLoS One*, 6(9):e24577, 2011.

Jessica H McCoy and Hau L Lee. Using fairness models to improve equity in health delivery fleet management. *Production and Operations Management*, 23(6): 965–977, 2014.

Katie Kerwin McCrimmon. The truth about COVID-19 and asymptomatic spread: Its common, so wear a mask and avoid large gatherings. https://www.uchealth.org/today/the-truth-about-asymptomatic-spread-of-covid-19/, 2021. Accessed February 13, 2021.

Sanjay Mehrotra, Hamed Rahimian, Masoud Barah, Fengqiao Luo, and Karolina Schantz. A model of supply-chain decisions for resource sharing with an application to ventilator allocation to combat COVID-19. *Naval Research Logistics (NRL)*, 2020.

Megan Meller. The asymptomatic and pre-symptomatic spread of COVID-19. https://www.gundersenhealth.org/covid19/the-asymptomatic-and-pre-symptomatic-spread-of-covid-19/#:~:text=We%20believe%20that%20the%20number,allergies%20or%20a%20cold., 2020. Accessed November 30, 2020.

Martin I Meltzer, Charisma Y Atkins, Scott Santibanez, Barbara Knust, Brett W Petersen, Elizabeth D Ervin, Stuart T Nichol, Inger K Damon, and Michael L Washington. Estimating the future number of cases in the Ebola epidemic–Liberia and Sierra Leone, 2014–2015. *CDC*, 2014.

Martin I Meltzer, Anita Patel, Adebola Ajao, Scott V Nystrom, and Lisa M Koonin. Estimates of the demand for mechanical ventilation in the United States during an influenza pandemic. *Clinical Infectious Diseases*, 60(suppl_1):S52–S57, 2015.

Lingzhong Meng, Haibo Qiu, Li Wan, Yuhang Ai, Zhanggang Xue, Qulian Guo, Ranjit Deshpande, Lina Zhang, Jie Meng, Chuanyao Tong, et al. Intubation and ventilation amid the COVID-19 outbreak: Wuhans experience. *Anesthesiology*, 132(6):1317–1332, 2020.

Stefano Merler, Marco Ajelli, Laura Fumanelli, Stefano Parlamento, Ana Pastore y Piontti, Natalie E Dean, Giovanni Putoto, Dante Carraro, Ira M Longini Jr, M Elizabeth Halloran, et al. Containing Ebola at the source with ring vaccination. *PLoS Neglected Tropical Diseases*, 10(11):e0005093, 2016.

Naomi Miller and Andrzej Ruszczyński. Risk-averse two-stage stochastic linear programming: Modeling and decomposition. *Operations Research*, 59(1): 125–132, 2011.

Kenji Mizumoto, Amna Tariq, Kimberlyn Roosa, Jun Kong, Ping Yan, and Gerardo Chowell. Spatial variability in the reproduction number of ebola virus disease, democratic republic of the congo, january–september 2019. *Eurosurveillance*, 24(42), 2019.

Ebola MSF. Crisis update - march 2020. https://www.msf.org/drc-ebola-outbreak-crisis-update, 2020. Accessed March 23, 2020.

Mudatsir Mudatsir, Samsul Anwar, Jonny K Fajar, Amanda Yufika, Muhammad N Ferdian, Salwiyadi Salwiyadi, Aga S Imanda, Roully Azhars, Darul Ilham, Arya U Timur, et al. Willingness-to-pay for a hypothetical Ebola vaccine in Indonesia: a cross-sectional study in Aceh. *F1000Research*, 8, 2019.

Sebastian A Müller, Michael Balmer, William Charlton, Ricardo Ewert, Andreas Neumann, Christian Rakow, Tilmann Schlenther, and Kai Nagel. Predicting the effects of COVID-19 related interventions in urban settings by combining activity-based modelling, agent-based simulation, and mobile phone data. *MedRxiv*, 2021.

China News. Year-end observation: Behind the new crown pandemic, historical reincarnation, world reshaping, and great changes in the future. http://www.chinanews.com/gj/2020/12-29/9373444.shtml, 2020. Accessed June 10, 2021.

Van Kinh Nguyen, Rafael Mikolajczyk, and Esteban A Hernandez-Vargas. Multiscale modeling to explore Ebola vaccination strategies. *BioRxiv*, page 133421, 2017.

Ebola NIH. Ebola vaccines. https://www.niaid.nih.gov/diseases-conditions/ebola-vaccines, 2019. Accessed September 23, 2019.

NJ.GOV. COVID-19 vaccine. https://covid19.nj.gov/pages/vaccine, 2021. Accessed July 10, 2021.

NJIT. NJIT to host community COVID-19 vaccination center. https://news.njit.edu/njit-host-community-covid-19-vaccination-center, 2021. Accessed June 10, 2021.

Nilay Noyan. Risk-averse two-stage stochastic programming with an application to disaster management. *Computers & Operations Research*, 39(3):541–559, 2012.

Elaine Nsoesie, Madhav Mararthe, and John Brownstein. Forecasting peaks of seasonal influenza epidemics. *PLoS Currents*, 5, 2013a.

Elaine O Nsoesie, Richard J Beckman, Sara Shashaani, Kalyani S Nagaraj, and Madhav V Marathe. A simulation optimization approach to epidemic forecasting. *PloS One*, 8(6):e67164, 2013b.

National Academies of Sciences Engineering, Medicine, et al. Framework for equitable allocation of covid-19 vaccine. *National Academies Press*, 2020.

Sevilay Onal, Najmaddin Akhundov, İ Esra Büyüktahtakın, Jennifer Smith, and Gregory R Houseman. An integrated simulation-optimization framework to optimize search and treatment path for controlling a biological invader. *International Journal of Production Economics*, page 107507, 2019.

Irem Sengul Orgut, Julie Ivy, Reha Uzsoy, and James R Wilson. Modeling for the equitable and effective distribution of donated food under capacity constraints. *IIE Transactions*, 48(3):252–266, 2016.

Abhishek Pandey, Katherine E Atkins, Jan Medlock, Natasha Wenzel, Jeffrey P Townsend, James E Childs, Tolbert G Nyenswah, Martial L Ndeffo-Mbah, and Alison P Galvani. Strategies for containing Ebola in West Africa. *Science*, 346 (6212):991–995, 2014.

Felix Parker, Hamilton Sawczuk, Fardin Ganjkhanloo, Farzin Ahmadi, and Kimia Ghobadi. Optimal resource and demand redistribution for healthcare systems under stress from COVID-19. *arXiv preprint arXiv:2011.03528*, 2020.

Purvi Patel, Aditya Athotra, TP Vaisakh, Tanzin Dikid, Sudhir Kumar Jain, et al. Impact of nonpharmacological interventions on covid-19 transmission dynamics in india. *Indian Journal of Public Health*, 64(6):142, 2020.

Paul Vieira Peter Loftus. Vaccine manufacturing issues force Moderna to cut supplies to Canada, U.K. https://www.wsj.com/articles/vaccine-manufacturing-issues-force-moderna-to-cut-supplies-to-canada-u-k-11618600046, 2021a. Accessed July 10, 2021.

Paul Vieira Peter Loftus. COVID-19 vaccines work. https://www.cdc.gov/coronavirus/2019-ncov/vaccines/effectiveness/work.html, 2021b. Accessed July 10, 2021.

Pfizer. Manufacturing and distributing the COVID-19 vaccine. https://www.pfizer.com/science/coronavirus/vaccine/manufacturing-and-distribution, 2021. Accessed July 10, 2021.

Georg Ch Pflug and Alois Pichler. Dynamic generation of scenario trees. *Computational Optimization and Applications*, 62(3):641–668, 2015.

Travis C Porco, Karen A Holbrook, Susan E Fernyak, Diane L Portnoy, Randy Reiter, and Tomás J Aragón. Logistics of community Smallpox control through contact tracing and ring vaccination: A stochastic network model. *BMC Public Health*, 4(1):34, 2004.

Victor M Preciado, Michael Zargham, Chinwendu Enyioha, Ali Jadbabaie, and George Pappas. Optimal vaccine allocation to control epidemic outbreaks in arbitrary networks. In *Proceedings of the 52nd IEEE Conference on Decision and Control*, pages 7486–7491. IEEE, 2013.

Maciel M Queiroz, Dmitry Ivanov, Alexandre Dolgui, and Samuel Fosso Wamba. Impacts of epidemic outbreaks on supply chains: mapping a research agenda amid the covid-19 pandemic through a structured literature review. *Annals of Operations Research*, pages 1–38, 2020.

Amira Rachah. A mathematical model with isolation for the dynamics of ebola virus. In *Journal of Physics: Conference Series*, volume 1132, page 012058. IOP Publishing, 2018.

Megan L Ranney, Valerie Griffeth, and Ashish K Jha. Critical supply shortagesthe need for ventilators and personal protective equipment during the COVID-19 pandemic. *New England Journal of Medicine*, 382(18):e41, 2020.

Mehdi Rastegar, Madjid Tavana, Afshin Meraj, and Hassan Mina. An inventory-location optimization model for equitable influenza vaccine distribution in developing countries during the COVID-19 pandemic. *Vaccine*, 39(3):495–504, 2021.

Yingtao Ren, Fernando Ordóñez, and Shinyi Wu. Optimal resource allocation response to a Smallpox outbreak. *Computers & Industrial Engineering*, 66 (2):325–337, 2013.

Steven Riley and Neil M Ferguson. Smallpox transmission and control: Spatial dynamics in Great Britain. *Proceedings of the National Academy of Sciences*, 103(33):12637–12642, 2006.

Caitlin M Rivers, Eric T Lofgren, Madhav Marathe, Stephen Eubank, and Bryan L Lewis. Modeling the impact of interventions on an epidemic of Ebola in Sierra Leone and Liberia. *PLoS Currents*, 6, 2014.

Ralph Tyrrell Rockafellar and Stanislav Uryasev. Conditional value-at-risk for general loss distributions. *Journal of Banking & Finance*, 26(7):1443–1471, 2002.

Nick Routley. Charts: The economic impact of COVID-19 in the U.S. so far. https://www.visualcapitalist.com/economic-impact-of-covid-h1-2020/, 2020. Accessed September 8, 2020.

Fernando Saldaña, Hugo Flores-Arguedas, José Ariel Camacho-Gutiérrez, and Ignacio Barradas. Modeling the transmission dynamics and the impact of the control interventions for the covid-19 epidemic outbreak. *Math. Biosci. Eng*, 17(4): 4165–4183, 2020.

Emanuel S Savas. On equity in providing public services. *Management Science*, 24 (8):800–808, 1978.

Harvard Medical School. Symptoms, spread and other essential information about Coronavirus and COVID-19. https://www.health.harvard.edu/diseases-and-conditions/covid-19-basics#:~:text=and%20body%20ache.-,In%20some%20people%2C%20COVID%2D19%20causes%20more%20severe%20symptoms%20like,a%20short%20period%20of%20time., 2021. Accessed February 12, 2021.

Rüdiger Schultz and Stephan Tiedemann. Conditional value-at-risk in stochastic programs with mixed-integer recourse. *Mathematical Programming*, 105(2-3): 365–386, 2006.

Jill Seladi-Schulman. What we know about the effectiveness of the Johnson & Johnson COVID-19 vaccine. https://www.healthline.com/health/adult-vaccines/johnson-and-johnson-vaccine-efficacy, 2021. Accessed June 10, 2021.

Md Salman Shamil, Farhanaz Farheen, Nabil Ibtehaz, Irtesam Mahmud Khan, and M Sohel Rahman. An agent-based modeling of covid-19: Validation, analysis, and recommendations. *Cognitive Computation*, pages 1–12, 2021.

Leah B Shaw and Ira B Schwartz. Enhanced vaccine control of epidemics in adaptive networks. *Physical Review E*, 81(4):046120, 2010.

Eunha Shim. Optimal allocation of the limited covid-19 vaccine supply in south korea. *Journal of Clinical Medicine*, 10(4):591, 2021.

Mark J Siedner, Lawrence O Gostin, Hilarie H Cranmer, and John D Kraemer. Strengthening the detection of and early response to public health emergencies: lessons from the West African Ebola epidemic. *PLoS Medicine*, 12(3), 2015.

Constantinos Siettos, Cleo Anastassopoulou, Lucia Russo, Christos Grigoras, and Eleftherios Mylonakis. Modeling the 2014 Ebola virus epidemic–agent-based simulations, temporal analysis and future predictions for Liberia and Sierra Leone. *PLoS Currents*, 7, 2015.

Sina. A failed infectious disease containment, starting from the 2009 H1N1 epidemic in the United States. https://tech.sina.cn/2020-01-30/detail-iimxxste7650292.d.html, 2021. Accessed June 10, 2021.

Hamed Soleimani and Kannan Govindan. Reverse logistics network design and planning utilizing conditional value at risk. *European Journal of Operational Research*, 237(2):487–497, 2014.

Deborah Stone. Policy paradox: the art of political decision-making, new york: W. w, 2002.

Xuanming Su and Stefanos A Zenios. Recipient choice can address the efficiency-equity trade-off in kidney transplantation: A mechanism design model. *Management Science*, 52(11):1647–1660, 2006.

Matthew W Tanner, Lisa Sattenspiel, and Lewis Ntaimo. Finding optimal vaccination strategies under parameter uncertainty using stochastic programming. *Mathematical Biosciences*, 215(2):144–151, 2008.

Radboud J Duintjer Tebbens and Kimberly M Thompson. Priority shifting and the dynamics of managing eradicable infectious diseases. *Management Science*, 55 (4):650–663, 2009.

Sherry Towers, Oscar Patterson-Lomba, and Carlos Castillo-Chavez. Temporal variations in the effective reproduction number of the 2014 West Africa Ebola outbreak. *PLoS Currents*, 6, 2014.

Maduka Donatus Ughasoro, Dorothy Omono Esangbedo, Beckie Nnenna Tagbo, and Ijeoma Chigozie Mejeha. Acceptability and willingness-to-pay for a hypothetical Ebola virus vaccine in Nigeria. *PLoS Negl Trop Dis*, 9(6): e0003838, 2015.

United Nations. Resources for results v, office of the un special envoy on ebola. https://ebolaresponse.un.org/sites/default/files/resources_for_results_v.pdf, 2020. Accessed September 24, 2020.

Rae Wannier, Lee Worden, Nicole A Hoff, Eduardo Amezcua, Bernice Selo, Cyrus Sinai, Mathias Mossoko, Bathe Njoloko, Emile Okitolonda-Wemakoy, Placide Mbala-Kingebeni, et al. Estimating the impact of violent events on transmission in Ebola Virus Disease outbreak, Democratic Republic of the Congo, 2018–2019. *Epidemics*, 28:100353, 2019.

Chad Wells, Dan Yamin, Martial L Ndeffo-Mbah, Natasha Wenzel, Stephen G Gaffney, Jeffrey P Townsend, Lauren Ancel Meyers, Mosoka Fallah, Tolbert G Nyenswah, Frederick L Altice, et al. Harnessing case isolation and ring vaccination to control Ebola. *PLoS Neglected Tropical Diseases*, 9(5):e0003794, 2015.

Chad R Wells, Abhishek Pandey, Alyssa S Parpia, Meagan C Fitzpatrick, Lauren A Meyers, Burton H Singer, and Alison P Galvani. Ebola vaccination in the Democratic Republic of the Congo. *Proceedings of the National Academy of Sciences*, 116(20):10178–10183, 2019.

Amy Wesolowski, Caroline O Buckee, Linus Bengtsson, Erik Wetter, Xin Lu, and Andrew J Tatem. Commentary: Containing the Ebola outbreak-the potential and challenge of mobile network data. *PLoS Currents*, 6, 2014.

Douglas B White and Bernard Lo. A framework for rationing ventilators and critical care beds during the COVID-19 pandemic. *Jama*, 323(18):1773–1774, 2020.

WHO. Factors that contributed to undetected spread of the Ebola virus and impeded rapid containment. https://www.who.int/news-room/spotlight/one-year-into-the-ebola-epidemic/factors-that-contributed-to-undetected-spread-of-the-ebola-virus-and-impeded-rapid-containment, 2015. Accessed March 28, 2021.

WHO. Ebola situation reports: archive. https://www.who.int/csr/disease/ebola/situation-reports/archive/en/, 2016. Accessed November, 2019.

WHO. Ebola vaccine frequently asked questions. https://www.who.int/emergencies/diseases/ebola/frequently-asked-questions/ebola-vaccine, 2018. Accessed November 25, 2019.

WHO. Second Ebola vaccine to complement ring vaccination given green light in DRC. https://www.who.int/news-room/detail/23-09-2019-second-ebola-vaccine-to-complement-ring-vaccination-given-green-light-in-drc, 2019a. Accessed Jan 15, 2020.

WHO. SARS (SEVERE ACUTE RESPIRATORY SYNDROME). https://www.who.int/ith/diseases/sars/en/, 2019b. Accessed November 20, 2019.

WHO. Preliminary results on the efficacy of rVSV-ZEBOV-GP Ebola vaccine using the ring vaccination strategy in the control of an Ebola outbreak in the Democratic Republic of the Congo: An example of integration of research into epidemic response. https://www.who.int/csr/resources/publications/ebola/ebola-ring-vaccination-results-12-april-2019.pdf, 2019c. Accessed November 25, 2019.

WHO. Ebola vaccines. https://www.who.int/westernpacific/news/q-a-detail/ebola-vaccines, 2021a. Accessed March 28, 2021.

WHO. The top 10 causes of death. https://www.who.int/news-room/fact-sheets/detail/the-top-10-causes-of-death, 2021b. Accessed April 30, 2021.

WHO. Costs of delivering COVID-19 vaccine in 92 amc countries. https://www.who.int/publications/m/item/costs-of-delivering-covid-19-vaccine-in-92-amc-countries, 2021c. Accessed June 10, 2021.

WHO. Coronavirus disease (COVID-19): Vaccines. https://www.who.int/news-room/q-a-detail/coronavirus-disease-(covid-19)-vaccines, 2021d. Accessed June 10, 2021.

Ebola WHO. Ebola Virus Disease. https://www.who.int/health-topics/ebola, 2019d. Accessed May 30, 2019.

Ebola WHO. Ebola situation reports: Democratic Republic of the Congo (archive). https://www.who.int/ebola/situation-reports/drc-2018/en/, 2020a. Accessed November 30, 2019.

Ebola WHO. Ebola response roadmap. http://www.who.int/csr/resources/publications/ebola/response-roadmap/en/, 2020b. Accessed September 24, 2020.

Ebola WHO. Ebola Virus Disease. fact sheet, world health organization, geneva. http://www.who.int/mediacentre/factsheets/fs103/en/, 2020c. Accessed September 24, 2020.

Ebola WHO. Ebola situation report - 31 december 2014. https://apps.who.int/ebola/en/status-outbreak/situation-reports/ebola-situation-report-31-december-2014, 2020d. Accessed September 24, 2020.

Ebola WHO. Coronavirus. https://www.who.int/health-topics/coronavirus, 2020e. Accessed March 24, 2020.

WHO E. R. Team. Ebola Virus Disease in West Africa-The first 9 months of the epidemic and forward projections. *New England Journal of Medicine*, 371 (16):1481–1495, 2014.

Lee Worden, Rae Wannier, Nicole A Hoff, Kamy Musene, Bernice Selo, Mathias Mossoko, Emile Okitolonda-Wemakoy, Jean Jacques Muyembe Tamfum, George W Rutherford, Thomas M Lietman, et al. Projections of epidemic transmission and estimation of vaccination impact during an ongoing Ebola Virus Disease outbreak in Northeastern Democratic Republic of Congo, as of feb. 25, 2019. *PLoS Neglected Tropical Diseases*, 13(8):e0007512, 2019.

Xiaomin Xi, Ramteen Sioshansi, and Vincenzo Marano. Simulation–optimization model for location of a public electric vehicle charging infrastructure. *Transportation Research Part D: Transport and Environment*, 22:60–69, 2013.

Zhifu Xie. Data fitting and scenario analysis of vaccination in the 2014 Ebola outbreak in Liberia. *Osong Public Health and Research Perspectives*, 10(3):187, 2019.

Hamed Yarmand, Julie S Ivy, Brian Denton, and Alun L Lloyd. Optimal two-phase vaccine allocation to geographically different regions under uncertainty. *European Journal of Operational Research*, 233(1):208–219, 2014.

Xuecheng Yin and İ. Esra Büyüktahtakın. A multi-stage stochastic programming approach to epidemic resource allocation with equity considerations. *Published online ahead of print in Health Care Management Science*, pages 1–26, 2021a.

Xuecheng Yin and İ. Esra Büyüktahtakın. Risk-averse multi-stage stochastic programming to optimizing vaccine allocation and treatment logistics for effective epidemic response. *IISE Transactions on Healthcare Systems Engineering*, (just-accepted):1–52, 2021b.

Xuecheng Yin, İ. Esra Büyüktahtakın, and Bhumi P Patel. Covid-19: Optimal allocation of ventilator supply under uncertainty and risk. *Available at SSRN 3801183*, 2021.

Peyton Young. *Equity: in theory and practice*. Princeton University Press, 1995.

Gregory S Zaric and Margaret L Brandeau. Resource allocation for epidemic control over short time horizons. *Mathematical Biosciences*, 171(1):33–58, 2001.

Gregory S Zaric and Margaret L Brandeau. A little planning goes a long way: multilevel allocation of HIV prevention resources. *Medical Decision Making*, 27(1):71–81, 2007.

Gregory S Zaric, Margaret L Brandeau, and Paul G Barnett. Methadone maintenance and HIV prevention: A cost-effectiveness analysis. *Management Science*, 46 (8):1013–1031, 2000.

Stephanie Zaza, Lisa M Koonin, Adebola Ajao, Scott V Nystrom, Richard Branson, Anita Patel, Bruce Bray, and Michael F Iademarco. A conceptual framework for allocation of federally stockpiled ventilators during large-scale public health emergencies. *Health Security*, 14(1):1–6, 2016.

Kevin Zhang, Thomas N Vilches, Mehreen Tariq, Alison P Galvani, and Seyed M Moghadas. The impact of mask-wearing and shelter-in-place on COVID-19 outbreaks in the united states. *International Journal of Infectious Diseases*, 101:334–341, 2020a.

Nan Zhang, Wei Jia, Hao Lei, Peihua Wang, Pengcheng Zhao, Yong Guo, Chung-Hin Dung, Zhongming Bu, Peng Xue, Jingchao Xie, et al. Effects of human behaviour changes during the COVID-19 pandemic on influenza spread in Hong Kong. *Clinical Infectious Diseases*, 2020b.

Weini Zhang, Hamed Rahimian, and Güzin Bayraksan. Decomposition algorithms for risk-averse multistage stochastic programs with application to water allocation under uncertainty. *INFORMS Journal on Computing*, 28(3):385–404, 2016.